INTERFERENCE EFFECTS

IN SUPERSONIC FLOW

Thesis by

Zegmund O. Bleviss

In Partial Fulfillment of the Requirements

For the Degree of

Doctor of Philosophy

California Institute of Technology

Pasadena, California

1951

ACKNOWLEDGMENTS

The writer wishes to acknowledge his deep indebtedness to Professor P. A. Lagerstrom for his constant interest, advice, and many stimulating discussions. He wishes, further, to express his appreciation to M. Hunter, D. Delameter, and, in particular, E. W. Graham of the Douglas Aircraft Co., Santa Monica, for many helpful discussions.

The writer wishes to thank Mrs. Elizabeth Fox for her part in the preparation of this thesis and J. Carp for his timely help with the figures.

ABSTRACT

A study is made of interference problems with emphasis on low-aspect-ratio supersonic missile configurations. The configurations are composed of slender pointed bodies with circular cross section, plane or cruciform delta wings, and tails which are not specified. For fin-fin interference (no body) general multi-fin delta wings are studied for the roll problems.

Three types of interferences are studied. They are (1) fin-fin interference, (2) fin-fin and wing-body interferences combined, and (3) wing-body-tail interference. Where possible, three aerodynamic problems are studied under each of these interferences. They are (1) lift and incidence, (2) roll due to aileron deflection, and (3) damping in roll.

A survey of the theoretical work on supersonic interference problems is included.

Linearized theory is used throughout for all problems treated by the writer. Work by other writers which fits naturally into the scheme of the present work is summarized briefly. For most of the problems it is not possible to obtain exact linearized solutions without excessive labor. Where possible, approximations to or estimates of the exact solutions are obtained. It is hoped that these results will be useful for engineering estimates of the interference effects.

Theoretical results for the roll problems--exact, approximate, and estimated--are presented for fin-fin interference for cruciform and more general multi-fin delta wings with subsonic and supersonic leading edges.

For fin-fin and wing-body interferences combined, theoretical results which bracket the exact solutions are obtained for the roll problems.

For wing-body-tail interference, the vorticity distributions, rolled-up vortex strengths, and initial vortex positions at the trailing edges are estimated for lift, incidence, aileron deflection, and damping in roll problems. Both plane and cruciform delta wing-body configurations are studied.

A qualitative discussion of some of the nonlinear, viscous, and gap effects is included.

Recommendations for future research are made.

TABLE OF CONTENTS

TABLE OF CONTENTS (Cont'd)

TABLE OF CONTENTS (Cont'd)

LIST OF FIGURES

LIST OF FIGURES (Contd)

LIST OF FIGURES (Cont'd)

LIST OF FIGURES (Cont'd)

SYMBOLS AND NOTATION

For convenience, a plane wing is considered to be oriented so that it lies in the horizontal (x-z) plane and a cruciform wing is considered to be oriented so that one pair of fins is horizontal and the other pair vertical.

Notations and coordinates for plane and cruciform wings and wing-body combinations are shown in Figures 1 and 2.

Wide Delta--All leading edges supersonic.
Narrow-Delta--All leading edges subsonic.
Plane Wing--Flat plate unless otherwise stated of zero thickness.
Plane Delta Wing--Plane wing with delta planform. The two halves of the delta wing are called fins.
Plane Aileron--Plane wing with aileron deflection, i.e. the two halves (fins) of the plane wing deflected in opposite directions by $\pm \delta$.
Cruciform Wing--Two plane wings with the same planform normal to each other and symmetrically arranged about the line of intersection (see Figure 1(b)). This is a special case of a multi-fin wing with N = 4.
Cruciform Aileron--Cruciform wing with the horizontal or vertical or both pairs of fins deflected as ailerons. This is a special case of a multi-fin aileron with N = 4.
Mixed Cruciform Aileron--Cruciform aileron with wide-delta vertical fins and narrow-delta horizontal fins.
Multi-Fin Wing--A wing composed of two or more plane wings all having the same planform and symmetrically disposed about the wing axis.
Multi-Fin Aileron--A multi-fin wing with one or more of the plane wings deflected as ailerons.

A = body diameter/wing span = $2r/b$

A_L = value of A above which the fins do not interact

AR = aspect ratio

b = span of wing extended through the body (see Figure 2)

$b^*/2$ = span of fin (see Figure 2)

c = chord of delta wing extended into the body (Figure 2)

c^* = chord of half-delta fin

c' = chord of elementary strip (Figures 27, 28, and 29)

C_L = lift coefficient based on the area of the delta wing extended into the body

C_l = rolling moment coefficient based on the area and span of the delta wing extended into the body

C_L^* = lift coefficient based on the area of two half-delta fins

C_l^* = rolling moment coefficient based on the area of two half-delta fins and on the span b

C_p = pressure coefficient

C_R = resultant force coefficient for banked wing

C_S = side force coefficient

$C_{L_\alpha} = C_L/\alpha = \left(\frac{\partial C_L}{\partial \alpha}\right)_{\alpha=0}$

$C_{l_p} = C_l \Big/ \frac{pb}{2U} = \left[\partial C_l \Big/ \partial\left(\frac{pb}{2U}\right)\right]_{p=0}$ = rolling moment coefficient for damping in roll

$C_{l_\delta} = C_l/\delta = \left(\frac{\partial C_l}{\partial \delta}\right)_{\delta=0}$ = rolling moment coefficient for aileron deflection

$(C_{l_\delta})_H$ = rolling moment coefficient for horizontal fins

$(C_{l_\delta})_V$ = rolling moment coefficient for vertical fins

$d = \frac{\tan \omega}{\tan \mu} = \frac{b}{2mc}$ (for subsonic leading edges)

dL = differential lift of elementary strip

dM = differential rolling moment about the axis of the elementary strip. Positive when counterclockwise facing upstream

e = distance downstream of wing trailing edge at which vortex sheet is essentially rolled up

$E(\sqrt{1-d^2})$ = complete elliptic integral of the second kind with modulus $\sqrt{1-d^2}$

$f = \frac{\tan \mu}{\tan \omega} = \frac{2mc}{b} = \frac{1}{d}$ (for supersonic leading edges)

K = constant of proportionality depending upon concentration of vorticity at trailing edge (see Equation (4.61))

$K(\sqrt{1-d^2})$ = complete elliptic integral of the first kind with modulus $\sqrt{1-d^2}$

$l(x), l(y)$ = spanwise load distribution

L = lift

$m = \frac{1}{\sqrt{M^2-1}}$

M = free-stream Mach number

M_Γ = moment of vorticity distribution at trailing edge about wing-body juncture

$M(k)$ = defined on page 118

N = number of fins

p = angular rolling velocity

P = pressure

P_∞ = free-stream pressure

$q = \frac{1}{2}\rho U^2$ = free-stream dynamic pressure

$Q(k')$ = defined on page 118

r = body radius

$r^* = r/mc^*$

R = resultant force normal to plane wing

RM^* = rolling moment of fin about the wing-body juncture

S = side force

U = free-stream velocity

u, v, w = perturbation velocities in x, y, and z directions respectively

x, y, z = coordinates (see Figures 1 and 2)

$\bar{x}, \bar{y}$ = x/mc, y/mc

x^* = x/mc*

$x_{c.v.}$ = distance to centroid of vorticity distribution (initial position of rolled-up vortex)

x_1, z_1 = coordinates for elementary strip (Figures 27 and 28)

α = angle of attack. Positive when wing noses up

α_a = apparent angle of attack

α_u = upwash flow angle due to body upwash (see Figure 5)

α_v = upwash flow angle at the tail due to the vortices from the wing (see Figure 5)

α_B = angle of attack of the body

β = $\sqrt{M^2-1} = \frac{1}{m}$

γ = vorticity at trailing edge of wing

Γ = circulation at trailing edge of wing (strength of rolled-up vortex)

δ = deflection angle for aileron deflection or incidence angle for lift

θ = angle of bank

μ = Mach angle

ξ, η, ζ = running coordinates for integrations (see Figure 1)

ξ^* = $\frac{\xi}{mc^*}$

ξ' = $\frac{\xi}{mc'}$

ξ_1, ζ_1 = running coordinates for elementary strip (Figures 27 and 28)

ρ = free-stream density

φ = perturbation velocity potential

ω = half vertex angle of delta planform

I. INTRODUCTION

1.1 Meaning and Importance of Interference

The phenomenon of aerodynamic interference is very important in the design of airplanes and missiles. The word "interference" in this context denotes the interaction between two or more components which may or may not be directly connected but which somehow influence each other while passing through the air. The components are generally chosen so that by themselves they are relatively simple geometric configurations (e.g. a wing or a fuselage) for which aerodynamic characteristics may be calculated without too great mathematical difficulties. Any particular aerodynamic characteristic of these components when each is taken alone will usually be changed when the components interact. Hence, a simple combination of the aerodynamic characteristics of the components alone will generally not yield the correct overall characteristics of the single configuration composed of the interacting components. This difference between the characteristics of the components alone and in combination is generally defined as being caused by interference effects. The magnitudes of the interference effects depend upon the particular interference under consideration, the aerodynamic characteristic being studied, the geometry of the components, and the relative positions of the components.

The supersonic missiles are a particular example where interference effects often are so large that a simple combination of the aerodynamic characteristics of the components alone gives quite erroneous results. In general, a good knowledge of interference effects is necessary before practical engineering calculations of the performance and stability characteristics of an airplane or a missile can be carried out. The lack of such knowledge requires extensive time- and money-consuming experimental testing. Any contributions to the understanding of interference effects, both qualitatively and quantitatively, can be expected to reduce the amount of experimental testing which is necessary to design an airplane or a missile.

1.2 The Subsonic Airplane

Before restricting the subject matter to supersonic problems, it is convenient, for purposes of illustration, to review very briefly the interference problems for the familiar low-subsonic-speed airplane.

The basic airplane is composed of a high-aspect-ratio wing whose span is much greater than the diameter of the body. This fact about the airplane geometry is important from the point of view of interference since it generally leads to small wing-body interference effects for many of the aerodynamic problems and thus makes it

possible to combine the results for the wing and for the body according to some simple rule. This standard wing-body geometry also simplifies greatly the wing-body-tail interference problem. The complete airplane has numerous other components such as nacelles, propellers, rudder, etc. whose interference effects must be studied.

A large number of interferences have been considered, e.g. wing-body, wing-body-tail, wing-nacelle, propeller slip stream-wing, and so on. References 1 and 2 discuss the various interferences mostly from a qualitative point of view. Reference 3 summarizes the more recent work done by the Germans during World War II. The difficulty of the subject is illustrated by the relatively small number of good theoretical papers. See, for example, the extensive bibliography of recent German experimental and theoretical work in Reference 3. Theoretical results were usually obtained by making simplifying assumptions and studying idealized configurations (see, for example, Reference 4). The usual simplifying assumptions lead to the well known linearized theory for steady subsonic irrotational inviscid flow. Even with this simplification, the boundary value problems for the nonplanar three-dimensional configurations were so difficult that highly idealized configurations had to be studied. The linearized solutions for these ideal configurations were used as approximations to the linearized solutions for the actual configurations. The accuracies of these approximations were generally not known; however,

the solutions for the ideal configurations still proved useful as guides for design. It will be seen later that, for supersonic problems, the situation is different: although linearized methods are also used here, the boundary value problems are much easier. The nature of the hyperbolic equation which governs this flow is such that the actual configuration can be decomposed into a sum of idealized configurations by an exact superposition scheme.

By combining the available theoretical work with a large amount of experimental research and testing, the aerodynamicist has been able to develop a good understanding of interferences along with quantitative design rules to account for interference effects. The extent of the experimental work can be seen by the large number of reports issued by the NACA alone. The main reason that such design rules could be developed without an inordinate amount of testing was the fact that the basic configurations of all low-speed airplanes were similar.

1.3 Supersonic Aircraft Configurations

With the advent of supersonic flight speeds, the basic aircraft configurations were considerably changed. These changes are particularly noticeable in the supersonic missile but are less pronounced in the supersonic airplane.

One important combination of changes was the use of wings and tails of low aspect ratio in conjunction with body diameters which were not small compared with the wing and tail spans. The ratio of

the body diameter to the wing span is a geometric parameter which could be ignored for the subsonic airplane since this parameter was generally quite small. However, for the supersonic missile, the body diameter may be of the order of the wing span and the variation of interference effects with this parameter must be considered. It should be obvious that, with these changes, proportionately larger portions of the wing and tail will be affected by the body. Then it would be expected that the wing-body interference effects might be considerably increased. Other not-so-obvious considerations show that the wing-body-tail interference effects may be and generally are completely changed.

The difficulties with the theoretical problems for subsonic flight speeds which were mentioned previously are greatly magnified because of these changes in geometry. Consequently the theoretical work on interference effects is practically nonexistent for such low-aspect-ratio wing-body-tail configurations at subsonic speeds. The experimental work is probably all classified and generally not available.

For supersonic speeds the theoretical outlook is quite promising. It is frequently true that the solution of an aerodynamic problem is much easier for supersonic speeds than for subsonic speeds. It is still true that the low-aspect-ratio problems are more difficult than the high-aspect-ratio problems but even the low-aspect-ratio problems can be attacked theoretically with some success. A fair amount of theoretical work can be found in the literature. Although there has been much experimental work, it is practically all classified and must be considered as unavailable for the purposes of this thesis.

Another important change was the introduction of multi-fin wings and tails. This change refers primarily to supersonic missiles. The multi-fin wings and tails which are most widely used are of the cruciform type. However, multi-fin wings composed of more than two plane wings are being contemplated. With this change from planar to nonplanar wings, it is convenient to introduce another type of interference which will be called fin-fin interference. In general, fin-fin interference refers to the interaction between the fins of a multi-fin wing-body configuration which are not in the same plane. It should be quite apparent that this fundamental change in the geometry of the lifting surfaces must lead to new interference effects. There is relatively little theoretical work available on cruciform interference problems and even less on multi-fin problems. The experimental results are again mostly classified and unavailable.

In the relatively new field of supersonic interference research, the theoretical studies have generally been restricted to simplified configurations. The configurations were usually composed of a slender pointed body with circular cross section combined with a plane or cruciform wing which had either a high or a low aspect ratio. The low-aspect-ratio wings generally had delta planforms and the high-aspect-ratio wings had either delta or rectangular planforms. Some studies have included other planforms.

Three basic types of interferences have been studied. The first and most popular type is wing-body interference. In connection

with the study of lift problems, it was necessary to decompose the problem further into wing-body interference problems with and without afterbody. The afterbody is that part of the body which is downstream of the wing trailing edge. Fin-fin interference is the second type which has been studied. The theoretical work has, until recently, been restricted to cruciform configurations. The third and most difficult type studied is wing-body-tail interference. Most of these studies considered plane wing-body-tail configurations and restricted themselves to the lift problem.

All of the above types of interference will enter into the calculation of any particular aerodynamic characteristic for a missile if the missile has a multi-fin wing or tail or both. Of course, if both the wing and the tail are plane, fin-fin interference does not occur. Five different aerodynamic problems have been considered in the literature. Some have been studied extensively and others have hardly more than been discussed qualitatively. Furthermore, for some of the problems results have been obtained for all of the interferences mentioned above while, for others, even the simplest type of interference is difficult to discuss.

The aerodynamic problems which have been considered are lift, roll due to aileron deflection, damping in roll, roll due to combined pitch and yaw, and wave drag. Most of the effort has been

expended on the lift problem. Although the literature on the lift problem contains mainly wing-body interference studies, this is the only aerodynamic problem for which any wing-body-tail interference effects have been investigated to the point where practical engineering calculations can be made. Little work has been done on fin-fin interference lift problems. The problems of roll due to aileron deflection and damping in roll can be lumped together as far as the types of interference effects which have been studied and the extent of these studies. Most of the work has been on wing-body and fin-fin interference. The problem of roll due to combined pitch and yaw is exceedingly difficult and this shows up in the literature in that practically all references to this problem are of a qualitative nature. This situation is rather unfortunate because this problem is very important in supersonic missile stability. The wave drag problem is the least important. The total drag is composed of the wave drag plus the viscous shear and separation drags. The changes in wave drag due to interference effects will generally be small compared with the total drag. The drag problem is important primarily for performance calculations such as, for example, the computation of missile trajectories. Reasonable estimates of the wave drag can be made and errors can be allowed for by simply supplying the airplane or missile with enough power. This problem

will not be mentioned further except to remark here that practically no theoretical results have been obtained.

1.4 Survey of the Literature

At this point it is useful to make a brief but rather complete survey of the theoretical papers on interference effects in supersonic flow. It is expected that, besides being a guide to the literature on interference, such a survey will also act as a guide to those parts of the subject which require the greatest future theoretical work. Those papers which appear to be of immediate use for engineering calculations will be pointed out. Many of these papers will be elaborated upon later wherever they fit the purposes of the present study.

The survey will first cover the papers which have attempted to obtain detailed linearized solutions for the velocity and pressure distributions on wing-body configurations. Such studies will obviously not depend on aspect ratio as long as the aspect ratio is high enough so that the wing tip does not intersect the region of interest about the wing-body juncture. The remaining papers will be divided into high- and low-aspect-ratio problems. This division is not absolute and many papers will fall into both categories. Under each of these categories, the survey will be further divided into lift and roll problems.

In all of the papers where wing-body or fin-fin interference were studied, linearized irrotational inviscid stationary supersonic flow theory or slender body theory was used. In the studies of wing-body-tail interference, the nonlinear effects downstream of the wings cannot be neglected. These effects were approximated by various methods which will be elaborated upon in a later section of this thesis.

Consider first the papers on linearized velocity and pressure distributions on wing-body configurations. These papers are all concerned with the lift problem. Ferrari's first paper (Reference 5) was the first attempt to obtain the detailed pressure distribution for a wing-body problem. Unfortunately, some of the methods and results are incorrect. In a later paper (Reference 6), Ferrari attempts to modify and correct his results and compares them with some experimental data. In both of these papers the configuration consisted of a slender pointed body with circular cross section and a rectangular wing far back on the body in a region where the body diameter is practically constant. A third paper by Ferrari (Reference 7) considers the application of the method of characteristics to the wing-body interference problem, but no calculations are made. Morikawa (Reference 8) studies the problem in a different and more general way and presents

some approximate pressure distributions. In Reference 9 Morikawa compares the experimental data from Reference 6 with his theoretical results from Reference 8. Browne, Friedman, and Hodes (Reference 10) have obtained results for a conical wing-body configuration. They present pressure distributions for both subsonic and supersonic leading edges. Lagerstrom and Van Dyke (Reference 11) discuss some approximate source-sink methods for obtaining pressure distributions.

Now consider the literature on high-aspect-ratio lift problems. Browne, Friedman, and Hodes (Reference 10) also obtained some integrated lift results for the conical wing-body configuration. Since the wing is triangular, their results apply to either the high- or low-aspect-ratio problems. Lagerstrom and Van Dyke (Reference 11) consider the problem from the overall viewpoint of understanding the integrated lift effects. They present some useful engineering estimates for wing-body configurations with no afterbody. In Reference 12 Morikawa presents some useful wing-body engineering results. He presents integrated lift results for three types of wing-body configurations. In all cases the body is a circular cylinder extending infinitely far upstream but cut off at the wing trailing edges (no afterbody). He presents results for the delta, the clipped-delta, and the rectangular wings covering the complete range from zero to infinite aspect ratio.

Furthermore, he separates the lift carried on the wing and on the body. Morikawa and Coleman (Reference 13) present some results for center of pressure for the clipped-delta wing-body configuration. Kirby and Robinson (Reference 14) have made some computations for a rectangular wing on a conical body. Lagerstrom and M. E. Graham (References 15 and 16) are generally concerned with low-aspect-ratio problems, however their ideas on afterbody lift also apply to the high-aspect-ratio problem. Spreiter and Sacks (Reference 17) study the rolling up of the trailing vortex sheets for the wing-body-tail interference problem.

All of the papers on high-aspect-ratio roll problems assume a circular cylindrical body at zero angle of attack. All but one of the papers give results for delta wings. These results will then apply to both the high- and low-aspect-ratio cases. In Reference 18 this writer studied fin-fin interference for roll due to aileron deflection (cruciform wide-delta aileron with no body). Some calculations were made for the crossflow field behind the cruciform aileron assuming no deflection or distortion of the vortex sheets. In a second paper (Reference 19), this writer extended the fin-fin interference studies to damping in roll for the cruciform wide-delta wing and to the cruciform narrow-delta aileron and obtained estimates of wing-body and fin-fin interference for plane and cruciform delta wings for roll due to aileron deflection and damping

in roll. Further computations on wing-body-tail interference were presented. Reference 19 was essentially a summary of methods and results which will be found included and extended in some detail in the present study. Tucker and Piland (Reference 20) have estimated the wing-body interference for plane wide-delta wing-body combinations. Bolz and Nicolaides (Reference 21) study a cruciform wing-body combination which has high-aspect-ratio rectangular wings. They estimate the effects of wing-body interference for roll due to aileron deflection, damping in roll, and equilibrium rate of roll and they present some comparisons with experiments. E. W. Graham (Reference 22) has studied a very interesting limiting case for missile rolling moments. He considers a configuration composed of an infinite number of plane delta wings symmetrically arranged about an axis in the free-stream direction. Another paper by E. W. Graham (Reference 23) extends his results to more cases. In these two papers he presents results for roll due to aileron deflection, damping in roll, and equilibrium rate of roll for the wing alone and also presents results for roll due to aileron deflection and damping in roll for the wing combined with a body. He gets results for both supersonic and subsonic leading edges.

The literature on low-aspect-ratio lift problems includes many of the papers previously listed under high-aspect-ratio

lift problems. The results of Reference 10 apply here since the wing has a delta planform. Certain considerations on wing-body interference in Reference 11 where delta wings were studied will also apply here. Morikawa's paper (Reference 12) on wing-body lift with no afterbody was discussed previously. Laitone (Reference 24) has discussed some wing-body interference effects for a rectangular wing-body combination using, among other things, apparent mass considerations. The remaining papers in this category on wing-body and fin-fin interferences utilize slender body methods which, when properly understood and interpreted, act as useful limiting cases. It is to be particularly noted that Lagerstrom and M. E. Graham (References 15 and 16) have used slender body theory to estimate afterbody lift. Spreiter (Reference 25) published the first paper on slender body methods applied to wing-body interference problems. Ward (Reference 26), in a general study of slender body methods, obtained Spreiter's results independently. In another paper, Spreiter (Reference 27) extends his slender body methods to cruciform wing-body configurations. Three papers on wing-body-tail interference complete this section. Martha Graham (Reference 28) studied the simplified problem of wing-tail interference using two alternate extreme assumptions about the vortex sheet behind the wing. The configuration consisted of two narrow-delta wings

connected by a rigid line. The two alternate assumptions about the vortex sheet were, first, that the sheet was deflected but undistorted or, second, that the sheet was completely rolled up and could be represented by two deflected vortices. This study intended to consider the low-aspect-ratio problem and was made before it was known which of these assumptions was the more realistic. However, since delta wings were used, the study also applies to the high-aspect-ratio problem. It is now known that, for a low-aspect-ratio wing, the assumption of rolled up vortices is generally more realistic, however, if the aspect ratio of the wing is high enough, the undistorted vortex sheet might be the more realistic picture. Spreiter and Sacks' paper on the rolling up of the trailing vortex sheet (Reference 17) shows that the vortex sheet will generally be rolled up within a short distance downstream of the wing if the wing has a low aspect ratio. They studied the motion of the vortex sheet behind the wing and the size of the vortex core when the sheet was rolled up and they present photographs of the rolling-up process which were taken in simple water tank experiments. Lagerstrom and M. E. Graham (Reference 15) reached the same conclusion about the rolling up of the vortex sheet behind low-aspect-ratio wings from some rather simple studies of the motion of two-dimensional vortices. They have carried out in great detail a study of the motion of two vortices in the presence of a circular body.

The literature on low-aspect-ratio roll problems will include all but one of the papers listed previously in the section on high-aspect-ratio roll problems (i.e. References 18, 19, 20, 22, and 23). The remaining papers on wing-body and fin-fin interference have used slender body methods. Spreiter (Reference 27) has presented some results for roll due to combined pitch and yaw. Heaslet and Lomax (Reference 29) have obtained the solution for the damping in roll of a plane delta wing-body combination. In a recent paper, Adams (Reference 30) obtained the solutions for the cruciform delta aileron and for the damping in roll of a cruciform delta wing. E. W. Graham (Reference 31) obtained the solution for the damping in roll of a cruciform delta wing independently. The few results of References 18 and 19 and some discussion by Lagerstrom and M. E. Graham (Reference 15) of the application of their methods to the roll problems represent virtually all the work that has been done on wing-body-tail interference effects for the roll problems.

1.5 Purpose of the Present Study

At the present time there is a great need for practical answers to the interference effects in a variety of aerodynamic problems. This need is particularly severe for supersonic missiles where added roll problems are encountered which previously were of little importance or were not even present. The complete

solutions to these problems are beyond present-day mathematics. The best that can be hoped for at present are linearized solutions for fin-fin and wing-body interference problems. Where exact linearized solutions are not possible, approximations to or estimates of the exact solutions can be useful. For wing-body-tail interference problems, linearized theory cannot be used for the motion of the vortex sheets downstream of the wing and other assumptions are made to approximate the nonlinear effects. The usefulness of the quantitative results obtained by these methods can only be evaluated by experiment. However, past experience has shown that such results can be useful qualitatively for the understanding of the phenomena and very often the results are quantitatively useful for engineering calculations.

With this in mind, the basic purpose of this thesis is to obtain and present methods and results which may be useful for engineering calculations. In general, the aim is to study integrated quantities such as lifts and moments. The emphasis will always be on the possible applicability of the methods and results to engineering calculations. Methods of solution which require long and tedious calculations will be avoided, for it is felt that, in view of the assumptions already made and the basic purpose of this thesis, such methods are unwarranted.

In more detail, the purpose of the present study is five-fold.

First, to summarize and present in their proper perspective in a unified study the theoretical work to date which fits into the scheme of the present study. Second, to present new theoretical results which have been obtained by the writer for some of the interference problems. Third, to discuss the effects of the various parameters and their importance. Fourth, to discuss qualitatively, where possible, the effects of parameters and phenomena which have been neglected--that is, gap, high angle of attack, nonlinear, viscous, and nonstationary effects. Fifth and last, to make some recommendations for future theoretical and experimental research.

1.6 Outline of the Present Study

The subject matter contained in the present study will now be outlined very briefly.

The basic configuration studied has a slender pointed body with circular cross section with a wing far back on the body in a region where the body is nearly cylindrical. It is assumed that the body is a circular cylinder from the wing to the tail. Both high- and low-aspect-ratio wings are considered, but the major emphasis is on the more difficult low-aspect-ratio case. Most of the low-aspect-ratio wing studies are for wings with delta planforms. The high-aspect-ratio wing studies generally treat wings with either delta or rectangular planforms. Both plane and cruciform configurations are studied with about equal emphasis and some results

are presented for multi-fin wings composed of more than two plane wings.

Three aerodynamic problems are studied. They are (1) lift and incidence, (2) roll due to aileron deflection, and (3) damping in roll. Fin-fin, wing-body, and wing-body-tail interference effects are studied for each of these aerodynamic problems.

In general, for all calculations which do not involve the trailing vortex sheets downstream of the wings, linearized or slender body theory or both are used. These calculations include lifts carried by the body and by the wings, rolling moments about the body axis for aileron deflection and damping in roll, and vorticity distributions at the trailing edges of the wings. Linearized theory cannot be used for the motion of the vortex sheets downstream of the wings. Although no new calculations are made for the motion of the vortex sheets, the assumptions for and the methods of carrying out such calculations are considered, particularly for the roll problems.

II. CONFIGURATIONS

2.1 Types of Configurations Considered

The types of wing-body configurations which have been investigated by the writer are described in this section.

The major emphasis throughout this thesis will be placed on the low-aspect-ratio delta wing supersonic missile-type configuration. Figure 3 shows a typical configuration with a cruciform wing. All configurations are assumed to have a slender pointed body with circular cross section. Three wing planforms are studied. They are (1) the low-aspect-ratio delta wing, (2) the high-aspect-ratio delta wing, and (3) the high-aspect-ratio rectangular wing planforms. Unless otherwise specified, the term "high aspect ratio" will always refer to configurations where the body diameter is much less than the span of the high-aspect-ratio wing. This is illustrated in Figures 4(a) and 4(b) as opposed to the cases illustrated in Figures 4(c) and 4(d) where the body diameter is not small compared with the wing span. In general, both plane and cruciform wings are studied. Furthermore, for the case of no body, multi-fin delta wings composed of more than two plane wings are also considered. It will be assumed that the wing is located far back on the body where the body is nearly cylindrical. From the wing to the tail section, the body is assumed to be a circular cylinder. The tail configuration will remain

unspecified since no explicit calculations are made for it.

2.2 Linearized Superposition

Except for the motion of the vortex sheets downstream of the wing, linear theories will be used. The motion of the vortex sheets downstream of the wing is a highly nonlinear problem whose nonlinear character must be retained if any useful results for wing-body-tail interference are to be obtained. However, for fin-fin and wing-body interference problems, linear theories can be expected to yield useful results.

The use of linear theory permits solutions to be superimposed. Hence the general problem can be simplified by decomposing it into the sum of simpler problems. Figure 9.1 of Reference 11 illustrates a superposition scheme for the wing-body interference lift problem. Figure VII-2 of Reference 15 illustrates the basic superposition scheme for the wing-body-tail interference lift problem. These superposition schemes may be generalized in an obvious way to include the roll problems and multi-fin configurations.

Figure 5 illustrates the superposition scheme for all the aerodynamic problems studied in this thesis. The complete configuration in Figure 5(a) is to be considered as representative of the more general configurations studied. The most general configuration would be composed of the body with a multi-fin wing and tail whose individual fins may have different angles of attack but will always have the same

apparent twist and will always be uncambered.

Figure 5(a) shows how the wing-body-tail interference problems may be decomposed into the sum of several simpler problems. The complete configuration consists of the body with a plane wing and a plane tail. α_{w_1} and α_{w_2} denote the geometrical angles of attack of the two wing fins or, for damping in roll, they denote the geometrical angles of attack plus the apparent linear twists of the two fins (the usual assumption for the damping in roll problem). α_{T_1} and α_{T_2} have the same meanings for the tail fins. The decomposition into problems A' and B' illustrates the superposition scheme which is used to calculate wing-body-tail interference. α_u denotes the distribution of upwash flow angle due to body angle of attack and α_v denotes the distribution of upwash flow angle (positive and negative) due to the vortex system from the wing. B' is a wing-body interference problem with the wing (tail fins) twisted in some complicated manner given by the apparent angle of attack, α_a. Linear theories can be used for problem B' and hence it can be decomposed into the three simpler problems B, C, and D. It is important to point out that problem A' cannot be decomposed into simpler problems for calculating α_v. This is where part of the essential nonlinearity of the wing-body-tail interference problem is encountered. However, A' can be decomposed into simpler problems for the calculation of wing-body (and fin-fin) interference effects. This is il-

lustrated in Figure 5(b). First the problem is decomposed into E' and F and then E' is further decomposed into E and G. If the wing or tail is of the multi-fin type, the superposition scheme is identical except that α_u and α_v must be interpreted as angles measured in a plane normal to the plane of the fin whose apparent angle of attack distribution is desired.

From this discussion it is apparent that, for fin-fin and wing-body interference problems, the study of the general wing-body configuration can be reduced to the study of a wing-body configuration consisting of a circular cylindrical body at zero angle of attack which extends infinitely far upstream but which may or may not extend downstream beyond the trailing edges of the wing (the afterbody problem) and a wing whose fins may be twisted in some complicated manner.

2.3 Reasons for Choice and Expected Applicability

The choice of the geometry of the configurations which are studied was dictated by the simplification of the theoretical problems and, more practically, by the actual use of such geometry in some supersonic missiles.

From the theoretical point of view, the body with circular cross section is practically a necessity for all of the interference studies if any results are to be obtained. In fact, many of the results in this thesis are valid exactly only if the body cross section is circular.

The choice of the delta planform for the wings is not necessary but many of the theoretical problems are considerably simpler, particularly for low-aspect-ratio wings. Furthermore, for many of the problems, a single calculation yields results for both high- and low-aspect-ratio wings. Although the delta planform can be expected to be useful for applications to supersonic missiles, it is not a likely planform shape for the high-aspect-ratio supersonic airplane. This is the reason that the rectangular wing is included in the study of high-aspect-ratio wing problems.

The cruciform wing is studied because of its wide use on supersonic missiles. The basic purpose of a cruciform wing is to be able to supply lift equally in any desired lateral direction by some combination of deflections of the fins. Although any wing composed of a finite number of nonplanar lifting surfaces has this property, calculations are simplest for the cruciform configuration.

III. BASIC THEORY AND ASSUMPTIONS

Some of the basic theory and assumptions which can be conveniently separated from the text are discussed in this section.

3.1 Linearized Theory

The basic assumptions of stationary linearized supersonic flow lead to the wave equation for the perturbation velocity potential, φ,

$$\varphi_{xx} + \varphi_{yy} - (M^2 - 1)\varphi_{zz} = 0 \tag{3.11}$$

where M is the Mach number of the free stream and the free stream velocity, U, is nominally in the positive z direction. Viscosity and heat transfer have been neglected and the flow is isentropic and irrotational. The perturbation velocity vector is given by

$$(u, v, w) = \text{grad } \varphi \tag{3.12}$$

where u, v, and w are the perturbation velocity components in the x, y, and z directions, respectively. The condition for irrotational flow may be expressed by

$$\text{curl } (u, v, w) = 0 \tag{3.13}$$

The pressure for a planar system is given by

$$p - p_\infty = -\rho U w = -\rho U \varphi_z \tag{3.14}$$

and the pressure coefficient is

$$C_p = \frac{P-P_\infty}{\frac{1}{2}\rho U^2} = -\frac{2w}{U} = -\frac{2\Phi_z}{U} \qquad (3.15)$$

It is important to note that Equations (3.14) and (3.15) apply only to the planar parts of a wing-body configuration, i.e. the fins. On the body, more perturbation velocity terms would have to be included in the expansion of the isentropic pressure relation or the exact pressure relation itself could be used.

The boundary conditions are the usual ones which are imposed when viscosity is neglected. The flow is assumed to be tangent to any solid surface at the surface and the flow is assumed to be uniform and undisturbed upstream of any disturbing bodies.

This basic theory is well known and will not be elaborated upon further. The application of this theory to the exact solution of wing-body problems is not well known. Although such exact solutions will not be attempted here, it is of interest to note where such attempts have been made. Most of the work which has been done on the exact solutions of wing-body problems will be found in References 5 through 11.

In the present study, linearized theory for planar systems is used to make estimates of or approximations to the exact linearized solutions of several fin-fin and wing-body interference problems. Certain fin-fin interference problems can be reduced exactly to

planar wing problems and, hence, these solutions will be exact. Since the nonplanar problems are approximated by planar problems, the pressure relations, Equations (3.14) and (3.15), may be used.

The linearized supersonic theory of planar wings is so well known that the pertinent results will be given here without further discussion. The general solution of Equation (3.11) for the perturbation velocity potential when the downwash on the wing is prescribed is given by (see, for example, Reference 32)

$$\varphi(x,y,z) = -\frac{1}{\pi}\iint \frac{\varphi_y(\xi,0,\zeta)\,d\xi\,d\zeta}{\sqrt{(z-\zeta)^2-(M^2-1)[(x-\xi)^2+y^2]}} \qquad (3.16)$$

For the lifting wing, this equation gives the potential at any point (x,y,z) above the wing (y positive). The potential below the wing is obtained from symmetry. ξ and ζ are running coordinates on the wing. The region of integration is that part of the wing which is contained within the upstream Mach cone from (x,y,z) if the leading edge is supersonic. If the upstream Mach cone from (x,y,z) encounters a subsonic leading edge, the region of integration must be modified according to Evvard (Reference 33). The line of intersection of the upstream Mach cone and the wing is a parabola which degenerates into two straight lines when the potential on the top side of the wing is desired, i.e. for y = 0+.

Linearized theory is not used to study the motion of the vortex sheets downstream of the wings. As mentioned previously,

the nonlinear character of this motion must be retained. However, linearized theory is used to solve other parts of the wing-body-tail interference problem such as the vorticity at the wing trailing edges and the forces induced on the tail by the vortex system from the wing.

3.2 Slender Body Theory

There have been many applications of slender body theory to wing, body, and wing-body problems. Applications to fin-fin and wing-body interference problems will be found in References 15, 16, 25, 26, 27, 29, and 30. The theory and its application are well known and will not be reproduced here. However, it is desirable to have a clear physical picture of what the slender body assumptions imply in order that the extent to which slender body theory can be used for approximating wing-body problems be understood. Excellent discussions from this point of view will be found in References 15 and 16. Although the following discussion is somewhat different from that of References 15 and 16, all of the essential ideas are from these papers. The discussion will be brief and the proofs of most of the statements will be found in the two papers mentioned above or any others mentioned in the discussion.

The basic idea behind slender body theory is that under certain conditions the term $(M^2-1)\varphi_{zz}$ in Equation (3.11) will be negligible compared with the other terms. Then Equation (3.11) reduces to the

much simpler equation

$$\varphi_{xx} + \varphi_{yy} = 0 \tag{3.21}$$

Now the problem has been reduced to solving a two-dimensional incompressible flow problem in the x-y plane. Powerful general methods are available for solving such problems.

The term $(M^2-1)\varphi_{zz}$ can be made small by making either (M^2-1) or φ_{zz} or both small. If the Mach number is unity, the factor (M^2-1) is identically zero and Equation (3.21) is obtained exactly. Then any configuration is a slender body at M = 1. But this is obvious since, for M = 1, the Mach waves are normal to the free stream direction and every point will influence every other point in any section of the configuration taken normal to the free stream direction. This is just what Equation (3.21) expresses. Since slender body theory is exact for M = 1, velocities and pressures computed this way will be correct. For Mach numbers greater than one, the Mach waves are no longer normal to the free stream direction and any point influences only those regions which lie within its downstream Mach cone. This is the typical delayed action in supersonic flow. Now velocities and pressures computed by slender body theory will not be correct. The error in the velocity and pressure distributions will obviously increase with increasing Mach number.

Now consider the factor $\varphi_{\xi\xi} = w_{\xi}$. This is essentially the pressure gradient in the streamwise direction. It is known that, for a low-aspect-ratio wing or wing-body configuration, the pressure equalization around the subsonic edges will cause the pressure perturbation to approach zero in the streamwise direction (see also Reference 34). At the same time, the streamwise gradient of the pressure will also approach zero. The rapidity with which this gradient approaches zero will depend on the rapidity of pressure equalization which in turn depends upon the number of times the Mach wave from a point of disturbance has been reflected from a subsonic edge. In the final analysis, the rate of pressure equalization depends upon the Mach number and the geometry of the configuration. To illustrate, consider Figure 6

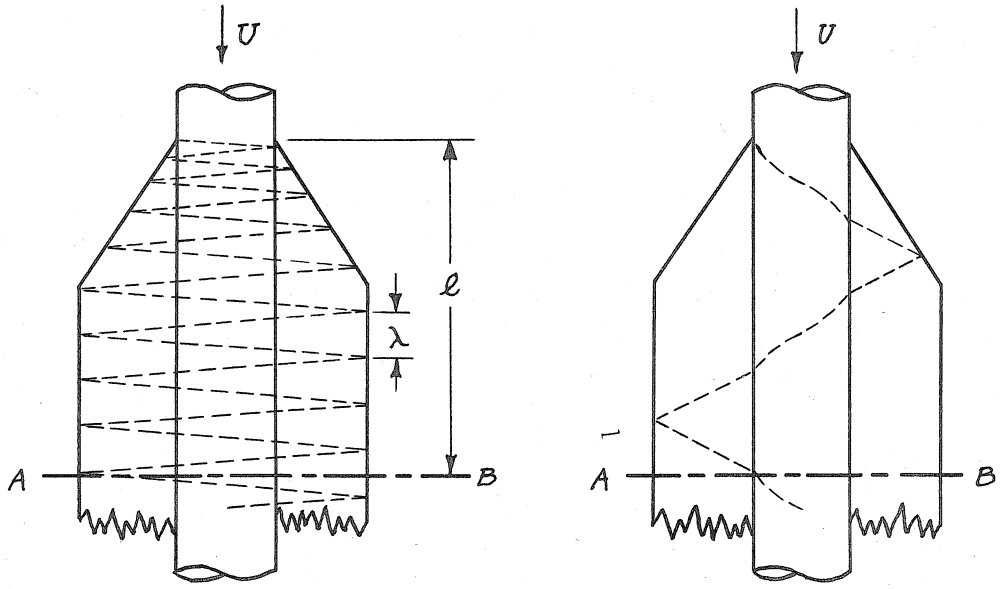

(a) M slightly greater than one.

(b) M definitely greater than one.

Figure 6

The delta wing is continued downstream with sides parallel to the free-stream direction. In Figure 6(a) the Mach number is slightly greater than one and a disturbance wave starting at the wing leading edge-body juncture reflects several times at subsonic or side edges before reaching section AB. If the Mach number is definitely greater than one as in Figure 6(b), fewer reflections occur before section AB is reached. Note that if M = 1 the wave system contracts to a single line normal to the free stream direction and, in a sense, an infinite number of reflections have occurred by the time section AB is reached.

By taking section AB far enough downstream, $\varphi_{\bar{z}\bar{z}}$ can then be made small enough so that $(M^2-1)\varphi_{\bar{z}\bar{z}}$ can be neglected. Then the solution of Equation (3.21) at this section will give nearly the correct solution. But the potential, φ, at section AB is directly proportional to the spanwise lift distribution of the part of the configuration upstream of AB. Hence, if AB is the trailing edge of the wing-body combination, slender body theory will give nearly the correct spanwise lift distribution and, thus, lift, rolling moment, and lateral center of pressure. It should be pointed out, however, that this is not true for the pitching moment and chordwise center of pressure. The exact slender body result is obtained if the aspect ratio of the configuration is zero, that is if section AB is infinitely far downstream. In a sense, slender body theory

anticipates the complete wave system.

The factors (M^2-1) and φ_{zz} are seen to be interrelated through the configuration geometry. This interrelation can be expressed as follows: If the maximum wave length of the wave system, λ, is small compared with the length of the configuration, ℓ, [see Figure 6(a)] slender body theory will approximate well to the lift and rolling moment of the configuration.

The aspect ratio of a wing or a wing-body configuration which has a finite length can be made to approach zero by simply letting the lateral dimensions approach zero. Slender body theory will then give the correct result for the limiting case of zero aspect ratio. For a delta wing, plane or multi-fin, this limit is approached as the apex angle approaches zero.

Slender body theory is used in interference problems in two ways. First, to give the exact limiting values for certain integrated aerodynamic quantities when the lateral dimensions of the configuration approach zero and, second, to estimate the lift of a wing-body configuration with an afterbody.

3.3 Vortex Sheets Downstream of the Wing

As mentioned previously, nonlinearity must be retained in this problem. The assumptions and approximations used in computing the motion of the vortex sheets are fully explained in a

later section. Briefly, for low-aspect-ratio wings, the vortex sheets are replaced by vortices which start at the centroids of the vorticity distributions at the trailing edges of the wing. Incompressible two-dimensional flow theory is then used to calculate the motion of these vortices as they pass downstream to the tail position.

3.4 Gap Effects

In all cases where fins are deflected so that gaps are produced the effects of the gap are neglected.

IV. THEORETICAL RESULTS

Some of the results for the roll problems were previously published by the writer in Reference 19 in a very condensed form. Since then, new results have been obtained and a relatively minor error has been discovered in one of the computed curves in Reference 19. Most of the methods and results in Reference 19 together with the new results are presented here in detail. Results from other papers will also be included here whenever they fit into the scheme of this study. In general, only the important results from these papers will be included with a minimum of details.

4.1 Interference Definitions

There is no standard definition of interference. Until recent years the interference studies were confined to the lift problem for wing-body-tail configurations with high-aspect-ratio wings and tails. It was natural, then, for interference to be defined as the difference between the sum of the lifts of the components taken separately and the lift of the combination. The use of low-aspect-ratio missile configurations has made it necessary to include roll problems in interference studies and to introduce fin-fin interference when multi-fin wings or tails are used. Interference, as defined above, is not quite as natural for the low-aspect-ratio problems. However, this definition will be used where possible for

the three types of interferences considered here.

It will be assumed that a multi-fin wing is always composed of an even number of fins symmetrically located about the body axis. In other words, a multi-fin wing will always be composed of two or more plane wings. This is assumed so that the plane delta wing is the basic plane configuration. If the multi-fin wing with an odd number of fins were included, it would be logically necessary to consider the half delta wing as the basic configuration.

The word "wing" will be used in its general sense and may refer to the lift, aileron deflection, or damping in roll problems, i.e. the "wing" may be lifting, may be deflected as an aileron, or may have an apparent linear twist. Whenever the terms "multi-fin wing", "plane wing", and "plane wing-body combination" are used in connection with a general multi-fin wing-body configuration, they will have special meanings. Consider a general multi-fin wing-body configuration. The basic wing formed when the body diameter shrinks to zero is called the "multi-fin wing". The term "plane wing" refers to any of the plane wings which compose the "multi-fin wing". A "plane wing-body combination" is formed by combining a "plane wing" with the body of the general configuration.

When the components of a multi-fin wing-body combination are considered separately, they are assumed to have the same angles of attack, angles of bank, aileron deflection, and twist

which they have in the combination. It should be noted that the body alone never develops any lift or rolling moment. This is apparent from the superposition scheme shown in Figure 5 where the wing-body problems are always decomposed so that the body is at zero angle of attack.

Using these definitions and explanations, the various interferences are defined for any particular aerodynamic characteristic as follows:

Fin-fin interference--Consider a multi-fin wing-body combination. Fin-fin interference is defined as the difference between the sum of the forces or moments on the plane wing-body combinations taken separately and the force or moment on the complete configuration. This definition is illustrated schematically in Figure 7.

Wing-body interference--Consider a multi-fin wing-body combination. Consider the sum of the forces or moments on the plane wings and body when all are taken separately. Then consider the sum of the forces or moments on the plane wing-body combinations all taken separately. The difference between these total forces or moments is defined as wing-body interference. Note that this definition has been specifically constructed to exclude any fin-fin interference effects. This definition is illustrated schematically in Figure 8.

Wing-body-tail interference--Consider a general wing-body-tail configuration which may have any kind of multi-fin wing and tail. Wing-body-tail interference is defined as the difference between the sum of the forces or moments on the wing-body and tail-body combinations taken separately and the force or moment on the combined configuration. This difference will be caused by the vortex system from the wing which induces forces or moments on the tail. Although no quantitative calculations are carried out, this definition is used in the discussion of methods and procedures for carrying out such calculations.

If the differences which are referred to in these definitions are to represent interferences, they must always be described relative to the case of no interference. In future discussions of results, these differences will usually be described by percentage changes based on the case of no interference.

4.2 Fin-Fin Interference--Low Aspect Ratio

Configurations which give rise only to fin-fin interferences are studied in this section. These configurations will obviously be wings. These results will be useful for the wing-body problems of section 4.4 as endpoints (when the body diameter is zero, i.e. $A = 0$) in the estimating procedures.

Only delta wings are studied here. Then the results will apply as well to high-aspect-ratio wings. However, fin-fin inter-

ference and roll due to aileron deflection problems are not likely to occur in the high-aspect-ratio problems, hence it is desirable to make this division of subject matter into low- and high-aspect-ratio problems.

A. Lift

Plane wide-delta wing--Consider an unyawed flat plane wide-delta wing in the horizontal (x-z) plane which is at an angle of attack α (measured in a plane normal to the plane of the wing). The lift coefficient based on the wing area is well known and is given by

$$C_L = 4m\alpha \quad \text{or} \quad \beta C_{L_\alpha} = 4 \tag{4.21}$$

If the wing is banked about its axis of symmetry (z-axis) through the bank angle θ, the resultant force, R, on the wing will always be normal to the wing and the effective angle of attack in the plane normal to the plane of the wing will be $\alpha \cos\theta$. The resultant force coefficient will be

$$C_R = 4m\alpha \cos\theta \tag{4.22}$$

Decomposing this into lift and side force coefficients for the banked wing gives

$$C_L = 4m\alpha \cos^2\theta \tag{4.23}$$

and

$$C_S = 4m\alpha \cos\theta \sin\theta \tag{4.24}$$

These relations are very simply obtained and should be apparent from the schematic illustration of the banked wing shown in Figure 9. When the wing is banked 90 degrees all the forces are zero. This is, of course, apparent physically without the above equations.

Cruciform wide-delta wing--Consider an unyawed and unbanked cruciform wide-delta wing. No forces will be developed on the vertical fins and, from symmetry, the horizontal fins act like a plane wide-delta wing. The lift coefficient is then given by Equation (4.21).

Now let the wing be banked about its axis of symmetry (z-axis). This situation is equivalent to pitching and yawing the wing through small angles. No side forces are developed and the resultant lift force is the same as when the wing is unbanked. Letting L be the lift of the unbanked wing, this result can be shown readily by the vector diagrams in Figure 10. Then the lift of the cruciform wing is independent of bank angle and its lift coefficient is always given by Equation (4.21). It should be noted that this is only true for cruciform wings whose horizontal and vertical fins have identical planforms as is always the case in this thesis.

According to the definition, the fin-fin interference for the banked cruciform wing is given by the difference between the

sum of the forces on the two plane wings taken separately and the force on the cruciform wing. This difference is zero and, hence, there is no fin-fin interference for the cruciform wing in lift. This fact should be obvious from Figure 10 where it is noted that only the result for the plane wing was needed in order to obtain the result for the cruciform wing. This result is peculiar to any cruciform wing because of its 90 degree geometry. For other multi-fin wings the fin-fin interference will generally not be zero.

Plane narrow-delta wing--For a plane narrow-delta wing at an angle of attack α the results are well known (see Reference 35) and the lift coefficient is

$$C_L = \frac{2\pi m \alpha d}{E(1-d^2)} \tag{4.25}$$

The previous remarks about the effects of bank for the plane wide-delta wing obviously apply here as well.

Cruciform narrow-delta wing--From the previous discussion of the effects of bank on the lift of a cruciform wing, it is seen that the lift coefficient of a cruciform narrow-delta wing is given by Equation (4.25). The previous remarks on fin-fin interference are true here also.

B. Roll Due to Aileron Deflection

For high-aspect-ratio wings, sufficient rolling moments

can usually be generated by the familiar trailing-edge or possibly leading-edge ailerons. However, for low-aspect-ratio wings, different types of ailerons are generally necessary in order to generate satisfactory rolling moments because of the reduced wing area and moment arms.

One type of aileron which has been used and the one which is treated here is formed by deflecting the entire wing so that the two halves of the wing have equal but opposite angles of attack. Other types of ailerons which have been used are formed by deflecting relatively large portions of the wing. The largest interference effects will be obtained for the aileron formed by deflecting the entire wing. For other types of ailerons, the methods used in this thesis will generally apply and will yield closer estimates of or approximations to the exact linearized results because of the smaller interference effects.

For the general multi-fin wing, aileron deflection denotes the equal and opposite deflection of the two halves (fins) of one or more of the plane wings which compose it. If the solution is obtained for just one pair of fins deflected, the solution for any number of pairs of fins deflected can be obtained by superposition. Only the rolling moments are to be considered and, hence, the axis of symmetry of the multi-fin wing is oriented in the free-stream direction so that no net lateral forces arise. The wing

or wing-body combinations will be so oriented for all roll problems. The lateral forces (lift and side forces) can be included by superposition.

Plane wide-delta aileron--Consider an unyawed plane wide-delta aileron in the horizontal plane. This terminology is used interchangeably to denote a wide-delta wing with aileron deflection, i.e. with its two fins deflected equally in opposite directions. Looking upstream, the right fin is deflected by $+\delta$ and the left fin by $-\delta$ so that positive rolling moments (see Figure 1) are generated. This is illustrated in Figure 11. Also shown is the leading edge parameter, f, which enters the results for wings (and wing-body configurations) with supersonic leading edges.

The result for this aileron was obtained in Reference 18 (there the effects of yaw are included) and is

$$\beta C_{l_\delta} = \frac{2}{3} \tag{4.26}$$

Note that this result is independent of the leading edge sweepback (f) as was also the lift result (Equation (4.21)). There is a general theorem which shows that this is true for any angle of attack distribution (see Reference 11).

Cruciform wide-delta aileron--It is convenient to consider this aileron to be oriented so that one pair of fins is horizontal

and the other pair is vertical. In general, both pairs of fins might be deflected as ailerons with different deflection angles. The general case can always be obtained by an obvious superposition from the case where just one pair of fins is deflected. In the present work, when both pairs of fins are deflected they will have the same deflection angles and the configuration will be denoted by "4 fins deflected". The rolling moment is obtained by just doubling the result for "2 fins deflected".

Consider the cruciform aileron with the horizontal fins deflected by $\pm \delta$ and the vertical fins undeflected. This configuration is obtained if undeflected vertical fins with supersonic leading edges are added to the plane aileron discussed above. These vertical fins prevent the equalization of pressure which takes place across the top and bottom sides of the plane aileron and, hence, the horizontal fins of the cruciform aileron will carry more rolling moment than the plane aileron. However, the results show that this effect is more than counteracted by the counter-roll induced on the vertical fins.

That a counter-roll is induced on the vertical fins can be shown from simple physical considerations. Figure 12 illustrates the signs of the pressures on the various fins of the cruciform aileron at a cross section of the aileron. The right horizontal fin is deflected by $+\delta$ and hence will have suction

(indicated by minus signs) on the top side and overpressure (indicated by plus signs) on the bottom side. Suction and overpressure will be induced on the vertical fins within the Mach cone as shown in Figure 12. It is apparent that the vertical fins carry a rolling moment which opposes that of the horizontal fins.

The fact that all leading edges are supersonic means that there is no communication between the quadrants shown in Figure 12. Hence the flow fields in the quadrants are independent of each other and, in particular, the flow fields separated by the vertical fins are independent of each other. When the flow conditions to the right of the vertical fins are known, those to the left are immediately obtained by symmetry. In particular, the pressure is antisymmetric about the plane of the vertical fins.

The presence of the vertical fins requires that the sidewash be zero in the plane of these fins. Hence, by symmetry, the flow conditions to the right of the vertical fins are exactly those obtained from a wide-delta lifting wing whose angle of attack is everywhere $+\delta$. Then the solution of the cruciform wide-delta aileron problem can be reduced exactly to the solution of planar wing problems. The solution was obtained in Reference 18 using known conical wing results for the pressure distributions and integrating over the horizontal and vertical fins. These results are summarized here for completeness.

The rolling moment coefficient for the horizontal fins is given by

$$\beta\left(C_{l_\delta}\right)_H = \frac{4}{3\pi}\left(\frac{\cos^{-1}f}{\sqrt{1-f^2}} + f\right) \tag{4.27}$$

There are two limiting cases which greatly simplify the results: f = 0 (infinite aspect ratio ($\omega = 90^\circ$) or M = ∞ ($\mu = 0$)) and f = 1 (sonic leading edges). For f = 0, Equation (4.27) becomes

$$\beta\left(C_{l_\delta}\right)_H\Big|_{f=0} = \frac{2}{3} \tag{4.27a}$$

This is the result for the plane aileron. For f = 1, Equation (4.27) is indeterminate and, by usual methods, becomes

$$\beta\left(C_{l_\delta}\right)_H\Big|_{f=1} = \frac{8}{3\pi} \tag{4.27b}$$

The counter-roll induced on the vertical fins is given by

$$\beta\left(C_{l_\delta}\right)_V = -\frac{4f^2}{3\pi}\left[\frac{\cos^{-1}f - f\sqrt{1-f^2}}{(1-f^2)^{3/2}}\right] \tag{4.28}$$

$$\beta\left(C_{l_\delta}\right)_V\Big|_{f=0} = 0 \tag{4.28a}$$

$$\beta\left(C_{l_\delta}\right)_V\Big|_{f=1} = -\frac{8}{9\pi} \tag{4.28b}$$

Adding these results, the rolling moment coefficient for the complete cruciform aileron is

$$\beta C_{l_\delta} = \frac{4}{3\pi(1-f^2)}\left[\frac{(1-2f^2)\cos^{-1}f}{\sqrt{1-f^2}} + f\right] \tag{4.29}$$

$$\beta C_{l_\delta}\Big|_{f=0} = \frac{2}{3} \tag{4.29a}$$

$$\beta C_{l_\delta}\Big|_{f=1} = \frac{16}{9\pi} \tag{4.29b}$$

These results are shown in Figure 13. According to the definition, the fin-fin interference is given by the difference between the results for the plane aileron and the cruciform aileron for a given value of f. It is seen that fin-fin interference generally is detrimental since it decreases the aileron effectiveness. The magnitude of the interference is zero for f = 0 and increases monotonically to a maximum of 15 percent when the leading edges are sonic (f = 1).

The result that there is no fin-fin interference when f = 0 is quite general and applies to the multi-fin wing-body configuration as well. Simple physical considerations can be used to prove this result. There are two physical interpretations for f = 0: either the wing has finite geometry and M = ∞ (μ = 0) or the Mach number is finite and the aspect ratio of the wing is infinite. Interference can only be generated if part of a fin lies within the region of influence of another fin not in the same plane. When the Mach angle, μ, is zero, the region of influence vanishes and,

hence, all fin-fin interference effects must vanish.

Plane narrow-delta aileron-- This aileron is similar to that shown in Figure 11 except that here the leading edges are subsonic. The notation for this case is shown in Figure 14. The leading edge parameter here, d, is the reciprocal of the parameter for supersonic leading edges, f.

The solution for this aileron was obtained in Reference 18 and is given by

$$\beta C_{l_\delta} = \frac{2}{3} d \tag{4.210}$$

It should be noted that this result is actually independent of Mach number since there is a β hidden in the parameter d on the right hand side which will cancel the β on the left. This solution is then the slender body result as well.

Cruciform narrow-delta aileron-- This configuration is the same as that for the cruciform wide-delta aileron except that here the leading edges are subsonic. The horizontal fins are deflected by $\pm \delta$ and the vertical fins are undeflected. The addition of the vertical fins to the plane aileron to form this aileron will reduce but not eliminate the equalization of pressure which takes place across the top and bottom sides of the plane aileron. Then the horizontal fins of the cruciform aileron will carry more rolling

moment than the plane aileron just as in the wide-delta case. Again the vertical fins must carry a counter-rolling moment and, it will be seen, this moment more than counteracts the increase in rolling moment carried by the horizontal fins and leads to larger interference effects than for the wide-delta case.

Since the leading edges are subsonic, the flow conditions on the two sides of the vertical fins are not independent of each other and this problem cannot be reduced exactly to planar wing problems as in the wide-delta case. As yet, the exact solution is not known and this writer has not attempted to obtain it. Instead, an approximate solution is obtained by studying exact limiting cases combined with under- and overestimates. This approximate solution is obtained graphically by fairing a curve which satisfies the exact limiting cases and the under- and overestimates. Such a procedure was carried out in Reference 19 before the slender body solution was available. The slender body solution is included here and should improve considerably the accuracy of the approximation.

What is desired here is an approximation to the plot of βC_{l_δ} versus d. The results are shown in Figure 15 and all the discussion concerning the approximate solution will refer to this figure. First consider what exact limiting values are known for the cruciform aileron. The exact values for d = f = 1 are given by Equations (4.27b), (4.28b), and (4.29b) (or Figure 13) for the horizontal fins, the vertical

fins, and the complete aileron respectively. At d = 0, C_{l_δ} will be zero for the horizontal and vertical fins and for the complete aileron. The slender body solution supplies the exact slopes of the curves at d = 0. These results were published recently in Reference 30. The results for the horizontal fins, vertical fins, and complete aileron respectively are given by

$$\beta \left(C_{l_\delta}\right)_H = 1.128\, d \tag{4.211}$$

$$\beta \left(C_{l_\delta}\right)_V = -0.620\, d \tag{4.212}$$

$$\beta C_{l_\delta} = 0.508 \tag{4.213}$$

It is possible to obtain some further information about the complete aileron by bracketing the exact solution. Take a fixed value of d for the horizontal fins. Then let the vertical fins increase in size from the limiting case of no fins (plane aileron) to the other limiting case of fins with sonic leading edges (mixed cruciform aileron). It seems reasonable that the variations in rolling moment during this process will be continuous and monotonic and that the value of rolling moment for the cruciform aileron will lie somewhere between the two limits. The solution for the plane aileron is given by Equation (4.210) and is plotted in Figure 15. The slender body result for the complete aileron (Equation (4.213)) is also shown. Since the slender body result and the correct endpoint at

d = 1 lie below the plane aileron solution, the plane aileron must overestimate the correct solution. Then the mixed cruciform aileron underestimates the correct solution.

The mixed cruciform aileron is the only multi-fin configuration treated in this thesis which does not have the same planform for all of its component plane wings. It should first be noted that, when d = 1, all leading edges are sonic and the mixed aileron has the correct value. Since the vertical fins have sonic leading edges, the flow conditions on its right and left sides are completely independent of each other. Then the flow conditions to the right of the vertical fins are exactly those obtained from a narrow-delta lifting wing whose angle of attack is everywhere + δ . The same arguments which were used for the cruciform wide-delta aileron apply here. The details of the calculations will not be presented since this solution is of no great importance.

The pressure distributions can be obtained from Reference 35 where the conical solution for the complete flow field of a narrow-delta lifting wing is given. The pressure distribution on the upper side of the right horizontal fin is given essentially by

$$w = \frac{m \delta U d}{E(\sqrt{1-d^2})\sqrt{1-(t/d)^2}} \qquad (4.214)$$

where t denotes the usual conical variable in the horizontal plane. The pressure distribution on the right side of the upper vertical

fin is given by

$$W = \frac{m\,\delta U d\sqrt{1-s^2}}{E(\sqrt{1-d^2})\sqrt{1+s^2\left(\frac{1}{d^2}-1\right)}} \tag{4.215}$$

where s denotes the conical variable in the vertical plane. Integrating these pressure distributions over the horizontal and vertical fins using the symmetries depicted in Figure 12, the rolling moment coefficients based on the area and span of the narrow-delta horizontal fins are given by

$$\beta\left(C_{l_\delta}\right)_H = \frac{4}{3}\frac{d}{E(\sqrt{1-d^2})} \tag{4.216}$$

$$\beta\left(C_{l_\delta}\right)_V = -\frac{2}{3(1-d^2)E(\sqrt{1-d^2})}\left(\frac{\cos^{-1}d}{\sqrt{1-d^2}} - d\right) \tag{4.217}$$

$$\beta C_{l_\delta} = \frac{2}{3(1-d^2)E(\sqrt{1-d^2})}\left[d(3-2d^2) - \frac{\cos^{-1}d}{\sqrt{1-d^2}}\right] \tag{4.218}$$

for the horizontal fins, vertical fins, and complete mixed aileron respectively. These three equations are plotted in Reference 19.

Only the result for the complete aileron can be used for estimating purposes. This is plotted in Figure 15. It is seen that this solution starts at the correct value for d = 1 but rapidly moves away from the overestimate (plane aileron) as d decreases. Then, as an underestimate, the mixed aileron is of little use except near d = 1 where it attains the correct value. The slope of the mixed aileron curve at d = 1 will act as a guide for fairing in the approxi-

mate solution by limiting the slope of the approximate curve so that it does not pass below the mixed aileron curve. Differentiating Equation (4.218) with respect to d and evaluating the indeterminate expression when d = 1, the slope is given by

$$\beta\left(\frac{\partial C_{l_\delta}}{\partial d}\right)_{d=1} = \frac{104}{45\pi} \tag{4.219}$$

and is shown in Figure 15.

Using the known endpoints at d = 0 and d = 1, the known slope at d = 0, and the limiting nature of the slope of the mixed aileron curve at d = 1, the cruciform aileron approximation can be drawn in a reasonable manner which leaves little to the imagination. The cruciform aileron approximation shown in Figure 15 is expected to approximate quite well to the correct solution.

The magnitude of the fin-fin interference is given by the difference between the plane aileron and the cruciform aileron approximation for a given value of d. It is seen that fin-fin interference reduces the aileron effectiveness. The magnitude of the interference is 15 percent for d = 1 and increases with decreasing d until it attains the limiting value of about 24 percent for d = 0.

Reviewing the cruciform aileron results briefly, it is seen that, for nearly all leading edge conditions (subsonic and supersonic), fin-fin interference is detrimental in that it reduces the rolling moment carried by the cruciform aileron below the moment

carried by the plane aileron. The one leading edge condition for which this statement is not true is f = 0----a condition which is obviously not attainable physically. Hence, for practical purposes, fin-fin interference is always detrimental. Starting from zero for f = 0 (d = ∞), the magnitude of the interference increases with increasing f (decreasing d). It is 15 percent for d = f = 1 and attains its maximum value of about 24 percent when f = ∞ (d = 0). It is apparent physically that the variation of f from zero to infinity is equivalent to the variation of the interaction between the fins from no interaction to complete interaction. Then, qualitatively, the results are not surprising.

Multi-fin ailerons--In this section, roll due to aileron deflection is studied for multi-fin wings other than the cruciform. The method used for estimating the solutions restricts the study to multi-fin wings whose fins are all deflected equally and in the same direction, i.e. all component plane ailerons of the multi-fin aileron are deflected by $\pm \delta$ so as to produce rolling moments of the same sign. Since the multi-fin wing is assumed to be axially symmetric, the basic case where only one component plane wing is deflected as an aileron is obtained from the superposition principle by dividing the results by the number of plane wings.

E. W. Graham (References 22 and 23) has studied a very interesting limiting case which makes it possible to estimate the results for the multi-fin aileron. He has studied the limiting case when the multi-fin wing is composed of an infinite number of fins all of which are deflected equally as ailerons. This problem is easily solved by simple angular-momentum considerations. The result is

$$\beta C_{l_\delta} = \frac{2\pi}{3} d = \frac{2\pi}{3f} \tag{4.220}$$

This result is actually independent of Mach number since the β hidden in the d or f cancels the β on the left. Then Equation (4.220) gives the solution for all leading edge conditions (supersonic and subsonic).

Equation (4.220) is plotted against d in Figure 16 for $0 \leq d \leq 1$ (subsonic leading edges). Also shown are the results for the plane aileron and for the cruciform aileron approximation with all fins deflected. N denotes the number of fins. The results for N = 2 and N = ∞ will bracket the results for any aileron with an even number of fins (all deflected). Since these bracketing results are straight lines, they do not supply enough information about the shape of the curves for $2 < N < \infty$. The curve for N = 4, although approximate, supplies additional information for estimating the shapes of the curves for $4 < N < \infty$. The ordinate at d = 0 will obviously be zero for all multi-fin ailerons. If the endpoints are

known at d = 1, approximate solutions can be faired in for any multi-fin aileron. The endpoints at d = 1 can be estimated by plotting $\beta \hat{C}_{l_\delta}$ against 1/N using the known exact solutions for N = 2, 4, and ∞ . Such a plot is shown in Figure 17 with a reasonable curve drawn through the three known points. A few estimated endpoints at d = 1 are shown in Figure 16.

In order to estimate the solutions for multi-fin ailerons with supersonic leading edges, the known results for N = 2, 4, and ∞ are plotted against f in Figure 18. The results are also shown for part of the range of subsonic leading edges ($1 \leq f \leq 4$). Since there are no interference effects for f = 0, the ordinate for any multi-fin aileron with N even is obtained as a multiple of the known ordinate for N = 2. At f = 1, the ordinates can be estimated as described above and a few are indicated in Figure 18. Using the exact values at f = 0, the estimated values at f = 1, and the result for N =4 to indicate the shape, the results for wide-delta multi-fin ailerons can be estimated.

It should be pointed out that this procedure can also be used for ailerons with N odd.

In Figures 16 and 18, fin-fin interference is given by the difference between $\beta \hat{C}_{l_\delta}$ for the multi-fin aileron with all fins deflected and $\beta \hat{C}_{l_\delta}$ for the plane aileron multiplied by the number (N/2) of plane ailerons which form the multi-fin aileron.

For f = 0 the interference is zero for all N. For any other f, the interference increases with increasing N to a maximum value of 100% when $N = \infty$. For any given N, the variation of interference with f ($0 \leq f \leq \infty$) is qualitatively the same as for the cruciform aileron which was discussed previously.

C. Damping in Roll

Consider a multi-fin wing which is rotating about its axis of symmetry with constant angular velocity p. The axis of symmetry is assumed to be oriented in the free-stream direction so that no lateral forces are generated. The usual assumption that the effect of rolling can be represented by an apparent linear angle of attack distribution will be made. Then the rolling wing is replaced by a stationary wing whose fins are linearly twisted. The results for such a wing will be qualitatively the same as for the aileron. The two problems differ only quantitatively because of the different angle-of-attack distributions of the fins.

Plane wide-delta wing--The solution for this wing can be obtained from Reference 36 and is

$$\beta C_{l_p} = -\frac{1}{3} \tag{4.221}$$

As expected, the result is independent of leading edge sweepback, f.

Cruciform wide-delta wing-- Assume, for convenience, that the wing is oriented so that one pair of fins is horizontal and the other pair vertical. The complete problem with all fins twisted can be decomposed into the sum of simpler problems as shown in Figure 19. The dotted lines represent the linear angle of attack distributions spanwise. The two simpler problems A and B are essentially the same. This is evident if either is rotated by 90 degrees. Then the solution will be obtained for problem B and doubled for the final result.

In problem B, the vertical fins are untwisted and undeflected and will carry a counter-roll just as in the aileron case. The horizontal fins are twisted linearly with the angles of attack negative for the right fin and positive for the left fin. The horizontal fins will generate a negative rolling moment and a positive counter-moment will be induced on the vertical fins. In the final results, the rolling moment carried by the horizontal fins will be called "direct damping" and the roll carried by the vertical fins will be called "fin-fin induced roll" since horizontal and vertical fins have little physical significance for this problem.

Using the same arguments as for the cruciform wide-delta aileron, the flow field to the right of the vertical fins is the same as the flow field for a plane wide-delta wing which has linear symmetric twist. The upwash is known at all points on the wing and is

a function of x only (i.e. wing is uncambered). Since the problem has been reduced to a planar wing with prescribed upwash, Equation (3.16) can be used to determine the flow field. The right half of the plane wing corresponds to the right horizontal fin of the cruciform wing and the vertical plane of symmetry of the plane wing corresponds to the right side of the vertical fins of the cruciform wing. Obtaining the solutions in these two planes will then provide the data for computing the rolling moment for the complete cruciform wing.

The potential at the trailing edge of the horizontal fins, $\varphi_{T.E.}(x)$, is directly proportional to the spanwise lift distribution, $\Gamma(x)$. This is also true for the vertical fins if y replaces x and $\Gamma(y)$ represents the spanwise side-force distribution. If the subscripts L and U denote quantities on the lower and upper sides of the horizontal fins, the known symmetries for this problem show that

$$p_L = -p_U$$

and, hence,

$$p_L - p_U = -2p_U = 2\rho U (\varphi_z)_U$$

The spanwise lift distribution is given by integrating this quantity from the leading edge (L.E.) to the trailing edge (T.E.).

$$\Gamma(x) = \int_{L.E.}^{T.E.} (p_L - p_U)\, dz = 2\rho U \int_{L.E.}^{T.E.} \left[\varphi_z(x,z)\right]_U dz \qquad (4.222)$$

$$= 2\rho U \left[\varphi_{T.E.}(x)\right]_U = \frac{4g}{U} \left[\varphi_{T.E.}(x)\right]_U$$

In the same way, the spanwise side-force distribution is given by

$$\ell(y) = \frac{4q}{U}\left[\varphi_{T.E.}(y)\right]_R \tag{4.223}$$

where the subscript R denotes the right side of the vertical fins. Note that $\varphi_{L.E.} \equiv 0$.

The spanwise lift distribution will now be obtained for the right horizontal fin. The equivalent planar wing problem with the regions of integration is shown in Figure 20. The potential at the trailing edge is $\varphi(x,0,c)$. Equation (3.16) reduces to the form

$$\varphi(x,0,c) = -\frac{1}{\pi}\iint \frac{\varphi_y(\xi)\,d\xi\,d\zeta}{\sqrt{(c-\zeta)^2-\beta^2(x-\xi)^2}}$$

There are two regions to be considered: $0 \le x \le mc$ $(0 \le \bar{x} \le 1)$ and $mc \le x \le b/2$ $(1 \le \bar{x} \le 1/f)$.

For the region $1 \le \bar{x} \le 1/f$, $\varphi(x,0,c)$ is given by

$$\varphi(x,0,c) = -\frac{b}{\pi}\left[\int_{c\left(\frac{x-mc}{b/2-mc}\right)}^{c\left(\frac{x+mc}{b/2+mc}\right)} d\zeta \int_{m\zeta+x-mc}^{\frac{b\zeta}{2c}} \frac{\xi\,d\xi}{\sqrt{(c-\zeta)^2-\beta^2(x-\xi)^2}} + \int_{c\left(\frac{x+mc}{b/2+mc}\right)}^{c} d\zeta \int_{m\zeta+x-mc}^{-m\zeta+x+mc} \frac{\xi\,d\xi}{\sqrt{(c-\zeta)^2-\beta^2(x-\xi)^2}}\right]$$

carrying out the ξ integration,

$$\varphi(x,0,c) = \frac{b}{\pi}\left[mx\int_{c\left(\frac{x-mc}{b/2-mc}\right)}^{c\left(\frac{x+mc}{b/2+mc}\right)} \sin^{-1}\frac{\left(x-\frac{b\zeta}{2c}\right)}{m(c-\zeta)}\,d\zeta + m\int_{c\left(\frac{x-mc}{b/2-mc}\right)}^{c\left(\frac{x+mc}{b/2+mc}\right)} \sqrt{m^2(c-\zeta)^2-\left(x-\frac{b\zeta}{2c}\right)^2}\,d\zeta - \right.$$

$$\left. - \frac{\pi m c x b}{2}\left(\frac{b/2-x}{b^2/4+m^2c^2}\right)\right]$$

By sufficient integration by parts all of these integrals can be found in integral tables such as Reference 37. The final result can be put into the following form:

$$\varphi(x,0,c) = \frac{p\left(\frac{b}{2}\right)^2 f^2(1-f\bar{x})}{(1-f^2)^{3/2}}\left[\frac{f}{2}(1+f\bar{x})-\bar{x}\right] \qquad \text{for} \qquad 1 \le \bar{x} \le \frac{1}{f} \tag{4.224}$$

For the region $0 \le \bar{x} \le 1$, $\varphi(x,0,c)$ is

$$\varphi(x,0,c) = -\frac{p}{\pi}\left[-\int_{\frac{b}{2}\left(\frac{x-mc}{b/2+mc}\right)}^{0} \xi\, d\xi \int_{-\frac{2c}{b}\xi}^{\frac{\xi-x}{m}+c} \frac{d\zeta}{\sqrt{(c-\zeta)^2-\beta^2(x-\xi)^2}} + \int_{0}^{x} \xi\, d\xi \int_{\frac{2c}{b}\xi}^{\frac{\xi-x}{m}+c} \frac{d\zeta}{\sqrt{(c-\zeta)^2-\beta^2(x-\xi)^2}} + \right.$$

$$\left. + \int_{x}^{\frac{b}{2}\left(\frac{x+mc}{b/2+mc}\right)} \xi\, d\xi \int_{\frac{2c}{b}\xi}^{\frac{x-\xi}{m}+c} \frac{d\zeta}{\sqrt{(c-\zeta)^2-\beta^2(x-\xi)^2}}\right]$$

Carrying out the inner integration

$$\varphi(x,0,c) = -\frac{p}{\pi}\left[\int_{0}^{\frac{b}{2}\left(\frac{x-mc}{b/2+mc}\right)} \xi \log\left|\frac{mc\left(1+\frac{2\xi}{b}\right)+\sqrt{m^2c^2\left(1+\frac{2\xi}{b}\right)^2-(x-\xi)^2}}{(x-\xi)}\right| d\xi + \right.$$

$$\left. + \int_{0}^{\frac{b}{2}\left(\frac{x+mc}{b/2+mc}\right)} \xi \log\left|\frac{mc\left(1-\frac{2\xi}{b}\right)+\sqrt{m^2c^2\left(1-\frac{2\xi}{b}\right)^2-(x-\xi)^2}}{(x-\xi)}\right| d\xi\right]$$

This can be reduced finally to the result

$$\varphi(x,0,c) = -\frac{p}{\pi}\left(\frac{b}{2}\right)^2 f^2\left[\bar{x}^2 \operatorname{sech}^{-1}\bar{x} + \frac{1}{(1-f^2)^{3/2}}\left\{\sqrt{(1-\bar{x}^2)(1-f^2)} - (1+f\bar{x})\left[\frac{f}{2}+\left(1-\frac{f^2}{2}\right)\bar{x}\right]\cos^{-1}\left(\frac{f+\bar{x}}{1+f\bar{x}}\right) - \right.\right.$$

$$\left.\left. -(1-f\bar{x})\left[\frac{f}{2}-\left(1-\frac{f^2}{2}\right)\bar{x}\right]\cos^{-1}\left(\frac{f-\bar{x}}{1-f\bar{x}}\right)\right\}\right] \tag{4.225}$$

For f = 1, sonic leading edges, this reduces to

$$\varphi(x,0,c)\Big|_{f=1} = -\frac{p}{\pi}\left(\frac{b}{2}\right)^2\left(\bar{x}^2 \operatorname{sech}^{-1}\bar{x} + \frac{1}{3}\sqrt{1-\bar{x}^2}\right) \tag{4.226}$$

The rolling moment coefficient for direct damping for the complete cruciform wing, $(C_{l_p})_H$, is obtained by integrating $l(x)$ (see Equation (4.222)) over the right horizontal fin and multiplying the result by four.

$$C_l = \frac{4\int_0^{b/2} x l(x)\,dx}{q\frac{bc}{2}b} = \frac{32}{b^2 c U}\int_0^{b/2} x\,\varphi(x,0,c)\,dx \tag{4.227}$$

Substituting Equations (4.224) and (4.225) for their respective regions of validity into Equation (4.227) and carrying out the indicated integrations will yield finally

$$\beta(C_{l_p})_H = -\frac{2}{3\pi(1-f^2)^{3/2}}\left[(2-f^2)\sqrt{1-f^2} + (2-3f^2)\cos^{-1}f\right] \tag{4.228}$$

When f = 0

$$\beta(C_{l_p})_H\Big|_{f=0} = -\frac{2}{3} \tag{4.228a}$$

This is the result for two plane wings (see Equation (4.221)) as expected for this case of no interference. For sonic leading edges

$$\beta(C_{l_p})_H\Big|_{f=1} = -\frac{20}{9\pi} \tag{4.228b}$$

The spanwise side-force distribution will now be obtained for the upper vertical fin. This is essentially given by the potential at the trailing edge of the right side, $\varphi(0,y,c)$, by Equation (4.223). This potential is given by the solution of the equivalent plane wing along the line x = 0, z = c for positive y. The region of integration

is symmetric about the z-axis and is shown in Figure 21. Equation (3.16) becomes

$$\varphi(o,y,c) = -\frac{1}{\pi}\iint \frac{\varphi_y(\xi)\, d\xi\, d\zeta}{\sqrt{(c-\zeta)^2 - \beta^2(\xi^2+y^2)}} \tag{4.229}$$

Because the integrand is symmetric in ξ, the integration in ξ can be carried out over half the region and the result doubled. Then the potential is

$$\varphi(o,y,c) = -\frac{2m\rho}{\pi}\int_0^{\frac{\sqrt{m^2c^2-(1-f^2)y^2}-mfc}{1-f^2}} \xi\, d\xi \int_{\frac{2c}{b}\xi}^{c-\frac{1}{m}\sqrt{\xi^2+y^2}} \frac{d\zeta}{\sqrt{m^2(c-\zeta)^2-(\xi^2+y^2)}}$$

and carrying out the first integration

$$\varphi(o,y,c) = -\frac{2\rho}{\pi}\int_0^{\frac{\sqrt{m^2c^2-(1-f^2)y^2}-mfc}{1-f^2}} \xi\, \cosh^{-1}\left|\frac{mc-f\xi}{\sqrt{\xi^2+y^2}}\right| d\xi$$

The final result is

$$\varphi(o,y,c) = -\frac{b}{\pi}\left(\frac{b}{2}\right)^2 f^2 \left\{ \frac{\sqrt{1-\bar{y}^2}}{1-f^2} - \bar{y}^2 \operatorname{sech}^{-1}\bar{y} - \frac{f}{(1-f^2)^{3/2}}\cos^{-1}\left(\frac{f}{\sqrt{1-(1-f^2)\bar{y}^2}}\right) + \right.$$

$$\left. + \frac{f\bar{y}^2}{2\sqrt{1-f^2}}\left[\sin^{-1}\left(\frac{\sqrt{1-f^2}-\bar{y}}{1-\sqrt{1-f^2}\,\bar{y}}\right) + \sin^{-1}\left(\frac{\sqrt{1-f^2}+\bar{y}}{1+\sqrt{1-f^2}\,\bar{y}}\right)\right] \right\} \tag{4.230}$$

This result applies of course for $0 \le \bar{y} \le 1$ since induced effects occur only within the Mach cone.

The rolling moment coefficient for fin-fin induced roll for the complete cruciform wing, $(C_{l_p})_V$, is obtained by integrating

the spanwise side-force distribution just as was done previously for the lift distribution. The final result is

$$\beta\left(C_{l_p}\right)_V = \frac{2f^3}{3\pi(1-f^2)^{3/2}}\left[(2+f^2)\sqrt{1-f^2} - 3f\cos^{-1}f\right] \tag{4.231}$$

$$\beta\left(C_{l_p}\right)_V\Big|_{f=0} = 0 \tag{4.231a}$$

$$\beta\left(C_{l_p}\right)_V\Big|_{f=1} = \frac{4}{15\pi} \tag{4.231b}$$

Combining the results for direct damping and fin-fin induced roll, the final result for the cruciform wing is

$$\beta C_{l_p} = -\frac{2}{3\pi(1-f^2)^2}\left[f(2-5f^2) + (2-5f^2+6f^4)\frac{\cos^{-1}f}{\sqrt{1-f^2}}\right] \tag{4.232}$$

$$\beta C_{l_p}\Big|_{f=0} = -\frac{2}{3} \tag{4.232a}$$

$$\beta C_{l_p}\Big|_{f=1} = -\frac{88}{45\pi} \tag{4.232b}$$

The results for the cruciform wide-delta wing are plotted in Figure 22. For interference effects, the comparison must be made with the result for two plane wings which is also shown. These results are qualitatively the same as for the cruciform wide-delta aileron (see Figure 13). The primary difference is that here the magnitude of the interference is consistently less than for the aileron. For f = 1, fin-fin interference decreases the roll damping by about 7 percent compared with 15 percent for the aileron.

From physical considerations it would be expected that fin-fin interference has a greater effect for aileron deflection than for

damping in roll. Fin-fin interference will obviously depend on the angle-of-attack distributions of the fins. For distributions which are concentrated inboard the interference effects will be greater than for distributions concentrated outboard. The distribution of angle of attack is concentrated further inboard for the aileron deflection case relative to the damping in roll case and, thus, higher interference effects would be expected.

Whether or not this decrease in roll damping is detrimental depends entirely on the problem being considered. For the aileron problem, this decrease in damping is beneficial since it is generally desired that the rolling be as rapid as possible. For other cases such as roll induced by combined pitch and yaw, high damping is generally desirable for stability.

Plane narrow-delta wing--The roll damping coefficient was obtained in Reference 36. The result is

$$\beta C_{l_p} = -\frac{\pi}{4} \frac{d(1-d^2)}{\left[(2-d^2)E(\sqrt{1-d^2}) - d^2 K(\sqrt{1-d^2})\right]} \tag{4.233}$$

Reference 38 gives the slender body result

$$\beta C_{l_p} = -\frac{\pi}{8} d \tag{4.234}$$

which is the correct slope of the roll damping curve at d = 0.

Cruciform narrow-delta wing-- The exact solution of this problem is even more difficult than for the corresponding aileron.

The reason is that this configuration is not conical whereas the aileron is and, hence, the aileron can be treated by the powerful methods of potential theory. Just as for the aileron, an approximate solution is obtained here by graphically fairing in a reasonable curve based on exact limiting values for endpoints and slopes.

The endpoints are known at d = 0 and at d = 1. At d = 0, $C_{l_p} = 0$ and, at d = 1, the solution is known from the supersonic-leading-edge case. The slender body solution gives the exact slope at d = 0. This solution was obtained recently in References 30 and 31 and is given by

$$\beta C_{l_p} = -\frac{2}{\pi} d \tag{4.235}$$

This information turns out to be sufficient to establish a reasonable faired approximation to the exact solution.

These results are shown in Figure 23. It is seen that even the slender body solution is a good approximation to the exact solution. The curve for $N = \infty$ is also shown. This result was obtained in Reference 23 and is given by

$$\beta C_{l_p} = -\frac{\pi}{2} d = -\frac{\pi}{2f} \tag{4.236}$$

Note that the cruciform wing approximation fits the expected change of shape of the solutions as N varies from 2 to ∞.

The interference effects are qualitatively the same as for

the corresponding aileron. Again, the interference is less than for the aileron. The interference increases from about 7 percent for d = 1 to about 19 percent for d = 0.

Multi-fin wings--The same procedure as was used for multi-fin ailerons can be used here to estimate the solutions for multi-fin wings. Estimated endpoints are obtained from Figure 17 for d = f = 1. Some endpoints are shown in Figures 23 and 24. These two graphs can be used to estimate the multi-fin wing solutions knowing the endpoints and the shapes of the curves for N = 4 and N = ∞ .

Except for the formulas, the discussion of the effects of interference for the multi-fin ailerons applies here as well.

D. Equilibrium Rate of Roll.

When any of the fins of a multi-fin wing are suddenly deflected as ailerons, the wing will begin to roll. The rate of roll will eventually become constant. This constant rate of roll is what is referred to as the equilibrium rate of roll and it is determined by the fact that the roll due to aileron deflection is equal to the roll due to damping for steady conditions. The equilibrium rate of roll will obviously depend on the aileron deflection and it is generally expressed in a parameter formed by the ratio of the tip helix angle $\left(\frac{pb}{2V}\right)_e$ to the aileron deflection angle δ . Since

the rolling moments due to aileron deflection and damping are equal, the equilibrium rate of roll is obtained by a simple division

$$\left(\frac{pb}{2V}\right)\Big/_{\delta} = -\frac{\beta C_{l_\delta}}{\beta C_{l_p}} \tag{4.237}$$

Results are shown in Figures 25 and 26 for all the cases for which C_{l_δ} and C_{l_p} have been obtained. The estimated multi-fin points at d = f = 1 are obtained from the estimated points previously obtained for C_{l_δ} and C_{l_p} or from the interpolation curve in Figure 17. Note in Figure 25 that the values at d = 0 are known only for N = 2, 4 and ∞ . Multi-fin points can be estimated at d = 0 exactly the same way they were estimated at d = 1. At f = 0 all the curves start from $\left(\frac{pb}{2V}\right)\Big/_{\delta} = 2$ if all fins are deflected. Using these endpoints and the known curves as guides, the general multi-fin wing results can be estimated. It should be noted that, for $0 \leq f \leq 1$, the curve for N = 4 exhibits an inflection point which is necessary if the curve for N = ∞ is to be approached as N increases.

Also shown in Figures 25 and 26 is the cruciform wing approximation with only two fins deflected. This result is just half of the result for N = 4. This curve is shown to indicate that all fins of a multi-fin wing need not be deflected and that this may lead to much lower equilibrium rates of roll than generally indicated in these graphs.

Fin-fin interference is given by the difference between the curve for a particular multi-fin wing (all fins deflected) and the curve for N = 2. In general, it is desired to have an equilibrium rate of roll which is as high as possible. Then fin-fin interference is always detrimental. The reason for this is that the interference effects are always greater for C_{l_δ} than for C_{l_p}. It should be noted that the interference effects for N = 4 do not increase with increasing f for the whole range $0 \leq f \leq \infty$: at f = 0 there is no interference, at f=1 the interference is about 9 percent, and at $f = \infty$ the interference is about 6%. For a given value of f, fin-fin interference increases as N increases to a maximum value for $N = \infty$. The maximum interference for $N = \infty$ is about 30%.

4.3 Fin-Fin Interference--High Aspect Ratio

The designation "high aspect ratio" is generally intended to refer to supersonic airplane problems. The supersonic airplane will generally have plane wings and, hence, no fin-fin interference effects. It is likely, however, that some missiles will have nonplanar high-aspect-ratio wings or tails or both. With this in mind, this brief section is included.

Delta Wings--All of the results which have been presented will, of course, apply here. The supersonic flight speeds which are generally expected for supersonic airplanes and missiles are

well above M = 1. Then the leading edges of these wings will usually be supersonic and, further, the leading edge parameter, f, will usually be small. For this range, the cruciform results are exact and the results for multi-fin wings can be easily estimated.

Rectangular Wings--The methods for the delta wings can be used here as long as the wing tips do not intersect the Mach cone from the axis of symmetry. As a matter of fact, the calculations are considerably simpler for this case because the leading edges are normal to the free-stream direction. The applications of the previous methods to this problem should be obvious and will not be discussed further.

4.4 Fin-Fin and Wing-Body Interference--Low Aspect Ratio

Plane and multi-fin wing-body interference problems are studied in this section. Since multi-fin wing-body combinations are to be included, there may be both fin-fin and wing-body interferences occurring simultaneously or either interference might occur by itself depending on the ratio of the body diameter to the wing span of the combination (a parameter denoted by A).

It was seen that, for certain fin-fin interference problems, exact linearized solutions could be obtained easily. The presence of a body makes the interference problems much more difficult. As yet no exact linearized solutions have been obtained for general

lift and roll problems. However, estimates of or approximations to the exact solutions are usually useful qualitatively and are often useful quantitatively for engineering calculations.

The lift problem for plane wing-body configurations is the wing-body interference problem which has been studied most widely. Three recent papers (References 12, 15, and 16) have presented methods and results for plane wing-body lift problems for a wide variety of useful configurations. The important results will be reviewed here briefly. The difficulty with the plane wing-body problem has precluded any work on multi-fin wing-body problems other than cruciform.

The roll problems are easier than the lift problems because the circular body contributes nothing to the rolling moments. In the present work the writer studies roll due to aileron deflection and damping in roll for plane and cruciform delta wing-body configurations. No attempt is made to obtain exact solutions. Instead, the exact solutions are bracketed by over- and underestimates from which results can be estimated.

A. Lift.

The term "lift", when used for wing-body configurations, will denote lift problems where the wings are undeflected relative to the body unless specifically stated otherwise. If the wings are deflected relative to the body, the effects of "incidence" must be

included. The papers which will be reviewed here briefly have considered only the "lift" problem for plane wing-body configurations.

Plane wing-body configurations--It is necessary to decompose the problem into configurations with and without afterbody particularly for the missile configurations where a sizeable lift can be carried by the afterbody. The tail problem, aside from the induced effects due to the vortex sheets, is generally a wing-body problem for a configuration with little or no afterbody.

Morikawa (Reference 12) has presented results for three wing-body configurations with no afterbody. He treats the delta, clipped-delta, and rectangular wings. The results are bracketed by the solutions for slender bodies (zero aspect ratio) and wings of infinite aspect ratio. Using results obtained from some of his previous work (Reference 8), he presents estimates for some of the configurations lying between these two limiting cases. For each of the wings he shows how much of the lift is carried by the body and how much is carried by the wing.

Lagerstrom and M. E. Graham (References 15 and 16) have used slender body theory to estimate the lift carried by plane wing-body combinations with afterbodies. These are the first papers which present methods for obtaining reasonable estimates of the afterbody lift. Furthermore, these papers give a good physical

picture of the mechanism of afterbody lift and they show how this lift varies with the two important parameters A and afterbody length.

Using the previous discussion of slender body theory, the methods and results of References 15 and 16 will now be summarized very briefly. If, in Figure 6 (see Section 3.2), the wing-body configuration ends where the wing becomes parallel to the free-stream direction, the lift of the resulting delta wing-body configuration (without afterbody) can be obtained from Morikawa's paper. This lift is generally considerably less than the slender body result. Let the configuration be continued downstream as shown in Figure 6 (wing continued parallel to free-stream direction). This continuation will be denoted as the afterbody whether or not the wing is continued. As the afterbody increases in length, the lift will increase, eventually become greater than the slender body value, reach a maximum value, and then decrease and approach the slender body value as the afterbody length approaches infinity.

Now let the body alone be continued downstream so that the resulting configuration is a delta wing-body combination with an afterbody. As this afterbody increases in length, the lift will again increase but not as much as before. The lift may or may not exceed the slender body result as the afterbody length is

increased. As the afterbody length approaches infinity, the lift will approach a value which is less than the slender body value. These variations of lift with afterbody length will obviously depend upon the ratio of the body diameter to the wing span (A).

Then, for any afterbody problem, the lift will depend on A and on the afterbody length. For small values of A, the afterbody lift will be very small but, for values of A near unity, the lift carried by a long afterbody must be taken into account.

From these considerations it is seen that the afterbody lift carried by a high-aspect-ratio supersonic airplane configuration will generally be negligible. The afterbody lift carried by a supersonic missile configuration is much greater than for the airplane primarily because of the increased value of A. The fact that the afterbody length of a missile (distance from wing to tail) is generally much greater than for an airplane may or may not increase the afterbody lift.

Lagerstrom and M. E. Graham have estimated the results by a double interpolation using known results for limiting values of A and afterbody length. The details are described in Reference 15.

When the wing-body configuration is banked about the body axis, the results are modified as discussed previously for the plane wing.

Cruciform wing-body configurations--Except for the wing-body interference effects, the effects of bank and the fin-fin interference are the same as for the cruciform wing. Then, banking about the body axis does not change the lift and the fin-fin interference is zero because of the 90 degree geometry of the fins. For the general multi-fin wing-body configuration, the fin-fin interference will not be zero unless A is large enough so that the fins cannot interact.

B. Elementary Strip

It is convenient for many of the future calculations to use the elementary strip (see References 11, 18, 19, and 28). It is useful for the applications to interpret the strip as a lifting wing of width $d\xi$ whose long dimension is in the free-stream direction. Since no cambered wings are considered, the angle of attack of the strip will be constant. Adjacent to the wing on both sides are flat plates at zero angle of attack. On one side, the plate always extends upstream of any disturbances from the strip whereas, on the other side, the leading edge of the plate is straight and may be subsonic or supersonic depending on the wing to which the calculations are to be applied. The results for this strip, interpreted as an elementary lifting strip, can be obtained by symmetry considerations (see Reference 11).

The potential due to this strip may be obtained also by

interpreting the strip as a line of sources of constant strength $\varphi_y/\pi = -\frac{\alpha(\xi)U}{\pi}$ in the z-direction determined by the downwash prescribed along the line ξ = constant.

These strips will always be used here for calculations with delta wings which are uncambered. Their usefulness is derived from the fact that the strips represent results for which the ζ integration of Equation (3.16) has already been carried out. As shown by this equation, the strips can then be integrated over ξ to obtain results for twisted wings.

Supersonic leading edge--Consider the elementary strip adjacent to a supersonic leading edge as shown in Figure 27. The coordinate system for the strip is shown. The potential, spanwise lift distribution, and sidewash velocity at the trailing edge, (x_1, o, c'), are the quantities which are desired for the present work.

The potential is given by Equation (3.16). If, in Equation (3.16), the ξ_1 integration is carried out from 0 to $d\xi_1$, and the mean value theorem is used, the equation can be reduced to

$$\varphi(x_1, o, c') = \frac{\alpha(\xi)U\,d\xi}{\pi}\int_0^{c'-\beta x_1} \frac{d\zeta_1}{\sqrt{(c'-\zeta_1)^2-\beta^2 x_1^2}}$$

$$= \frac{\alpha(\xi)U}{\pi}\,\mathrm{sech}^{-1}\left|\frac{x_1}{mc'(\xi)}\right| d\xi \qquad (4.41)$$

Then the spanwise lift distribution is given by

$$l(x_1) = \frac{4q}{U}\varphi(x_1, 0, c') = \frac{4q\alpha(\xi)}{\pi} \operatorname{sech}^{-1}\left|\frac{x_1}{mc'(\xi)}\right| d\xi \tag{4.42}$$

Differentiating Equation (4.41) with respect to x_1 gives the sidewash velocity on the top side at the trailing edge

$$\frac{\partial \varphi}{\partial x_1} = u(x_1, 0, c') = -\frac{\alpha(\xi) U m c'(\xi)\, d\xi}{\pi x_1 \sqrt{m^2 c'(\xi)^2 - x_1^2}} \tag{4.43}$$

All of these equations are applicable for $|x_1| \leq mc'$. The total lift due to the pressures induced on the flat plates can be obtained by integrating the spanwise lift distribution with respect to x_1 over the limits $-mc' \leq x_1 \leq mc'$. However it is known that the lift coefficient is two-dimensional based on the deflected area $c'd\xi$ (see Reference 11) and, hence, the differential lift is

$$dL = 4mq\,\alpha(\xi)\, c'(\xi)\, d\xi \tag{4.44}$$

It is also known that the center of pressure is at the centroid of the strip so that the differential rolling moment about the axis of the strip is

$$dM = 0 \tag{4.45}$$

Subsonic leading edge--The corresponding sketch of the elementary strip adjacent to a subsonic leading edge is shown in Figure 28. The region of integration for using Evvard's method is shown.

The potential at the trailing edge is given by

$$\varphi(x_1, 0, c') = \frac{\alpha(\xi) U \, d\xi}{\pi} \int_{(c'+\beta x_1)\left(\frac{1-d}{1+d}\right)}^{c'-\beta x_1} \frac{d\zeta_1}{\sqrt{(c'-\zeta_1)^2 - \beta^2 x_1^2}}$$

$$= \frac{\alpha(\xi) U}{\pi} \operatorname{sech}^{-1} \left| \frac{\frac{x_1}{mc'}(1+d)}{2d - \frac{x_1}{mc'}(1-d)} \right| \tag{4.46}$$

The spanwise lift distribution is

$$\Delta(x_1) = \frac{4q\alpha(\xi)}{\pi} \operatorname{sech}^{-1} \left| \frac{\frac{x_1}{mc'}(1+d)}{2d - \frac{x_1}{mc'}(1-d)} \right| \tag{4.47}$$

The sidewash velocity is

$$u(x_1, 0, c') = -\frac{\alpha(\xi) U m c'(\xi) \sqrt{d} \; d\xi}{\pi x_1 \sqrt{m^2 c'(\xi)^2 d - (1-d) m c'(\xi) x_1 - x_1^2}} \tag{4.48}$$

These results hold for $-mc' \leq x_1 \leq mc'd$. The differential lift due to the pressure distribution and the differential rolling moment about the axis of the strip were obtained in Reference 28 and are

$$dL = 4mq\,\alpha(\xi)\, c'(\xi) \sqrt{d} \; d\xi \tag{4.49}$$

$$dM = -mq\,\alpha(\xi)\, c'(\xi)(1-d) \sqrt{d} \; d\xi \tag{4.410}$$

where the sign convention for the moment about the strip is the same as shown in Figure 1.

C. Elementary Strip Over- and Underestimates

Consider the elementary strip as a deflected element in one fin of a delta wing-body combination as shown in Figure 29. When the strip is close enough to the body, disturbances will strike the body at the wing-body juncture. Part of the disturbances will be diffracted and pass onto the body downstream of a helical path and the rest will be reflected back onto the fin. That part which passes onto the body can contribute nothing to the rolling moment about the body axis since the body cross section is circular. It is this fact which makes a simple estimation of the wing-body interference possible. The disturbances which are reflected back onto the fin increase the lift on the fin and, hence, increase the rolling moment carried by the fin.

It is now apparent how the contribution of a fin to the rolling moment may be bracketed by over- and underestimates. The estimates are illustrated in Figure 29 for the case of supersonic leading edges. The same estimates are used for subsonic leading edges. An underestimate is obtained by assuming that no reflection takes place at the wing-body juncture. With the elementary strip this amounts to using only that portion of the pressure distribution which is crosshatched in Figure 29(a). An overestimate is obtained by assuming that complete reflection takes place. This is realized if the body is replaced at the wing-body juncture

by a reflecting wall which has supersonic leading edges. This is illustrated in Figure 29(b) where the region with double cross-hatching indicates the added pressures due to reflection.

These same limiting cases of no reflection and complete reflection will also bracket the velocity (and pressure) distributions on the fins. This will be utilized in a later section for estimating the vorticity distributions at the trailing edges of the fins of plane and cruciform delta wing-body configurations.

Supersonic leading edge--The differential lifts and rolling moments for the over- and underestimates can now be derived by utilizing the spanwise lift distribution for the strip as given by Equation (4.42).

If the strip is far enough from the body so that no disturbances strike the body $(m c' \leq \xi \leq \frac{b^*}{2})$, the over- and underestimates are the same and, obviously, are exact and the lift and rolling moment about the axis of the strip are given by Equations (4.44) and (4.45) respectively.

When the strip lies in the range $0 \leq \xi \leq mc'$, disturbances will strike the body and the estimates must be derived. For the underestimate, the lift is changed and the asymmetry in the pressure distribution shows that the center of pressure moves to the outboard side of the strip and, hence, a positive rolling moment about the strip axis results. The method of computing the lift and

rolling moment should be obvious and only the result will be given here. The lift is given by

$$dL = \frac{4mqc'(\xi)\alpha(\xi)}{\pi}\left(\pi + \xi' \operatorname{sech}^{-1}\xi' - \cos^{-1}\xi'\right) d\xi' \tag{4.411}$$

where $\xi' = \xi/mc'$ and the rolling moment about the axis of the strip is given by

$$dM = \frac{2m^2qc'(\xi)^2\alpha(\xi)}{\pi}\left(\sqrt{1-\xi'^2} - \xi'^2 \operatorname{sech}^{-1}\xi'\right) d\xi \tag{4.412}$$

For the overestimate, the lift is the same as when no disturbances strike the body since the disturbances which strike are completely reflected back onto the fin. Then the lift is given by Equation (4.44). Since the pressure distribution is not symmetric, a rolling moment is developed which, by obvious integrations, is given by

$$dM = \frac{4m^2qc'(\xi)^2\alpha(\xi)}{\pi}\left(\sqrt{1-\xi'^2} + \xi'^2 \operatorname{sech}^{-1}\xi' - 2\xi' \cos^{-1}\xi'\right) d\xi \tag{4.413}$$

Subsonic leading edge--For a subsonic leading edge, only the underestimate is easy to derive. The reflecting wall in the overestimate will cause the disturbances to be reflected back onto the fin and, if the strip is near enough to the body, the disturbances will encounter the leading edge before passing off the trailing edge. Some reflection phenomenon takes place at the leading edge and the reflected waves might strike the body again. As the strip approaches the wing-body juncture, this reflection between the wall and the

leading edge occurs progressively more and more times before all of the disturbances from the strip pass off the trailing edge. This problem requires repeated use of Evvard's method and would lead to very complicated expressions for the lift and the moment. This solution has not been carried out.

When the disturbances do not strike the body $(mc' \leq \xi \leq \frac{b^*}{2})$ the over- and underestimates are the same and are given by Equations (4.49) and (4.410).

When the strip lies in the range $0 \leq \xi \leq mc'$, the underestimate is obtained by obvious integrations using Equation (4.47). The lift is given by

$$dL = \frac{4mq\,c'(\xi)\alpha(\xi)}{\pi}\left\{\xi' \operatorname{sech}^{-1}\left[\frac{\xi'(1+d)}{2d+\xi'(1-d)}\right] + \sqrt{d}\cos^{-1}\left[\frac{(1-d)-2\xi'}{1+d}\right]\right\} d\xi \qquad (4.414)$$

and the moment is

$$dM = \frac{2m^2q\,c'(\xi)^2\alpha(\xi)}{\pi}\left\{\sqrt{d}\sqrt{d+(1-d)\xi'-\xi'^2} - \xi'^2 \operatorname{sech}^{-1}\left[\frac{\xi'(1+d)}{2d+\xi'(1-d)}\right] - \right.$$
$$\left. - \frac{\sqrt{d}(1-d)}{2}\cos^{-1}\left[\frac{(1-d)-2\xi'}{1+d}\right]\right\} d\xi \qquad (4.415)$$

It should be noted that an overestimate can be obtained if the fin has the same angle of attack throughout since the problem is reduced to a narrow-delta fin adjacent to a supersonic vertical fin. This is just the mixed cruciform aileron discussed previously.

All of these estimates will apply for any multi-fin delta wing-body configuration if the fins do not interact (see next section). By integrating with respect to ξ the proper expressions across the fin, the rolling moment about the body axis is obtained. The rolling moment coefficients will be based on the area $(\frac{bc}{2})$ and span (b) of one of the plane wings which compose the configuration, i.e. a pair of fins in the same plane extended into the body to form the basic plane wing (see Figure 2). The rolling moment coefficient for a single fin is given by

$$C_l = \frac{2}{gb^2C}\left\{\int_0^{\frac{mc^*}{1+f}}\left[(r+\xi)\,dL + dM\right] + \int_{\frac{mc^*}{1+f}}^{b/2}\left[(r+\xi)\,dL + dM\right]\right\} \qquad (4.416)$$

where the first integration is over the region of ξ where the disturbances from the elementary strip strike the body and the second integration covers the region where the disturbances do not strike the body. The proper expressions for dL and dM are to be substituted depending upon the estimate desired and the leading edge condition.

These estimates are of course equivalent to certain complete planar wing problems. The overestimate is just the half delta fin normal to a wall with supersonic leading edges or, by reflection, half of a delta wing which has symmetric twist (see previous discussion for cruciform wing roll problems in Section 4.2). The underestimate is the half delta fin adjacent to a flat

plate (in the same plane) which is at zero angle of attack and which extends ahead of any disturbances from the fin. If the lift and the rolling moment are known for the fin for either of these problems, the corresponding estimate is immediately obtained. These known results are usually in terms of the dimensions of the delta wing formed from two half delta fins (c* and b*). If C_L^* and C_l^* are the lift and moment (about the wing-body juncture) coefficients based on the area and span of the two half delta fins, the rolling moment coefficient about the body axis for a single fin based on the area and span of the delta wing extended into the body is given by

$$C_l = \frac{1}{2} A(1-A)^2 C_L^* + (1-A)^3 C_l^* \qquad (4.417)$$

D. Limits of Fin-Fin Interaction

The estimates discussed above can be used only if the disturbances which are propagated around the body do not encounter other fins. For, if this occurs, rolling moments will be induced which the estimates do not account for. For a given Mach number and a given fin, the body diameter can be made large enough so that the fins do not interact. Obviously this body diameter will be different for plane and cruciform wings. This is illustrated in Figure 30 where the limiting cases of a

disturbance from a fin leading edge-body juncture just striking the trailing edge of the next fin are shown for the plane and cruciform cases.

The disturbance which passes onto the body propagates along the Mach angle at all points on the body. From this fact, the path of the disturbance from the wing leading edge-body juncture is easily determined.

Supersonic leading edges--For the plane wing, it is readily seen that the fins do not interact if $\pi r \geq mc^*$ or, in another form, if

$$A \geq \frac{f}{\pi + f} \tag{4.418}$$

The estimates can be applied to a cruciform wing if $\pi r/2 \geq mc^*$ or if

$$A \geq \frac{2f}{\pi + 2f} \tag{4.419}$$

Note that if f = 0 the estimates apply for all values of A as would be expected since this is the case for no fin-fin interference. As f increases from 0 to 1, the interval of A values decreases.

Subsonic leading edges--These results are easily obtained by substituting 1/d for f in Equations (4.416) and (4.417). Then,

the estimates apply for a plane wing if

$$A \geq \frac{1}{1+\pi d} \tag{4.420}$$

and for a cruciform wing if

$$A \geq \frac{2}{2+\pi d} \tag{4.421}$$

Note that the estimates apply for a progressively smaller interval of A values as d approaches zero. When d = 0, the estimates cannot be applied since this is the slender body case and the fins may be considered as always interacting.

Using the estimates together with these limits on their validity, the strips can be superimposed by integration to give the over- and underestimates for any twisted wing. If the spanwise distribution of angle of attack is complicated, the integrations will probably have to be carried out graphically or numerically.

For general multi-fin wings, the interval of A values for which the estimates apply will decrease as the number of fins is increased. For $N = \infty$, the estimates cannot be used since the fins always interact (except for f = 0). However, this case has been solved exactly by E. W. Graham (References 22 and 23) and can be useful for estimating multi-fin problems.

E. Roll Due to Aileron Deflection

Results for plane and cruciform problems will be presented for both supersonic and subsonic leading edges. It will be assumed that only the horizontal fins are deflected by $\pm \delta$ for the

cruciform problem.

Supersonic leading edges--For the overestimate, the lift and rolling moment for a fin are known from the results for the horizontal fins of the cruciform wide-delta aileron with no body. Hence, Equation (4.417) may be used. The lift coefficient is two-dimensional based on the deflected area (fin area), hence

$$C_L^* = \frac{2\delta}{\beta}$$

since C_L^* is based on twice the area of the fin. C_l^* is obtained by taking half of the result for the horizontal fins of the cruciform wide-delta aileron (Equation (4.27)). Substituting these results into Equation (4.417) and doubling this result gives the overestimate for two deflected fins

$$\beta C_{l_\delta} = \frac{2(1-A)^2}{3\pi}\left[3\pi A + 2(1-A)\left(\frac{\cos^{-1} f}{\sqrt{1-f^2}} + f\right)\right] \tag{4.422}$$

$$\beta C_{l_\delta}\Big|_{f=0} = \frac{2}{3}(1-A)^2(1+2A) \tag{4.422a}$$

$$\beta C_{l_\delta}\Big|_{f=1} = \frac{2(1-A)^2}{3\pi}\left[4 + (3\pi - 4)A\right] \tag{4.422b}$$

For the underestimate, elementary strips will be integrated over the right horizontal fin using Equation (4.416). For the first integral dL and dM are given by Equations (4.411) and (4.412) respectively. For the second integral dM = 0 and dL is given by

Equation (4.44). Substituting into Equation (4.416) and multiplying by two will give

$$C_l = \frac{16m}{b^2 C}\left\{\int_0^{b^*/2}(r+\xi)\alpha(\xi)c'(\xi)\,d\xi + \frac{1}{\pi}\int_0^{\frac{mc^*}{1+f}}(r+\xi)\alpha(\xi)c'(\xi)\left(\xi' \operatorname{sech}^{-1}\xi' - \cos^{-1}\xi'\right)d\xi + \right.$$

$$\left. + \frac{m}{2\pi}\int_0^{\frac{mc^*}{1+f}}\alpha(\xi)\,c'(\xi)^2\left(\sqrt{1-\xi'^2} - \xi'^2 \operatorname{sech}^{-1}\xi'\right)d\xi\right\} \qquad (4.423)$$

Using the notations and relations

$$\xi^* = \xi/mc^* \qquad r^* = r/mc^* \qquad \xi' = \frac{\xi}{mc'(\xi)} = \frac{\xi^*}{1-f\xi^*}$$

$$c'(\xi) = c^*(1-f\xi^*)$$

and noting that for this case $\alpha(\xi) = \delta$, this equation can be put in the nondimensional form

$$\beta C_{l_\delta} = 4f^2(1-A)^3\left\{\int_0^{1/f}(r^*+\xi^*)(1-f\xi^*)\,d\xi^* + \frac{1}{2\pi}\int_0^{\frac{1}{1+f}}(1-f\xi^*)\sqrt{(1-f\xi^*)^2-\xi^{*2}}\,d\xi^* - \right.$$

$$\left. - \frac{1}{\pi}\int_0^{\frac{1}{1+f}}(r^*+\xi^*)(1-f\xi^*)\cos^{-1}\frac{\xi^*}{1-f\xi^*} + \frac{1}{\pi}\int_0^{\frac{1}{1+f}}\xi^*\left(r^*+\frac{\xi^*}{2}\right)\operatorname{sech}^{-1}\frac{\xi^*}{1-f\xi^*}\,d\xi^*\right\}$$

These integrations are tedious but straightforward and yield finally the underestimate

$$\beta C_{l_\delta} = \frac{2(1-A)^2}{3\pi}\left[(1+2A)\left(\frac{\pi}{2} + \frac{\cos^{-1}f}{\sqrt{1-f^2}}\right) + f(1-A)\right] \qquad (4.424)$$

$$\beta C_{l_\delta}\Big|_{f=0} = \frac{2}{3}(1-A)^2(1+2A) \qquad (4.424a)$$

$$\beta C_{l_\delta}\Big|_{f=1} = \frac{2(1-A)^2}{3\pi}\left[(1+\pi)A + 2 + \frac{\pi}{2}\right] \qquad (4.424b)$$

Results for plane and cruciform wing-body combinations are shown in Figures 31 and 32 respectively for three values of the parameter f. For a given value of f, the curves for the under- and overestimates are indicated by the same type of line. Each pair of curves is broken at a value of A indicated by a short solid line. These are the values of A above which the estimates are valid and, for the sake of brevity, will be denoted by A_L. A_L is given by Equations (4.418) and (4.419) when the equal signs are taken. For $A \geq A_L$ the curves are given by Equations (4.422) and (4.424). The endpoints for A = 0 are known exactly from Figure 13. The curves are then completed by drawing in curves between the known values at A = 0 and the known estimates at $A = A_L$. These curves are not drawn tangent to the estimate curves since it is expected that the exact solution to this problem will consist of two different expressions exhibiting the same type of slope discontinuity. Furthermore, the curves are drawn convex upward since this appears to be the most reasonable shape. In most cases it is rather easy to complete the curves in a reasonable fashion.

As f decreases from unity, the over- and underestimate curves approach each other and A_L decreases. This trend is evident when it is remembered that f = 0 means no fin-fin interference and, hence, $A_L = 0$. Furthermore, f = 0 means that the over- and underestimates coincide to a single exact curve.

According to the definition, wing-body interference is given in Figure 31 by the difference between the one value of βC_{l_δ} for A = 0 (plane aileron) and βC_{l_δ} for any desired values of A and f. Obviously, for A = 1, the body covers the plane aileron completely and the interference is 100 percent.

Fin-fin interference for the cruciform aileron is given by the difference between the ordinates of Figures 31 and 32 for given values of A and f. It is apparent that this difference arises because the vertical fins have been added to the plane wing-body configuration. As expected, fin-fin interference decreases with decreasing f.

For A = 0 only fin-fin interference occurs. For $0 < A < A_L$ both interferences contribute to the reduction in rolling moment. For $A \geq A_L$ only wing-body interference occurs.

For multi-fin wing-body combinations other than cruciform, the same methods can be applied. The values of A_L will increase with N and this will make the curves which are drawn in for $0 \leq A \leq A_L$ less convincing. Furthermore the ordinates for A = 0 are estimates from previous results.

Subsonic leading edges--As mentioned previously, the overestimate can be obtained since the problem for the horizontal fins of a mixed cruciform aileron reduces to a plane narrow-delta wing problem for which the solution is known. The pressure distribution on the wing is given by Equation (4.214). Using this pressure

distribution and Equation (4.417), the overestimate is easily obtained. It is

$$\beta C_{l_s} = \frac{(1-A)^2 d}{3E(\sqrt{1-d^2})}\left[4 + (3\pi - 4)A\right] \tag{4.425}$$

$$\beta C_{l_s}\Big|_{d=1} = \frac{2(1-A)^2}{3\pi}\left[4 + (3\pi - 4)A\right] \tag{4.425a}$$

The underestimate can be obtained by integration of elementary strips using Equation (4.416). Substitution of Equations (4.414) and (4.415) into the first integral and Equations (4.49) and (4.410) into the second integral, integration, and a great deal of algebra will reduce finally to

$$\beta C_{l_s} = \frac{2(1-A)^2}{3\pi}\left\{\left[3d(1+A) - (1-A)\right]\frac{\tan^{-1}\sqrt{d}}{\sqrt{d}} + \frac{3d(1+A)+(1-A)}{1+d}\right\} \tag{4.426}$$

$$\beta C_{l_s}\Big|_{d=1} = \frac{2(1-A)^2}{3\pi}\left[(1+\pi)A + 2 + \frac{\pi}{2}\right] \tag{4.426a}$$

Results are shown in Figures 33 and 34 for the plane and cruciform configurations respectively. The complete curves have been constructed using the same procedure as described above for supersonic leading edges. For the cruciform case, it will be remembered that the endpoints for A = 0 are approximate. As d decreases, A_L increases and the curves which are drawn between A = 0 and A = A_L become increasingly difficult to define. However,

it is expected that such curves still supply reasonable estimates.

F. Damping in Roll

The over- and underestimates for damping in roll can be obtained using the methods described for the aileron problem. For this case the angle of attack distribution is no longer constant over the fin but is expressed by

$$\alpha(\xi) = -\frac{p(r+\xi)}{U} \tag{4.427}$$

for the right horizontal fin. Since the plane and cruciform cases are to be considered, results will be presented for four fins, i.e. two plane wings or a cruciform wing.

The estimates have been obtained only for supersonic leading edges. The underestimate for subsonic leading edges can be obtained using the elementary strip. However, the overestimate for subsonic leading edges requires the solution for a twisted narrow-delta wing. This problem is very difficult and the writer has not attempted to obtain the solution.

Supersonic leading edges-- Both estimates were obtained by integrating the elementary strip estimates across the fin. The details of the calculations will not be given.

The overestimate is given by

$$\beta C_{l_p} = -\frac{2(1-A)^2}{3\pi(1-f^2)}\left\{(1-A)\left[(2-3f^2)+A(2-f^2)\right]\frac{\cos^{-1}f}{\sqrt{1-f^2}} + 2\pi A(1-f^2)(1+2A) + \right.$$

$$\left. + f(1-A)\left[(2-f^2)+A(2-3f^2)\right]\right\} \tag{4.428}$$

$$\beta C_{l_p}\Big|_{f=0} = -\frac{2}{3}(1-A)^2(1+2A+3A^2) \tag{4.428a}$$

$$\beta C_{l_p}\Big|_{f=1} = -\frac{4}{9\pi}(1-A)^2\left[5+(2+3\pi)A+(6\pi-7)A^2\right] \tag{4.428b}$$

The underestimate is given by

$$\beta C_{l_p} = -\frac{(1-A)^2}{3\pi(1-f^2)}\left\{\left[(2-3f^2)(1+2A)+3A^2(2-f^2)\right]\frac{\cos^{-1}f}{\sqrt{1-f^2}} + \pi(1-f^2)(1+2A+3A^2) + \right.$$

$$\left. + f(2-f^2)(1-A)(1+3A)\right\} \tag{4.429}$$

$$\beta C_{l_p}\Big|_{f=0} = -\frac{2}{3}(1-A)^2(1+2A+3A^2) \tag{4.429a}$$

$$\beta C_{l_p}\Big|_{f=1} = -\frac{(1-A)^2}{9\pi}\left[(10+3\pi)(1+2A)+3(2+3\pi)A^2\right] \tag{4.429b}$$

These results are shown in Figures 35 and 36 for two plane wings and for the cruciform wing respectively. The results for two plane wings are shown in Figure 35 so that a direct comparison with Figure 36 will give the fin-fin interference for the cruciform wing. The underestimate for f = 1 was incorrectly calculated in Reference 19 and has been corrected here.

These results are qualitatively identical with those for the aileron problem and will not be discussed further.

Improved Underestimate--It would be very desirable if, in some relatively simple way, it could be determined which of the estimates is closer to the exact solution. This would act as a guide for taking data from the graphs, particularly for the cases where the over- and underestimate curves are not very close together.

For the particular case of damping in roll for a plane wide-delta wing-body combination, Tucker and Piland (Reference 20) have used an underestimate which is different from that used here. Their underestimate appears to be valid for the rolling moment, although it is not as convincing as the one used here. It does not seem possible to determine whether or not their underestimate will bracket the actual velocity distributions. Even for this one case their underestimate is particularly interesting because it lies much closer to the overestimate used here (and used also in Reference 20). This would mean that the actual solution is closer to the overestimate than to the underestimate used here. Since their method does not generalize in any useful way to other roll problems or to multi-fin wing-body problems, it cannot be used to replace the underestimate used here. However, from their improved underestimate for this one case, it seems reasonable that

the exact solution will favor the overestimate for other roll problems and for multi-fin wing-body configurations. It will be seen later that other evidence helps to substantiate such a statement.

Tucker and Piland's reasoning and results will now be presented in an abbreviated discussion. First, they look at the limiting cases for the plane wing-body problem when A approaches zero and when A approaches unity. As A approaches zero the spanwise twist approaches that for the plane wing for damping in roll (antisymmetric linear twist). As A approaches unity, the body acts like a vertical wall. They use the vertical wall case as an overestimate just as used here. However, for the underestimate, they use the other limiting case of antisymmetric linear twist in such a way that, when A = 0, the correct twisted wing is obtained.

Their underestimate reduces to a planar wing problem for a twisted delta wing the right half of which has the angle of attack distribution of the fin and the left half of which has an angle of attack distribution determined by simply continuing this same twist to the left. This is shown in Figure 37 together with the underestimate used here. Figure 37(a) shows the angle of attack distribution for a fin of a wing-body configuration. Figure 37(b) shows the underestimate used by Tucker and Piland as an equivalent planar wing problem. The twist of the left half of the wing is obtained by just continuing the slope of the $\alpha(\bar{\zeta})$ curve to the

left. This problem can be decomposed as shown into a flat rolling wing plus a flat wing at a negative angle of attack. The corresponding underestimate used in this thesis is shown in Figure 37(c) where the left half of the wing is a flat plate at zero angle of attack.

It should be noted that Tucker and Piland's underestimate approaches the correct endpoints at A = 0 and A = 1. This single curve will then be the underestimate for the entire range $0 \leq A \leq 1$ without any regions limited by fin-fin interaction if the plane wing-body configuration is considered.

The solution may be obtained by calculating the lift and rolling moment coefficients for the right half of the wing shown in Figure 37(b) and then substituting into Equation (4.417). This solution was not given explicitly in Reference 20. It is easily obtained and is given by

$$\beta C_{l_p} = -\frac{2(1-A)^2}{3\pi}\left\{4A(1-A)\left[\frac{f(2-f^2)\sqrt{1-f^2}+(2-3f^2)\cos^{-1}f}{(1-f^2)^{3/2}}\right]+\pi\left[6A^2+(1-A)^2\right]\right\} \tag{4.430}$$

$$\beta C_{l_p}\Big|_{f=0} = -\frac{2}{3}(1-A)^2(1+2A+3A^2) \tag{4.430a}$$

$$\beta C_{l_p}\Big|_{f=1} = -\frac{2(1-A)^2}{9\pi}\left[3\pi+2(20-3\pi)A+(21\pi-40)A^2\right] \tag{4.430b}$$

These results are for four fins (i.e. two plane wing-body configurations) so that direct comparison with previous results can be made. The result for f = 1 is shown in Figure 38. Also shown are the over- and underestimates previously derived (see Figure 35). Note that, over most of the range of A, the exact solution must be closer to the overestimate than to the underestimate used here.

Although derived from arguments for the plane wing, this underestimate can be used for the cruciform wing if the curve is cut off when the fins interact. This is obvious since until the fins interact the number of fins is immaterial. The result for the cruciform wing for f = 1 is shown in Figure 39. Here it is seen that the exact solution definitely must favor the overestimate over the entire range of A.

G. Equilibrium Rate of Roll

Using Equation (4.237), the over- and underestimates for the equilibrium rate of roll for plane and cruciform wing-body combinations can be obtained. Since both $\beta \hat{C}_{l_p}$ and $\beta \hat{C}_{l_s}$ were obtained only for the wide-delta case, these are the results which can be presented.

Supersonic leading edges--The results are shown in Figures 40 and 41 for the plane and cruciform cases respectively.

The overestimate is obtained from Equations (4.422) and (4.428) and the underestimate is obtained from Equations (4.424) and (4.429). The remaining portions of the curves are constructed as before.

4.5 Fin-Fin and Wing-Body Interference--High Aspect Ratio.

The lift and roll problems are generally much easier for high-aspect-ratio problems. The afterbody problem can be neglected because of the very small lift carried by the afterbody relative to the lift of the wings. The wing-body lift results can be obtained from Reference 12 and some general remarks on lift will be found in Reference 11.

Delta Wings--The roll results presented here will apply. As explained in Section 4.3, f will generally be small and, hence, the over- and underestimate curves will be close together and approximate well to the exact solution.

Rectangular Wings--The remarks in Section 4.3 apply here also.

4.6 Wing-Body-Tail Interference

This is the most difficult type of interference to study in detail both theoretically and experimentally. It is in this interference that the really essential difference between high- and low-aspect-

ratio configurations arises. Whereas for the high-aspect-ratio subsonic airplane configuration it was possible to obtain engineering answers by linearized theory and some simple corrections for the deflection of the vortex sheets, it is not possible to use linear theories for the low-aspect-ratio configurations and further assumptions are necessary in order to account for the nonlinear behavior of the vortex sheets. Furthermore, the fact that the body diameter may be of the order of the wing span adds to the difficulties of the low-aspect-ratio configurations.

Two recent papers (References 15 and 17) on the lift problem represent the first good theoretical papers which have made it possible to obtain reasonable estimates of wing-body-tail interference for low-aspect-ratio configurations. In the following discussions this writer will use results from these papers without much explanation. For very complete and clear discussions of these results and the methods which lead to them the reader is referred to these papers.

A. Mechanism of Interference

As previously remarked, this interference problem is associated with the effects of the vortex sheets from the wing of a wing-body-tail configuration on the tail. The following description of the mechanism of this interference applies to general multi-fin

wing-body-tail configurations and to general aerodynamic problems.

Whenever any of the wing fins carries a spanwise lift distribution, a vortex sheet passes downstream from the trailing edge of that fin. For a general multi-fin wing, vortex sheets will generally pass downstream from one or more of the fins. These vortex sheets will trail downstream about the body and will deflect and distort under the influence of the body and the spatial distribution of vorticity. This is an extremely nonlinear problem whose exact solution is beyond present-day mathematics. Associated with these vortex sheets is a cross-flow velocity field. At the tail, this cross-flow field will introduce apparent angle of attack distributions on the tail fins which result in induced forces. This is what is referred to as wing-body-tail interference. This general mechanism is illustrated schematically in Figure 5(a) where α_v denotes the flow angle distributions induced by the cross-flow velocities.

For the usual type of wing-body-tail configurations where the span of the wing fins is greater than the span of the tail fins, the lifts and rolling moments induced on the tail generally oppose those of the wing. However, it is possible that, for other types of configurations such as the canard, the lifts and rolling moments induced on the tail (wing for the canard) may be in the same direction as those of the wing.

B. Background

The problem of wing-body-tail interference arose originally, of course, with the high-aspect-ratio subsonic airplane. It was found primarily through experiments that the vortex sheet from the wing was practically undistorted at the tail position although there was some deflection of the sheet away from the plane of the wing. By using linearized wing theory together with some small corrections for the deflection of the vortex sheet, it was possible to compute the cross-flow field at the tail with sufficient accuracy to supply good engineering results for wing-body-tail interference. Since the wing-body configurations were similar for most subsonic airplanes, it was further possible to develop general design rules for the effects of wing-body-tail interference.

As has so often happened at the start of investigations for supersonic flow, many of the methods and results of subsonic flow were carried over. This particular subject was no exception. Until recently most theoretical work on the cross-flow fields behind plane wings in supersonic flow assumed that linearized theory could be used throughout. According to linearized theory, the vortex sheet from the wing passes downstream undistorted and undeflected, i.e. it follows the linearized stream lines. Linearized calculations for the cross-flow field behind lifting wings can be found, for example, in References 39, 40, and 41 and further

references will be found listed in Reference 40. In Reference 39 it was found that the Trefftz-plane (infinitely far downstream) values of cross-flow velocities were obtained for all practical purposes a few chord lengths downstream of the wing. This led to the development of some elegant Trefftz-plane methods in References 39 and 42.

Experimental evidence soon showed that the undeflected undistorted vortex sheet did not give the correct answers for low-aspect-ratio configurations. This led to a study by Martha Graham (Reference 28) of the simplified case of wing-tail interference using two alternate extreme assumptions about the vortex sheet from the wing. The two alternate assumptions were, first, that the sheet was deflected but undistorted or, second, that the sheet was completely rolled up and could be represented by two deflected vortices. At the time it was not known which assumption, if either, was the more realistic picture and what governed the characteristics of the vortex sheet.

Recently two papers (References 15 and 17) showed that, for a low-aspect-ratio wing, the assumption of rolled up vortices is generally more realistic. Reference 17 studies the parameters which affect the rolling-up of the vortex sheet. Reference 15 uses the rolled-up vortices and studies in detail the incompressible

motion of two vortices in the presence of a circular cylinder as an approximation to the motion of the rolled-up vortex sheets for a low-aspect-ratio wing-body configuration.

All of these studies were concerned with the lift problem for plane wings or plane wing-body combinations. The first calculations for cruciform wings were made in Reference 18 assuming undistorted and undeflected vortex sheets for the roll due to aileron deflection problem. Some further remarks were made in Reference 19. In general, multi-fin problems other than cruciform are untouched.

C. Problems to be Solved

The first problem which must be solved for the wing-body-tail interference problem is the vorticity at the trailing edges of the wing fins of a wing-body combination. For plane wings and for cruciform wings with supersonic leading edges, exact linearized solutions have been obtained if there is no body for many planforms and many aerodynamic problems. However, if a body is present, there are practically no solutions even for the simplest cases. In general it is expected that linearized solutions will supply useful results.

The next important problem which must be solved is the motion of the vortex sheets as they move downstream to the tail. Contained in this problem is the calculation of the cross-flow

velocity field at the tail section. As mentioned before, References 15 and 17 are two excellent papers which have studied this problem for lift.

The final problem is the calculation of induced tail effects. Generally, this problem reduces to a wing-body problem with rather complicated distributions of angles of attack on the fins.

D. Rolling Up of the Vortex Sheets

It is the purpose here to discuss briefly the results of References 15 and 17 with reference particularly to the low-aspect-ratio missile configurations. These papers considered the lift problem for plane configurations and generally considered lift distributions which were nearly elliptic. It is important to point out how this work applies to the cruciform configuration and to the roll problems.

From similarity considerations, Spreiter and Sacks show that the distance downstream of the trailing edge of a fin at which the vortex sheet may be considered essentially rolled up, e, is given in terms of chord lengths by

$$\frac{e}{c^*} = K \frac{AR}{C_L} \left(\frac{b^*}{c^*} \right) \tag{4.61}$$

where AR is the aspect ratio and K is a constant of proportionality depending upon the spanwise lift distribution (or vorticity distribution at the trailing edge). It is evident that decreasing the aspect

ratio or increasing the lift coefficient will make the vortex sheet roll up faster. For a given type of planform and angle of attack distribution the vorticity distribution at the trailing edge is determined. This distribution of vorticity determines K which decreases as the concentration of vorticity increases. For elliptic lift distribution on the fins K is approximately 0.28.

It is useful to discuss the meaning of Equation (4.61) in more physical terms. The distortion and rolling up of a vortex sheet is caused by the velocities induced at all points of the sheet by the distributed infinitesimal vortices at all other points. It is convenient to consider the vortex sheet to be composed of a large number of discrete vortices equally spaced and having strengths determined by the areas under the vorticity distribution curve for the particular intervals which the discrete vortices replace. If these vortices are all weak, the sheet will move a relatively large distance downstream before it is appreciably distorted. Any effect which increases the strength of some or all of the vortices will increase the rate of rolling up. If the aspect ratio is decreased and the lift coefficient is held constant, the effect is to increase the strengths of all the vortices and, hence, to decrease e. Increasing the lift coefficient for a given aspect ratio has the same effect. If both the aspect ratio and the lift coefficient are kept constant, there is one other way by which the strengths of at least part of the vortices can

be increased. This can be done by varying the shape of the spanwise load curve which in turn changes the shape of the vorticity distribution curve. The greater the curvature of the spanwise load curve the greater will be the concentration of vorticity. This will mean that some of the vortices will be very strong and the rest relatively weak and the sheet will roll up rapidly in the vicinity of the concentration of vorticity. The rest of the vortices will roll up slowly, but the major part of the vorticity will be in the region where it is concentrated. As mentioned before, K is a measure of the concentration of vorticity and is large when the vorticity is uniformly distributed and small when the vorticity is concentrated in smaller regions.

Over the range of the usual operating lift coefficients for high-aspect-ratio subsonic airplanes the vortex sheet is relatively undistorted at the tail position. The supersonic missile generally differs from the subsonic airplane in three important ways with regard to the speed of the rolling up of the vortex sheets: first, the aspect ratio is much lower, second, the lift coefficient is higher in order to obtain reasonable lifts and rolling moments and, third, the wing to tail distance is much greater. The first two differences cause actual increases in the speed of the rolling-up process and the last difference may be considered as an apparent increase in the speed of the rolling-up process. In general, the vortex sheet

will be rolled up long before the tail section of the missile is reached. In fact, the vortex sheet will usually be rolled up within one or two chord lengths downstream of the wing trailing edge and very often within less than a chord length.

The lift problem for plane wing-body configurations as studied in References 15 and 17 leads to vorticity distributions at the trailing edges of the fins which are all of one sign. However, when the roll problems are considered and when cruciform wings are included, it will be seen that the vorticity distribution at the trailing edge of a fin often changes sign. This leads to the possibility of the vortex sheet rolling up into two distinct vortices of opposite sign and different strengths. In fact, for low aspect ratios it is expected that this will occur. For such cases the variables in Equation (4.61) must be properly interpreted for the regions of different sign. For each region of vorticity of different sign the aspect ratio and lift coefficient must refer to the portion of the fin upstream of that region and K is a measure of the concentration of the vorticity in that region.

E. Theoretical Work Contained in this Section

The theoretical work by the writer is restricted to the problem of determining the sidewash distributions at the trailing edges of plane and cruciform delta wing-body combinations. Emphasis will be placed on the low-aspect-ratio configurations where it can

be assumed that the trailing vortex sheets are completely rolled up a short distance downstream of the wing trailing edges. References 15 and 17 use incompressible two-dimensional nonstationary vortex theory to compute approximately the motion of these rolled-up vortices as they proceed downstream. They assume the vortices to start at the trailing edges at the centroids of their corresponding vorticity distributions and to have strengths given by the integrated strengths of the corresponding vorticity distributions. With this in mind, total strengths and centroids of vorticity distributions will be presented as starting points for the calculation of the motion of the vortices.

Lift, incidence, aileron deflection, and damping in roll problems are studied for plane and cruciform delta wing-body combinations. Where possible both subsonic and supersonic leading-edges are treated.

F. Vorticity at Trailing Edges--Low Aspect Ratio

The over- and underestimate ideas used previously will be utilized here to estimate the vorticity distributions at the trailing edges of plane and cruciform delta wing-body combinations. The strengths and centroids of the distributions will also be estimated.

The estimates will be computed as before by reducing the problems to equivalent planar wing problems which can be solved by well known linearized methods. These estimates can be used

as long as the fins do not interact. The estimates for the strengths and centroids of the vorticity distributions can be completed by calculating the exact endpoint at $A = 0$ and connecting this endpoint to the estimates at $A = A_L$.

All calculations will be made for flow quantities at the trailing edges of the fins and, when such notation is omitted, this is to be understood.

The vorticity distributions are obtained by computing the velocity distributions at and tangent to the trailing edges. The symmetries in all of these problems are such that the vorticity distributions are given by twice these velocity distributions with the signs determined by the signs of the velocities which are usually obvious physically.

Basic Relations--Here some of the basic relations between the vorticity at the trailing edge and the forces or moments on the fin are presented. These relations are easily derived and are well known.

Consider the right horizontal fin of a plane or cruciform delta wing-body combination. The basic relations will be derived for this fin and their application to the vertical fins should be obvious. The spanwise distance from the wing-body juncture is denoted by x (or ξ), the vorticity at the trailing edge is $\gamma(x)$, and the potential and sidewash on the top side of the fin at the trailing

edge are denoted by $\varphi(x)$ and $u(x) = \varphi_x(x)$ respectively. The notation $(x \to \frac{b^*}{2})$ following any quantity denotes that the quantity is given for the region from some variable distance x to the wing tip $x = \frac{b^*}{2}$. If x = 0, i.e. the complete fin is considered, this notation may be omitted.

Since negative sidewash on the top side of the fin means positive vorticity, it is obvious that

$$\gamma(x) = -2\,u(x) = -2\,\varphi_x(x) \tag{4.62}$$

As previously shown (see Equation (4.222)), the spanwise lift distribution is given by

$$l(x) = \frac{4q}{U}\,\varphi(x) \tag{4.63}$$

The total circulation between x and $\frac{b^*}{2}$, $\Gamma(x \to \frac{b^*}{2})$, is given by

$$\Gamma(x \to \tfrac{1}{2}b^*) = \int_x^{b^*/2} \gamma(\xi)\,d\xi = -2\int_x^{b^*/2} \varphi_\xi(\xi)\,d\xi$$
$$= 2\,\varphi(x) = \frac{U}{2q}\,l(x) \tag{4.64}$$

In order to determine the distance of the centroid of vorticity from the wing-body juncture, it is necessary to compute the moment of the vorticity distribution about the wing-body juncture, M_Γ. This is given by

$$M_\Gamma(x \to \tfrac{b^*}{2}) = \int_x^{b^*/2} \xi\,\gamma(\xi)\,d\xi = 2x\,\varphi(x) + \frac{U}{2q}\,L(x \to \tfrac{b^*}{2}) \tag{4.65}$$

where $L(x \to \frac{b^*}{2})$ is the lift on the fin between x and $\frac{b^*}{2}$.

If Equation (4.65) is divided by Equation (4.64), the centroid of vorticity, $x_{c.v.}(x \to \frac{b^*}{2})$, is obtained.

Γ and M_Γ represent essentially the zero-th and first moments of the vorticity distribution. The second moment will not generally be calculated but it is of interest because it is related to the rolling moment. The second moment about the wing-body juncture is given by

$$\int_x^{b^*/2} \xi^2 \gamma(\xi)\, d\xi = 2x^2 \Phi(x) + \frac{U}{\rho} RM^*(x \to \tfrac{b^*}{2}) \tag{4.66}$$

where RM* is the rolling moment about the wing-body juncture.

Some useful conclusions about the applicability of the over- and underestimates can be drawn from these relations. The over- and underestimates differ only within the Mach cone from the vertex of the fin, i.e. $0 \le x \le mc^*$. Since the estimates are obtained from conical wing problems, the vorticity distribution will always be expressible in terms of the conical variable $x^* = \frac{x}{mc^*}$. Then, within the Mach cone, the various moments can be expressed as integrals of the type

$$\int_0^1 \xi^{*n} \gamma(\xi^*)\, d\xi^*$$

where n has integer values. $\gamma(\xi^*)$ will be the same for both estimates at $\xi^* = 1$. At $\xi^* = 0$ the overestimate will give the correct endpoint $\gamma(0) = 0$. However, since the underestimate will generally

have an angle of attack discontinuity at $\xi^* = 0$, $\gamma(\xi^*)$ will have a logarithmic infinity at $\xi^* = 0$. Then the estimates for γ will differ markedly in the vicinity of the origin. The moments of the estimates of γ will approach each other as n increases and obviously coincide for $n = \infty$. Thus it is seen that the estimates will bracket the correct solution closest for the rolling moment and will be increasingly poor brackets for the lift, the spanwise lift distribution (or Γ), and the vorticity distribution respectively. It will be found that the underestimate is of little use as a bracket for the vorticity calculations.

Body incidence in lift--The lift problem with no incidence can be decomposed by superposition into two simpler problems. This is shown in Figure 5(b) where E' and F are called "body incidence in lift" and "wing incidence in lift" respectively. The solution of these two simpler problems will supply the information for calculating general lift and incidence problems.

The problem of body incidence is further decomposed into problems E and G. The over- and underestimate solutions of problem G with the apparent twist due to the upwash about the body will now be obtained.

The apparent angle of attack due to the upwash about the body is assumed to be given by the slender body solution for the body, i.e. by the two-dimensional incompressible flow about a circular

cylinder (see, for example, Reference 11). Then the apparent twist is given by

$$\alpha(\xi) = \alpha_B \frac{r^2}{(\xi+r)^2} \tag{4.67}$$

The planar wing problems corresponding to the over- and under-estimates are shown in Figure 42.

The vorticity distribution at a point x of the trailing edge can be obtained by integrating the contributions of all elementary strips which affect this point. The vorticity due to an elementary strip is given essentially by Equation (4.43). As is apparent from Figure 20, only those strips which intersect the forward Mach cone from the point x will affect that point. The integrations can be set up from the data in Figure 20 if the chord and span of the wing are c*' and b* respectively.

For $0 \leq x \leq mc^*$, both estimates can be written down as one expression

$$\gamma(x) = \frac{2Um}{\pi}\left\{\int_{\frac{x-mc^*}{1+f}}^{0} \frac{\alpha(\xi)\,c'(\xi)\,d\xi}{x_1\sqrt{m^2c'(\xi)^2 - x_1^2}} + \int_{0}^{\frac{x+mc^*}{1+f}} \frac{\alpha(\xi)\,c'(\xi)\,d\xi}{x_1\sqrt{m^2c'(\xi)^2 - x_1^2}}\right\} \tag{4.68}$$

where the overestimate is given by the complete expression and the underestimate is obtained by using only the second integral. Noting that

$$x_1 = x - \xi \qquad c'(\xi) = \frac{2c^*}{b^*}\left(\frac{b^*}{2} - \xi\right) \qquad \text{for} \qquad \xi \geq 0$$

$$c'(\xi) = \frac{2c^*}{b^*}\left(\frac{b^*}{2} + \xi\right) \qquad \text{for} \qquad \xi \leq 0$$

$$\alpha(\xi) = \alpha_B \frac{r^2}{(\xi + r)^2} \qquad \text{for} \qquad \xi \geq 0$$

$$\alpha(\xi) = \alpha_B \frac{r^2}{(\xi - r)^2} \qquad \text{for} \qquad \xi \leq 0$$

and substituting into Equation (4.68), there results

$$\gamma(x) = \frac{2Uf\alpha_B r^2}{\pi}\left\{\int_0^{\frac{x+mc^*}{1+f}} \frac{\left(\frac{b^*}{2} - \xi\right) d\xi}{(\xi+r)^2(x-\xi)\sqrt{f^2\left(\frac{b^*}{2} - \xi\right)^2 - (x-\xi)^2}} - \int_0^{\frac{x-mc^*}{1+f}} \frac{\left(\frac{b^*}{2} + \xi\right) d\xi}{(\xi-r)^2(x-\xi)\sqrt{f^2\left(\frac{b^*}{2} + \xi\right)^2 - (x-\xi)^2}}\right\}$$

where, here, the first integral gives the underestimate and the complete expression gives the overestimate. When these integrations were carried out it was found that each estimate was given by different expressions over different regions of x determined by the relationship between mc and r. These different expressions arose quite formally when integrating quadratic square root expressions and will not be discussed further. The resulting expressions are complicated and, to simplify the form, the following notations are used

$$J = A + fx^*(1-A) \qquad F = f^2 - J^2$$

$$\overline{J} = A - fx^*(1-A) \qquad \overline{F} = f^2 - \overline{J}^2$$

$$G = \frac{f - x^* J}{A(1 - fx^*)} \qquad H = \frac{\sqrt{F(1-x^{*2})} + f - x^* J}{A(1 - fx^*)} \tag{4.69}$$

$$\overline{G} = \frac{f + x^* \overline{J}}{A(1 + fx^*)} \qquad \overline{H} = \frac{\sqrt{\overline{F}(1-x^{*2})} + f + x^* \overline{J}}{A(1 + fx^*)}$$

The underestimate for $0 \leq x^* \leq 1$ is given by the following equations:

For $mc > r$

$$\frac{\gamma(x)}{\alpha_B U} = \frac{2fA^2}{\pi J^2}\left[-\frac{1}{f}\operatorname{sech}^{-1}x^* + \frac{f(1-A)\sqrt{1-x^{*2}}J}{AF} - \frac{f^2-2J^2+J^3}{(-F)^{3/2}}\cos^{-1}G\right] \tag{4.610}$$

if $x > mc-r$ and

$$\frac{\gamma(x)}{\alpha_B U} = \frac{2fA^2}{\pi J^2}\left[-\frac{1}{f}\operatorname{sech}^{-1}x^* + \frac{f(1-A)\sqrt{1-x^{*2}}J}{AF} + \frac{f^2-2J^2+J^3}{F^{3/2}}\log|H|\right] \tag{4.611}$$

if $x < mc-r$. For $mc < r$, Equation (4.610) gives the vorticity distribution for all x.

The overestimate for $0 \leq x^* \leq 1$ is given by the following equations:

For $mc > r$

$$\frac{\gamma(x)}{\alpha_B U} = \frac{2fA^2}{\pi}\left\{\frac{1}{J^2}\left[-\frac{1}{f}\operatorname{sech}^{-1}x^* + \frac{f(1-A)\sqrt{1-x^{*2}}J}{AF} - \frac{f^2-2J^2+J^3}{(-F)^{3/2}}\cos^{-1}G\right] - \right.$$
$$\left. - \frac{1}{\bar{J}^2}\left[-\frac{1}{f}\operatorname{sech}^{-1}x^* + \frac{f(1-A)\sqrt{1-x^{*2}}\bar{J}}{A\bar{F}} + \frac{f^2-2\bar{J}^2+\bar{J}^3}{\bar{F}^{3/2}}\log\bar{H}\right]\right\} \tag{4.612}$$

if $x > mc-r$ and

$$\frac{\gamma(x)}{\alpha_B U} = \frac{2fA^2}{\pi}\left\{\frac{1}{J^2}\left[-\frac{1}{f}\operatorname{sech}^{-1}x^* + \frac{f(1-A)\sqrt{1-x^{*2}}J}{AF} + \frac{f^2-2J^2+J^3}{F^{3/2}}\log|H|\right] - \right.$$
$$\left. - \frac{1}{\bar{J}^2}\left[-\frac{1}{f}\operatorname{sech}^{-1}x^* + \frac{f(1-A)\sqrt{1-x^{*2}}\bar{J}}{A\bar{F}} + \frac{f^2-2\bar{J}^2+\bar{J}^3}{\bar{F}^{3/2}}\log|\bar{H}|\right]\right\} \tag{4.613}$$

if $x < mc-r$.

For $mc < r$, $\gamma(x)$ is given by Equation (4.612) if $x < mc-r$ and

$$\frac{\gamma(x)}{\alpha_B U} = \frac{2fA^2}{\pi}\left\{\frac{1}{J^2}\left[-\frac{1}{f}\operatorname{sech}^{-1}x^* + \frac{f(1-A)\sqrt{1-x^{*2}}J}{AF} - \frac{f^2-2J^2+J^3}{(-F)^{3/2}}\cos^{-1}G\right] - \right.$$
$$\left. -\frac{1}{\bar{J}^2}\left[-\frac{1}{f}\operatorname{sech}^{-1}x^* + \frac{f(1-A)\sqrt{1-x^{*2}}\bar{J}}{A\bar{F}} - \frac{f^2-2\bar{J}^2+\bar{J}^3}{(-\bar{F})^{3/2}}\cos^{-1}\bar{G}\right]\right\} \qquad (4.614)$$

if $x > mc-r$.

The over- and underestimates are the same for x lying outside the Mach cone from the vertex ($1 \le x^* \frac{1}{f}$). This result is much simpler and can be obtained using the same procedure as above. The final result is

$$\frac{\gamma(x)}{\alpha_B U} = -\frac{2fA^2}{J^2(-F)^{3/2}}(f^2-2J^2+J^3) \qquad (4.615)$$

where J and F are given by (4.69).

Figures 43, 44, and 45 show vorticity distributions for three different pairs of values of f and A. It is obvious that the over- and underestimates do not bracket the exact solution very closely. The underestimate does not attain the correct value $\gamma(0) = 0$ but has the logarithmic singularity mentioned before. The overestimate does have the correct value at the origin and it is expected that the exact solution will favor this estimate. Note that the underestimate shows regions of negative vorticity. This is known to be incorrect and is one more reason why the underestimate should not be expected to be very useful as an estimate for the vorticity problems.

Since the exact vorticity distribution is not expected to have a change in sign, a single vortex will start at the centroid of the distribution and have the strength Γ given by the area under the complete vorticity distribution curve. From Equation (4.64) it is seen that $\Gamma(0 \to \frac{b^*}{2})$ may be computed by calculating $2\phi(0)$. Because of the symmetry of the region of integration when x = 0, it is seen that the result for the overestimate is just twice that for the underestimate. Using elementary strip integration,

$$\Gamma = 2\phi(0) = \frac{2\alpha_B U r^2}{\pi} \int_0^{\frac{mc^*}{1+f}} \frac{\operatorname{sech}^{-1}\left|\frac{\xi}{f(b^*/2-\xi)}\right|}{(\xi+r)^2}\, d\xi$$

will give the result for the underestimate which becomes finally

$$\frac{\Gamma}{\alpha_B U(\frac{b^*}{2})} = \frac{2Af}{\pi\sqrt{A^2-f^2}} \cos^{-1}\left(\frac{f}{A}\right) \qquad \text{for} \quad f<A \tag{4.616}$$

$$= \frac{2Af}{\pi\sqrt{f^2-A^2}} \operatorname{sech}^{-1}\left(\frac{A}{f}\right) \qquad \text{for} \quad f>A \tag{4.616a}$$

$$= \frac{2}{\pi} f \qquad \text{for} \quad f=A \tag{4.616b}$$

The overestimate is obtained by just doubling the above results. The results are plotted in Figure 46 for two values of f. As expected, the over- and underestimates are useless as bracketing curves since the ordinate of the overestimate is just twice that of the underestimate. The short solid lines indicate the values of A_L. The estimates would normally be connected from A_L to the correct value at A = 0, however, since all estimates have the

correct value at A = 0, there is little point in drawing in lines different from those supplied by the estimates. It should be pointed out that these results are not useless since the overestimate has the correct endpoints at A = 0 and A = 1. It is expected that the exact solution will start from the overestimate at A = 1, move away from this curve towards the underestimate and then move back to the overestimate as A approaches zero. The only use of the underestimate is to indicate on which side of the overestimate curve the exact solution lies.

The moment of the complete vorticity distribution $M_\Gamma(0 \to \frac{b^*}{2})$ is related to the lift on the fin through Equation (4.65) with x = 0. The overestimate is easily computed using elementary strips and Equation (4.44). The result is given by

$$\frac{M_\Gamma}{\alpha_B U (\frac{b^*}{2})^2} = \frac{2fA(1-A+A\log A)}{(1-A)^2} \tag{4.617}$$

The underestimate is somewhat more complicated. It can be set up as an integration of elementary strips using Equation (4.411). This would give

$$M_\Gamma = 2\rho U \int_0^{b^*/2} c'(\xi)\alpha(\xi)\,d\xi + \frac{2\alpha_B U r^2}{\pi}\left\{\int_0^{\frac{1}{1+f}} \frac{\xi^* \operatorname{sech}^{-1}\left(\frac{\xi^*}{1-f\xi^*}\right)}{(\xi^*+r^*)^2}\,d\xi^* - \int_0^{\frac{1}{1+f}} \frac{(1-f\xi^*)\cos^{-1}\left(\frac{\xi^*}{1-f\xi^*}\right)}{(\xi^*+r^*)^2}\,d\xi^*\right\}$$

Substituting the proper quantities into the first integral leads to Equation (4.617). In the process of solving the second integral, integrals of the type

$$\int_0^1 \frac{\log(1+kx)\,dx}{x\sqrt{1-x^2}} \qquad k \le 1 \text{ or } k \ge 1$$

were encountered. By differentiating with respect to k, solving, and then integrating again, the solution of this integral may be given as

$$\frac{\pi^2}{8} - \frac{(\cos^{-1}k)^2}{2} \qquad \text{for} \quad k \le 1$$

$$\frac{\pi^2}{8} + \frac{(\cosh^{-1}k)^2}{2} \qquad \text{for} \quad k \ge 1$$

The last integration led to integrals of the type

$$\int_0^1 \frac{\log(1+kx)\,dx}{\sqrt{1-x^2}} \qquad k \le 1 \text{ or } k \ge 1$$

It was found necessary to integrate this numerically. Using the procedure described above, this definite integral can be written as the following indefinite integrals

$$M(k) = \int_0^k \frac{1}{\xi}\left(\frac{\pi}{2} - \frac{\cos^{-1}\xi}{\sqrt{1-\xi^2}}\right) d\xi \qquad \text{for} \quad k \le 1$$

$$M(1) + \int_{1/k}^1 \frac{1}{\xi}\left(\frac{\pi}{2} - \frac{\xi\,\mathrm{sech}^{-1}\xi}{\sqrt{1-\xi^2}}\right) d\xi \qquad \text{for} \quad k' = \frac{1}{k} \le 1$$

For numerical integration, the second expression can be expressed as

$$M(1) - \left[\frac{\pi}{2}\log k' - k'\,\mathrm{sech}^{-1}k' + \cos^{-1}k'\right] + Q(k')$$

where $$Q(k') = \int_{k'}^1 \left(\mathrm{sech}^{-1}\xi - \frac{\mathrm{sech}^{-1}\xi}{\sqrt{1-\xi^2}}\right) d\xi$$

M(k) and Q(k') were integrated graphically by counting squares and are plotted in Figure 47. The final results for M_Γ are

$$\frac{M_\Gamma}{\alpha_B U\left(\frac{b^*}{2}\right)^2} = \frac{2A}{(1-A)^2}\left\{\frac{f(1-A)}{2} + fA\log A + \frac{A}{2\pi}\left[(\cos^{-1}f)^2 - (\cos^{-1}\tfrac{f}{A})^2\right] + \frac{Af}{\pi}\left[M\left(\tfrac{f}{A}\right) - M(f)\right]\right\} \qquad (4.618)$$

for $f < A$

$$\frac{M_\Gamma}{\alpha_B U\left(\frac{b^*}{2}\right)^2} = \frac{2A}{(1-A)^2}\left\{\frac{f(1-A)}{2} + fA\log A + \frac{A}{2\pi}\left[(\cos^{-1}f)^2 + (\operatorname{sech}^{-1}\tfrac{A}{f})^2\right] + \frac{Af}{\pi}\left[M(1) - M(f) - \frac{\pi}{2}\log\left(\tfrac{A}{f}\right) + \right.\right.$$
$$\left.\left. + \frac{A}{f}\operatorname{sech}^{-1}\left(\tfrac{A}{f}\right) - \cos^{-1}\left(\tfrac{A}{f}\right) + Q\left(\tfrac{A}{f}\right)\right]\right\} \qquad \text{for } f > A \qquad (4.618a)$$

$$\frac{M_\Gamma}{\alpha_B U\left(\frac{b^*}{2}\right)^2} = \frac{2A}{(1-A)^2}\left\{\frac{1-A}{2} + A\log A + \frac{(\cos^{-1}A)^2}{2\pi} - \frac{A}{\pi}\left[M(A) - M(1)\right]\right\} \qquad \text{for } f = A \qquad (4.618b)$$

Dividing equations for M_Γ by the corresponding equations for Γ gives the centroid of vorticity $X_{c.v.}$. This is plotted in Figure 48 for two values of f. Qualitatively, the same remarks that were made with reference to Figure 46 apply here.

Wing incidence in lift--Here, the body is at zero angle of attack and the two fins are deflected by δ in the positive direction. From the calculations above, the methods to be used here are taken for granted and only the results will be given. These same estimates will of course apply to the aileron deflection problem for supersonic leading edges.

Outside the Mach cone $\left(1 \le x^* \le \frac{1}{f}\right)$ the estimates are the

same and the vorticity at the trailing edge is the constant sweep-back value

$$\frac{\gamma(x)}{\delta U} = \frac{2f}{\sqrt{1-f^2}} \tag{4.619}$$

For $0 \leq x^* \leq 1$, the overestimate is obtained directly from the side-wash results for the cruciform wide-delta aileron given in Reference 18 and is

$$\frac{\gamma(x)}{\delta U} = \frac{2f}{\pi\sqrt{1-f^2}} \left(\cos^{-1} \frac{f-x^*}{1-fx^*} - \cos^{-1} \frac{f+x^*}{1+fx^*} \right) \tag{4.620}$$

$$\left.\frac{\gamma(x)}{\delta U}\right|_{f=1} = \frac{4x^*}{\pi\sqrt{1-x^{*2}}} \tag{4.620a}$$

The underestimate is easily found to be

$$\frac{\gamma(x)}{\delta U} = -\frac{2}{\pi} \left[\operatorname{sech}^{-1} x^* - \frac{f}{\sqrt{1-f^2}} \cos^{-1} \frac{f-x^*}{1-fx^*} \right] \tag{4.621}$$

Some vorticity distributions are shown in Figure 49.

The integrated vorticity for the entire fin can be obtained from Equations (4.616) by letting $A \to 1$. As $A \to 1$, the body acts like a vertical wall and the angle of attack becomes a constant given by α_B. Then the underestimate is

$$\frac{\Gamma}{\delta U\left(\frac{b^*}{2}\right)} = \frac{2f}{\pi\sqrt{1-f^2}} \cos^{-1} f \tag{4.622}$$

and the overestimate is just double this result. These results are independent of A and a plot against A would show constant values

for each f with the overestimate having the correct values at A = 0 and A = 1.

M_Γ is easily obtained by calculating the lift on the fin. The overestimate is

$$\frac{M_\Gamma}{\delta U\left(\frac{b^*}{2}\right)^2} = f \tag{4.623}$$

The underestimate is

$$\frac{M_\Gamma}{\delta U\left(\frac{b^*}{2}\right)^2} = \frac{f}{\pi}\left(\frac{\pi}{2} + \frac{\cos^{-1} f}{\sqrt{1-f^2}}\right) \tag{4.624}$$

The centroid of vorticity is independent of A and the same remarks made above about Γ follow. The over- and underestimates are plotted against f in Figure 50. The underestimate is plotted just to indicate on which side of the overestimate the exact solution will lie.

The estimates for subsonic leading edges can also be computed. The overestimate sidewash distribution is given in Reference 39 and is

$$\frac{\gamma(x)}{\delta U} = \frac{2\left[x/\left(\frac{b^*}{2}\right)\right]}{E\left(\sqrt{1-d^2}\right)\sqrt{1-\left(\frac{x}{b^*/2}\right)^2}} \tag{4.625}$$

The underestimate can be computed by integrating elementary strips and is given by

$$\frac{\gamma(x)}{\delta U} = \frac{2}{\pi}\left[\frac{2}{1+d}\frac{\sqrt{1+d\left(\frac{x}{b^*/2}\right)}}{\sqrt{1-\left(\frac{x}{b^*/2}\right)}} - \log\left|\frac{\sqrt{1+d\left(\frac{x}{b^*/2}\right)}+\sqrt{1-\left(\frac{x}{b^*/2}\right)}}{\sqrt{1+d\left(\frac{x}{b^*/2}\right)}-\sqrt{1-\left(\frac{x}{b^*/2}\right)}}\right|\right] \tag{4.626}$$

Results are plotted in Figure 51.

The remainder of the desired quantities have been computed only for the overestimate. The vortex strength is

$$\frac{\Gamma}{\delta U\left(\frac{b^*}{2}\right)} = \frac{2}{E\left(\sqrt{1-d^2}\right)} \tag{4.627}$$

The moment of the vorticity is

$$\frac{M_\Gamma}{\delta U\left(\frac{b^*}{2}\right)^2} = \frac{\pi}{2E\left(\sqrt{1-d^2}\right)} \tag{4.628}$$

and the centroid is

$$\frac{X_{c.v.}}{\left(b^*/2\right)} = \frac{\pi}{4} \tag{4.628a}$$

Lift--By adding the results for the wing and body incidence cases so that the resultant configuration is a lifting wing-body with no incidence, the results for the lift case are obtained. Only the case of supersonic leading edges has been treated.

The estimates for vortex strength and position are shown in Figures 52 and 53 respectively. Here again it is seen that the overestimate has the correct endpoints at A = 0 and A = 1.

Morikawa's paper (Reference 12) has treated the lift problem and presents results for the lift of the fin alone. A brief comparison of results will indicate how well the overestimate can be expected to approximate to the exact solution. Morikawa plots the ratio of the lift on the wing (both fins) when in combination with

the body to the lift on the two fins when they are removed from the combination and placed together so as to form a wing alone. He denotes this parameter by $K^{(w)}$ and this will be used here just for this discussion. He brackets the exact solution by the limiting cases of infinite aspect ratio (overestimate) and zero aspect ratio (underestimate). His overestimate coincides with that used here. He also shows an approximate curve for f = 1.

These results together with the underestimates used here are shown in Figure 54. It is seen that the overestimate used here is practically exact for supersonic leading edges (and probably for the usual subsonic leading edges) for A greater than about 0.5. Then it can be expected that the exact solution will be given essentially by the overestimate for A near unity for all the results already presented and for those results which will be presented. As A decreases the exact solution will deviate further from the overestimate. By taking this behavior of the overestimate into account, it should be possible to make reasonable estimates of the strengths and positions of the starting vortices and even to estimate the vorticity distribution.

It is possible to estimate the strength and position of the vortex for subsonic leading edges using a combination of known endpoints and known slopes at these points. The sonic leading edge case can be used as a guide to the shape of the curves for

both subsonic and supersonic leading edges. The endpoints for f = d = 1 are known and, from the above discussion, the slope of the curve at A = 1 is known to be essentially that of the overestimate. These data can be taken from Figures 52 and 53.

Lagerstrom and M. E. Graham (Reference 15) have provided additional estimates which appear to give information about the slope near A = 0. They noticed that the pressures on the fins of a delta wing-body combination differ but little from the pressures on the corresponding regions of a delta wing alone having the same total span as the combination if slender body theory is used. They assumed that this would also be the case for the nonslender body subsonic leading edge case. It is obvious that this assumption must become poor with increasing A for it would predict infinite Γ for A=1. However, this assumption is probably good for A near zero and, hence, supplies information about the shape of the curves there. Using this assumption, they get for the strength of the vortex

$$\frac{\Gamma}{\alpha U(\frac{b^*}{2})} = \frac{2}{E(\sqrt{1-d^2})}\sqrt{\frac{1+A}{1-A}} \tag{4.629}$$

and for the position

$$\frac{X_{c.v.}}{(b^*/2)} = \frac{(1+A)}{2}\left[\frac{\cos^{-1}A - A\sqrt{1-A^2}}{(1-A^2)^{3/2}}\right] \tag{4.630}$$

These equations are correct for A = 0 and increasingly poor as A approaches one. Note that the position of the vortex is independent of d.

Equation (4.629) is plotted in Figure 55 for three values of d. The endpoints at A = 1 are known to be just twice the values at A = 0. Also shown is the overestimate for f = 1 taken from Figure 52. The overestimate gives the shape of the curve near A = 1 and Equation (4.629) gives the shape of the curve near A = 0. For d = f = 1, a curve can be faired between the known endpoints and shapes as shown in Figure 55. For other values of d, the curves will probably have the same shape. The curves for supersonic leading edges can also be modified according to the f = 1 curve.

Equation (4.630) is plotted in Figure 56. Also shown is the curve for f = 1 taken from Figure 53. Using the same arguments as above, a curve can be faired which will represent the centroid position for all d. The modification of the curve f = 1 can then be used to modify the supersonic results shown in Figure 53.

Roll due to aileron deflection--For this case and the damping in roll case it will be found that most of the types of ailerons and wings treated lead to vorticity distributions at the trailing edges of the fins which have sign changes. It is assumed that the aspect ratio is low enough so that the two regions of different sign

roll up into two distinct vortices of different strengths and of opposite signs. These will be referred to as the inboard and outboard vortices.

Four different cases of delta wing-body combinations with aileron deflection will be studied. They are the plane wide-delta aileron, the plane narrow-delta aileron, and the cruciform wide-delta aileron for the two cases of 2 and 4 fins deflected. In all cases it will be assumed that there are no net lateral forces so that only the rolling moment problem is considered, i.e. the body axis is in the free-stream direction. It must be pointed out here that the results for the strengths and initial positions of the vortices when lateral forces are included cannot be obtained, generally, by any superposition of these results for the pure roll and pure lateral force cases. Instead, it is necessary to superimpose the vorticity distributions (which is valid because of the use of linear theory) for the rolling and lateral force cases and then, from the resultant vorticity distributions, the vortex strengths and positions are computed. That the strengths and positions of the vortices cannot generally be obtained directly by superposition is due to the fact that these quantities are computed in connection with nonlinear assumptions about the distortion of the vortex sheets. Then the results presented here will apply only for the particular cases described above. However,

from the methods used here it will be obvious how the results for other aerodynamic problems can be estimated.

For the pure lift and incidence problems it is possible to superimpose two problems by a simple addition of Γ's and M_Γ's because the vorticity distributions are one-signed. However, when sign changes occur in the vorticity distributions (as for the roll problems) this procedure does not work.

Because of these vorticity regions of different signs, it is desirable to compute for all possible cases which might be superimposed the Γ's and M_Γ's as functions of x so that these quantities can be determined for any portions of the vorticity distributions. Such equations are given here for many of the cases treated but not for all. Those cases for which these equations are not presented here can usually be derived easily and, if not, a simple graphical integration may be employed.

For the four problems studied in this section and for all the remaining problems in this thesis, only the overestimate will be used. It was explained in great detail previously why the underestimate supplies little information for estimating results. It was also explained how the exact solution and the overestimate are related. It will be taken for granted that all of these ideas will be used with the results presented from here on. The overestimates for all of the aileron deflection problems are indepen-

dent of A and have the correct endpoint at A = 1. However, in contradistinction to the lift and incidence problems, the overestimate does not have the correct endpoint at A = 0. It will be necessary to compute the A = 0 endpoints for each problem and then connect these endpoints to the overestimates at the appropriate values of A_L using some reasonable curves which, admittedly, are fairly arbitrary in shape.

Consider first the plane wide-delta aileron problem. The results will be computed for the right fin which is at the angle of attack + δ and the results for the other fin are obtained from obvious symmetries. The overestimates are the same as for the wide-delta wing-incidence problem studied previously. The overestimates for the vorticity distribution, the strength of the vortex, and the moment of the vorticity distribution are given by Equations (4.619) and (4.620), double Equation (4.622), and Equation (4.623) respectively.

The results for the endpoint (A = 0) plane wide-delta aileron are easily obtained and the details will be omitted. It is first necessary to plot the vorticity distributions for the different values of f to determine the regions of vorticity of different sign. All calculations will be carried out for the two values f = 1 and f = 0.5. The vorticity distribution can be obtained from

Reference 18 and is

$$\frac{\gamma(x)}{\delta U} = \frac{2f}{\pi\sqrt{1-f^2}}\left(\cos^{-1}\frac{f-\bar{x}}{1-f\bar{x}} + \cos^{-1}\frac{f+\bar{x}}{1+f\bar{x}}\right) - \frac{4}{\pi}\,\mathrm{sech}^{-1}\bar{x} \tag{4.631}$$

for $0 \leq \bar{x} \leq 1$ and

$$\frac{\gamma(x)}{\delta U} = \frac{2f}{\sqrt{1-f^2}} \tag{4.632}$$

for $1 \leq \bar{x} \leq \frac{1}{f}$. For f = 1 the result is

$$\left.\frac{\gamma(x)}{\delta U}\right|_{f=1} = \frac{4}{\pi}\left(\frac{1}{\sqrt{1-\bar{x}^2}} - \mathrm{sech}^{-1}\bar{x}\right) \tag{4.633}$$

This is, of course, valid for $0 \leq \bar{x} \leq 1$. Vorticity distributions are plotted in Figure 57. It is seen that, for a certain outboard region, the vorticity is positive and, for the remaining inboard region, the vorticity is negative.

The vortex strengths can be computed from the following formulas with the notations in parenthesis having been defined in the Section "Basic relations":

$$\frac{\Gamma(\bar{x}\to 1)}{\delta U\left(\frac{b}{2}\right)} = \frac{2f}{\pi\sqrt{1-f^2}}\left[-\pi(1-f) + (1-f\bar{x})\cos^{-1}\frac{f-\bar{x}}{1-f\bar{x}} - (1+f\bar{x})\cos^{-1}\frac{f+\bar{x}}{1+f\bar{x}}\right] + \frac{4f}{\pi}\,\bar{x}\,\mathrm{sech}^{-1}\bar{x} \tag{4.634}$$

$$\left.\frac{\Gamma(\bar{x}\to 1)}{\delta U\left(\frac{b}{2}\right)}\right|_{f=1} = \frac{4}{\pi}\,\bar{x}\,\mathrm{sech}^{-1}\bar{x} \tag{4.634a}$$

$$\frac{\Gamma(0\to 1)}{\delta U\left(\frac{b}{2}\right)} = -2f\sqrt{\frac{1-f}{1+f}} \tag{4.635}$$

$$\frac{\Gamma\left(0\to \frac{1}{f}\right)}{\delta U\left(\frac{b}{2}\right)} = 0 \tag{4.636}$$

The result expressed by Equation (4.636) is obvious physically if the circulation about the proper contour is considered and irrotationality is imposed.

M_Γ is given by

$$\frac{M_\Gamma(\bar{x}\to 1)}{\delta U\left(\frac{b}{2}\right)^2} = \frac{f}{\pi\sqrt{1-f^2}}\left[-\pi(1-f^2) + (1-f^2\bar{x}^2)\left(\cos^{-1}\frac{f-\bar{x}}{1-f\bar{x}} + \cos^{-1}\frac{f+\bar{x}}{1+f\bar{x}}\right)\right] + \frac{2f^2\bar{x}^2}{\pi}\operatorname{sech}^{-1}\bar{x} \tag{4.637}$$

$$\left.\frac{M_\Gamma(\bar{x}\to 1)}{\delta U\left(\frac{b}{2}\right)^2}\right|_{f=1} = \frac{2}{\pi}\left(\sqrt{1-\bar{x}^2} + \bar{x}^2\operatorname{sech}^{-1}\bar{x}\right) \tag{4.637a}$$

$$\frac{M_\Gamma(0\to 1)}{\delta U\left(\frac{b}{2}\right)^2} = f\left(\frac{2}{\pi}\frac{\cos^{-1}f}{\sqrt{1-f^2}} - \sqrt{1-f^2}\right) \tag{4.638}$$

$$\left.\frac{M_\Gamma(0\to 1)}{\delta U\left(\frac{b}{2}\right)^2}\right|_{f=1} = \frac{2}{\pi} \tag{4.638a}$$

$$\frac{M_\Gamma\left(1\to \frac{1}{f}\right)}{\delta U\left(\frac{b}{2}\right)^2} = f\sqrt{1-f^2} \tag{4.639}$$

The results for Γ and $x_{c.v.}$ are shown in Figures 58 and 59 respectively for the inboard and outboard vortices. These plots were constructed as explained previously. The horizontal solid lines

denote the overestimates. These are the same for all of the wide-delta ailerons. The short vertical solid lines denote the values of A_L. The labeled dashed curves are the curves which connect the estimates at A_L to the known endpoints at A = 0. Note that as A decreases from unity there is no inboard vortex until the fin interaction begins.

The plane narrow-delta wing-body combination with aileron deflection will now be studied. The overestimates are the same as for the narrow-delta wing-incidence problem. The overestimates for the vorticity distribution and the strength and position of the vortex are given by Equations (4.625), (4.627), and (4.628a) respectively.

For the plane narrow-delta aileron endpoint (A = 0), the vorticity distribution is obtained from Reference 42 and is given by

$$\frac{\gamma(x)}{\delta U} = \frac{4}{\pi}\left[\frac{1}{\sqrt{1-\left(\frac{x}{b/2}\right)^2}} - \operatorname{sech}^{-1}\left(\frac{x}{b/2}\right)\right] \tag{4.640}$$

for $0 \leq x \leq \frac{b}{2}$. Note that this equation is independent of d and is, in particular, true for d = f = 1. Then the results for this case are given by the previous results for the plane wide-delta aileron for f = 1 if $\bar{x}$ is replaced by $\frac{x}{b/2}$ in those equations (see Equations (4.633), (4.634a), (4.637a), and (4.638a)). The vorticity distribution is given by the f = 1 curve in Figure 57 and the strengths and positions of the (inboard and outboard) vortices are given in Figures 60 and 61 respectively for three values of d.

Consider the problem of the cruciform wide-delta aileron with 2 fins deflected, i.e. the horizontal fins deflected by $\pm \delta$. Results will be obtained for the right horizontal fin and for the upper vertical fin and the results for the other two fins are obtained from symmetry. As A decreases from unity, the vertical fin will be inactive until the fins interact ($A = A_L$) at which point a vortex will start at the wing-body juncture. As A decreases further, a negative vortex will move upward along the vertical fin. The overestimates for the horizontal fin are the same as those for the plane wide-delta aileron (and for wide-delta wing-incidence).

The endpoint ($A = 0$) results are now needed for the horizontal and vertical fins. It is evident that for this problem there will be no sign changes in the vorticity distributions on either fin. It is further evident that the results for the horizontal fin are given by the overestimates with x* replaced by $\bar{x}$. Although $\Gamma(0 \to \frac{b}{2})$ and $M_\Gamma(0 \to \frac{b}{2})$ are the only quantities needed for either fin for this case, the results for variable regions are given here since they will be needed when 4 fins are deflected and sign changes in the vorticity distributions do occur.

For the horizontal fin, the vorticity distribution is given by Equations (4.619) and (4.620). Plots of the vorticity distributions are given by the overestimates in Figure 49. $\Gamma(0 \to \frac{1}{f})$ and $M_\Gamma(0 \to \frac{1}{f})$ are given by two times Equation (4.622) and by

Equation (4.623) respectively. Other formulas which may be derived are summarized as follows:

$$\frac{\Gamma(\bar{x}\to 1)}{\delta U(\frac{b}{2})} = \frac{2f}{\pi\sqrt{1-f^2}}\left[-\pi(1-f) + (1-f\bar{x})\cos^{-1}\frac{f-\bar{x}}{1-f\bar{x}} + (1+f\bar{x})\cos^{-1}\frac{f+\bar{x}}{1+f\bar{x}}\right] \tag{4.641}$$

$$\left.\frac{\Gamma(\bar{x}\to 1)}{\delta U(\frac{b}{2})}\right|_{f=1} = \frac{4}{\pi}\sqrt{1-\bar{x}^2} \tag{4.641a}$$

$$\frac{\Gamma(0\to 1)}{\delta U(\frac{b}{2})} = \frac{4f}{\pi\sqrt{1-f^2}}\left(\frac{\pi}{2}f - \sin^{-1}f\right) \tag{4.642}$$

$$\frac{M_\Gamma(\bar{x}\to 1)}{\delta U(\frac{b}{2})^2} = \frac{f}{\pi\sqrt{1-f^2}}\left[-\pi(1-f^2) + (1-f^2\bar{x}^2)\left(\cos^{-1}\frac{f-\bar{x}}{1-f\bar{x}} - \cos^{-1}\frac{f+\bar{x}}{1+f\bar{x}}\right)\right] + \frac{2f}{\pi}\cos^{-1}\bar{x} \tag{4.643}$$

$$\left.\frac{M_\Gamma(\bar{x}\to 1)}{\delta U(\frac{b}{2})^2}\right|_{f=1} = \frac{2}{\pi}\left(\bar{x}\sqrt{1-\bar{x}^2} + \cos^{-1}\bar{x}\right) \tag{4.643a}$$

$$\frac{M_\Gamma(0\to 1)}{\delta U(\frac{b}{2})^2} = f\left(1-\sqrt{1-f^2}\right) \tag{4.644}$$

The vorticity distribution along the vertical fin is obtained from Reference 18 and is given by

$$\frac{\gamma(y)}{\delta U} = -\frac{4}{\pi}\tan^{-1}\frac{\sqrt{1-\bar{y}^2}}{\bar{y}f} \tag{4.645}$$

$$\left.\frac{\gamma(y)}{\delta U}\right|_{f=1} = -\frac{4}{\pi}\cos^{-1}\bar{y} \tag{4.645a}$$

Plots for f = 1 and 0.5 are shown in Figure 62. Results for the vertical fin are as follows:

$$\frac{\Gamma(\bar{y}\to 1)}{\delta U(\frac{b}{2})} = \frac{4f}{\pi}\left(\bar{y}\,\tan^{-1}\frac{\sqrt{1-\bar{y}^2}}{\bar{y}f} - \frac{1}{\sqrt{1-f^2}}\,\tan^{-1}\frac{\sqrt{(1-f^2)(1-\bar{y}^2)}}{f}\right) \tag{4.646}$$

$$\left.\frac{\Gamma(\bar{y}\to 1)}{\delta U(\frac{b}{2})}\right|_{f=1} = \frac{4}{\pi}\left(\bar{y}\cos^{-1}\bar{y} - \sqrt{1-\bar{y}^2}\right) \tag{4.646a}$$

$$\frac{\Gamma(0\to 1)}{\delta U(\frac{b}{2})} = -\frac{4}{\pi}\,\frac{f\cos^{-1}f}{\sqrt{1-f^2}} \tag{4.647}$$

$$\left.\frac{\Gamma(0\to 1)}{\delta U(\frac{b}{2})}\right|_{f=1} = -\frac{4}{\pi} \tag{4.647a}$$

(Note that Γ for the vertical fin is equal and opposite to that for the horizontal fin. This is evident if the circulation around a closed contour taken along the vertical fin, then along the horizontal fin, and then completed through the undisturbed fluid, is set equal to zero).

$$\frac{M_\Gamma(\bar{y}\to 1)}{\delta U(\frac{b}{2})^2} = -\frac{2f^2}{\pi}\left[\frac{1}{2(1-f^2)}\left(\pi - 2f\cos^{-1}\bar{y} + \sin^{-1}\frac{\sqrt{1-f^2}-\bar{y}}{1-\sqrt{1-f^2}\,\bar{y}} - \sin^{-1}\frac{\sqrt{1-f^2}+\bar{y}}{1+\sqrt{1-f^2}\,\bar{y}}\right) - \bar{y}^2\tan^{-1}\frac{\sqrt{1-\bar{y}^2}}{\bar{y}f}\right] \tag{4.648}$$

$$\left.\frac{M_\Gamma(\bar{y}\to 1)}{\delta U(\frac{b}{2})^2}\right|_{f=1} = -\frac{1}{\pi}\left[(1-2\bar{y}^2)\cos^{-1}\bar{y} + \bar{y}\sqrt{1-\bar{y}^2}\right] \tag{4.648a}$$

$$\frac{M_\Gamma(0\to 1)}{\delta U(\frac{b}{2})^2} = -\frac{f^2}{1+f} \tag{4.649}$$

$$\frac{y_{c.v.}(0\to 1)}{\left(\frac{b}{2}\right)} = \frac{\pi}{4}\,\frac{f\sqrt{1-f^2}}{(1+f)\cos^{-1}f} \tag{4.650}$$

$$\left.\frac{y_{c.v.}(0\to 1)}{\left(\frac{b}{2}\right)}\right|_{f=1} = \frac{\pi}{8} \tag{4.650a}$$

Results for 2 fins deflected are shown in Figures 58 and 59.

Consider the cruciform wide-delta aileron with 4 fins deflected. Now all fins are alike and only the right horizontal fin will be considered. This configuration is obtained by superposition of two of the above ailerons (with 2 fins deflected) where one of the ailerons has been banked 90 degrees. Such a superposition will lead to a sign change in the vorticity distribution when the fins interact. The endpoint result (A = 0) is easily obtained from the above results. The vorticity distribution is shown in Figure 63. Using the above equations, the results for the inboard and outboard vortices can be obtained. These results are shown in Figures 58 and 59.

Damping in roll--The calculations for this case follow the method used in the case of aileron deflection. One important difference arises and that is that here the vorticity distributions for the overestimate (for supersonic leading edges) vary with A and show sign changes for values of A for which the fins do not interact. Then the overestimate results for the inboard and outboard vortices must first be computed. The results for the

inboard and outboard vortices for the endpoints at A = 0 are then connected to the results for the corresponding overestimate at the proper value of A_L.

Plane and cruciform wide-delta wing-body combinations which have no lateral forces acting will be studied here. Only the overestimate will be used and it is the same for the plane and cruciform problems. The methods to be used should be apparent so that the details of the calculations will be omitted.

The vorticity distribution for the overestimate can be obtained from previous results for the cruciform wide-delta wing in roll. This result is obtained essentially by differentiating Equations (4.224) and (4.225) with respect to x and combining this result with the result for a plane lifting wing so as to satisfy the angle of attack distribution shown in Figure 37(a). The final result is given by

$$\frac{\gamma(x)}{p(\frac{b}{2})} = \frac{2f}{\pi}\left[2(1-A)x^*\operatorname{sech}^{-1}x^* + \frac{(1-A)}{(1-f^2)^{3/2}}\left\{\left[1-fx^*(2-f^2)\right]\cos^{-1}\frac{f-x^*}{1-fx^*} - \right.\right.$$

$$\left.\left. -\left[1+fx^*(2-f^2)\right]\cos^{-1}\frac{f+x^*}{1+fx^*}\right\} - \frac{A}{\sqrt{1-f^2}}\left(\cos^{-1}\frac{f-x^*}{1-fx^*} - \cos^{-1}\frac{f+x^*}{1+fx^*}\right)\right] \qquad (4.651)$$

and

$$\left.\frac{\gamma(x)}{p(\frac{b}{2})}\right|_{f=1} = \frac{4x^*}{\pi}\left[(1-A)\operatorname{sech}^{-1}x^* - \frac{(2+A)}{3\sqrt{1-x^{*2}}}\right] \qquad (4.651a)$$

for $0 \leq x^* \leq 1$ and

$$\frac{\gamma(x)}{p(\frac{b}{2})} = -\frac{2f}{\sqrt{1-f^2}}\left\{A - \frac{(1-A)}{(1-f^2)}\left[1-fx^*(2-f^2)\right]\right\} \qquad (4.652)$$

for $1 \leq x^* \leq \frac{1}{f}$.

The overestimate circulation for the complete fin will be given by

$$\frac{\Gamma(0 \to \frac{b^*}{2})}{p(\frac{b}{2})(\frac{b^*}{2})} = \frac{2f}{\pi(1-f^2)^{3/2}}\left[(f^2+Af^2-2A)\cos^{-1}f-(1-A)f\sqrt{1-f^2}\right] \tag{4.653}$$

$$\left.\frac{\Gamma(0 \to \frac{b^*}{2})}{p(\frac{b}{2})(\frac{b^*}{2})}\right|_{f=1} = -\frac{2}{3\pi}(1+5A) \tag{4.653a}$$

The moment of the overestimate vorticity distribution is given by

$$\frac{M_\Gamma(0 \to \frac{b^*}{2})}{p(\frac{b}{2})(\frac{b^*}{2})^2} = -\frac{f}{3}(1+2A) \tag{4.654}$$

The overestimate vorticity distribution is plotted in Figure 64 for f = 1 for various values of A. Γ's for the inboard and outboard vortices were obtained for each value of A by graphical integration together with the use of Equation (4.653a). M_Γ's for the two vortices were obtained by plotting the moment of the vorticity distribution (see Figure 65), integrating the inboard vortex graphically, and then using Equation (4.654). The same procedure was carried out for f = 0.5 and the overestimate results for these two values of f are shown by the solid lines in Figures 66, 67, and 68. Figure 66 gives the strength of the inboard vortex. It is seen that above A = .65 there is no inboard vortex. This value of A was obtained by extrapolating the overestimate results to $\Gamma = 0$ and it appeared to be the

same for both values of f. Figure 67 gives the position of the inboard vortex and Figure 68 gives the strength and position of the outboard vortex. The curves in these three graphs are completed by obtaining the correct values at A = 0 for the plane and cruciform problems.

The results for the plane rolling wing (A = 0) can be obtained by standard methods. The results will be summarized here. The vorticity distribution is

$$\frac{\gamma(x)}{p\left(\frac{b}{2}\right)} = -\frac{2f}{\pi(1-f^2)^{3/2}}\left\{2f\sqrt{(1-f^2)(1-\bar{x}^2)} - \left[1+f\bar{x}(2-f^2)\right]\cos^{-1}\frac{f+\bar{x}}{1+f\bar{x}} - \left[1-f\bar{x}(2-f^2)\right]\cos^{-1}\frac{f-\bar{x}}{1-f\bar{x}}\right\} \tag{4.655}$$

$$\left.\frac{\gamma(x)}{p\left(\frac{b}{2}\right)}\right|_{f=1} = \frac{8}{3\pi}\frac{(1-2\bar{x}^2)}{\sqrt{1-\bar{x}^2}} \tag{4.655a}$$

if $0 \leq \bar{x} \leq 1$ and is

$$\frac{\gamma(x)}{p\left(\frac{b}{2}\right)} = \frac{2f}{(1-f^2)^{3/2}}\left[1-f\bar{x}(2-f^2)\right] \tag{4.656}$$

if $1 \leq \bar{x} \leq \frac{1}{f}$. If $1 \leq \bar{x} \leq \frac{1}{f}$, $\Gamma\left(\bar{x} \to \frac{1}{f}\right)$ is given by

$$\frac{\Gamma\left(\bar{x} \to \frac{1}{f}\right)}{p\left(\frac{b}{2}\right)^2} = \frac{f^2(1-f\bar{x})}{(1-f^2)^{3/2}}\left[f-\bar{x}(2-f^2)\right] \tag{4.657}$$

and, if $0 \leq \bar{x} \leq 1$, $\Gamma\left(\bar{x} \to \frac{1}{f}\right)$ is given by

$$\frac{\Gamma\left(\bar{x} \to \frac{1}{f}\right)}{p\left(\frac{b}{2}\right)^2} = \frac{f^2}{\pi(1-f^2)^{3/2}}\left\{2f\bar{x}\sqrt{(1-f^2)(1-\bar{x}^2)} - (1+f\bar{x})\left[f+\bar{x}(2-f^2)\right]\cos^{-1}\frac{f+\bar{x}}{1+f\bar{x}} + \right.$$
$$\left. + (1-f\bar{x})\left[f-\bar{x}(2-f^2)\right]\cos^{-1}\frac{f-\bar{x}}{1-f\bar{x}}\right\} \tag{4.658}$$

$$\left.\frac{\Gamma(\bar{x}\to\frac{1}{f})}{p(\frac{b}{2})^2}\right|_{f=1} = -\frac{8}{3\pi}\,\bar{x}\sqrt{1-\bar{x}^2} \tag{4.658a}$$

$$\Gamma(0\to\tfrac{1}{f}) = 0 \tag{4.659}$$

The following expressions have been derived for M_Γ :

If $1 \le \bar{x} \le \frac{1}{f}$

$$\frac{M_\Gamma(\bar{x}\to\frac{1}{f})}{p(\frac{b}{2})^3} = -\frac{f}{3(1-f^2)^{3/2}}\left\{1-2f^2+f^2\bar{x}^2\left[3-2\bar{x}f(2-f^2)\right]\right\} \tag{4.660}$$

$$\frac{M_\Gamma(1\to\frac{1}{f})}{p(\frac{b}{2})^3} = -\frac{f}{3(1-f^2)^{3/2}}(1+f^2-4f^3+2f^5) \tag{4.660a}$$

and, if $0 \le \bar{x} \le 1$,

$$\left.\frac{M_\Gamma(\bar{x}\to\frac{1}{f})}{p(\frac{b}{2})^3}\right|_{f=1} = -\frac{8}{9\pi}(1+2\bar{x}^2)\sqrt{1-\bar{x}^2} \tag{4.661}$$

$$\frac{M_\Gamma(0\to\frac{1}{f})}{p(\frac{b}{2})^3} = -\frac{2f}{3\pi(1-f^2)^{3/2}}\left[f\sqrt{1-f^2}+(1-2f^2)\cos^{-1}f\right] \tag{4.662}$$

$$\left.\frac{M_\Gamma(0\to\frac{1}{f})}{p(\frac{b}{2})^3}\right|_{f=1} = -\frac{8}{9\pi} \tag{4.662a}$$

For f = 1, the value of $\bar{x}$ where the vorticity changes sign can be obtained without plotting the vorticity distribution. It is obtained by putting $\gamma' = 0$ in Equation (4.655a). Using this value of $\bar{x}$, the results for the inboard and outboard vortices can be obtained. For f = .5,

the vorticity distribution is shown in Figure 69. From this plot, it is seen that the vorticity changes sign in the region $1 \leq \bar{x} \leq \frac{1}{f}$. A complete set of formulas is available for this region and the results for the two vortices can be obtained. The plane aileron results are shown in Figures 66, 67, and 68.

The results for the cruciform wide-delta rolling wing (A=0) can be obtained using the same procedure as was used for the cruciform aileron. The original problem can be decomposed into simpler problems as shown in Figure 19. Problem B is similar to the cruciform aileron with 2 fins deflected. The results for the right horizontal fin of problem B are given by the overestimate with A = 0 (see Equations (4.651) through (4.654)). The vorticity distribution for f = 1 is shown in Figure 64 (curve labeled A = 0). The vorticity distribution along the upper vertical fin of problem B is given essentially by the y derivative of Equation (4.230). The result is

$$\frac{\gamma(y)}{p(\frac{b}{2})} = \frac{2f\bar{y}}{\pi}\left\{2\,\mathrm{sech}^{-1}\bar{y} - \frac{f}{\sqrt{1-f^2}}\left[\sin^{-1}\frac{\sqrt{1-f^2}-\bar{y}}{1-\sqrt{1-f^2}\,\bar{y}} + \sin^{-1}\frac{\sqrt{1-f^2}+\bar{y}}{1+\sqrt{1-f^2}\,\bar{y}}\right]\right\} \tag{4.663}$$

$$\left.\frac{\gamma(y)}{p(\frac{b}{2})}\right|_{f=1} = \frac{4\bar{y}}{\pi}\left(\mathrm{sech}^{-1}\bar{y} - \sqrt{1-\bar{y}^2}\right) \tag{4.663a}$$

Figure 70 shows the vorticity distribution for two values of f. Some useful formulas which have been derived for the vertical fin are

$$\frac{\Gamma(\bar{y}\to 1)}{p\left(\frac{b}{2}\right)^2} = \frac{2f^2}{\pi}\left\{\frac{\sqrt{1-\bar{y}^2}}{1-f^2} - \bar{y}^2 \operatorname{sech}^{-1}\bar{y} - \frac{f}{(1-f^2)^{3/2}}\cos^{-1}\frac{f}{\sqrt{1-(1-f^2)\bar{y}^2}} + \right.$$

$$\left. + \frac{f\bar{y}^2}{2\sqrt{1-f^2}}\left[\sin^{-1}\frac{\sqrt{1-f^2}-\bar{y}}{1-\sqrt{1-f^2}\,\bar{y}} + \sin^{-1}\frac{\sqrt{1-f^2}+\bar{y}}{1+\sqrt{1-f^2}\,\bar{y}}\right]\right\} \tag{4.664}$$

$$\left.\frac{\Gamma(\bar{y}\to 1)}{p\left(\frac{b}{2}\right)^2}\right|_{f=1} = \frac{2}{\pi}\left[\frac{(1+2\bar{y}^2)\sqrt{1-\bar{y}^2}}{3} - \bar{y}^2 \operatorname{sech}^{-1}\bar{y}\right] \tag{4.664a}$$

$$\frac{\Gamma(0\to 1)}{p\left(\frac{b}{2}\right)^2} = \frac{2f^2}{\pi}\left[\frac{\sqrt{1-f^2}-f\cos^{-1}f}{(1-f^2)^{3/2}}\right] \tag{4.665}$$

$$\left.\frac{\Gamma(0\to 1)}{p\left(\frac{b}{2}\right)^2}\right|_{f=1} = \frac{2}{3\pi} \tag{4.665a}$$

$$\left.\frac{M_\Gamma(\bar{y}\to 1)}{p\left(\frac{b}{2}\right)^3}\right|_{f=1} = \frac{1}{6\pi}\left[\cos^{-1}\bar{y} + \bar{y}\sqrt{1-\bar{y}^2}(1+6\bar{y}^2) - 8\bar{y}^3\operatorname{sech}^{-1}\bar{y}\right] \tag{4.666}$$

$$\frac{M_\Gamma(0\to 1)}{p\left(\frac{b}{2}\right)^3} = \frac{f^3}{3(1+f)^2} \tag{4.667}$$

If the results which have been obtained are superimposed as in Figure 19 to form the complete rolling wing, all of the fins are identical. Figure 71 shows the vorticity distribution on a typical fin for f = 1. The strength and position of the inboard and outboard vortices were obtained by combining the use of the formulas for this problem with graphical integrations. Results for f = 1 and f = .5 are shown in Figure 66, 67, and 68.

G. Vorticity at Trailing Edges--High Aspect Ratio

In practical cases, a high-aspect-ratio wing usually operates at a much lower angle of attack than a low-aspect-ratio wing and its lift coefficient is generally much smaller. Both the increase in aspect ratio and the decrease in lift coefficient increase the distance e and, if the aspect ratio is high enough, the vortex sheet from the wing can be considered essentially undistorted at the tail just as in the case of the subsonic airplane.

Delta wings--Since f is generally small for a high-aspect-ratio delta wing, the overestimate will approximate the exact solution closely (because only a relatively small portion of the wing is affected by interference). The results for vorticity distributions derived previously can be used here but the other calculations do not apply. Furthermore, few of the problems treated before are likely to occur for the high-aspect-ratio airplane. In particular, the aileron deflection and the cruciform problems are not to be included in high-aspect-ratio airplane problems.

Rectangular wings--The remarks above generally apply here. It is to be noted that the overestimate predicts no vorticity except at the tips. Actually there is some vorticity near the wing-body juncture but it is expected to be small and to have little effect on the tail.

H. Motion of the Vortex Sheets--Low Aspect Ratio

If the aspect ratio is low enough, as assumed here, this problem is concerned with the motion downstream of several distinct vortices whose strengths and initial positions may be estimated by the procedures described in previous sections. Lagerstrom and M. E. Graham (Reference 15) have presented in great detail assumptions and methods for computing the motion of vortices for plane wing-body combinations in lift. These same assumptions and methods can be used for the problems studied in this thesis. However most of the problems here lead to very difficult problems in two-dimensional nonstationary incompressible vortex motion primarily because of the large number of vortices involved. For example, it was seen that two vortices might trail from each fin of a cruciform wing-body configuration for certain roll problems. Together with the reflected vortices which are placed within the body to satisfy boundary conditions, it is seen that some problems can involve as many as sixteen vortices. In general it is to be expected that step-by-step graphical or numerical procedures will have to be employed to study the motion of the vortex systems as they move downstream for most of the cruciform roll problems considered in the present work.

I. Calculating Tail Effects

The cross-flow field at the tail due to the vortices will

generally be very complicated. If the tail is a plane or cruciform wide-delta wing-body configuration, the estimating procedures introduced in Section 4.4 may be used. Generally this will involve numerical or graphical integration of elementary strip estimates across the fins which will have complicated apparent twists due to the vortex system.

V. QUALITATIVE DISCUSSION

All of the theoretical results which have been presented in this thesis were based on linearized nonviscous theory. Although the nonlinear rolling up of the vortex sheets is retained in the problem of computing wing-body-tail interference, the strengths and the initial positions at the wing trailing edges of the vortices which are to approximate the effect of rolling up are calculated by linearized theory. In practical cases, a missile is often subjected to angles of attack far greater than those for which linearized theory can be expected to give reasonable results. At these high angles of attack the nonlinear and viscous effects and the effect of the gap between a deflected fin and the body will be considerable. Just as the nonlinear effects are far more severe downstream of the wing than on the wing so too it must be expected that the increased effects on the wing due to high angles of attack will be highly magnified downstream. It is the purpose of this section to discuss qualitatively the expected applicability of the theoretical results in view of the fact that many important phenomena have been neglected. Where possible, the qualitative effects of these phenomena on the various interferences and aerodynamic problems will be pointed out.

In general, real fluid effects will decrease the effectiveness of lifting surfaces so that integrated values of lift and rolling moment which are derived from linearized theory will probably be

too large. This is particularly severe for the low-aspect-ratio missiles studied because of the high lifts which the fins generally carry and because of the large interference effects.

5.1 Lift and Incidence

Consider first the lift case without incidence. If the wing (plane or cruciform) is banked, the lift can be calculated by the usual decomposition into angles of attack normal to the wings. For the cruciform wing the lift should still be practically independent of bank if the nonlinear effects are not too great. Generally, the lift predicted by linear theory will be optimistic. At high angles of attack the presence of the body may seriously affect the predicted lift of fins which lie roughly in the downstream shadow of the body. It is known that viscous separation of the flow from the upper side of the body occurs (see References 43 and 44) but little is known about its effects on any fins which might lie in the separated region.

It is expected that, for many of the low-aspect-ratio missiles, there will be a considerable afterbody lift. Part of this lift can be estimated from linear theory (see References 15 and 16). There is also a lift due to viscous separation from the body and it appears that this can be estimated satisfactorily (see References 43 and 44).

If a fin is at an angle of attack relative to the body axis

(incidence case) a gap will be produced at the wing-body juncture. The lift effectiveness of the fin will be reduced because some pressure equalization takes place through the gap. As the angle of attack of the missile is increased the lift effectiveness of the fins can be expected to decrease.

The fins of a missile are often deflected suddenly in flight. Then there will be a certain time interval before stationary flow is established. Little work has been done on such nonstationary problems. If A is small and if a wide-delta wing is being considered, Reference 45 will provide information on the transient lift during this period of nonstationary flow.

5.2 Aileron Deflection

If the body is at zero angle of attack, the theoretical results presented here will probably predict rolling moments which are too large because real fluid and gap effects reduce the lift effectiveness of the fins. Let the deflected fins be in the horizontal plane and consider the effect of angle of attack. If the body is at an angle of attack, one of the fins will have a higher angle of attack than the other. The fin at the higher angle of attack carries proportionately more of the lift which generates the rolling moment. At the same time the gap and separation losses will be more severe. The result is probably a decrease of aileron effectiveness with angle of attack.

This problem has generally been treated as a stationary flow problem. Actually, of course, when the fins are deflected in flight there is a time interval before equilibrium conditions are established. Knowledge of these transient rolling moments is important in stability and central considerations. As yet there are no theoretical results available. However, it appears that for cruciform wide-delta ailerons the methods of Reference 45 can be used to compute the transient rolling moments for suddenly deflected fins.

5.3 Damping in Roll

The theoretical results for damping in roll were obtained by replacing a nonstationary problem by what was assumed to be an equivalent stationary problem. Thus the rolling wing was replaced by a nonrolling wing with linear spanwise twist. The magnitudes of the nonstationary effects is not known for cruciform wings but there are indications from planar wings that they may be large (see Reference 46).

5.4 Roll Due to Combined Pitch and Yaw

This problem is particularly serious because these rolling moments are generally not desired. At high angles of pitch and yaw (or high angles of attack for a banked wing) large rolling moments are usually developed and serious stability problems arise.

There are linearized solutions available for plane wings. However, for cruciform wings linearized theory predicts that these rolling moments must be at least of second order due to the necessary restriction to small angles of pitch and yaw. It appears that this problem will have to be studied primarily by experiments.

In general, pitching and yawing of a missile will cause the flow over the various symmetrical pairs of fins to be asymmetrical with respect to the body axis. This must produce additional rolling moments about the body axis if the fins concerned carry lift. No theoretical solutions are known when a body is present and it is expected that the planar wing results will generally not be applicable to plane wing-body configurations.

5.5 Fin-Fin and Wing-Body Interference

Little is known about the nonlinear, viscous, and gap effects with regard to these interferences. It is expected, though, that the linearized results will provide good estimates of these interferences.

5.6 Wing-Body-Tail Interference

Certain assumptions have been used in the calculation of wing-body-tail interference. Because of the extreme difficulty of this problem both theoretically and experimentally, it is not known yet how good these assumptions are. However, it is expected

that, if the angle of attack of the missile is not too great, these assumptions will lead to reasonable estimates of wing-body-tail interference.

At high angles of attack it is known that the assumption of a completely rolled up vortex sheet is a good approximation to the nonlinear effects. It appears that, if incompressible vortices are assumed to start at the trailing edges of the wing, useful engineering results can be obtained. The strengths and positions of these vortices would be obtained from the vorticity distributions at the trailing edges of the wing. The strengths and positions of vortices for several aerodynamic problems have been computed in the present work by linearized theory estimates. At high angles of attack it is expected that nonlinear, viscous, and gap effects will alter the vorticity distributions at the trailing edges so much that linearized theory will be of little value. For example, if any fins are deflected the gap produced can be expected to produce trailing vortices of considerable strength at high angles of attack.

Whenever a missile is pitched or yawed the tail moves laterally away from the vortices which trail from the wing. This will usually reduce the induced effects on the tail. Thus it can be expected that wing-body-tail interference will decrease as the angle between the body axis and the free-stream direction increases.

VI. RECOMMENDATIONS FOR FUTURE RESEARCH

A number of aircraft companies and laboratories are now carrying on theoretical and experimental research in this field. Since a large part of this work is unpublished and, for the most part, the details not known to the writer, some of the research recommended here may well be on the way.

6.1 Theoretical Research

Exact solutions for plane and cruciform wing-body problems have been obtained only for the slender body case. It was seen that, when properly used, such solutions can be very useful for estimating linearized solutions. Generally, the slender body method will not provide information for the problem of roll due to combined pitch and yaw. Aside from this problem, there are numerous other aerodynamic problems for which slender body theory can provide useful results.

Research should be continued on exact linearized solutions to a few of the interference problems. Such solutions will generally be obtained by iteration or series expansion methods, particularly if a body is included. The solutions will usually be difficult and tedious to carry out but a few such solutions would provide very useful guides for the applicability of linearized methods (when compared with experiment) and for the development of approximate methods.

Some study should be made of the nonstationary problems. Results from nonstationary plane wing problems will be useful.

Work should be continued on obtaining vorticity distributions at the trailing edges of plane and cruciform wing-body configurations. Just as mentioned above, a few judicious exact solutions would be very useful as guides. It appears that, for low-aspect-ratio configurations, useful theoretical results will probably be obtained by studying the motion of incompressible two-dimensional vortices as approximations to the rolled up vortex sheets. Some work along this line is known to be in progress.

6.2 Experimental Research

Some experimental research is now in progress on many of the problems considered in this thesis. Unfortunately, little of this work is on fundamental research and thus provides little basic knowledge. A great deal more careful fundamental research is necessary particularly for those problems where linearized theory can yield no useful answers.

The really basic job of experimental research should be the systematic hunting down of nonlinear and viscous effects.

REFERENCES

1. W. F. Durand, "Aerodynamic Theory", Vol. VI, Division P, Durand Reprinting Committee, 1943.

2. K. F. Tupper, "Aerodynamic Interference--A Summary", National Research Council of Canada Report No. PAA-31, Ottawa, May 1937.

3. H. Schlichting, "Aerodynamics of the Mutual Influence of Aircraft Parts (Interference)", The Royal Aircraft Establishment, Farnborough, Library Translation No. 275, October 1948.

4. J. Lennertz, "On the Mutual Reaction of Wings and Body", NACA TM 400, February 1927.

5. Carlo Ferrari, "Interference Between Wing and Body at Supersonic Speeds--Theory and Numerical Application", Journal of the Aeronautical Sciences, Vol. 15, No. 6, pp. 317-336, June 1948.

6. Carlo Ferrari, "Interference Between Wing and Body at Supersonic Speeds--Note on Wind-Tunnel Results and Addendum to Calculations", Journal of the Aeronautical Sciences, Vol. 16, No. 9, pp. 542-546, September 1949.

7. Carlo Ferrari, "Interference Between Wing and Body at Supersonic Speeds--Analysis by the Method of Characteristics", Journal of the Aeronautical Sciences, Vol. 16, No. 7, pp. 411-434, July 1949.

8. George Morikawa, "The Wing-Body Problem for Linearized Supersonic Flow", California Institute of Technology (Thesis), Pasadena, California, June 1949.

9. George K. Morikawa, "On Wing-Body Interference at Supersonic Speeds", Journal of the Aeronautical Sciences, Readers' Forum, Vol. 17, No. 5, May 1950

10. S. H. Browne, L. Friedman, and I. Hodes, "A Wing-Body Problem in a Supersonic Conical Flow", Journal of the Aeronautical Sciences, Vol. 15, No. 8, pp. 443-452, August 1948.

11. P. A. Lagerstrom and M. D. Van Dyke, "General Considerations About Planar and Non-Planar Lifting Systems", Douglas Report No. SM-13432, Santa Monica, June 1949.

12. George Morikawa, "Supersonic Wing-Body Lift", presented at the Annual Summer Meeting, I.A.S., July 1950 (preprint No. 296).

13. G. K. Morikawa and T. F. Coleman, "On Supersonic Wing-Body Center of Pressure", Journal of the Aeronautical Sciences, Readers' Forum, Vol. 18, No. 2, February 1951.

14. S. Kirby and A. Robinson, "Wing-Body Interference at Supersonic Speeds", College of Aeronautics, Cranfield, Report No. 7, April 1947.

15. P. A. Lagerstrom and M. E. Graham, "Aerodynamic Interference in Supersonic Missiles", Douglas Report No. SM-13743, Santa Monica, July 1950.

16. P. A. Lagerstrom and M. E. Graham, "Remarks on Low-Aspect-Ratio Configurations in Supersonic Flow", Journal of the Aeronautical Sciences, Vol. 18, No. 2, pp. 91-96, February 1951.

17. John R. Spreiter and Alvin H. Sacks, "The Rolling Up of the Trailing Vortex Sheet and its Effect on the Downwash Behind Wings", Journal of the Aeronautical Sciences, Vol. 18, No. 1, pp. 21-32, January 1951.

18. Zegmund O. Bleviss, "Some Roll Characteristics of Plane and Cruciform Delta Ailerons and Wings in Supersonic Flow", Douglas Report No. SM-13431, Santa Monica, June 1949.

19. Zegmund O. Bleviss, "Some Roll Characteristics of Cruciform Delta Wings at Supersonic Speeds", presented at the Annual Summer Meeting, I.A.S., July 1950 (preprint No. 303).

20. Warren A. Tucker and Robert O. Piland, "Estimation of the Damping in Roll of Supersonic-Leading-Edge Wing-Body Combinations", NACA TN 2151, July 1950.

21. Ray E. Bolz and John D. Nicolaides, "A Method of Determining Some Aerodynamic Coefficients from Supersonic Free-Flight Tests of a Rolling Missile", Journal of the Aeronautical Sciences, Vol. 17, No. 10, pp. 609-621, October 1950.

22. Ernest W. Graham, "A Limiting Case for Missile Rolling Moments", Douglas Report No. SM-13812, Santa Monica, October 1950.

23. Ernest W. Graham, "A Limiting Case for Missile Rolling Moments", presented at the Annual Winter Meeting, I.A.S., January 1951.

24. E. V. Laitone, "First Order Wing-Body Interference Effects", Journal of the Aeronautical Sciences, Readers' Forum, Vol. 16, No. 8, August 1949.

25. John R. Spreiter, "Aerodynamic Properties of Slender Wing-Body Combinations at Subsonic, Transonic, and Supersonic Speeds", NACA TN 1662, July 1948.

26. G. N. Ward, "Supersonic Flow Past Slender Pointed Bodies", Quarterly Journal of Mechanics and Applied Mathematics, Vol. II, Part 1, 1949.

27. John R. Spreiter, "Aerodynamic Properties of Cruciform-Wing and Body Combinations at Subsonic, Transonic, and Supersonic Speeds", NACA TN 1897, June 1949.

28. Martha E. Graham, "Some Linearized Computations of Supersonic Wing-Tail Interference", Douglas Report No. SM-13430, Santa Monica, December 1948.

29. Max A. Heaslet and Harvard Lomax, "Damping-in-Roll Calculations for Slender Swept-Back Wings and Slender Wing-Body Combinations", NACA TN 1950, September 1949.

30. Gaynor J. Adams, "Theoretical Damping in Roll Effectiveness of Slender Cruciform Wings," NACA TN 2270, January 1951.

31. Ernest W. Graham, unpublished work, 1950.

32. Allen E. Puckett, "Supersonic Wave Drag of Thin Airfoils," Journal of the Aeronautical Sciences, Vol. 13, No. 9, pp. 475-484, September 1946.

33. J. C. Evvard, "Distribution of Wave Drag and Lift in the Vicinity of Wing Tips at Supersonic Speeds", NACA TN 1382, July 1947.

34. P. A. Lagerstrom and M. E. Graham, "Low Aspect Ratio Rectangular Wings in Supersonic Flow", Douglas Report No. SM-13110, Santa Monica, December 1948.

35. H. J. Stewart, "The Lift of a Delta Wing at Supersonic Speeds", Quarterly of Applied Mathematics, Vol. IV, No. 3, October 1946.

36. Clinton E. Brown and Mac C. Adams, "Damping in Pitch and Roll of Triangular Wings at Supersonic Speeds," NACA TR 892, 1948.

37. H. B. Dwight, "Tables of Integrals and Other Mathematical Data", Macmillan, New York, 1947.

38. Herbert S. Ribner, "The Stability Derivatives of Low-Aspect-Ratio Triangular Wings at Subsonic and Supersonic Speeds", NACA TN 1423, 1947.

39. P. A. Lagerstrom and M. E. Graham, "Downwash and Sidewash Induced by Three-Dimensional Lifting Wings in Supersonic Flow", Douglas Report No. SM-13007, Santa Monica, April 1947.

40. Harold Mirels and Rudolph C. Haefeli, "The Calculation of Supersonic Downwash Using Line Vortex Theory", Journal of the Aeronautical Sciences, Vol. 17, No. 1, pp. 13-21, January 1950.

41. Rudolph C. Haefeli, Harold Mirels, and John L. Cummings, "Charts for Estimating Downwash behind Rectangular, Trapezoidal, and Triangular Wings at Supersonic Speeds", NACA TN 2141, August 1950.

42. P. A. Lagerstrom and M. E. Graham, "Methods for Calculating

the Flow in the Trefftz-Plane Behind Supersonic Wings", Douglas Report No. SM-13288, Santa Monica, July 1948.

43. Milton D. Van Dyke, "First Order and Second Order Theory of Supersonic Flow Past Bodies of Revolution", Rand Report No. P-125, December 1949.

44. H. Julian Allen, "Pressure Distribution and Some Effects of Viscosity on Slender Inclined Bodies of Revolution", NACA TN 2044, March 1950.

45. W. J. Strang, "Transient Lift of Three-Dimensional Purely Supersonic Wings", Proceedings of The Royal Society, Vol. 202, No. 1068, p. 54, June 22, 1950.

46. H. J. Stewart--Review of paper "Damping in Pitch and Roll of Triangular Wings at Supersonic Speeds", by Clinton E. Brown and Mac C. Adams, NACA Report 892, 1948--Applied Mechanics Reviews, Vol. 3, No. 6, Review No. 1135, June 1950.

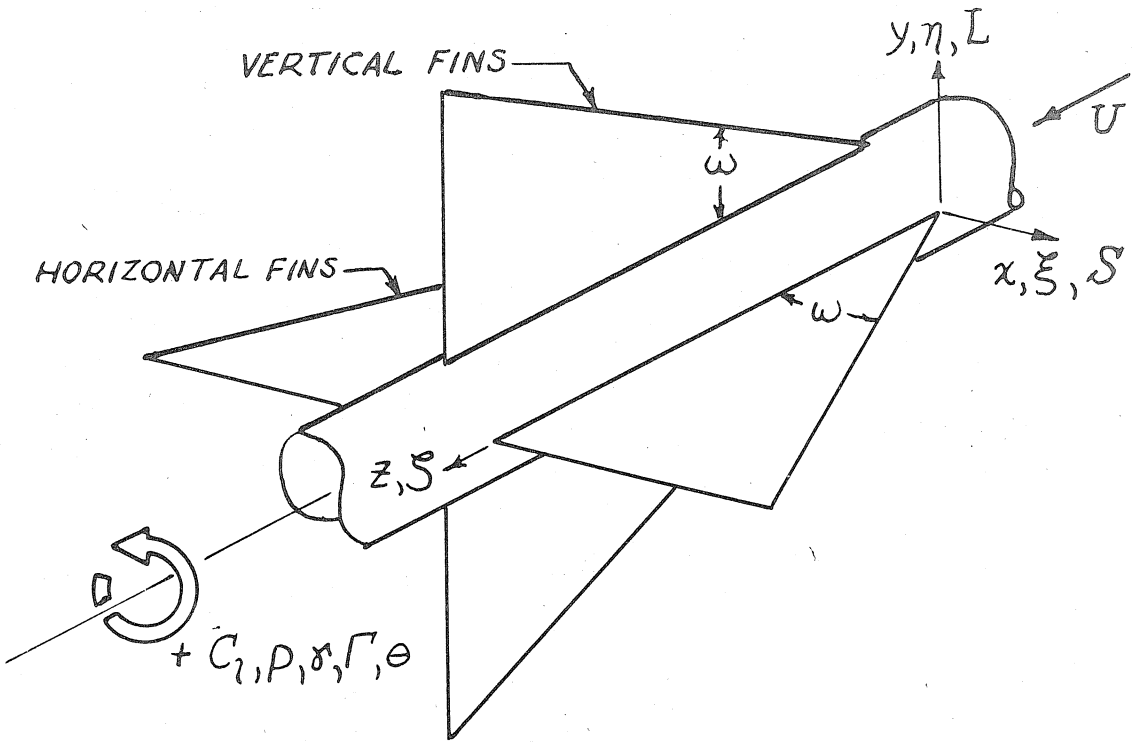

(a) CRUCIFORM DELTA WING-BODY

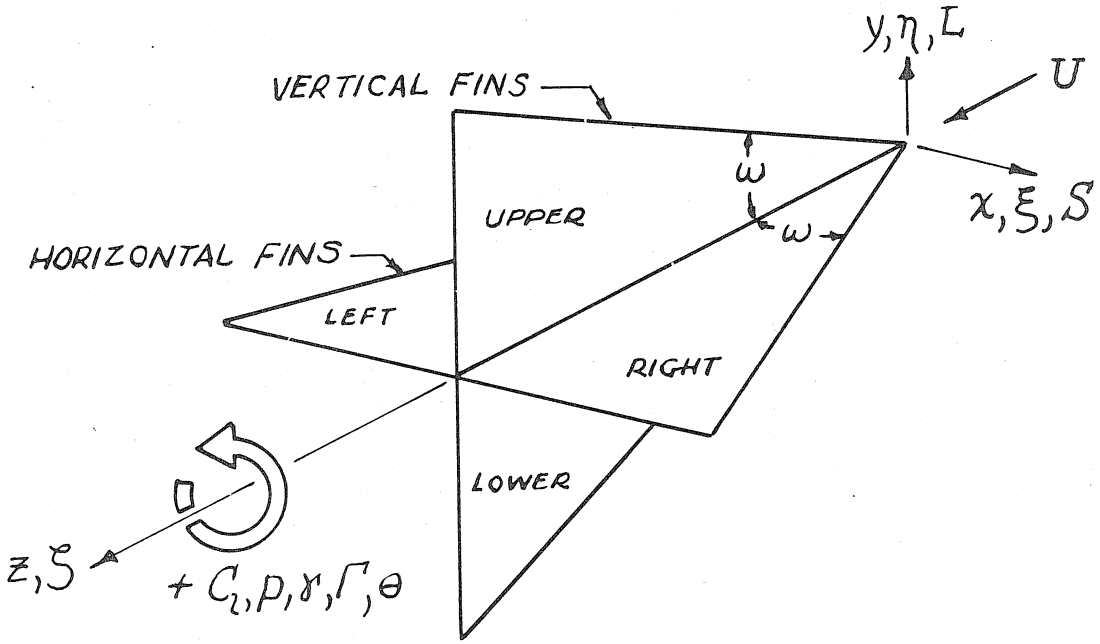

(b) CRUCIFORM DELTA WING

FIG.1. NOTATION AND COORDINATES

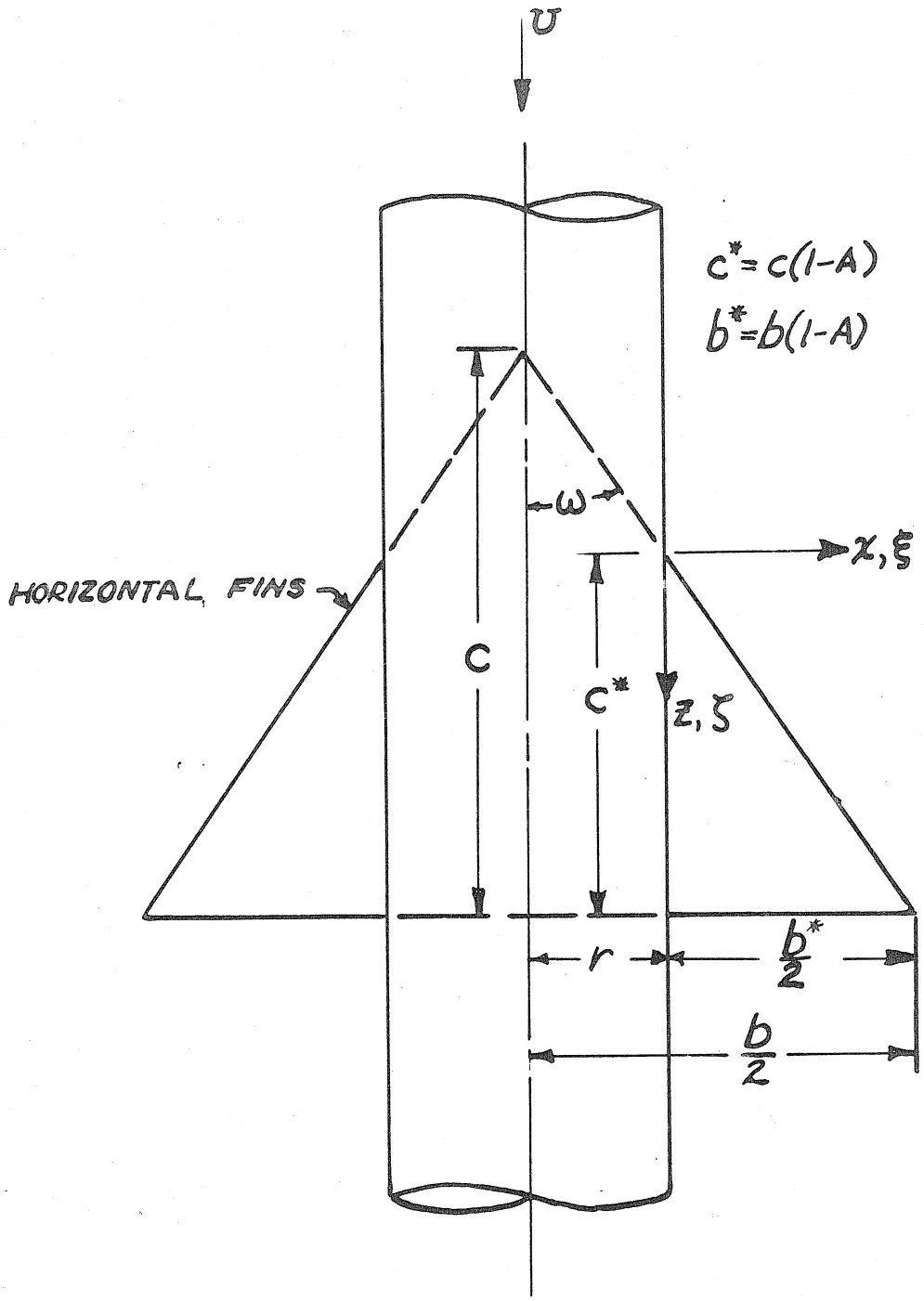

FIG. 2. NOTATION FOR DELTA WING-BODY CONFIGURATION

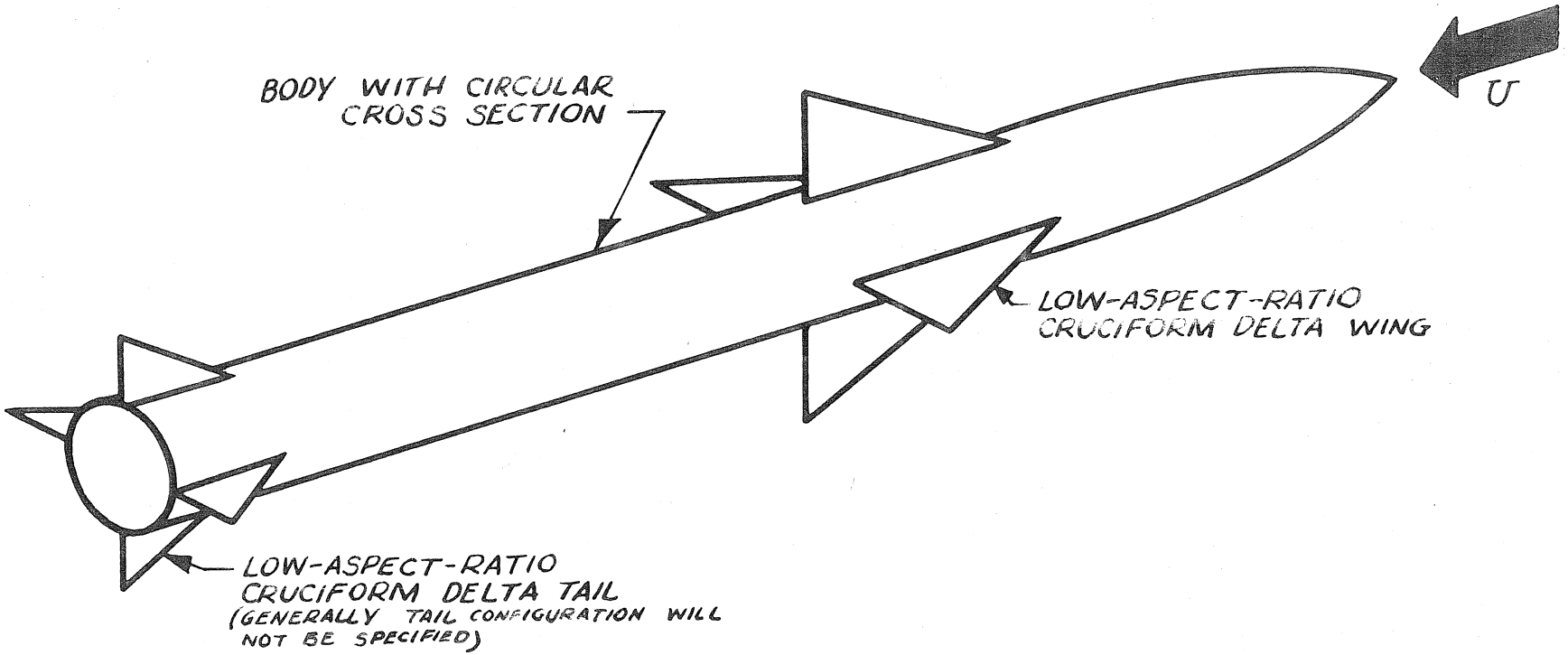

FIG.3 TYPICAL LOW-ASPECT-RATIO SUPERSONIC MISSILE-TYPE CONFIGURATION

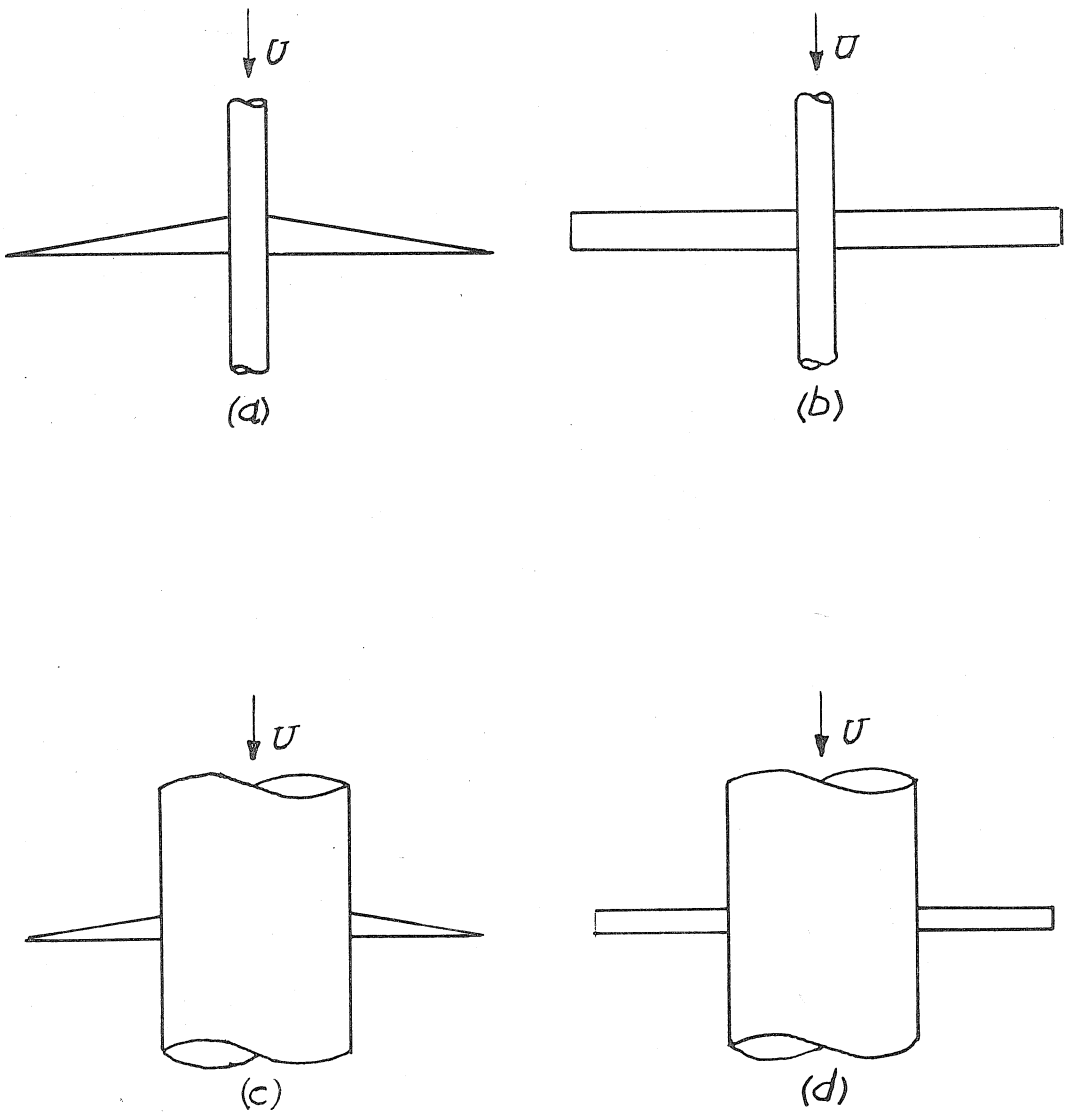

FIG. 4. HIGH ASPECT RATIO WING-BODY CONFIGURATIONS

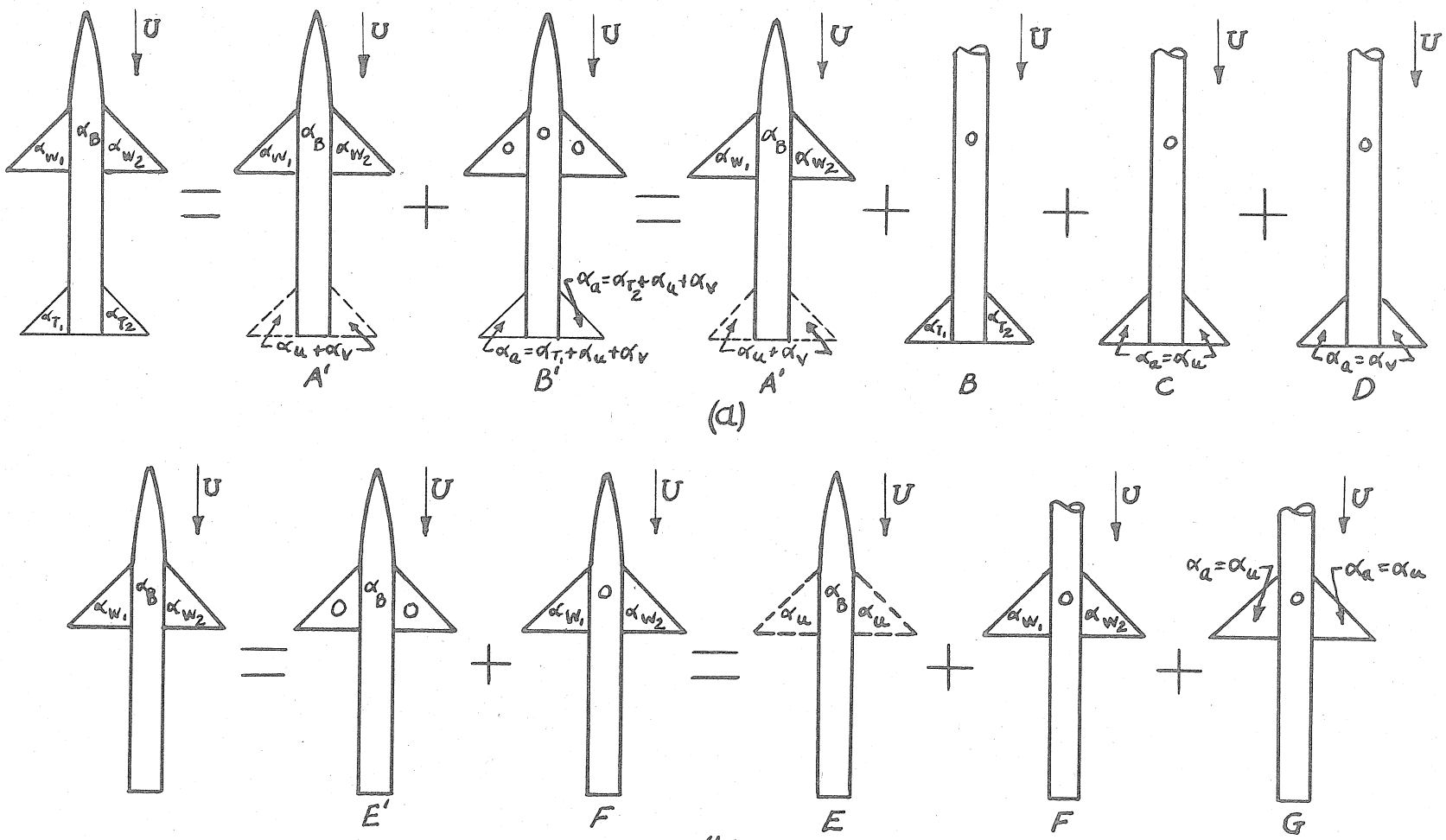

FIG. 5. SUPERPOSITION SCHEME FOR LINEARIZED PROBLEMS

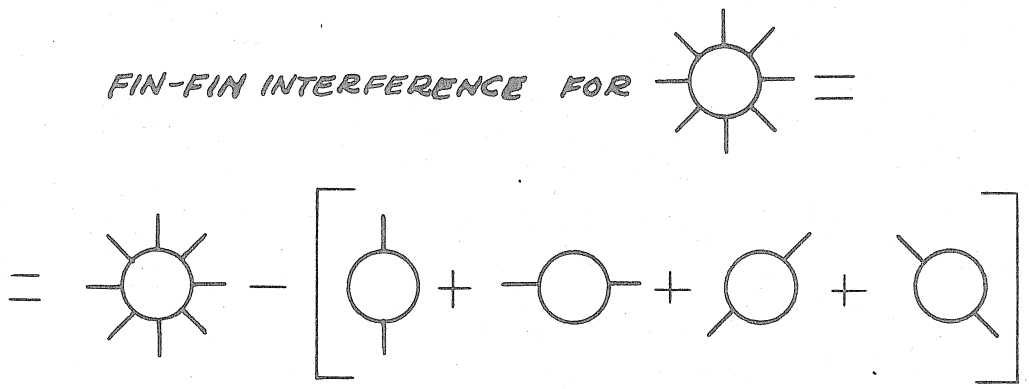

FIG. 7. FIN-FIN INTERFERENCE

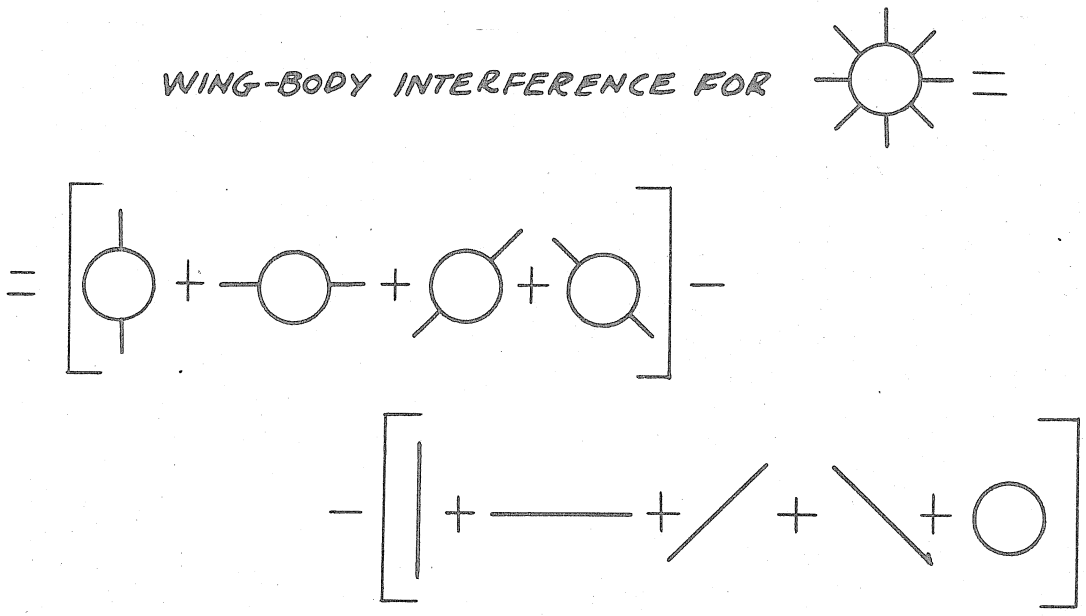

FIG 8. WING-BODY INTERFERENCE

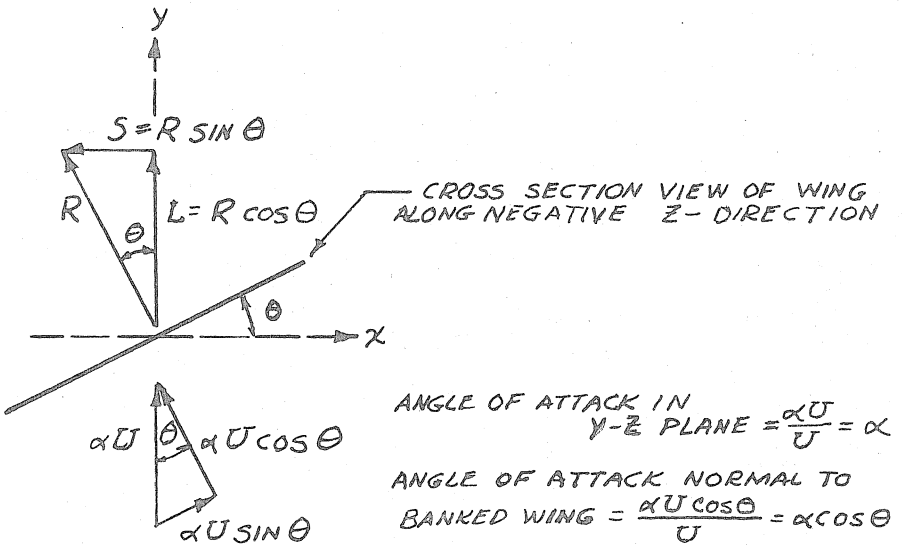

FIG. 9 BANKED PLANE WING

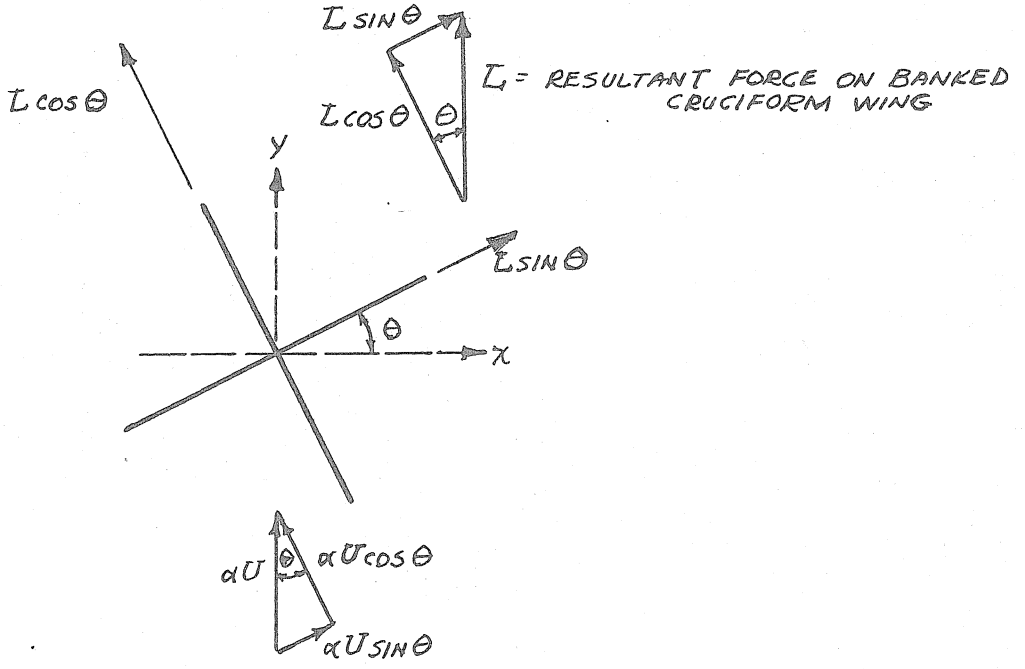

FIG. 10. BANKED CRUCIFORM WING

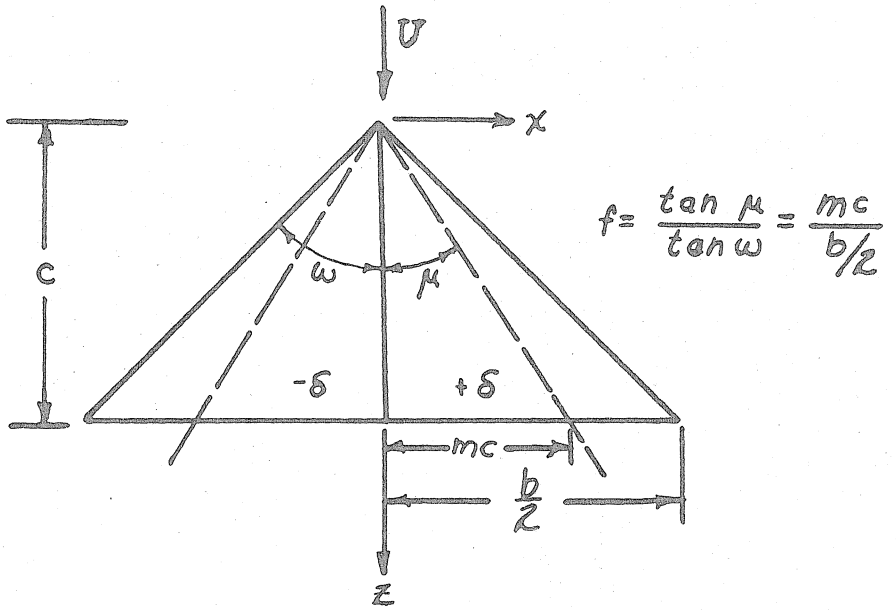

FIG. 11. PLANE WIDE-DELTA AILERON

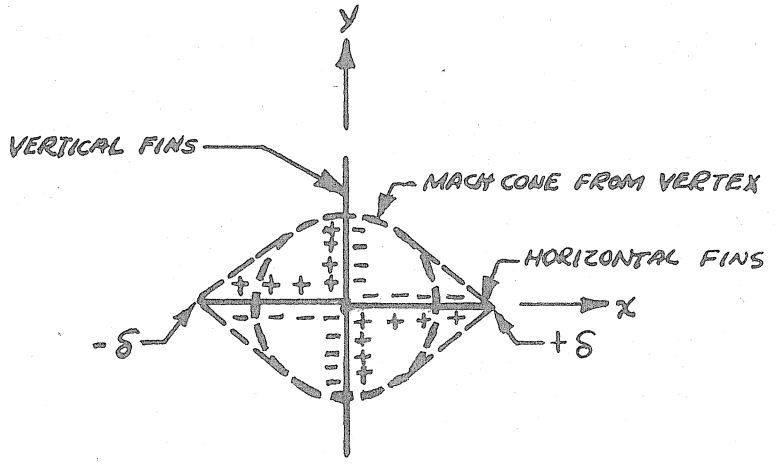

FIG. 12. PRESSURES ON CRUCIFORM AILERON

Fig. 13. Roll Due to Aileron Deflection for Cruciform Wide-Delta Wing

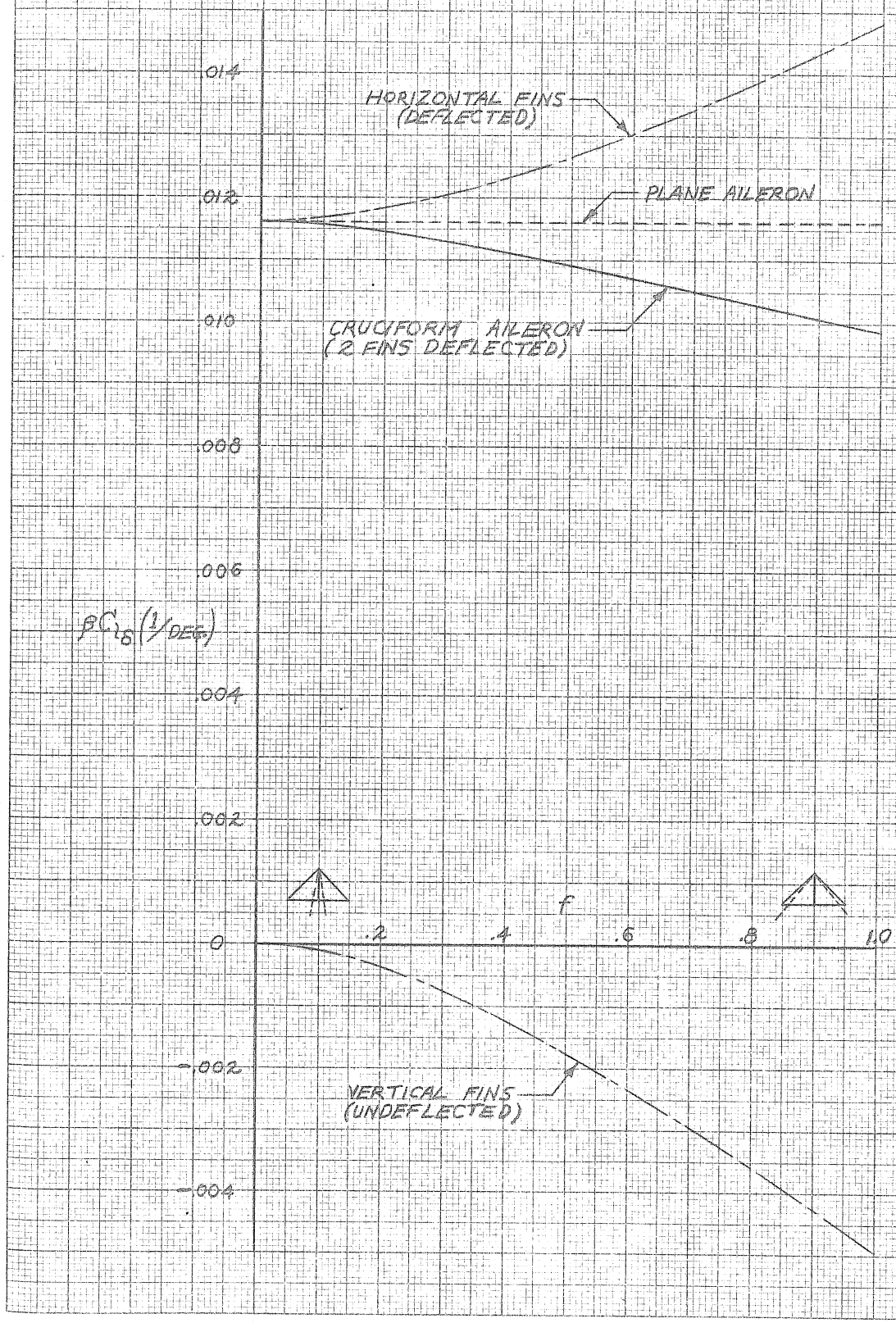

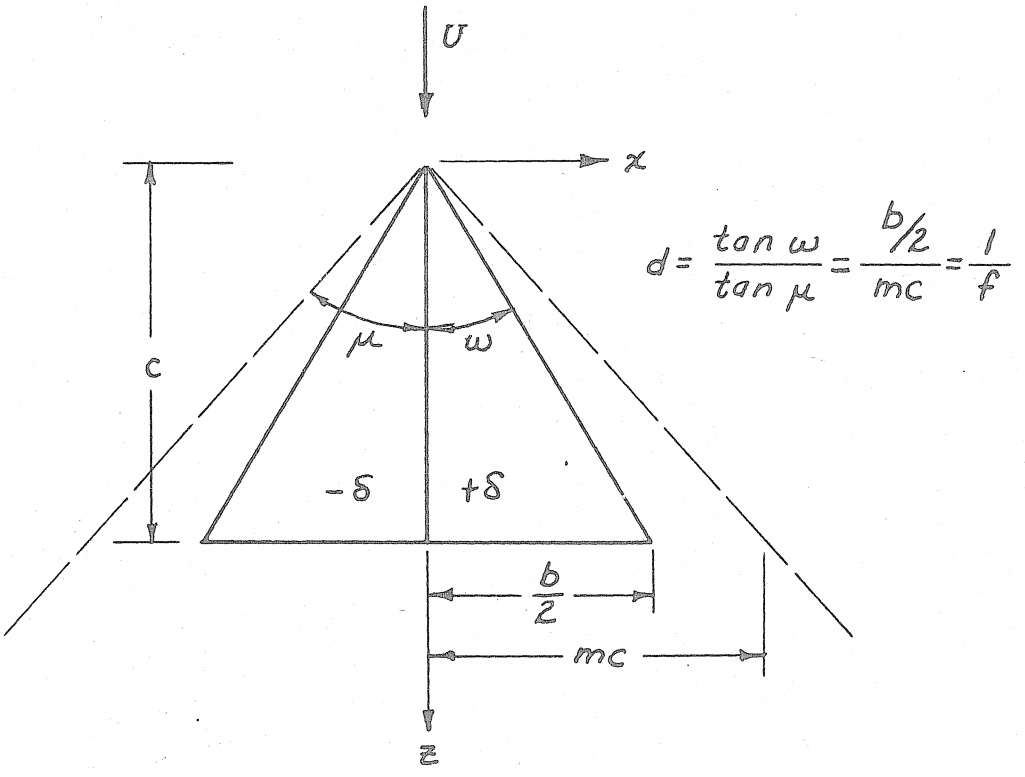

FIG. 14. PLANE NARROW-DELTA AILERON

Fig. 15. Approximation to Roll Due to Aileron Deflection for Cruciform Narrow-Delta Wing

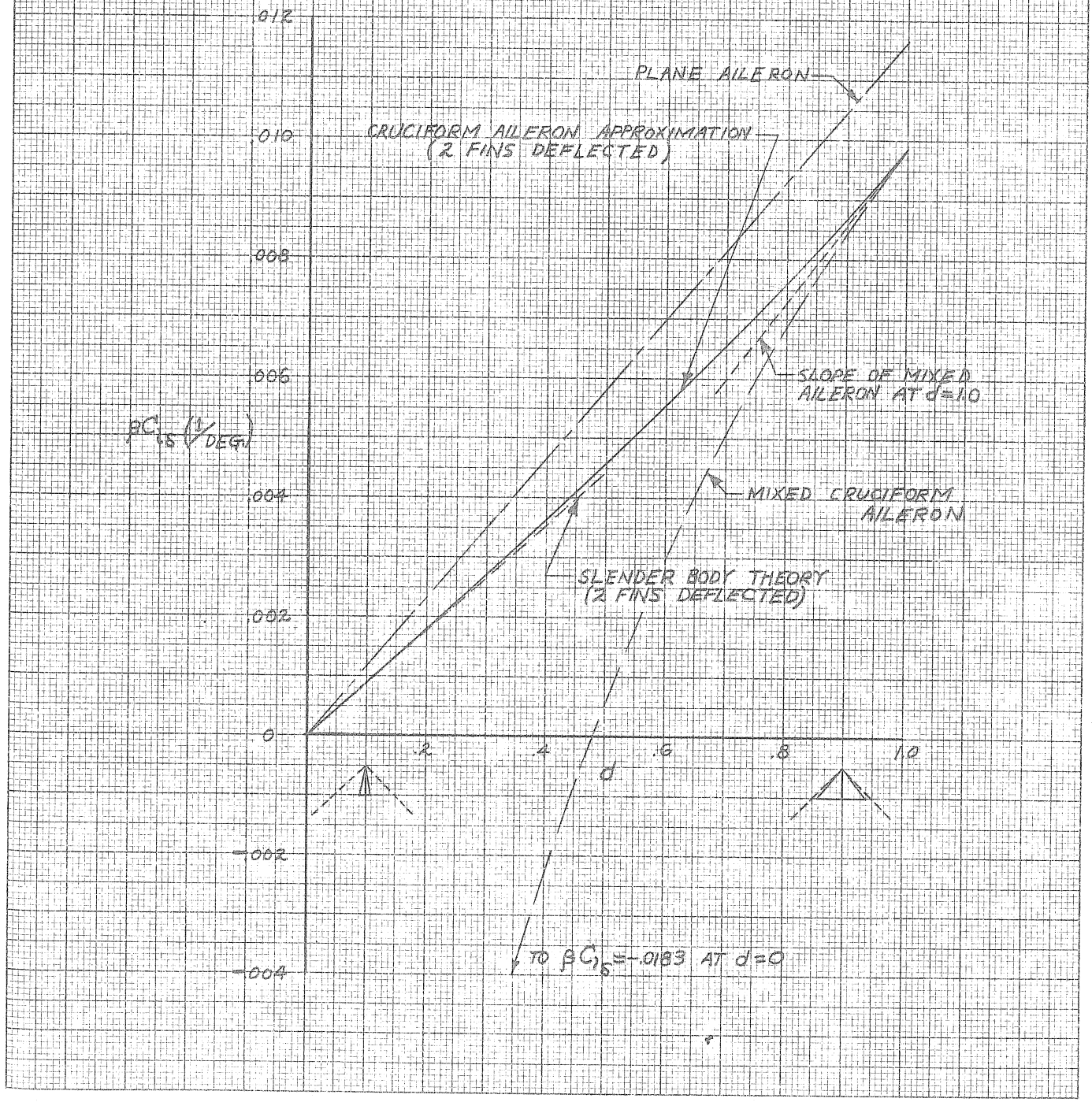

Fig. 16. Roll Due to Aileron Deflection for Multi-Fin Narrow-Delta Wings

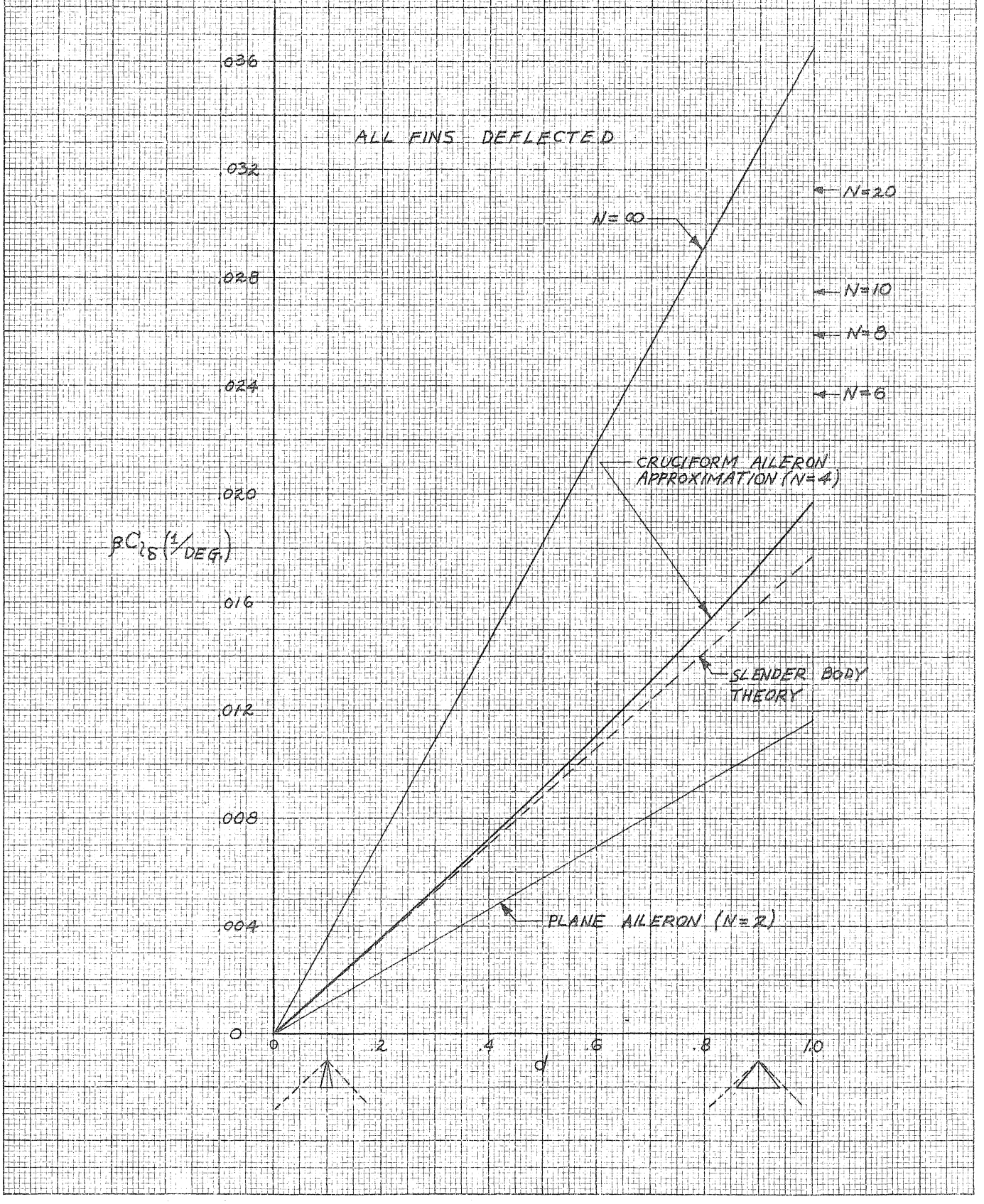

Fig. 17. Interpolation Curves for Multi-Fin Delta Wings with Sonic Leading Edges

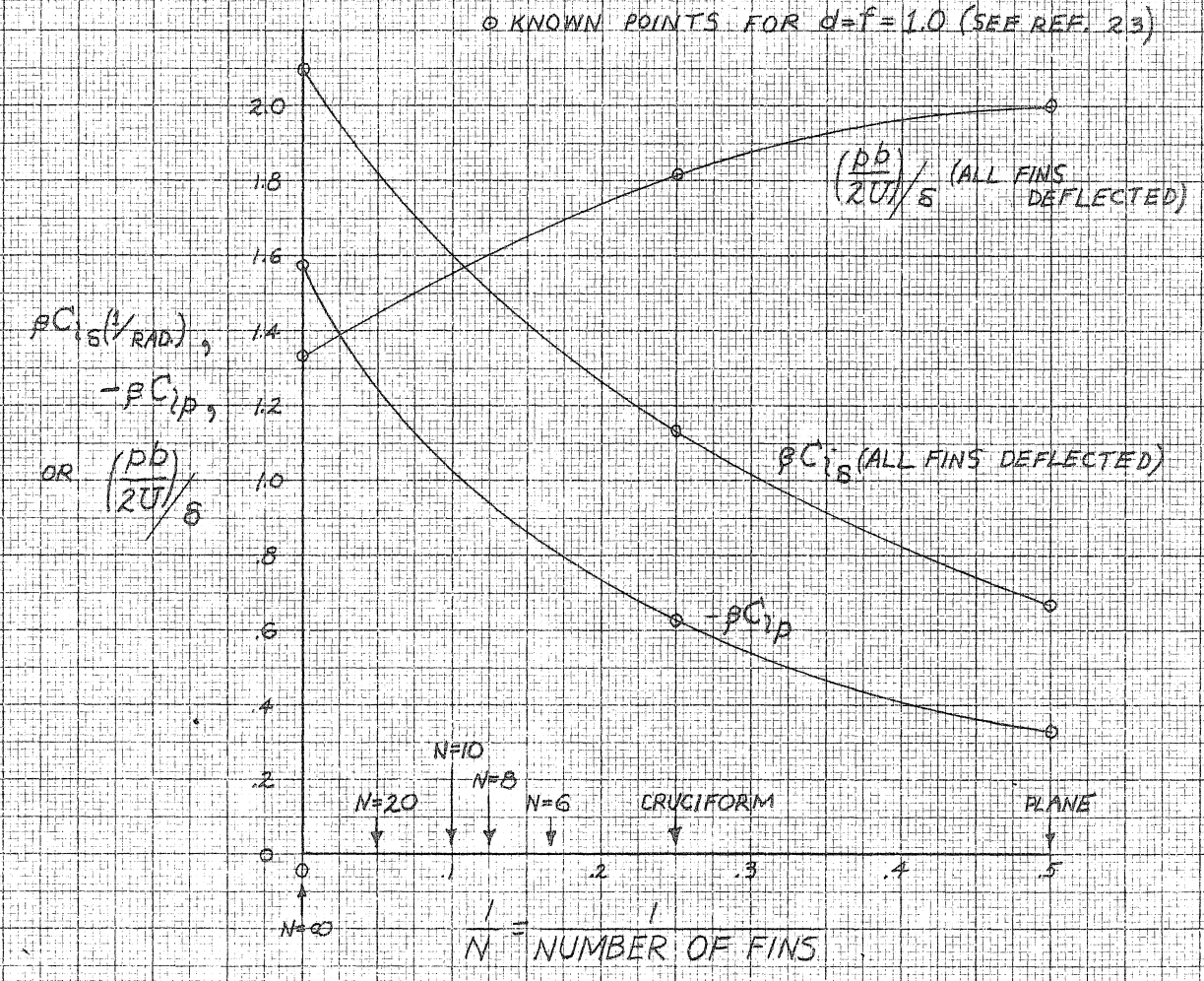

Fig. 18. Roll Due to Aileron Deflection for Multi-Fin Delta Wings

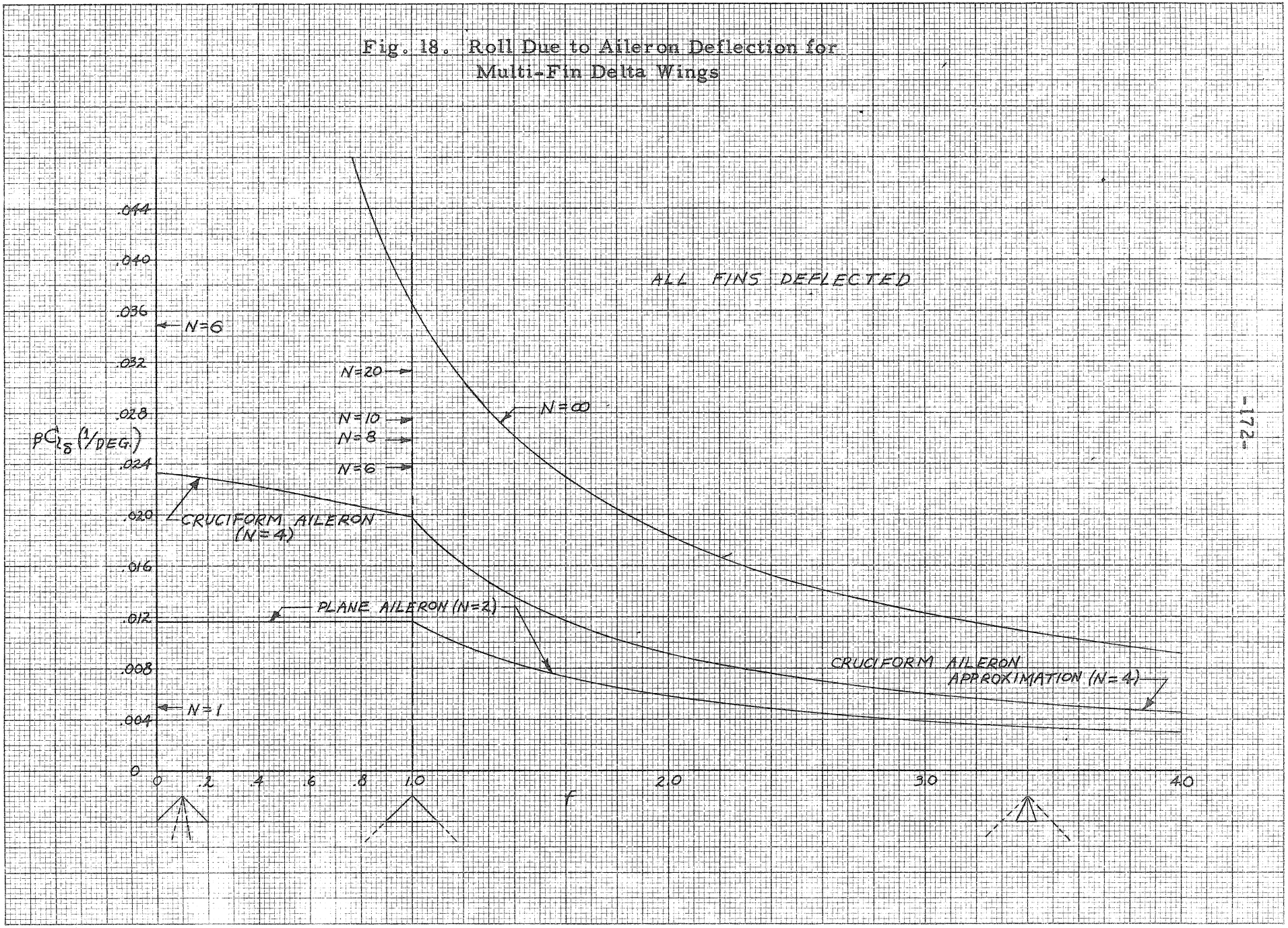

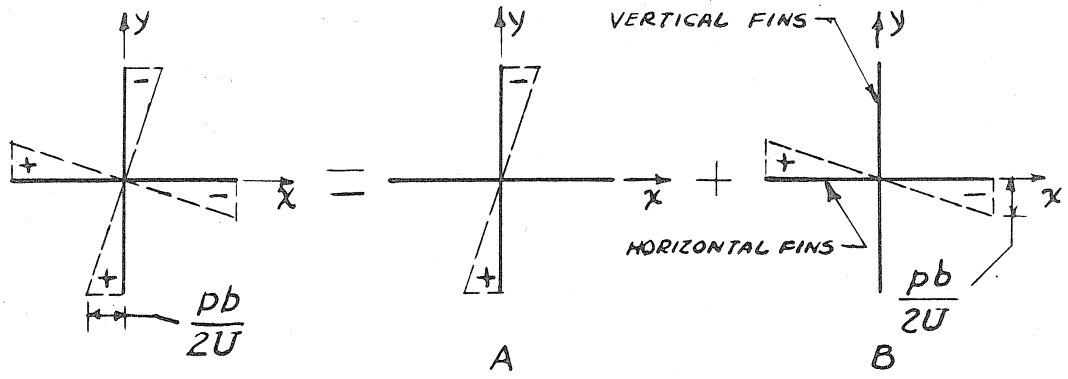

FIG. 19. DAMPING IN ROLL SUPERPOSITION

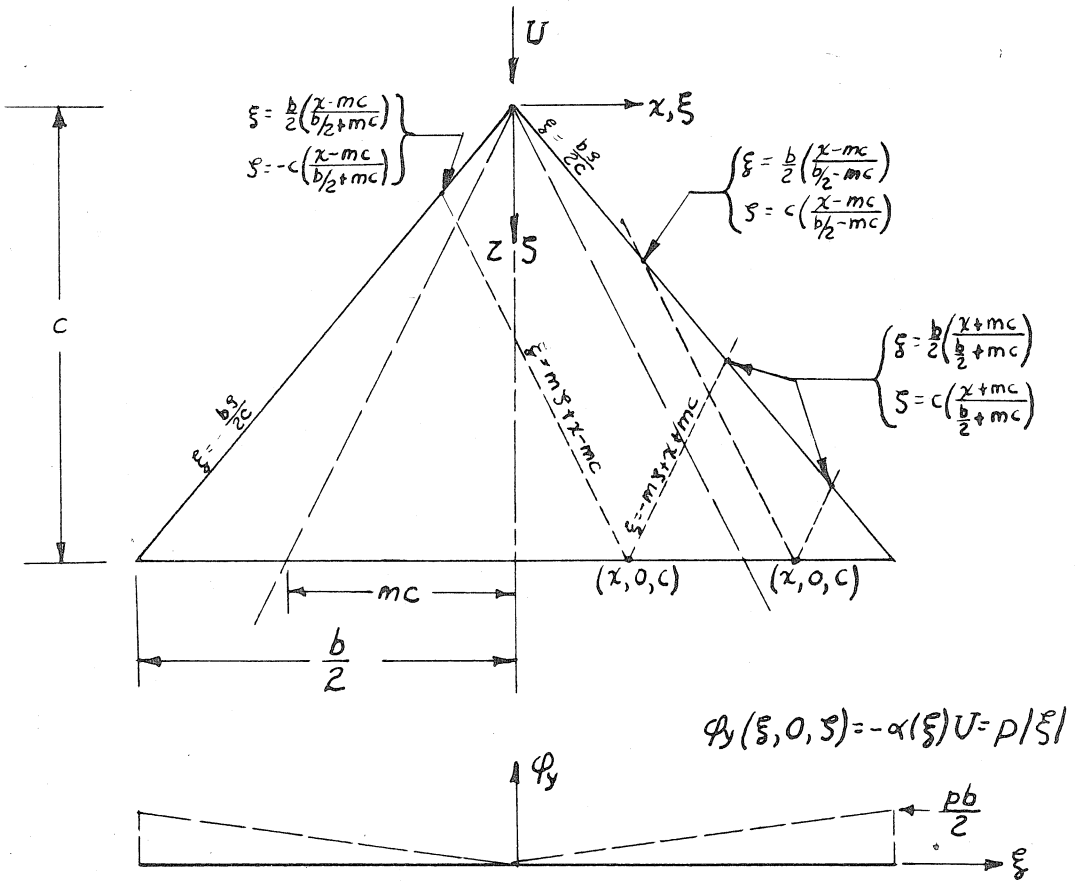

FIG. 20. EQUIVALENT PLANAR WING PROBLEM FOR HORIZONTAL FINS

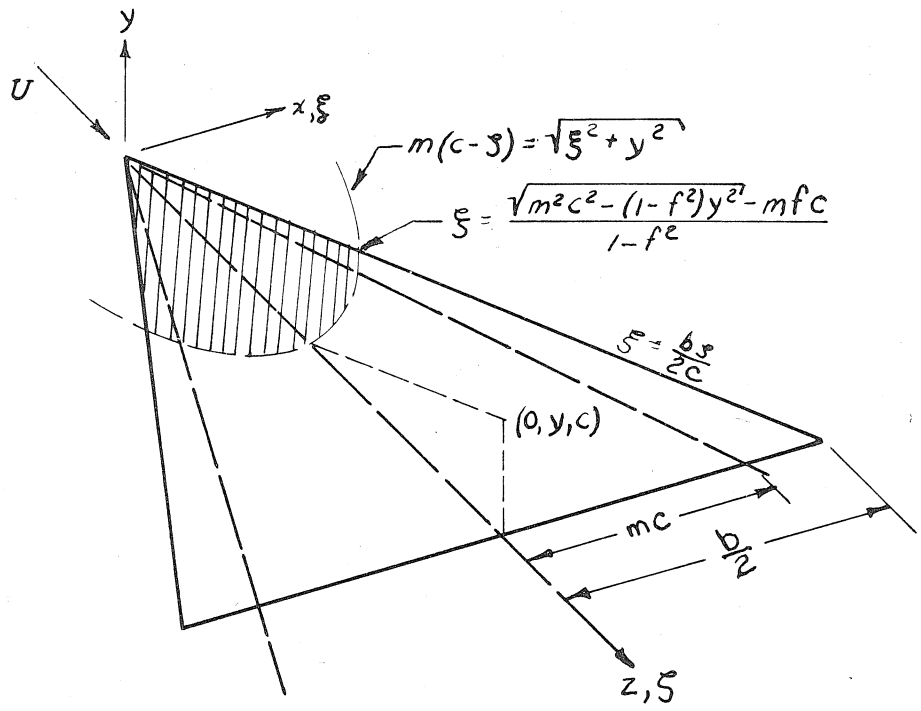

FIG. 21. EQUIVALENT PLANAR WING PROBLEM FOR VERTICAL FINS

Fig. 22. Damping in Roll for Cruciform Wide-Delta Wing

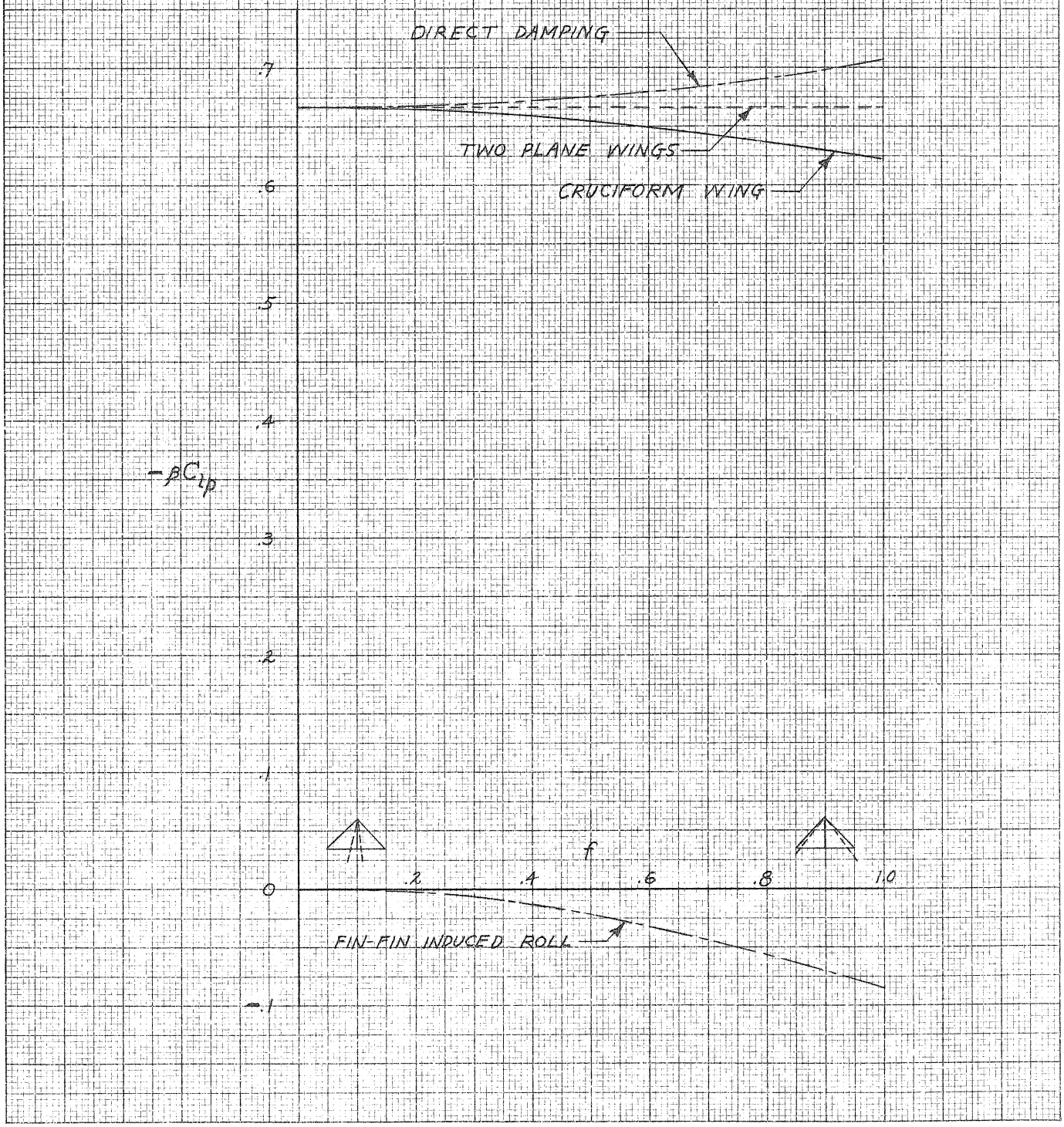

Fig. 23. Damping in Roll for Multi-Fin Narrow-Delta Wings

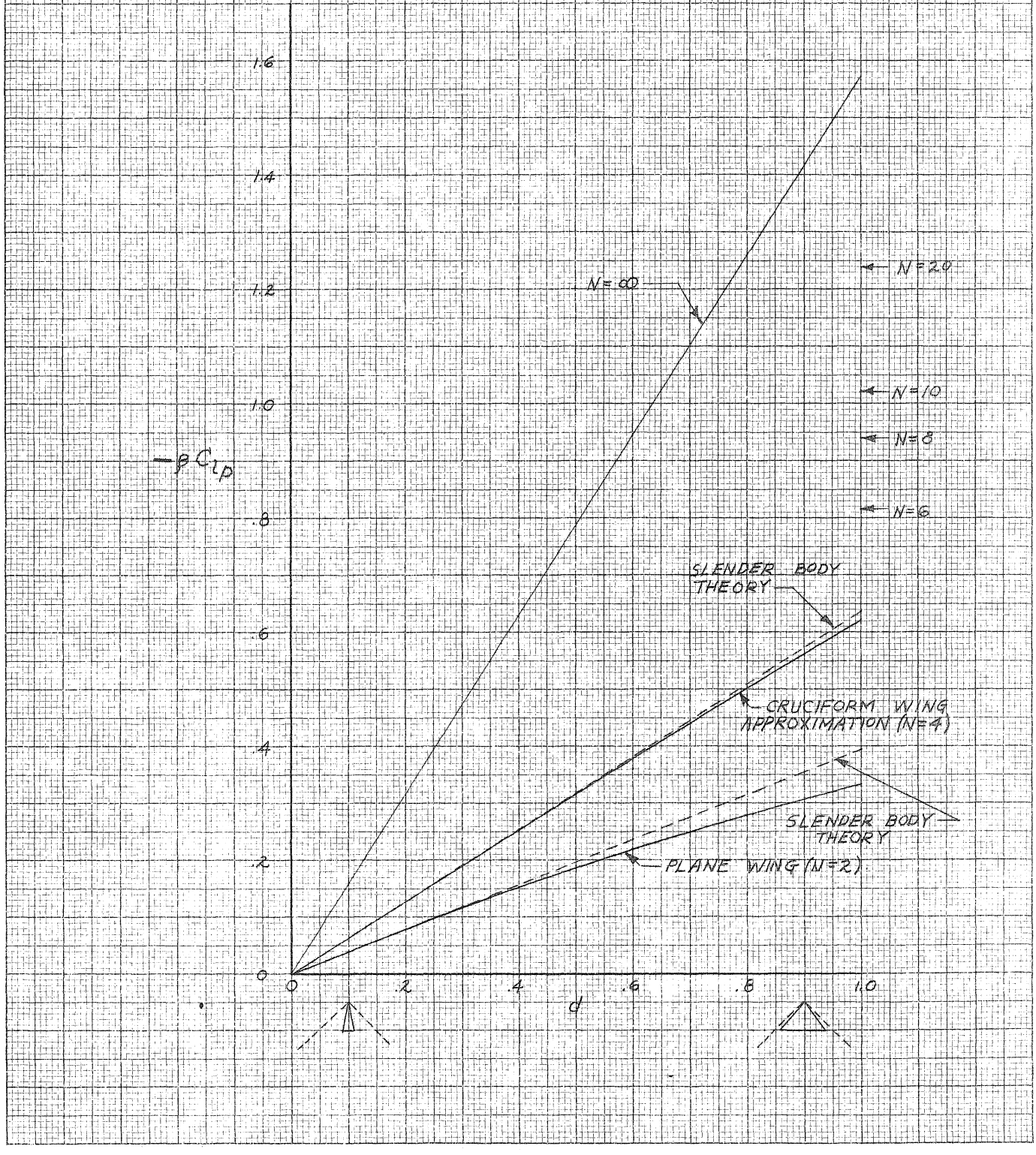

Fig. 24. Damping in Roll for Multi-Fin Delta Wings

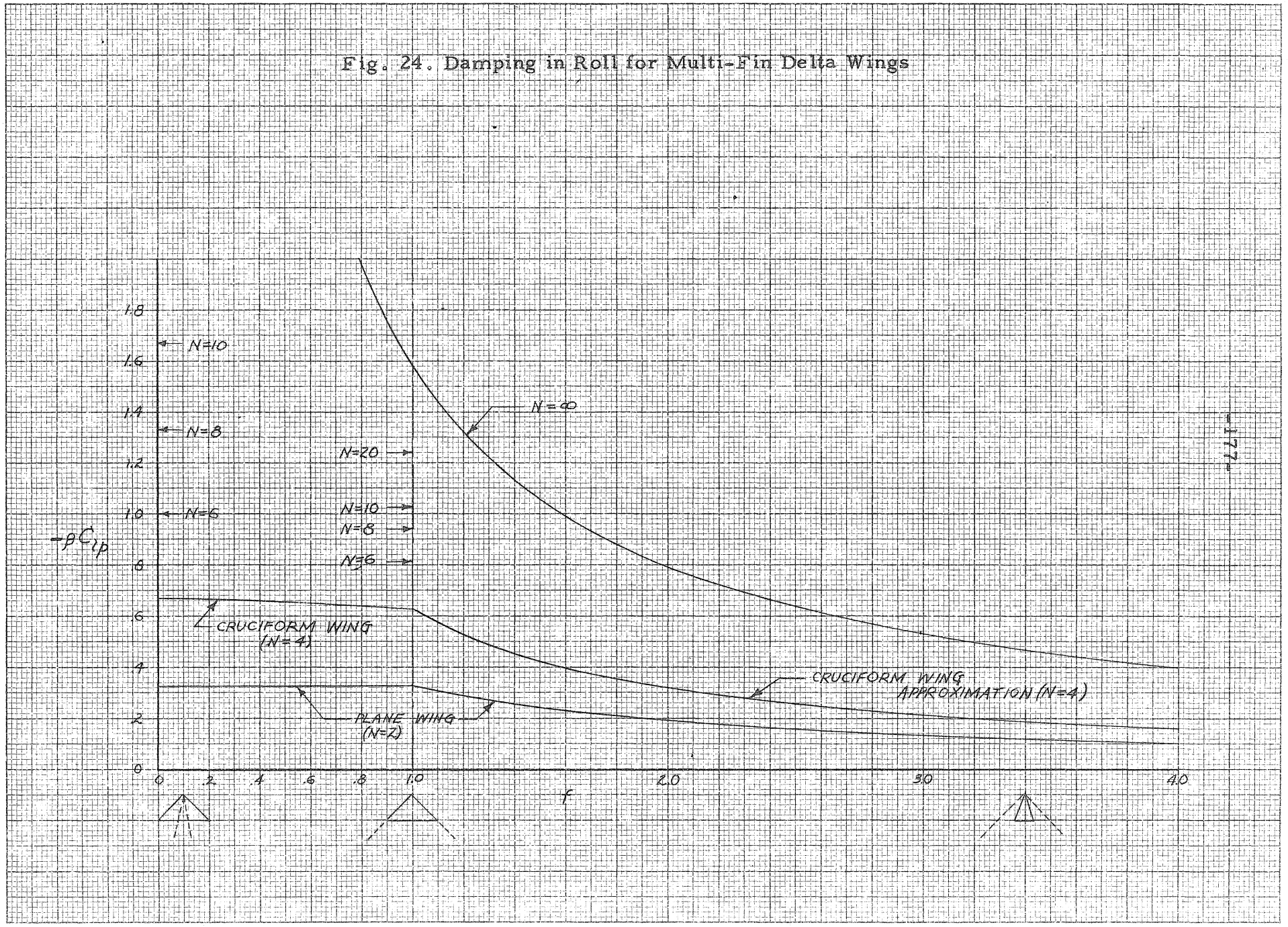

Fig. 25. Equilibrium Rate of Roll for Multi-Fin Narrow-Delta Wings

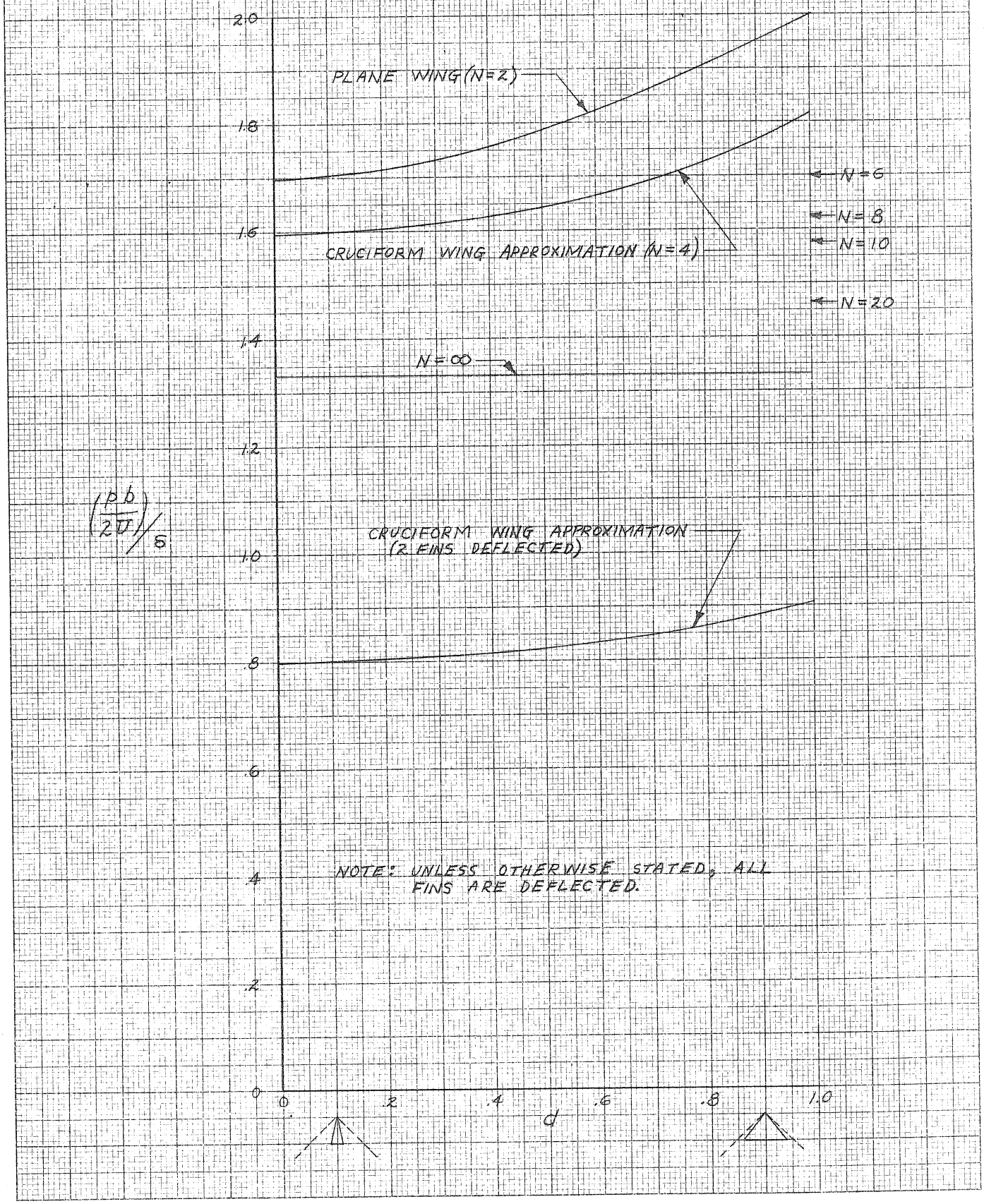

Fig. 26. Equilibrium Rate of Roll for Multi-Fin Delta Wings

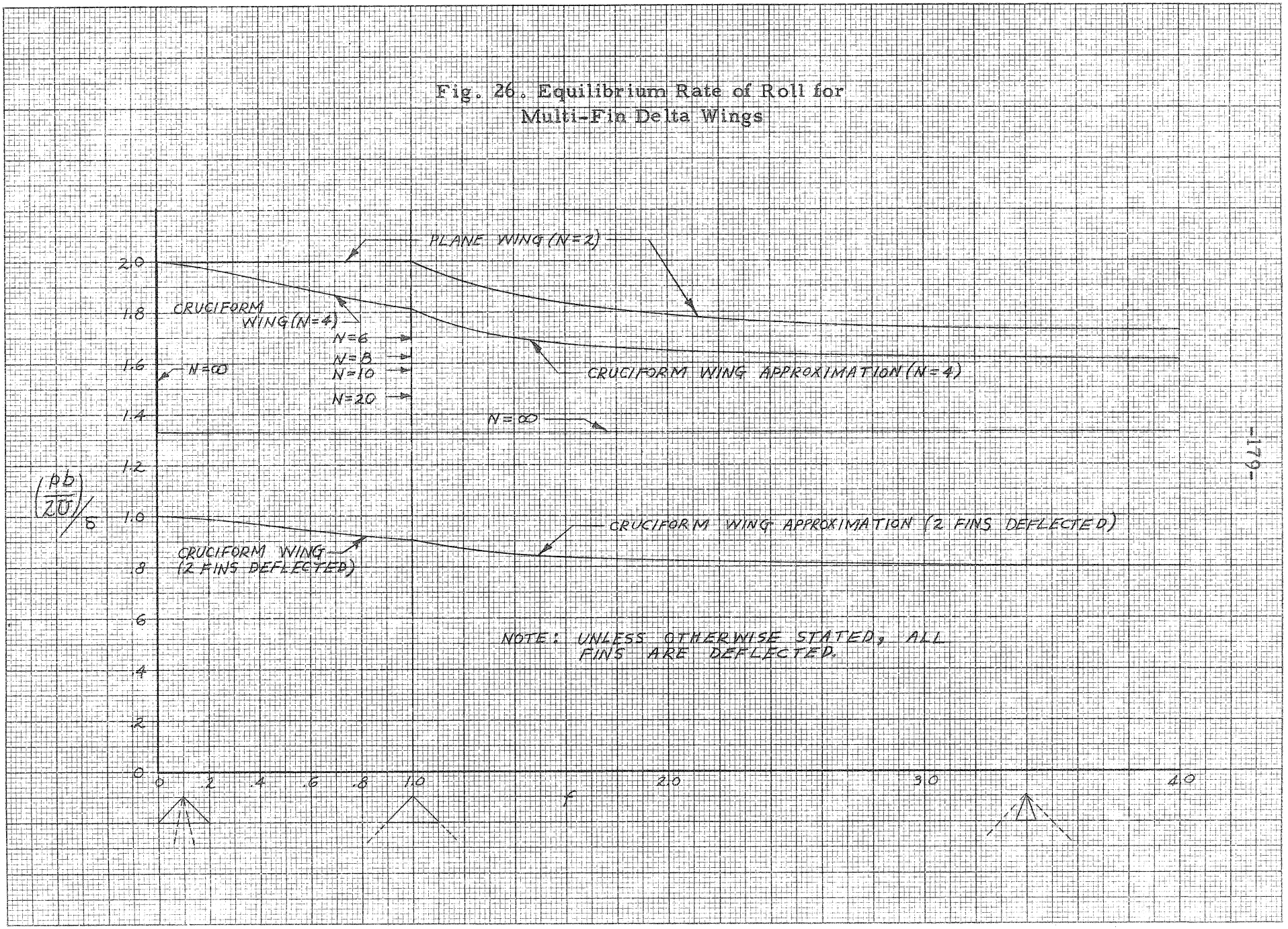

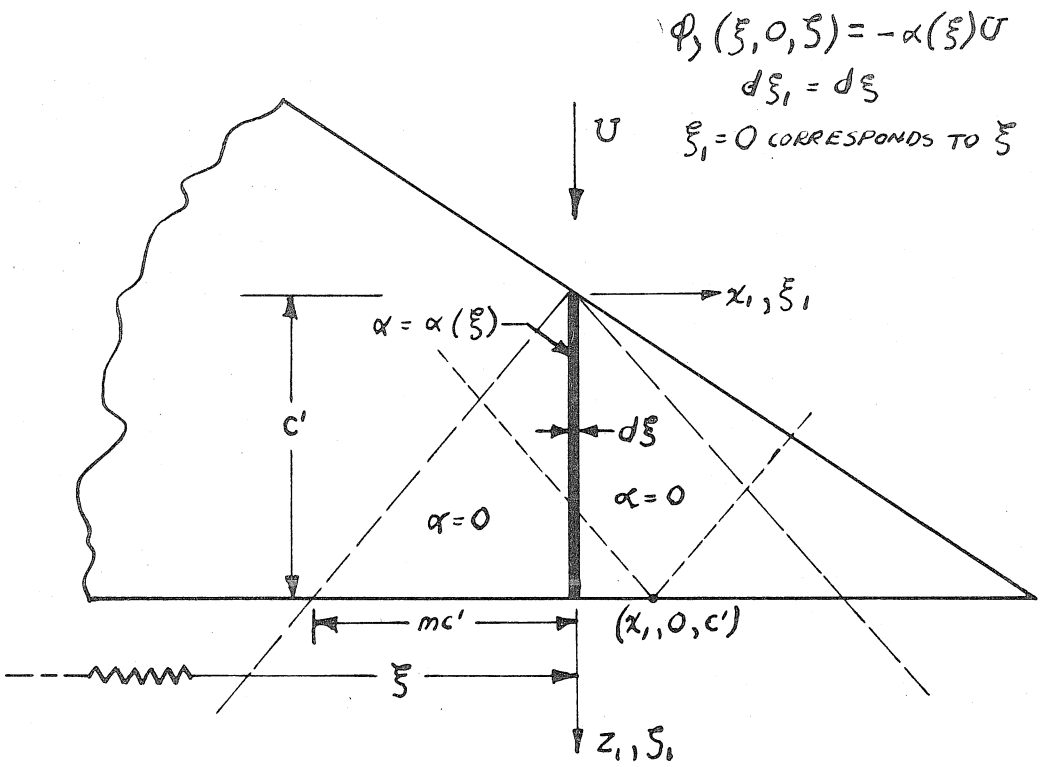

FIG. 27 ELEMENTARY STRIP ADJACENT TO SUPERSONIC LEADING EDGE

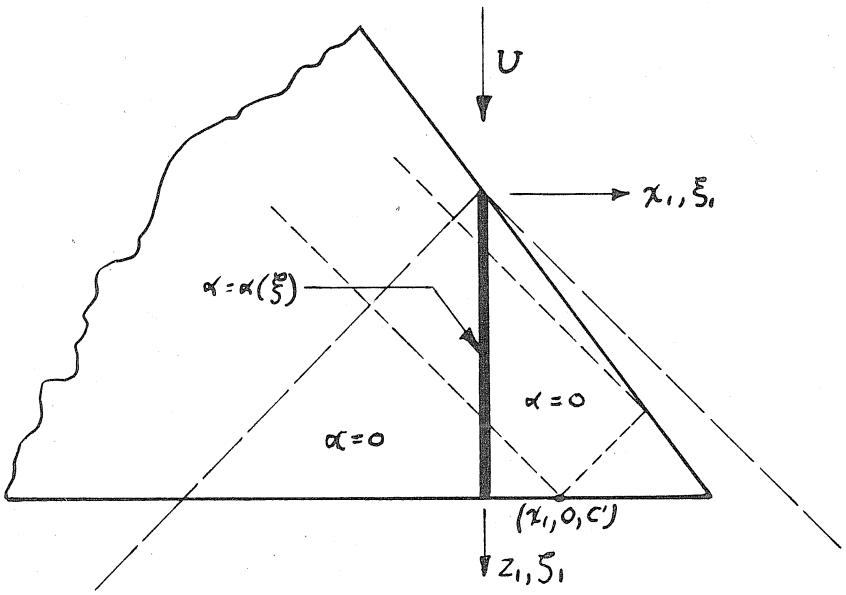

FIG 28. ELEMENTARY STRIP ADJACENT TO SUBSONIC LEADING EDGE

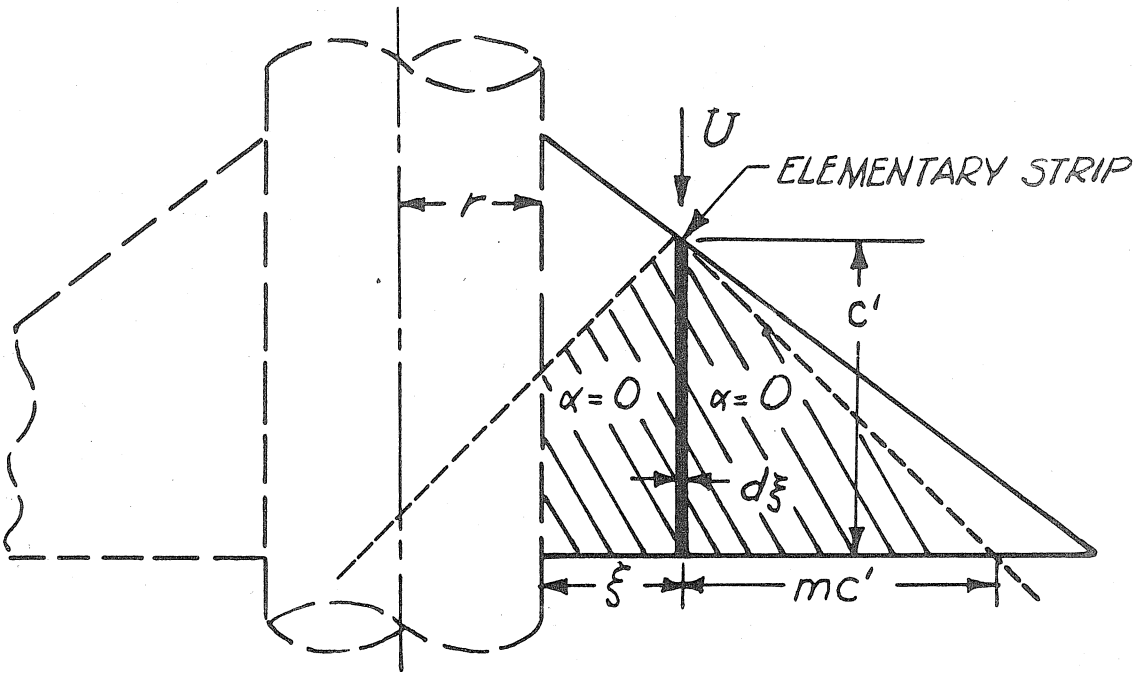

(a) UNDER ESTIMATE

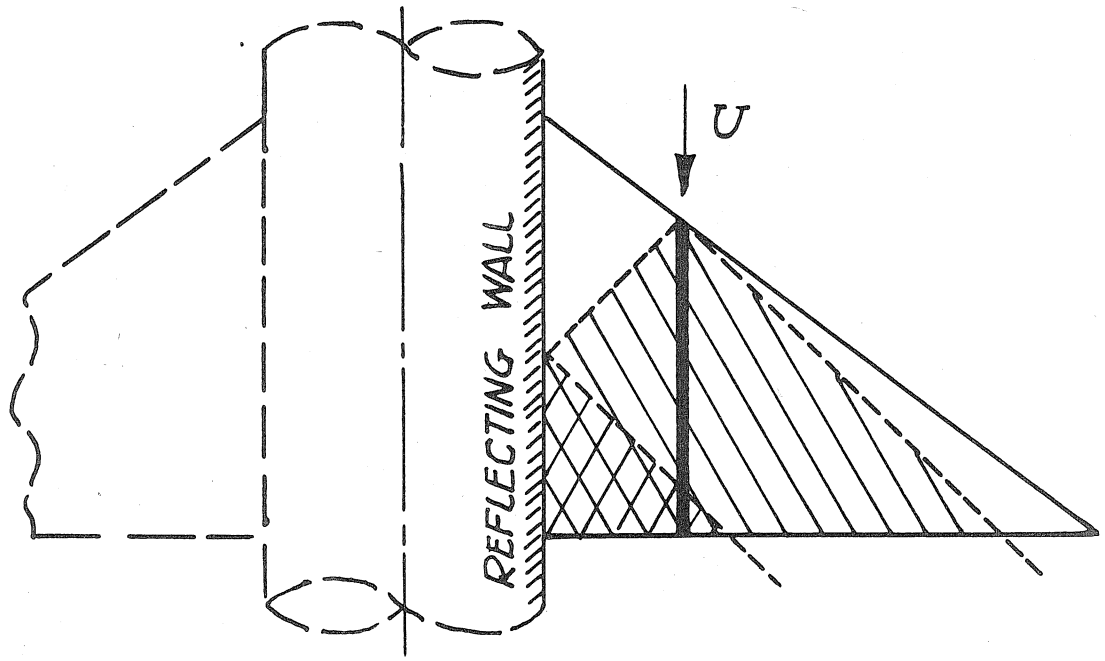

(b) OVER ESTIMATE

FIG. 29 ESTIMATES USING ELEMENTARY STRIP

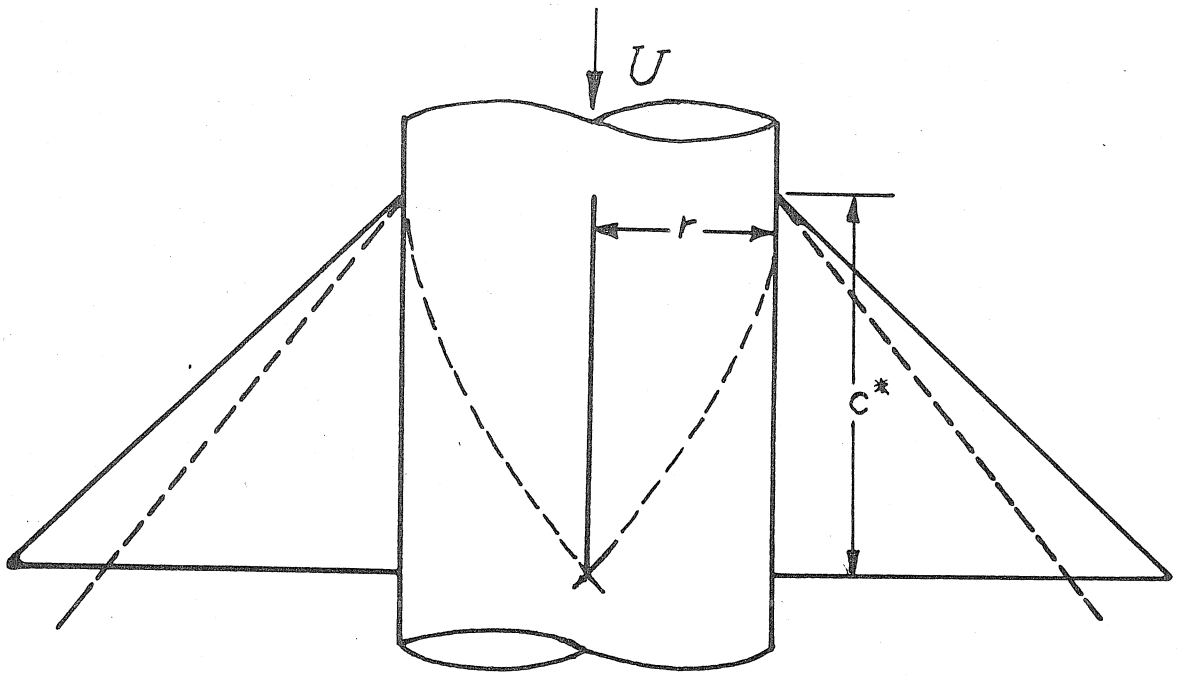

(a) CRUCIFORM WING

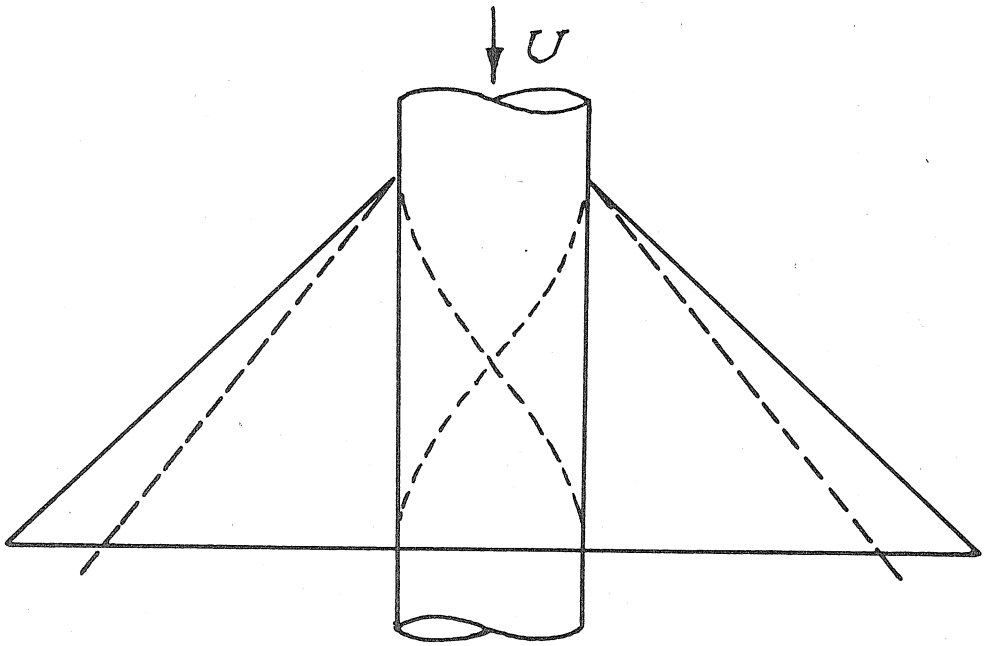

(b) PLANE WING

FIG. 30 LIMITS OF FIN-FIN INTERACTION

Fig. 31. Roll Due to Aileron Deflection for Plane Wide-Delta Wing-Body Combinations

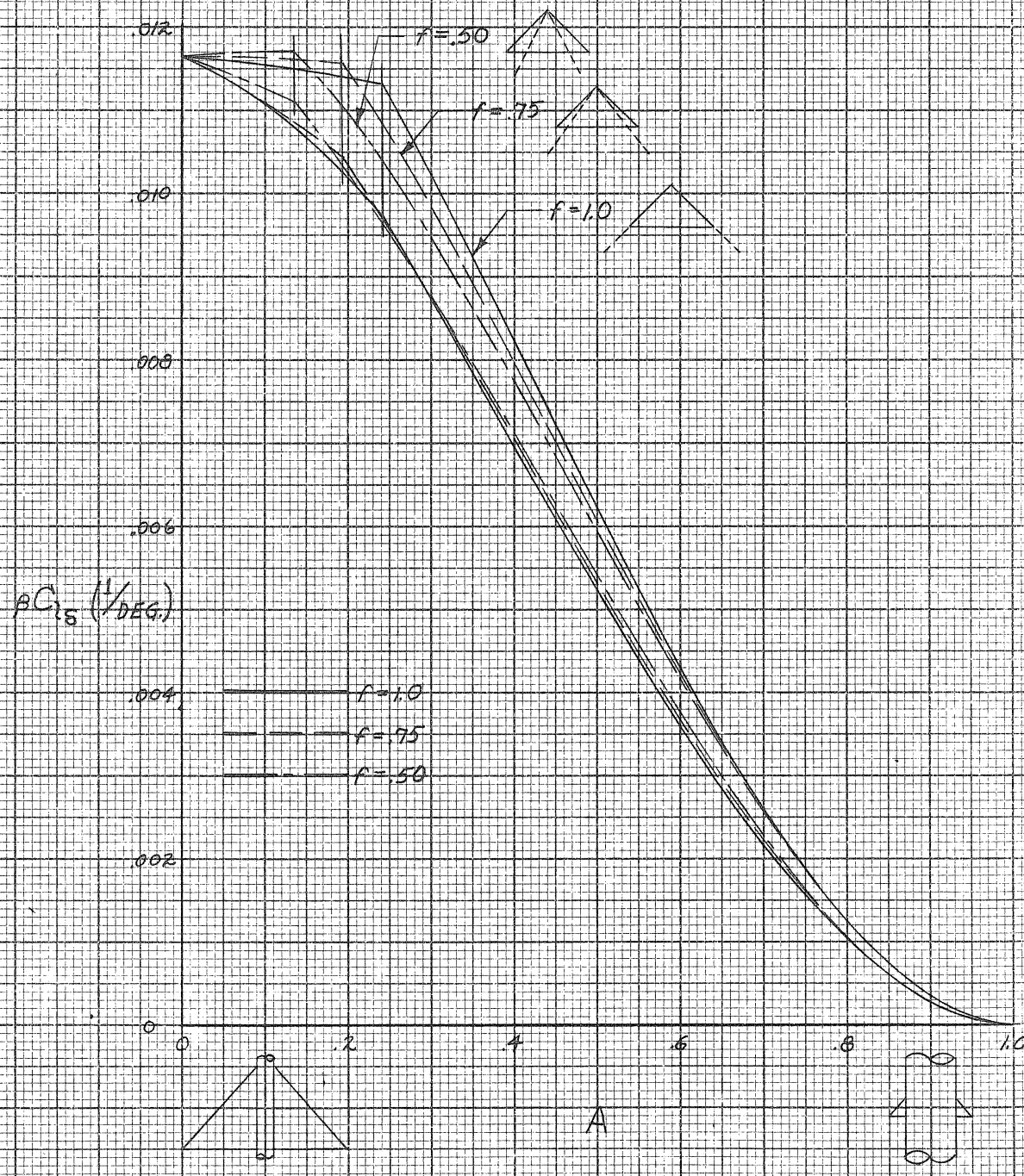

Fig. 32. Roll Due to Aileron Deflection for Cruciform Wide-Delta Wing-Body Combinations

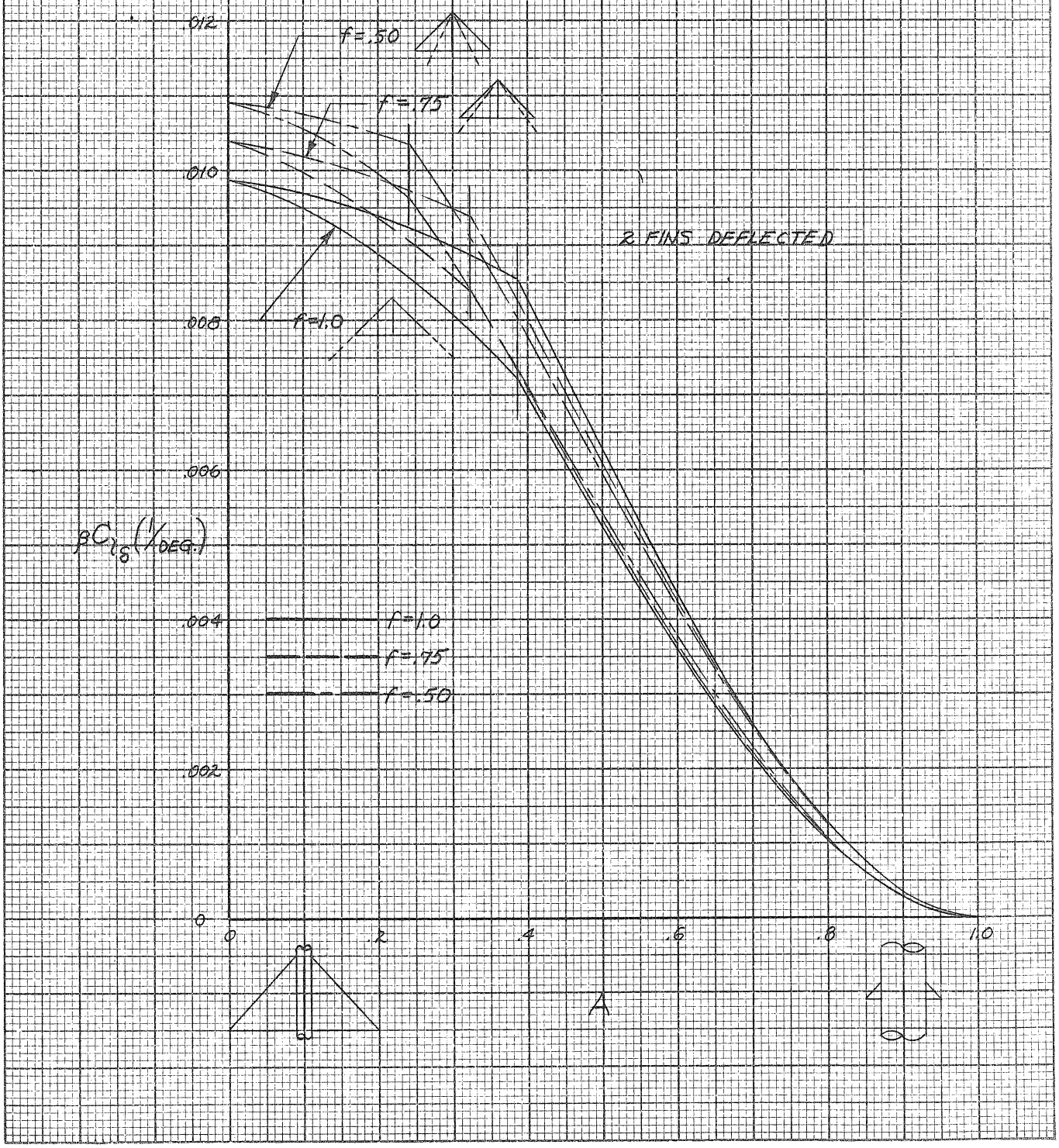

Fig. 33. Roll Due to Aileron Deflection for Plane Narrow-Delta Wing-Body Combinations

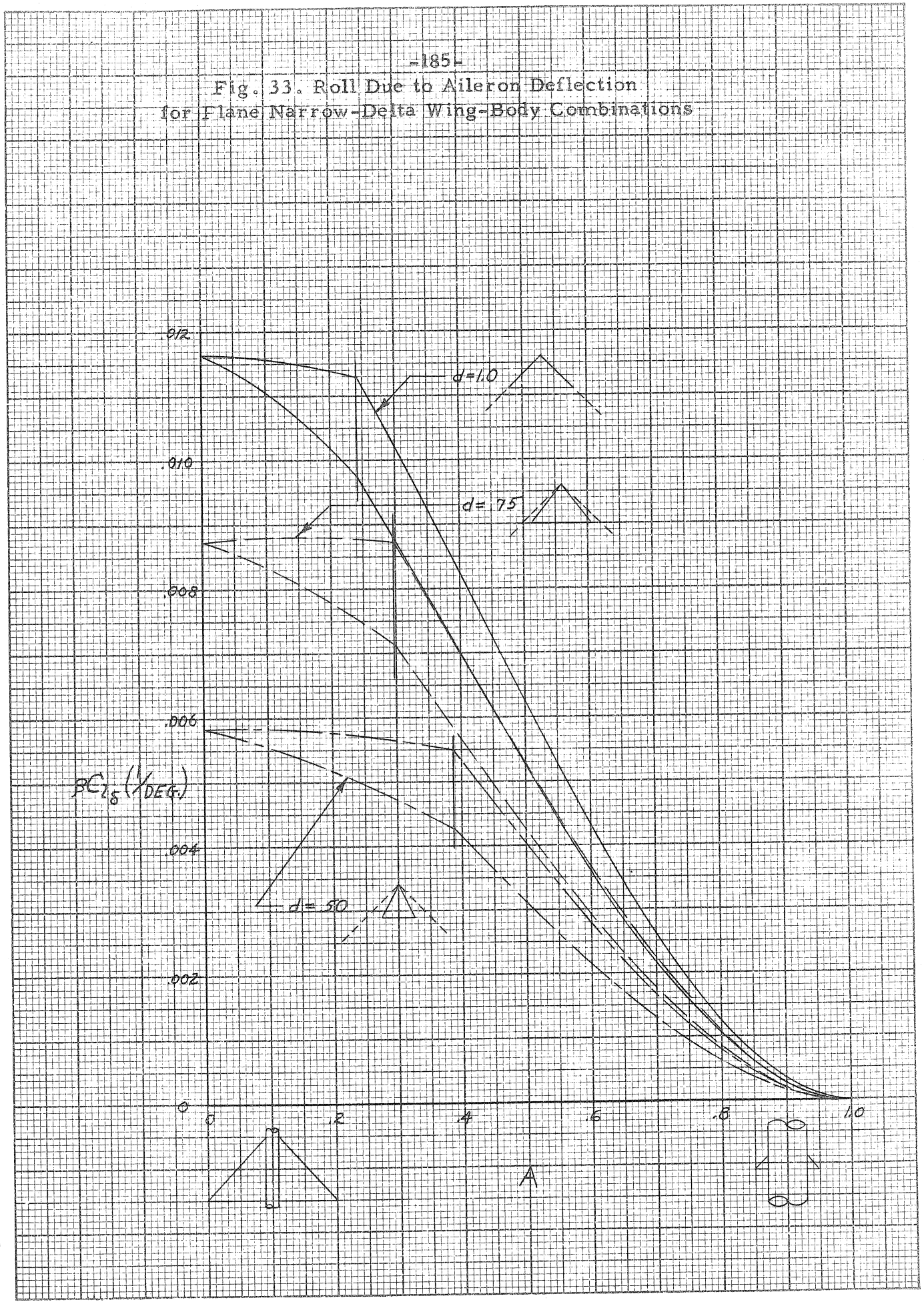

Fig. 34. Roll Due to Aileron Deflection for Cruciform Narrow-Delta Wing-Body Combinations

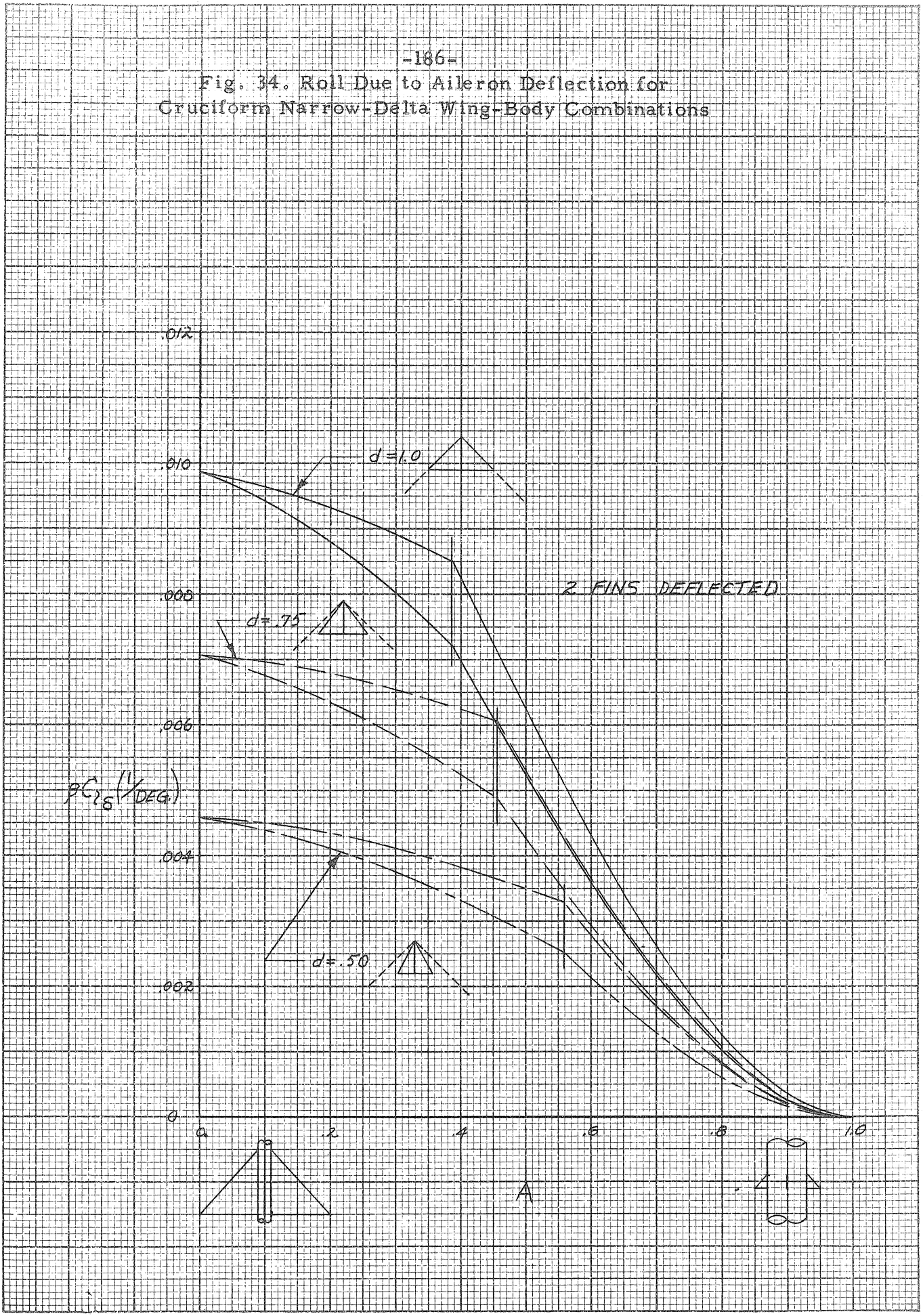

Fig. 35. Damping in Roll for Two Plane Wide-Delta Wing-Body Combinations

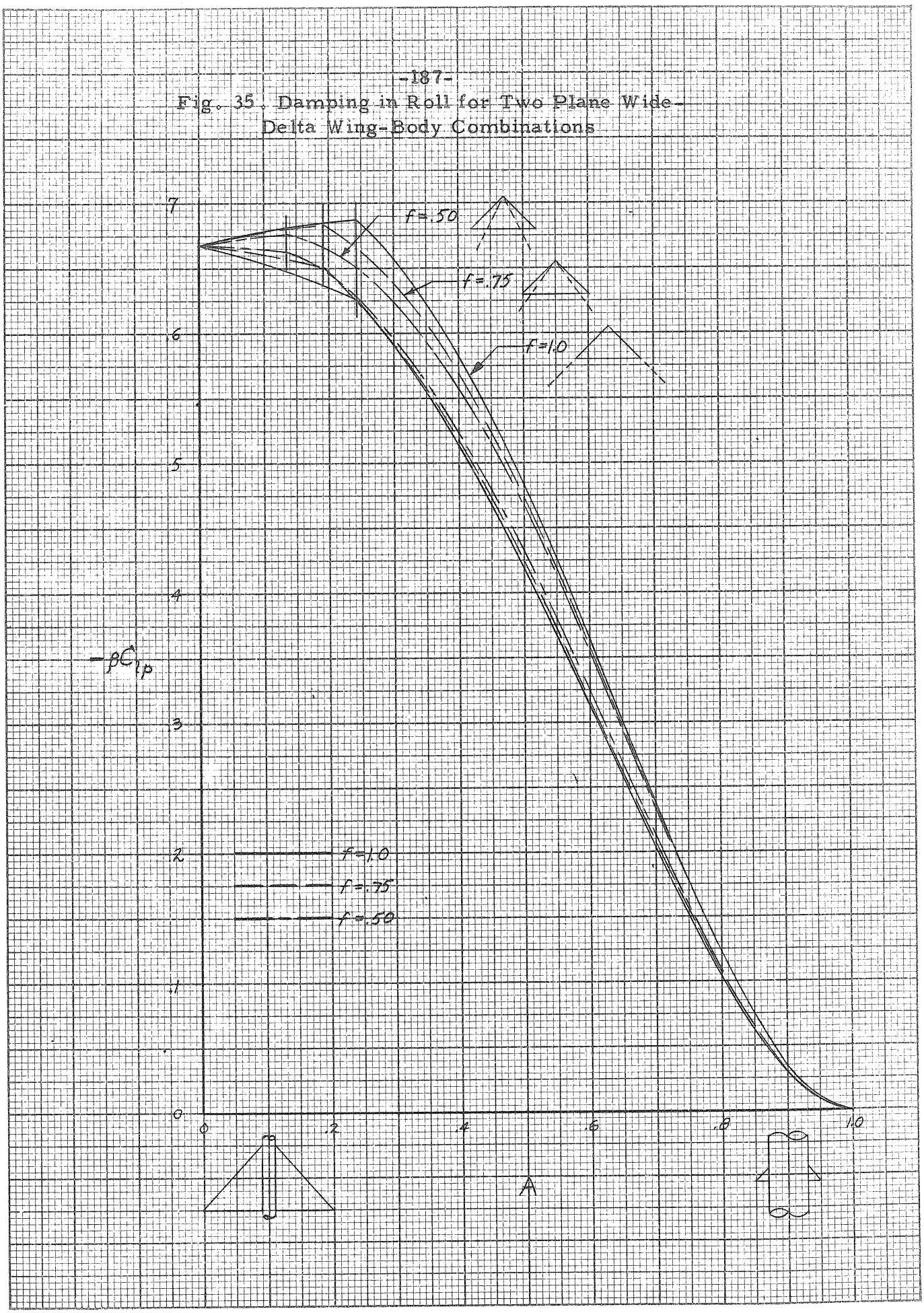

Fig. 36. Damping in Roll for Cruciform Wide-Delta Wing-Body Combinations

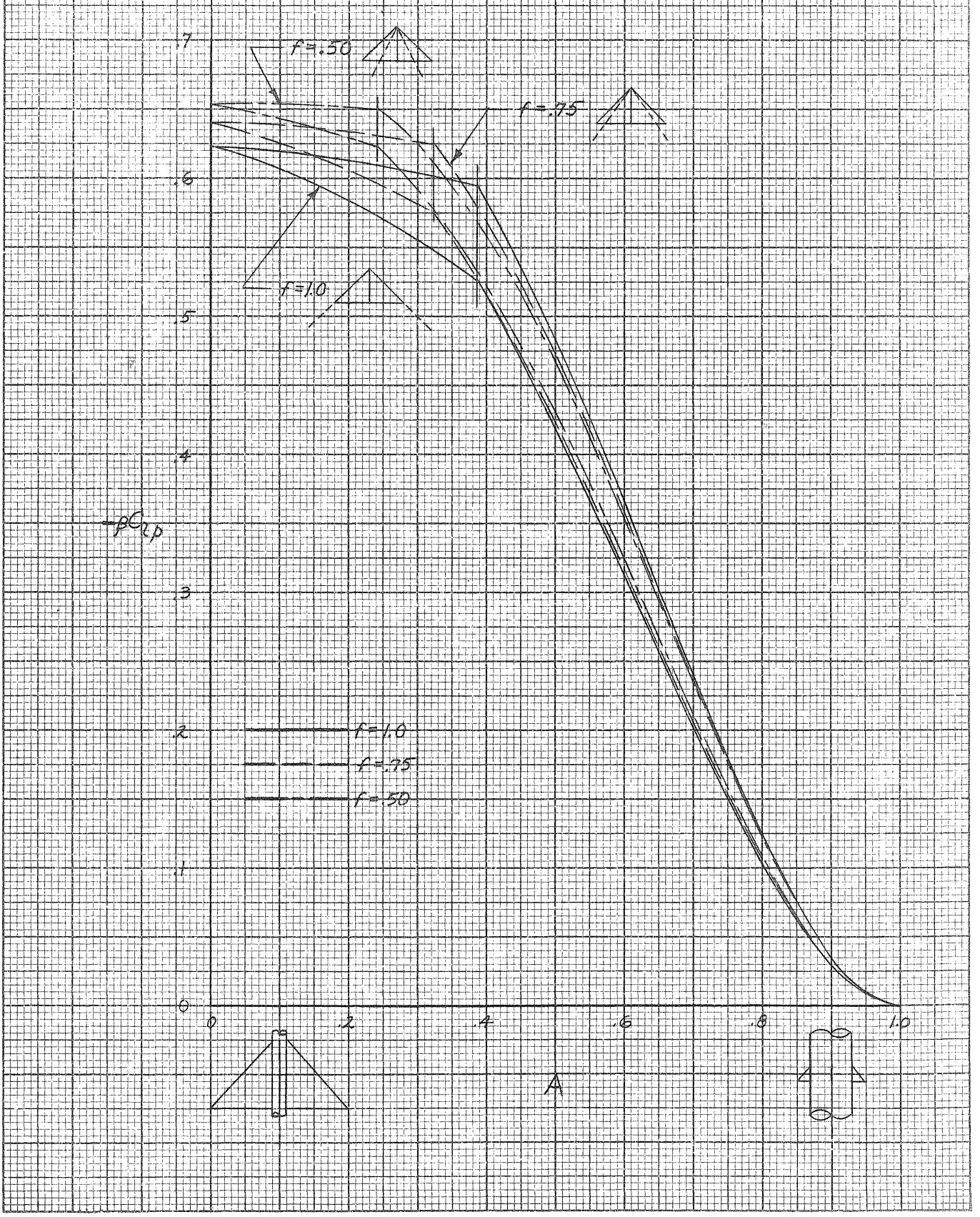

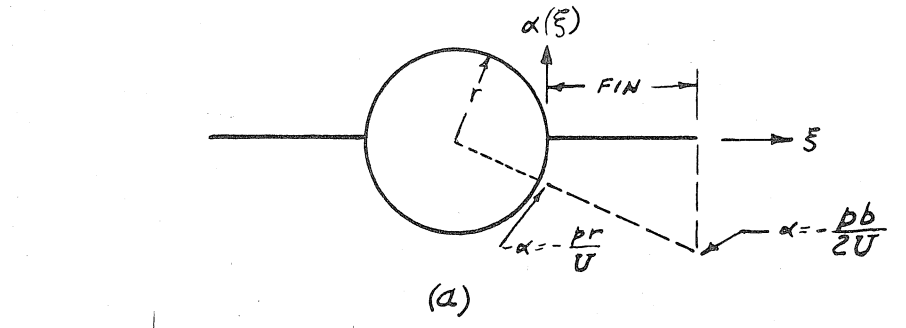

(a)

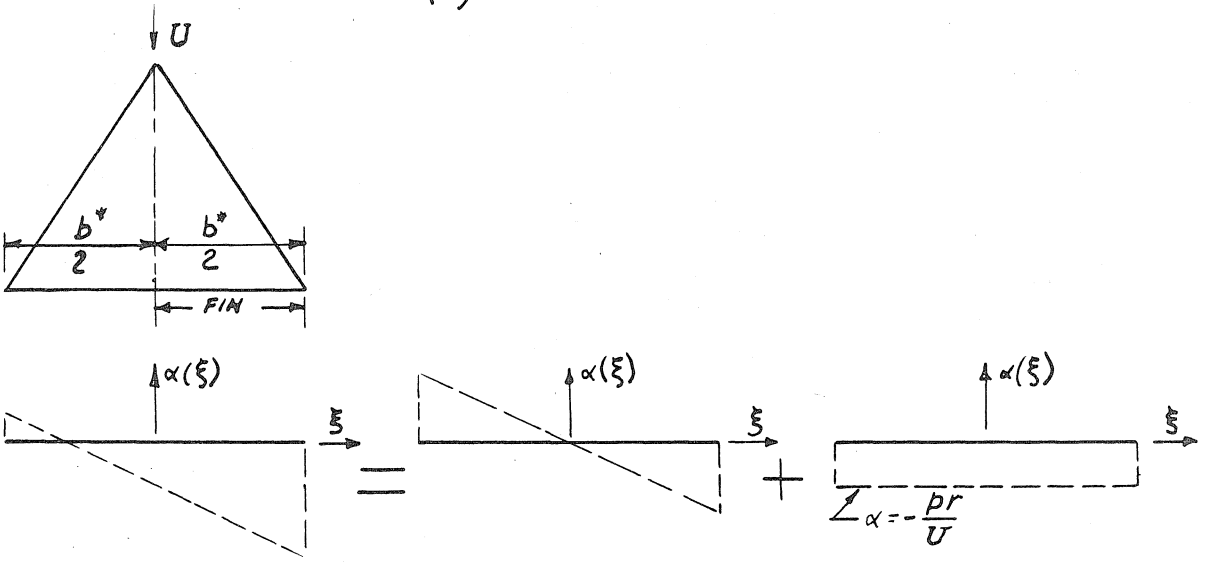

(b) IMPROVED UNDERESTIMATE

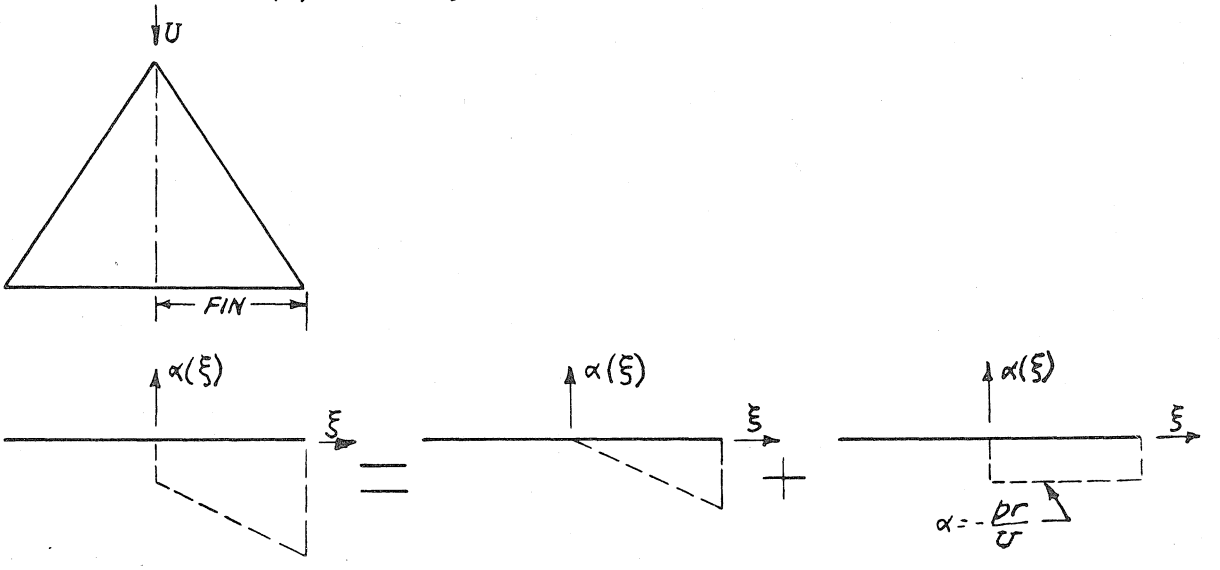

(c) UNDERESTIMATE USED HERE

FIG. 37. EQUIVALENT PLANAR WING PROBLEM FOR IMPROVED UNDERESTIMATE

Fig. 38. Improved Underestimate for Damping in Roll for Two Plane Wide-Delta Wing-Body Combinations

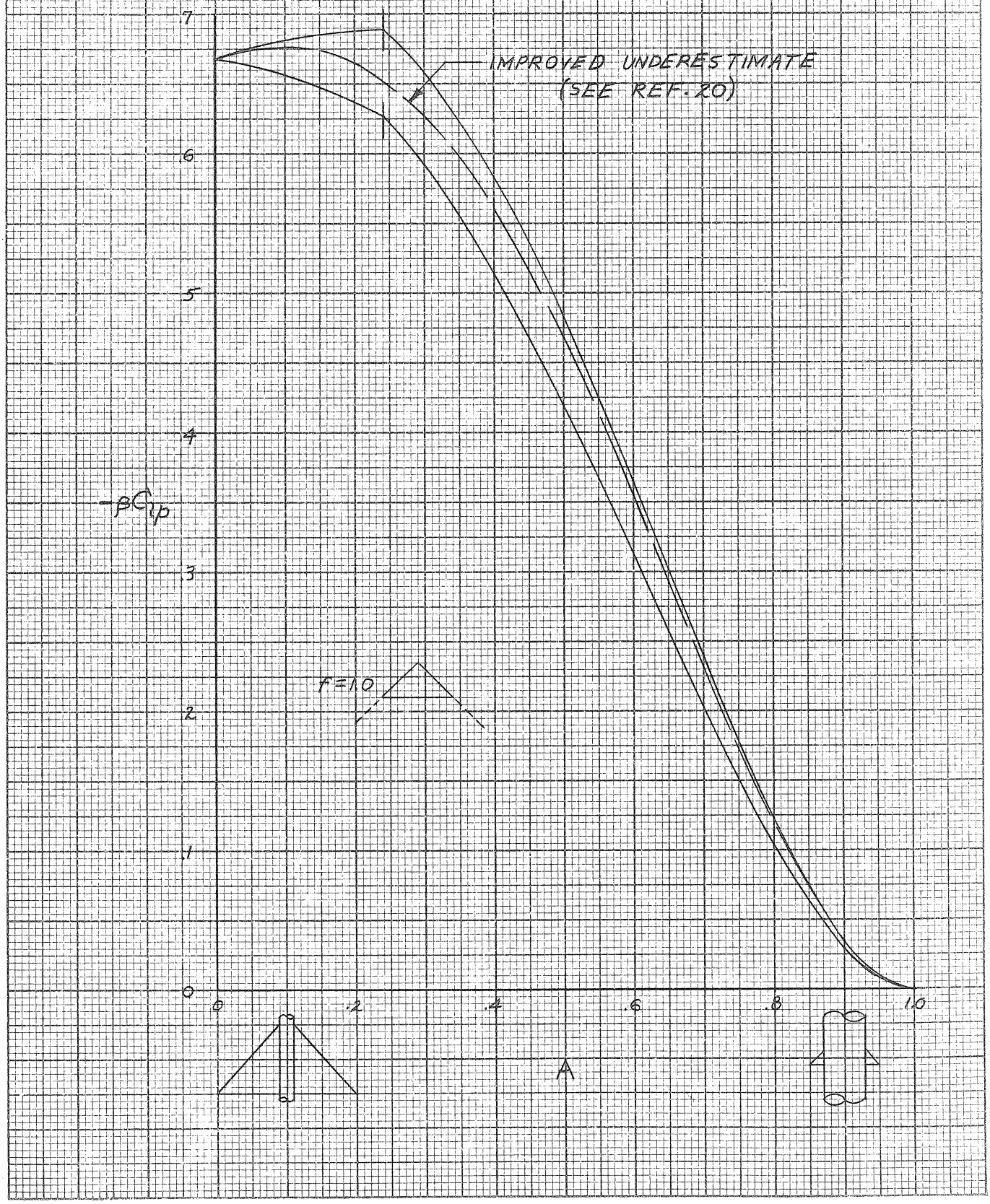

Fig. 39. Improved Underestimate for Damping in Roll for Cruciform Wide-Delta Wing-Body Combinations

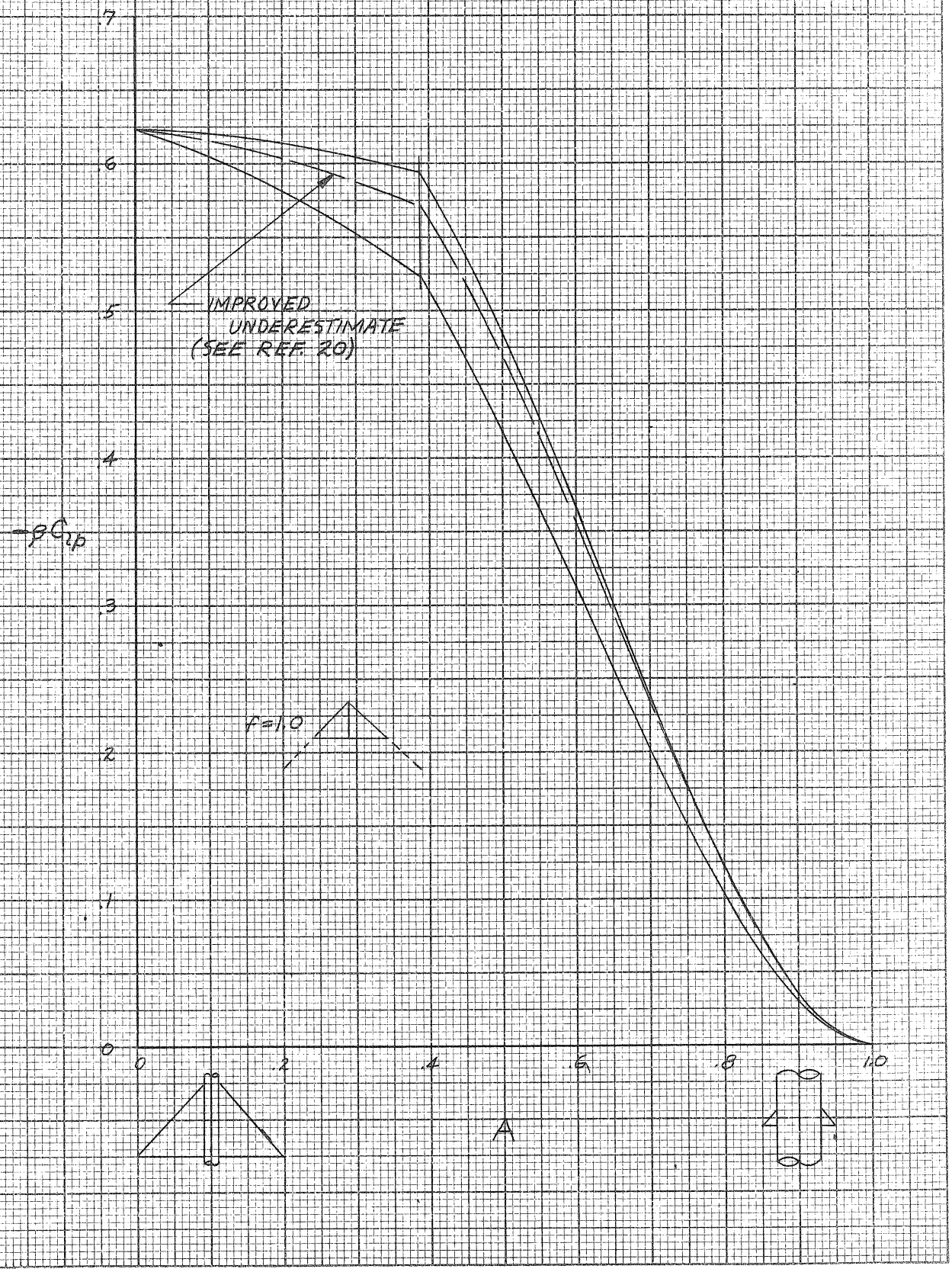

Fig. 40. Equilibrium Rate of Roll for Plane Wide-Delta Wing-Body Combinations

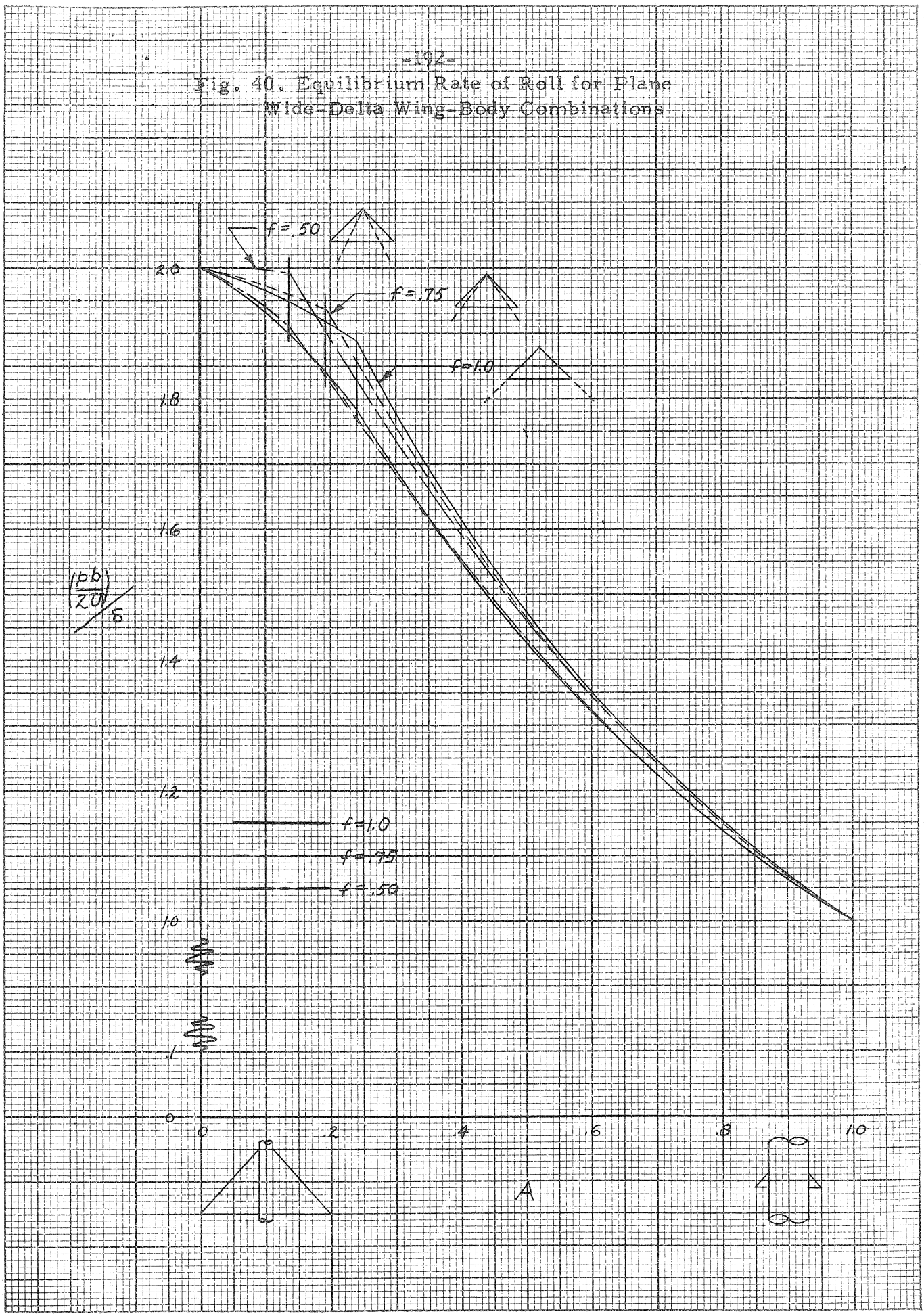

Fig. 41. Equilibrium Rate of Roll for Cruciform Wide-Delta Wing-Body Combinations

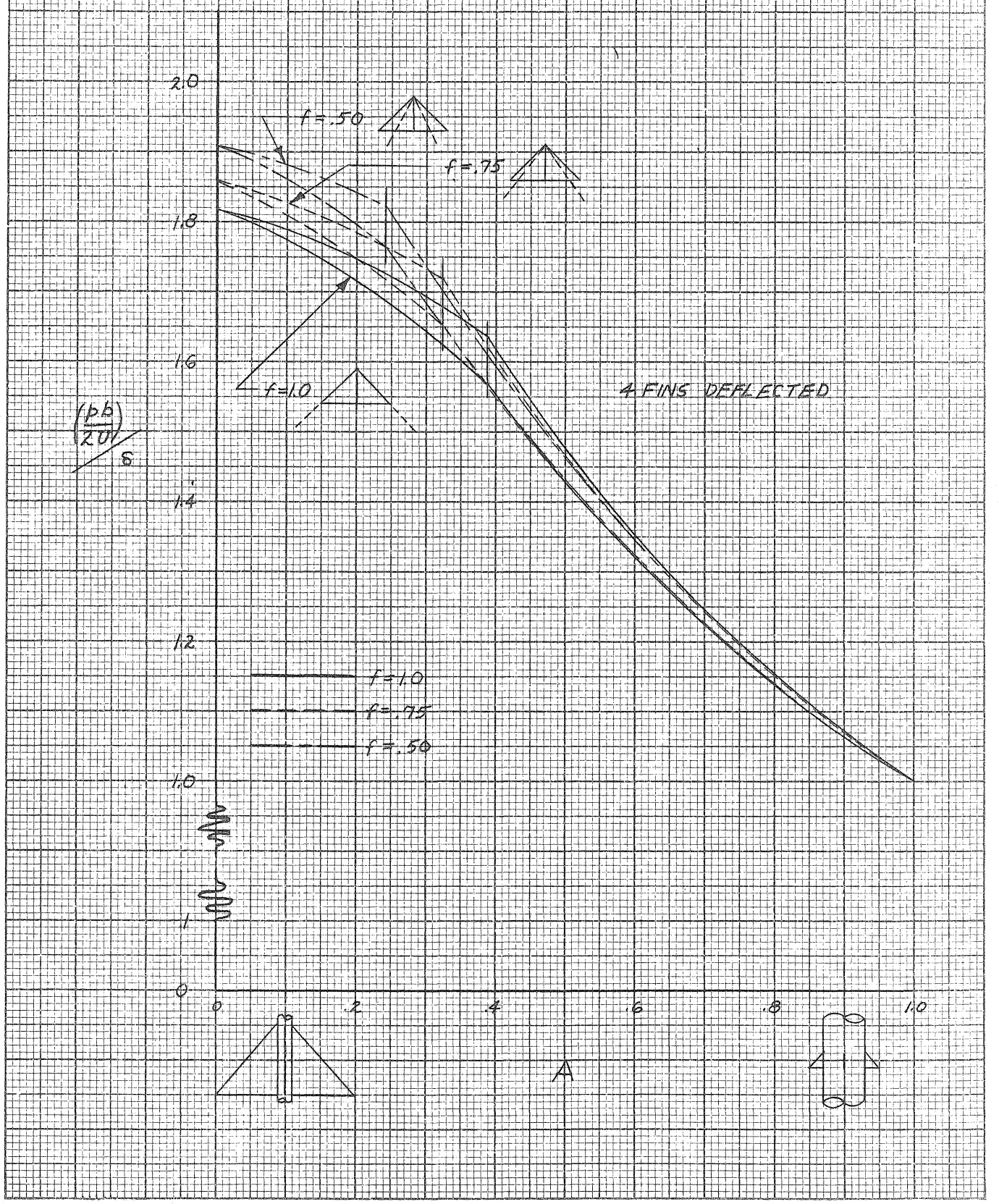

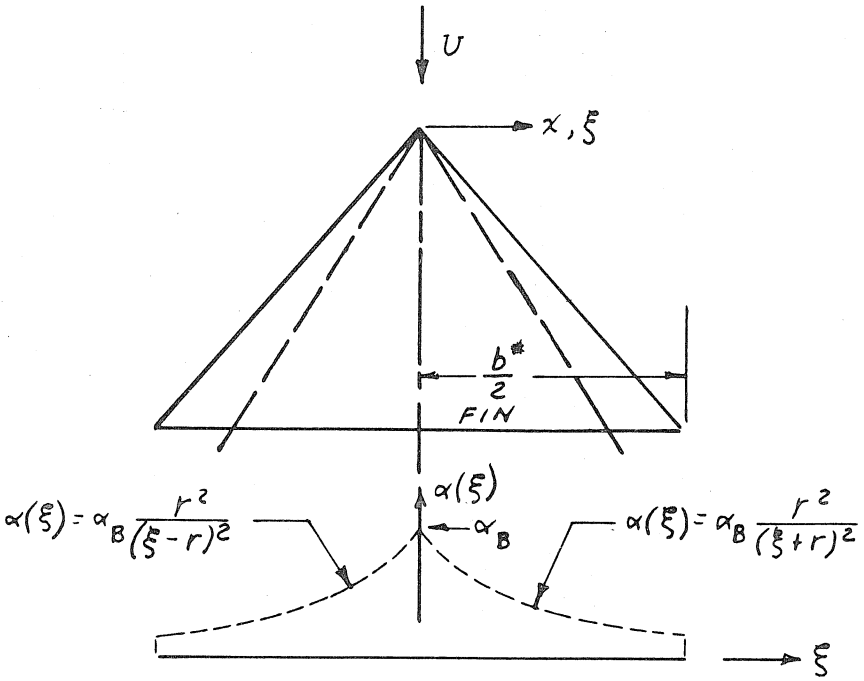

(a) OVERESTIMATE

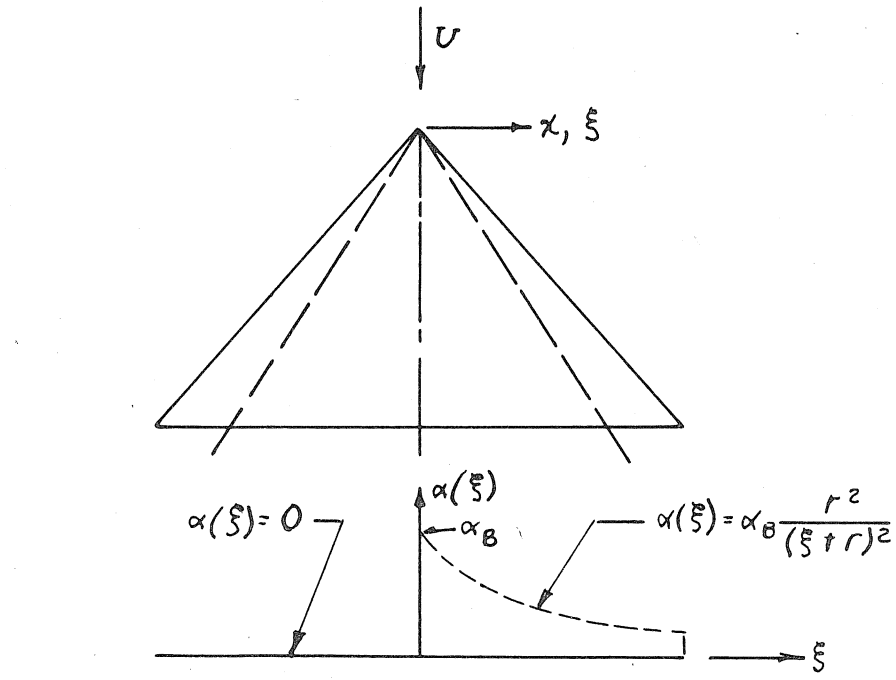

(b) UNDERESTIMATE

FIG. 42 OVER- AND UNDERESTIMATES FOR BODY INCIDENCE IN LIFT

Fig. 43. Vorticity Distribution Over- and Under-estimates for Body Incidence in Lift for f = 1, A = 1/4

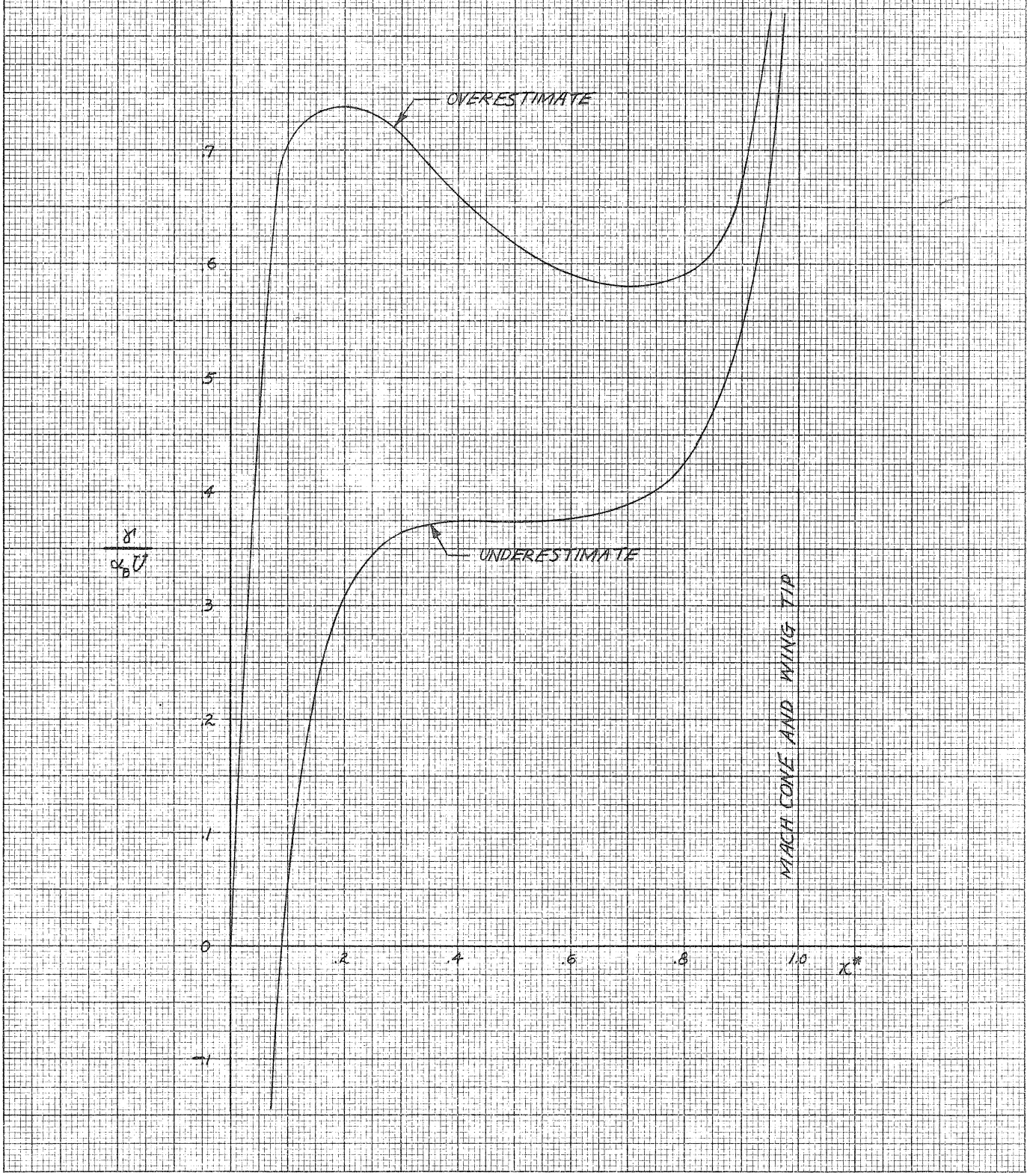

Fig. 44. Vorticity Distribution Over- and Under-estimates for Body Incidence in Lift for f = 3/4, A = 1/4

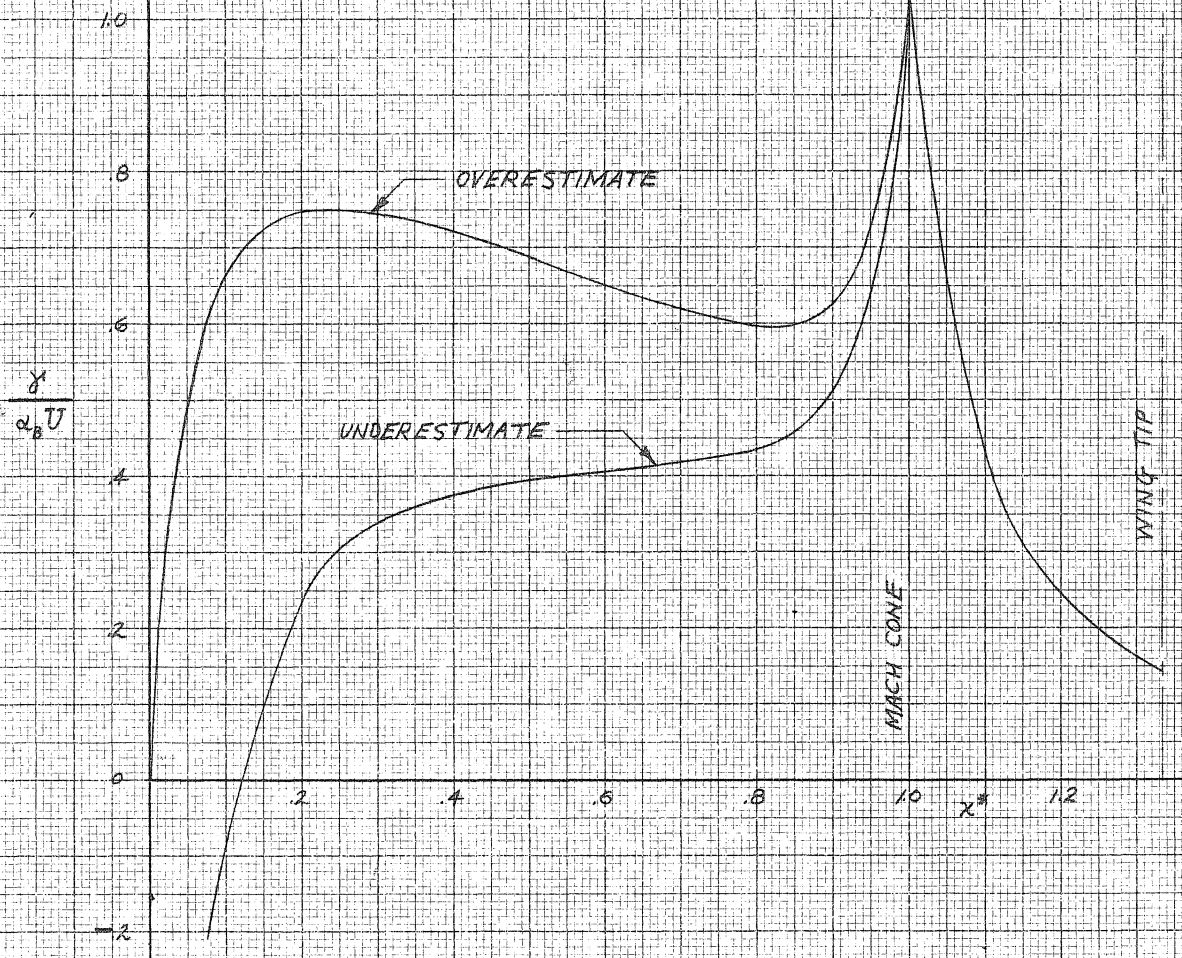

Fig. 45. Vorticity Distribution Over- and Under-estimates for Body Incidence in Lift for f = A = 3/4

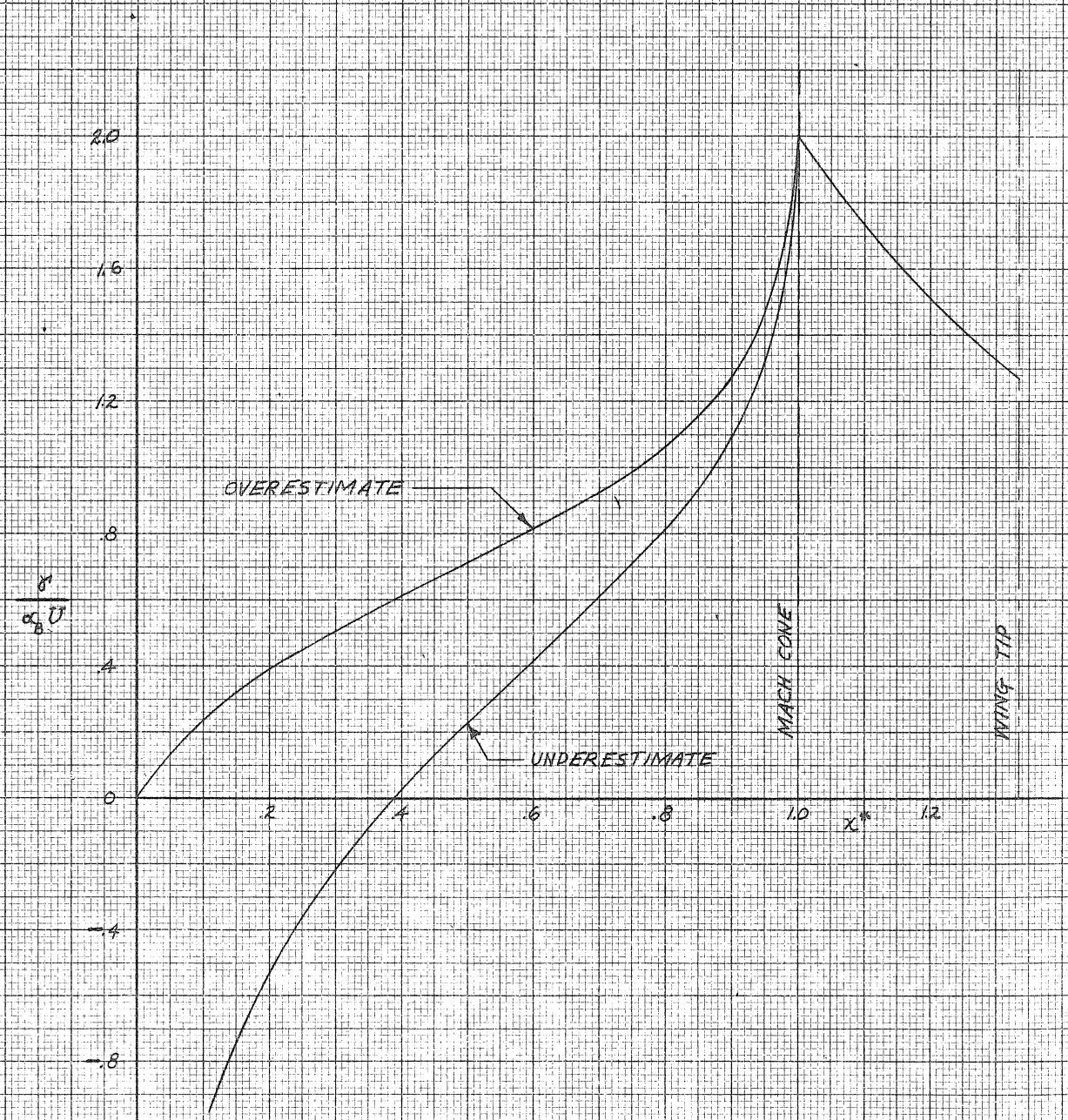

Fig. 46. Vortex Strength Over- and Underestimates for Body Incidence in Lift (Wide Delta)

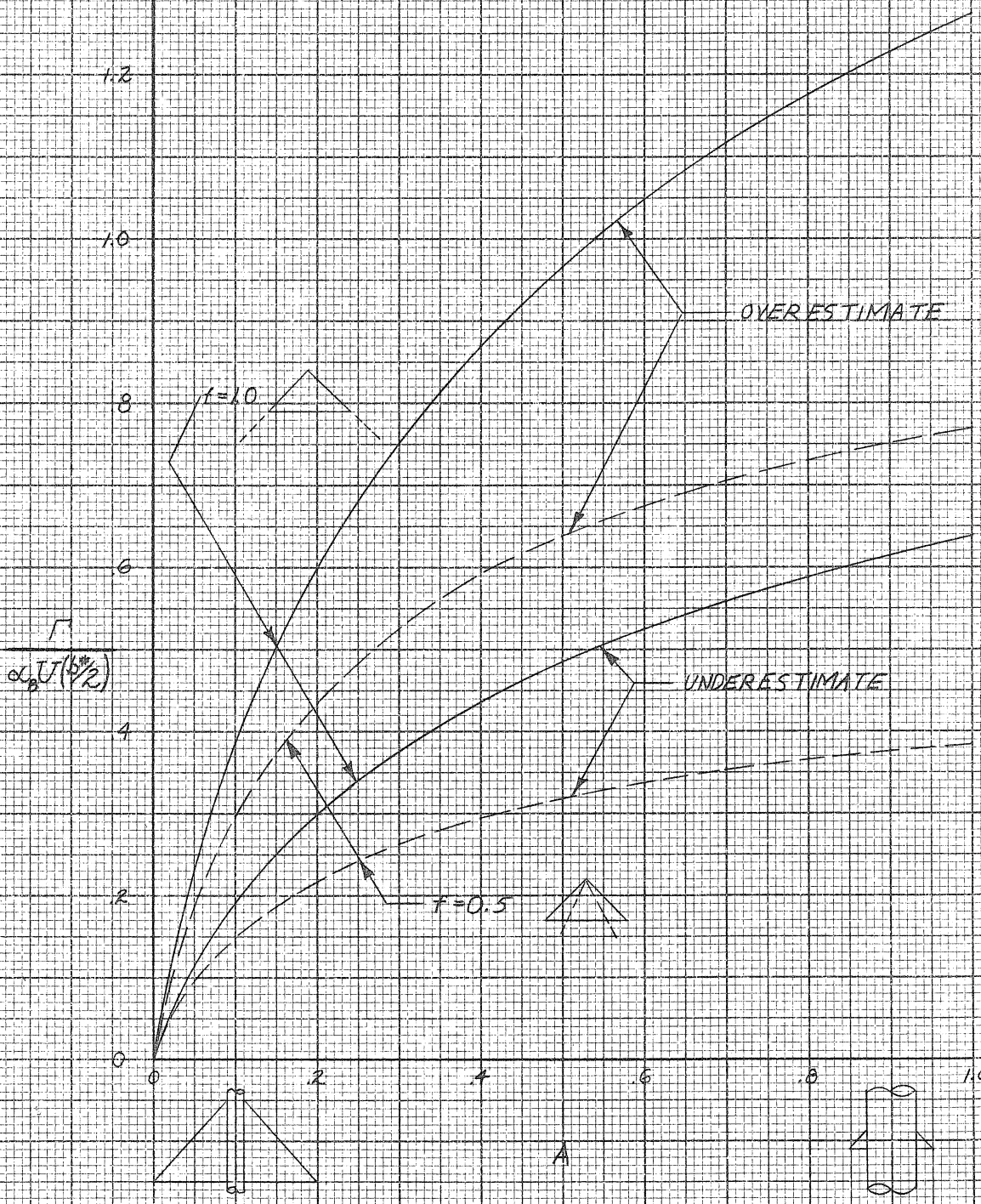

Fig. 47. Plots of Functions M(k) and Q(k')

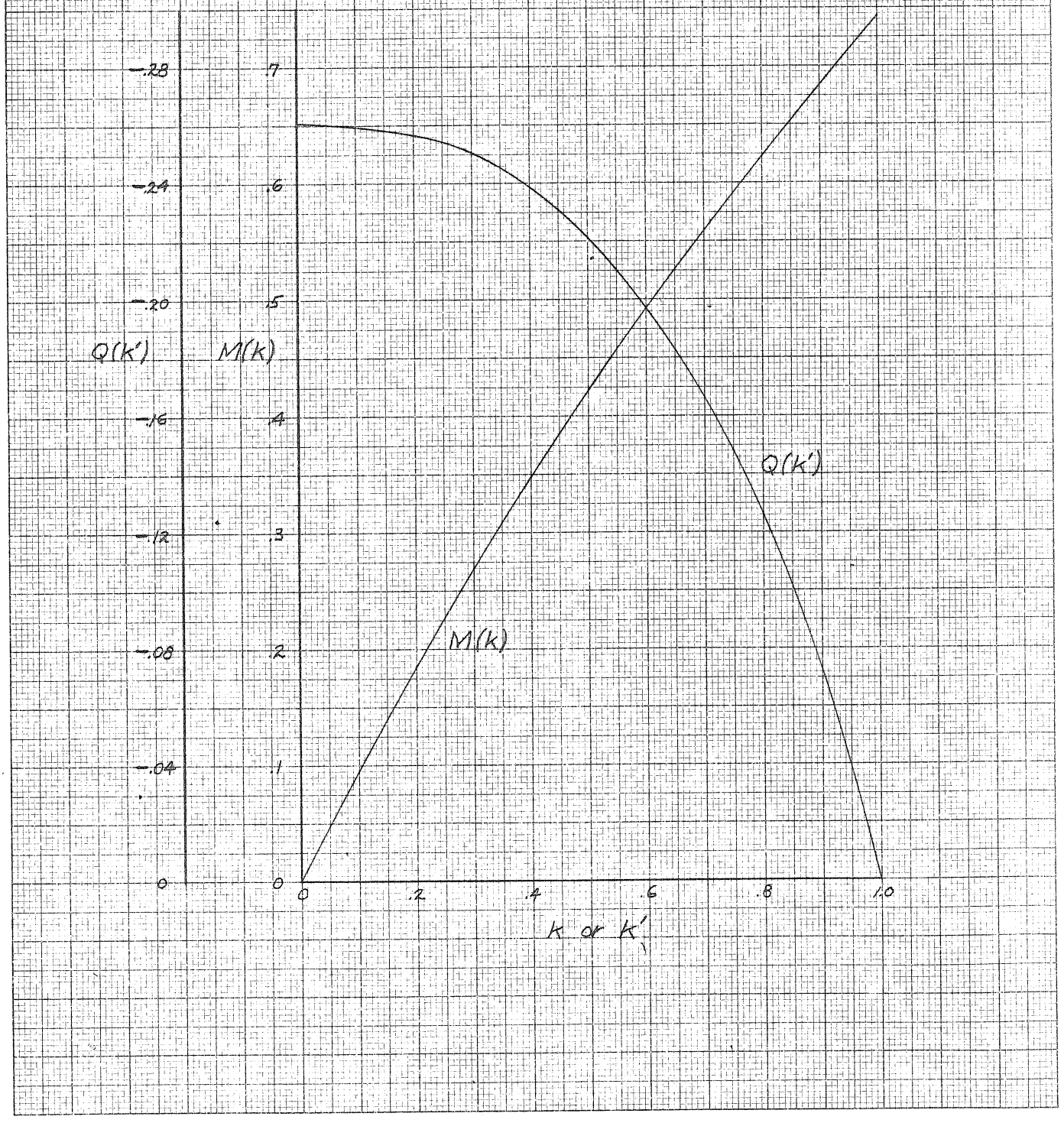

Fig. 48. Vortex Position Over- and Underestimates for Body Incidence in Lift (Wide Delta)

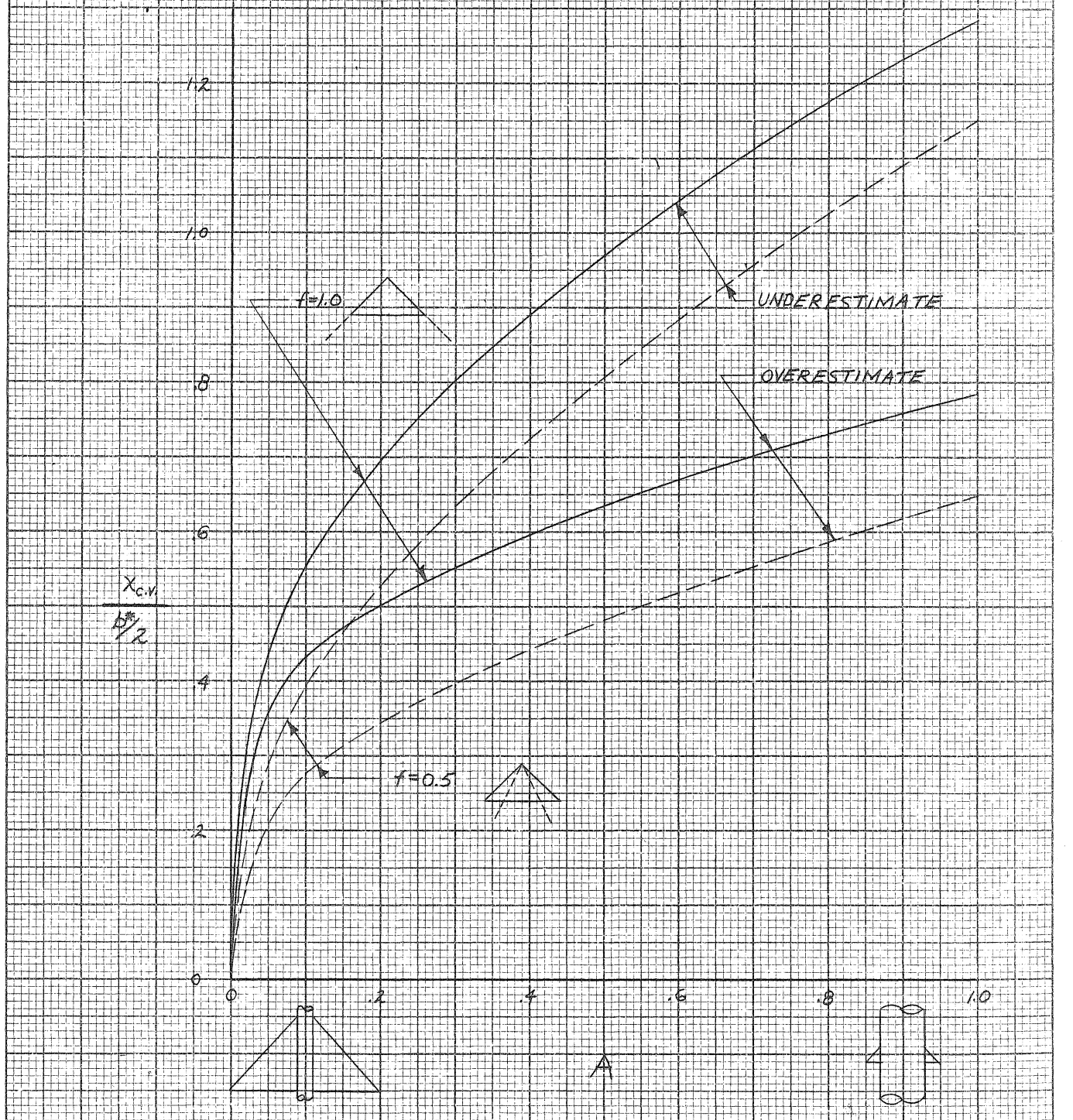

Fig. 49. Vorticity Distribution Over- and Underestimates for Wide-Delta Wing Incidence in Lift

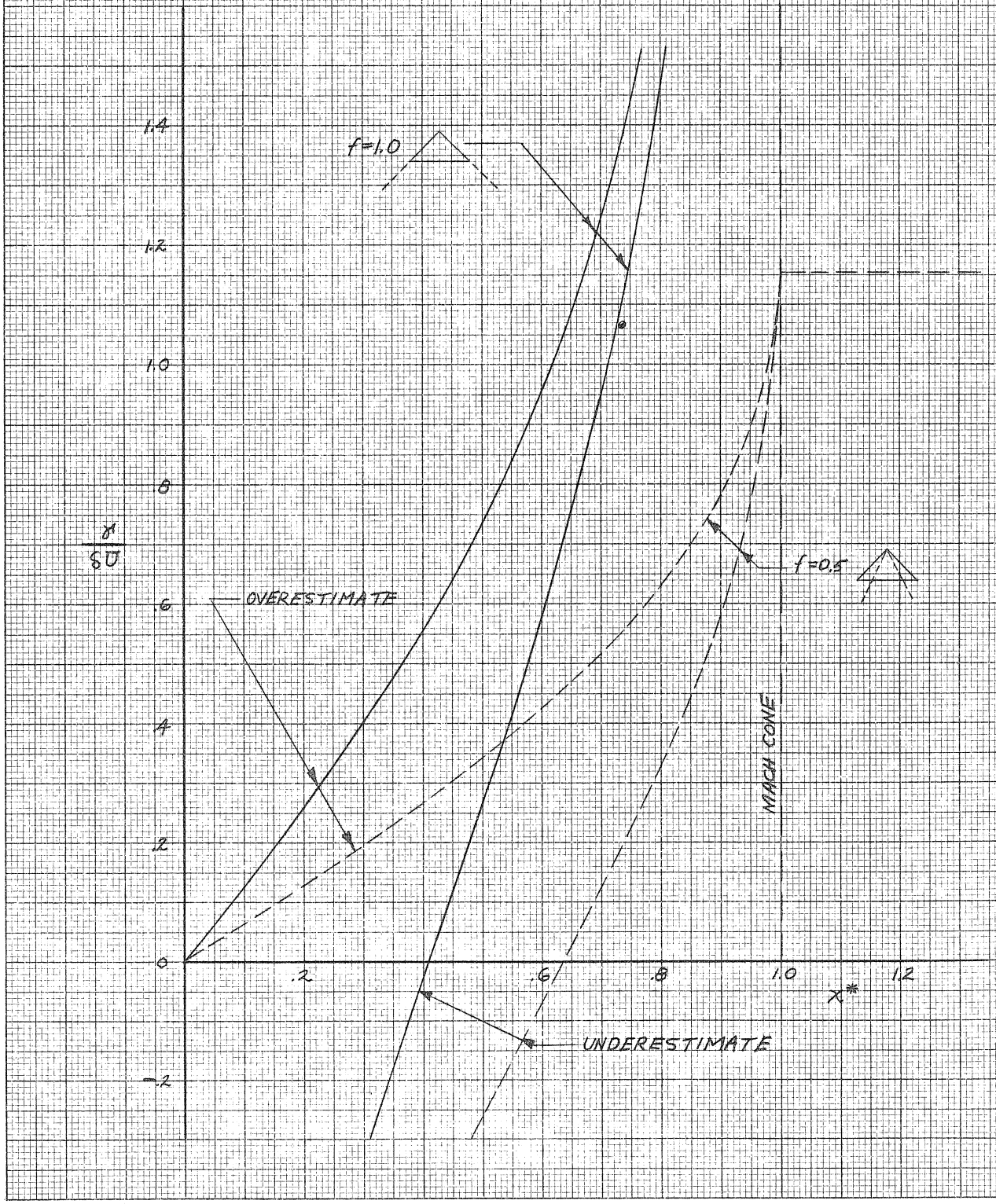

Fig. 50. Vortex Position Over- and Underestimates for Wide-Delta Wing Incidence in Lift

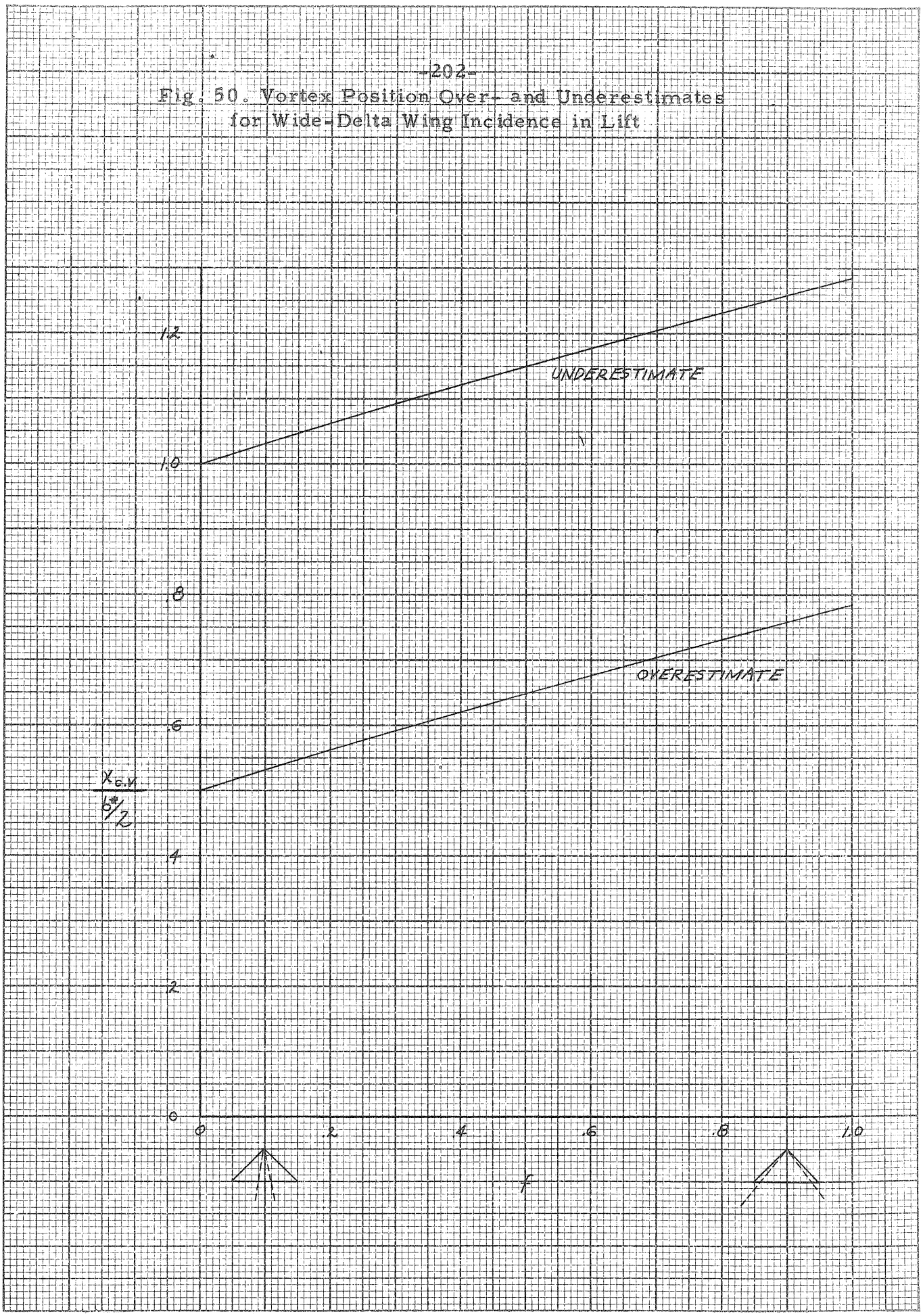

Fig. 51. Vorticity Distribution Over- and Under-estimates for Narrow-Delta Wing Incidence in Lift

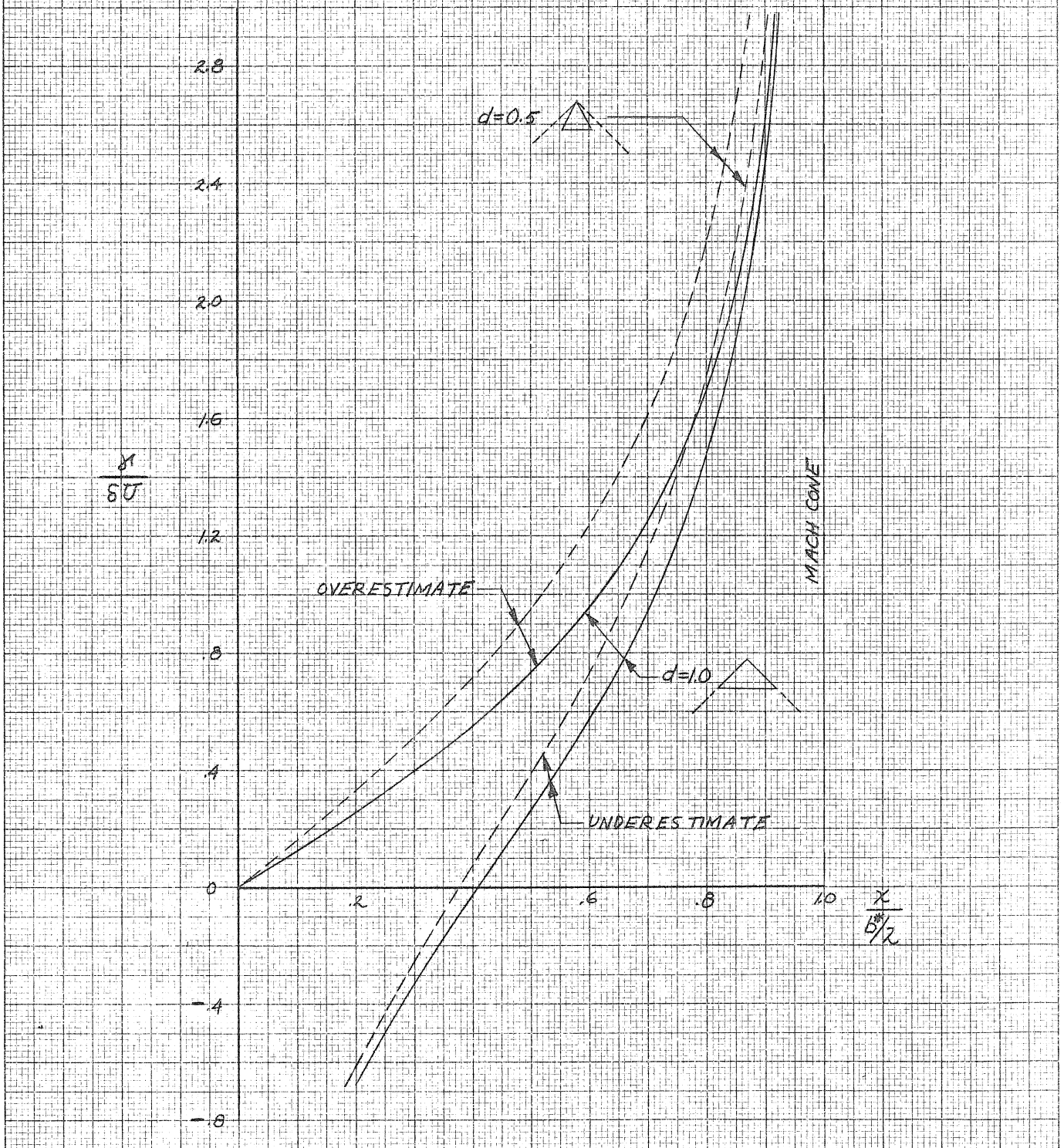

Fig. 52. Vortex Strength Over- and Underestimates for Lift (Wide Delta)

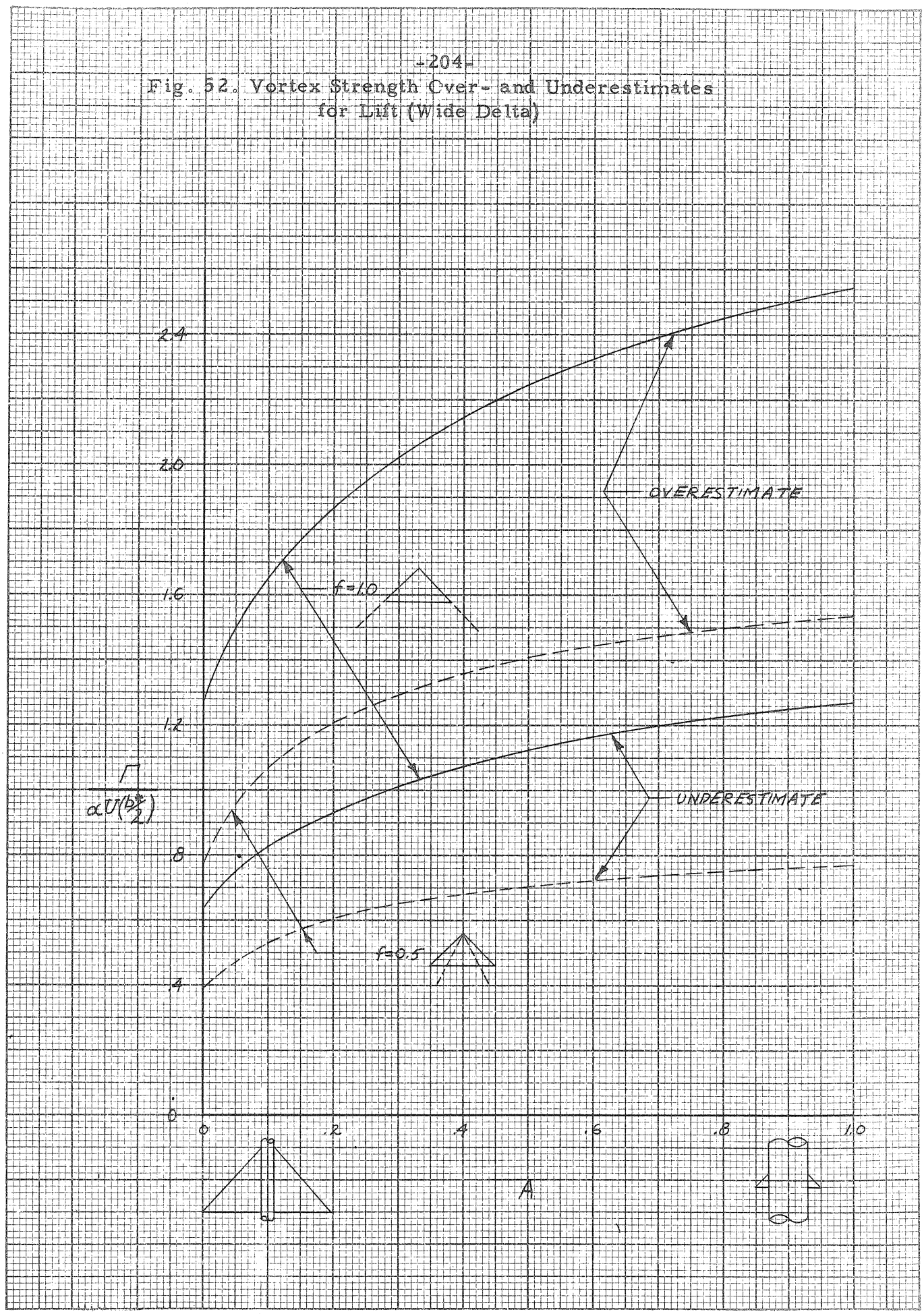

Fig. 53. Vortex Position Over- and Underestimates for Lift (Wide Delta)

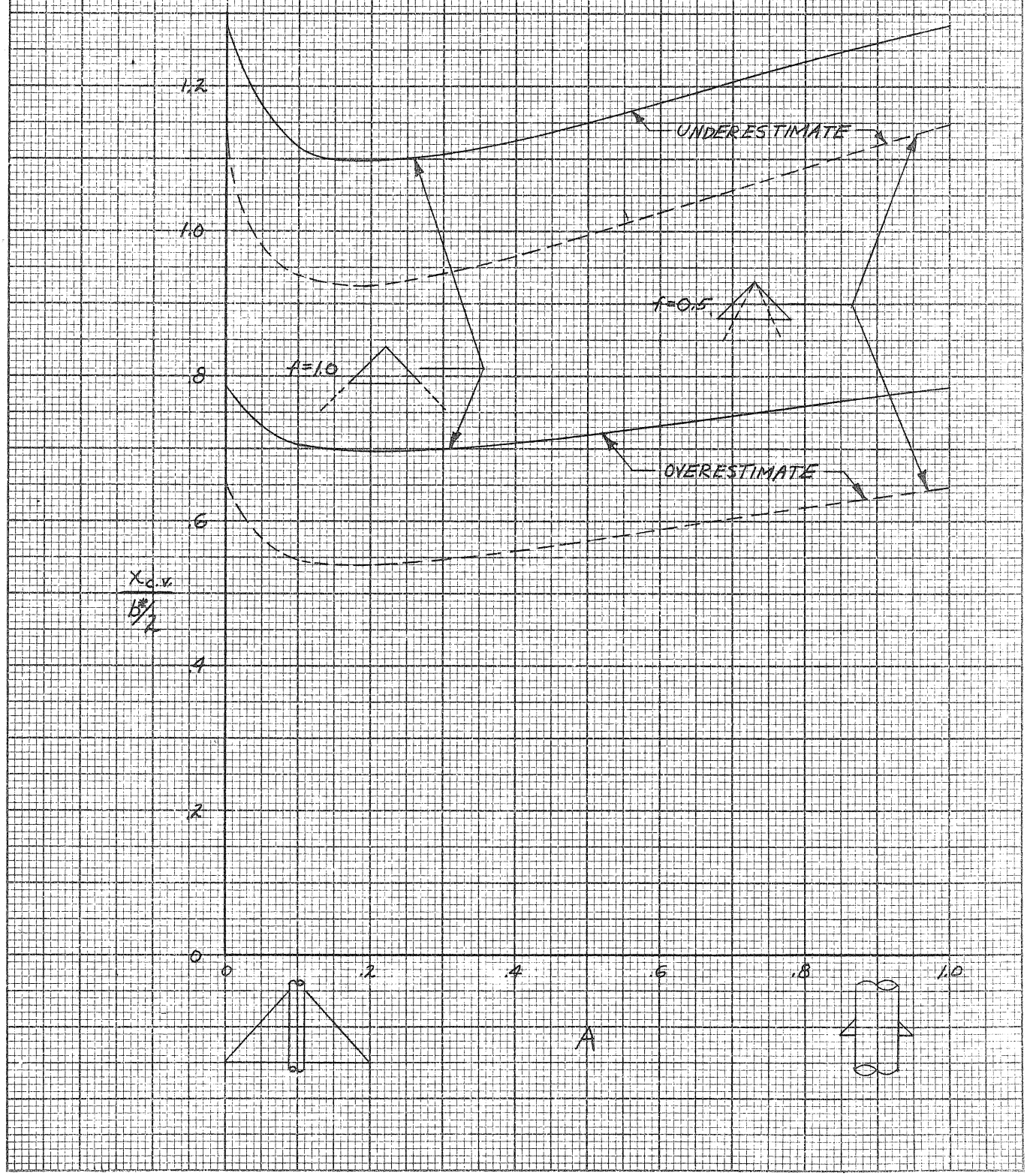

Fig. 54. Comparison with Morikawa's Estimates for Wing Lift

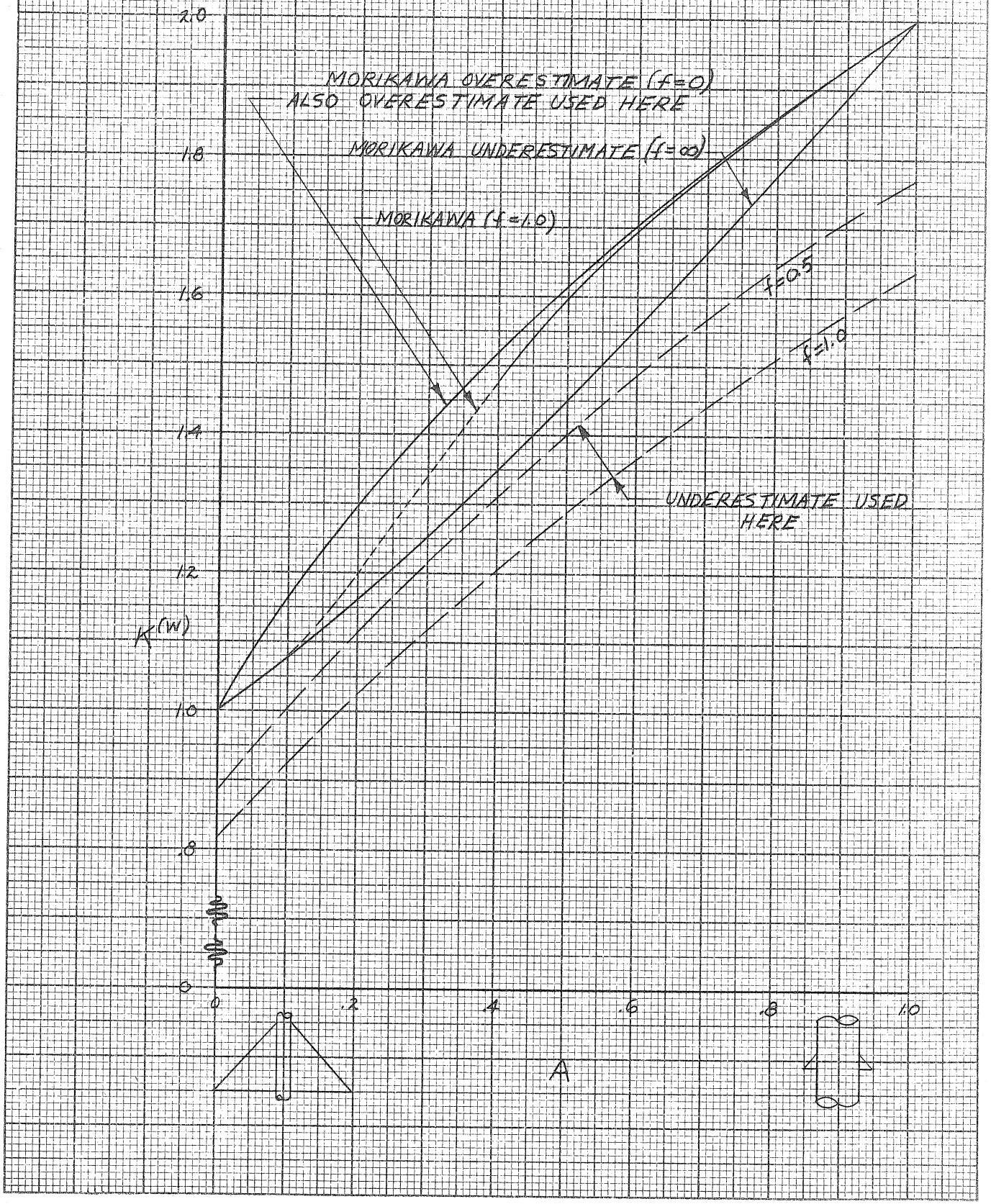

Fig. 55. Vortex Strength Estimates for Lift
(Wide and Narrow Delta)

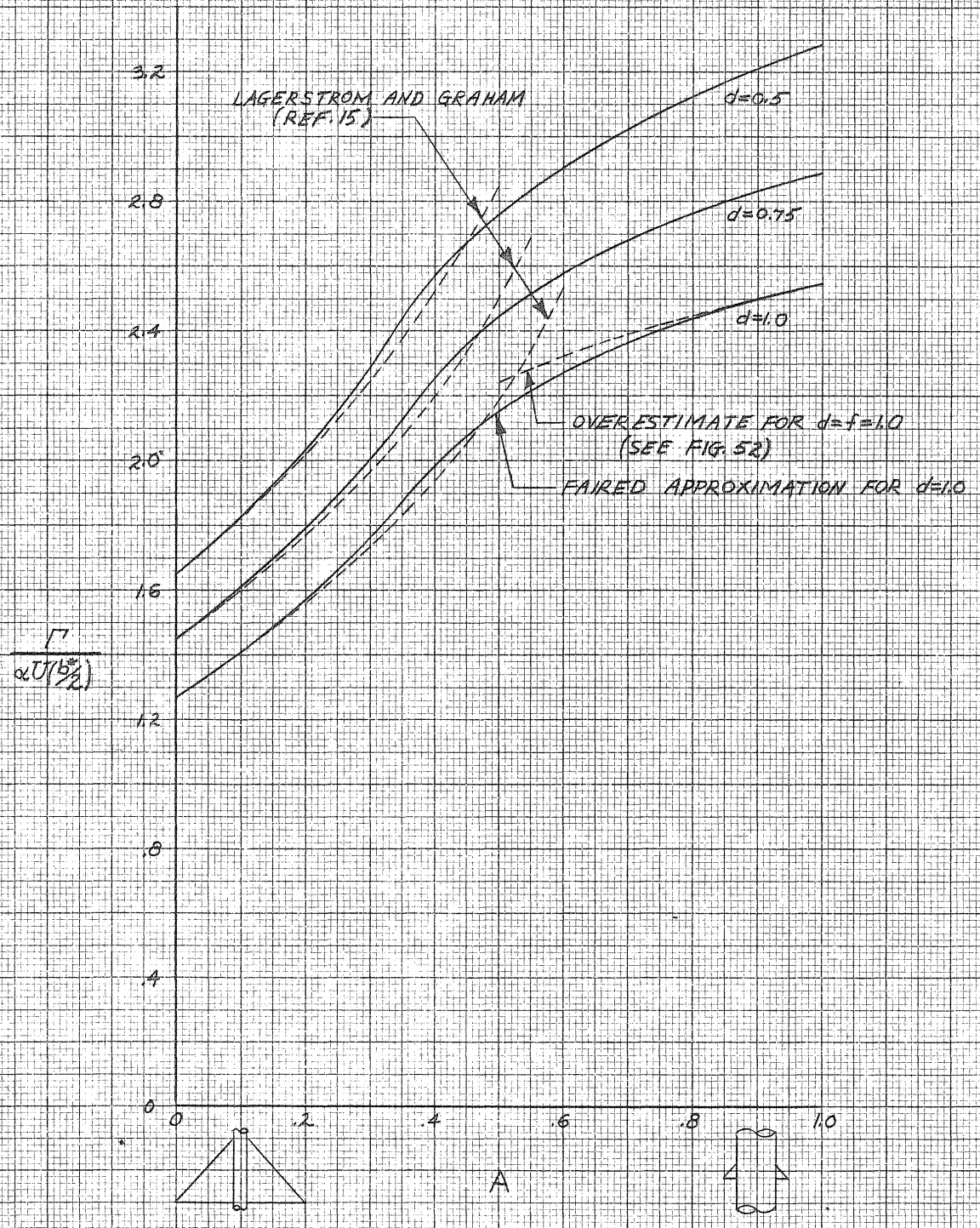

Fig. 56. Vortex Position Estimates for Lift (Wide and Narrow Delta)

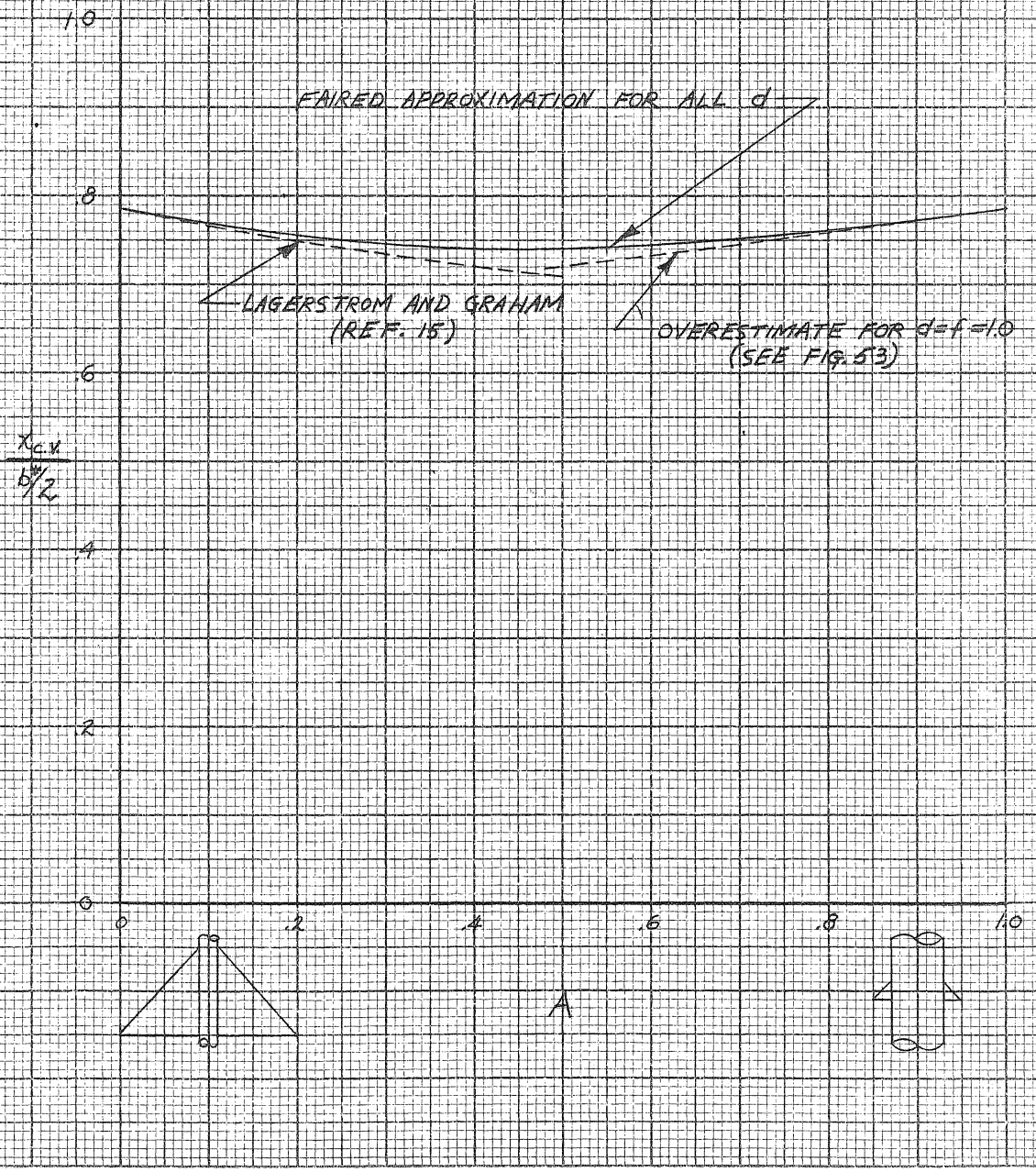

Fig. 5.7. Vorticity Distributions for Plane Wide-Delta Aileron

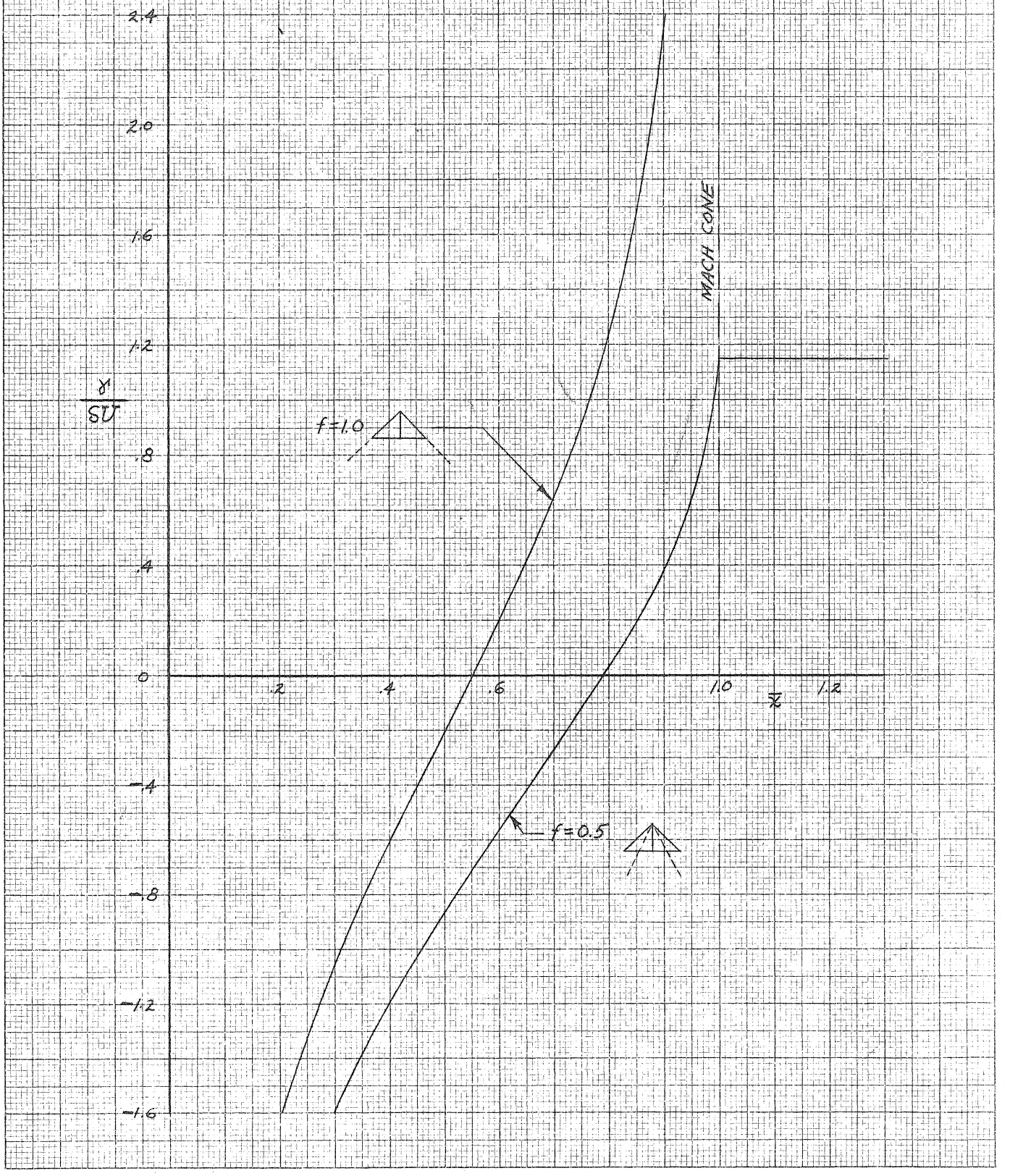

Fig. 58. Vortex Strength Estimates for Plane and Cruciform Wide-Delta Ailerons

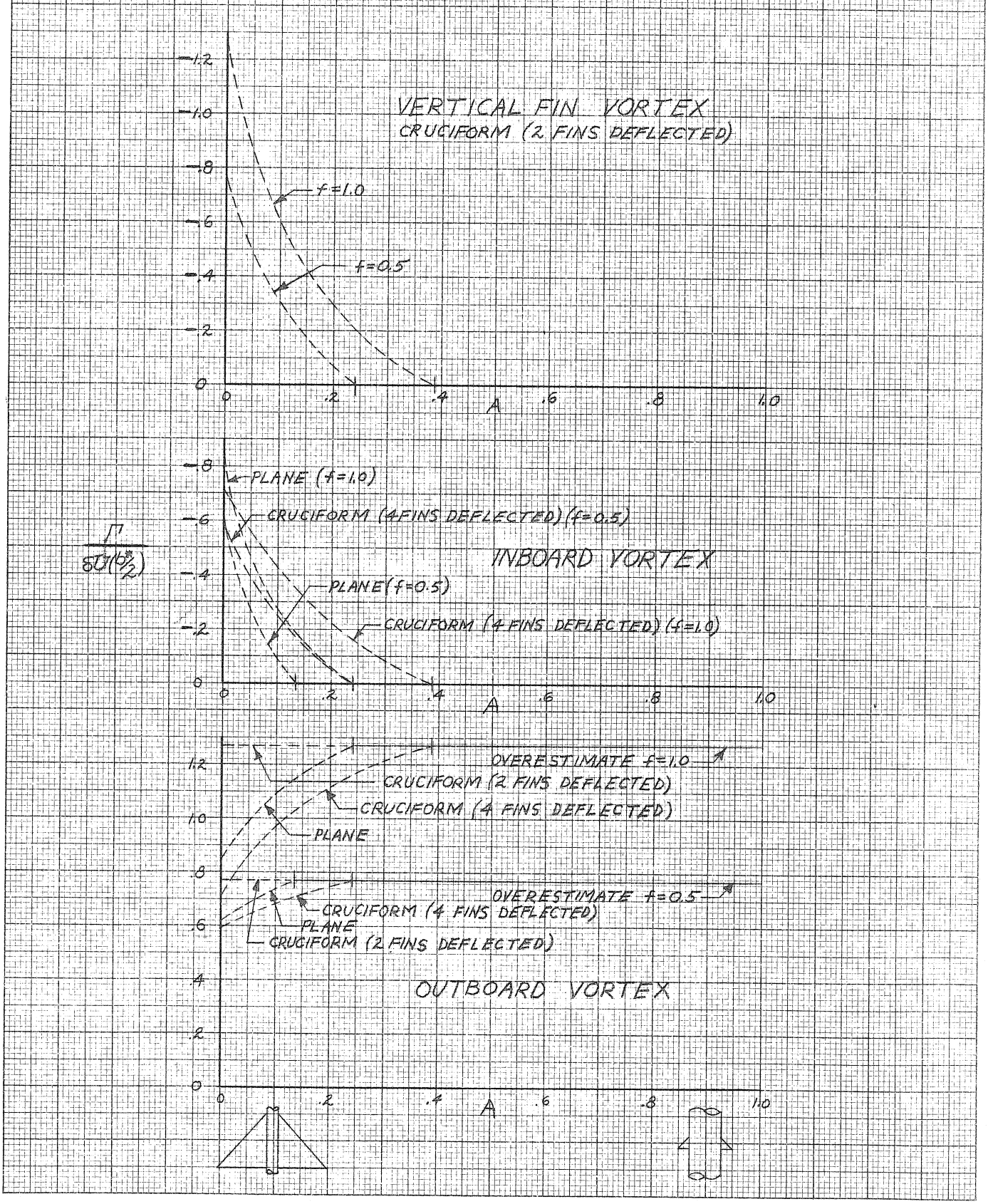

Fig. 59. Vortex Position Estimates for Plane and Cruciform Wide-Delta Ailerons

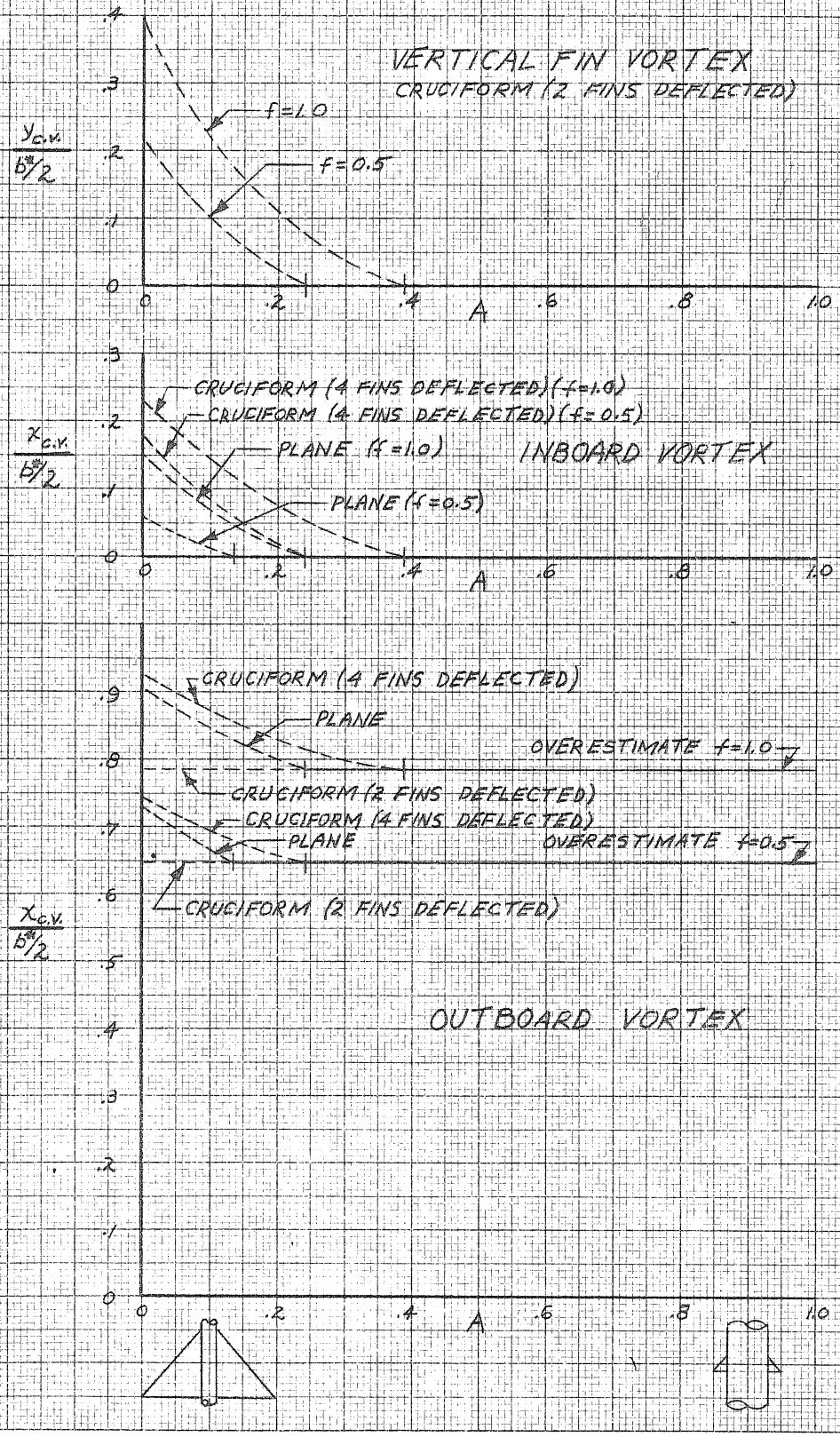

Fig. 60. Vortex Strength Estimates for Plane Narrow-Delta Ailerons

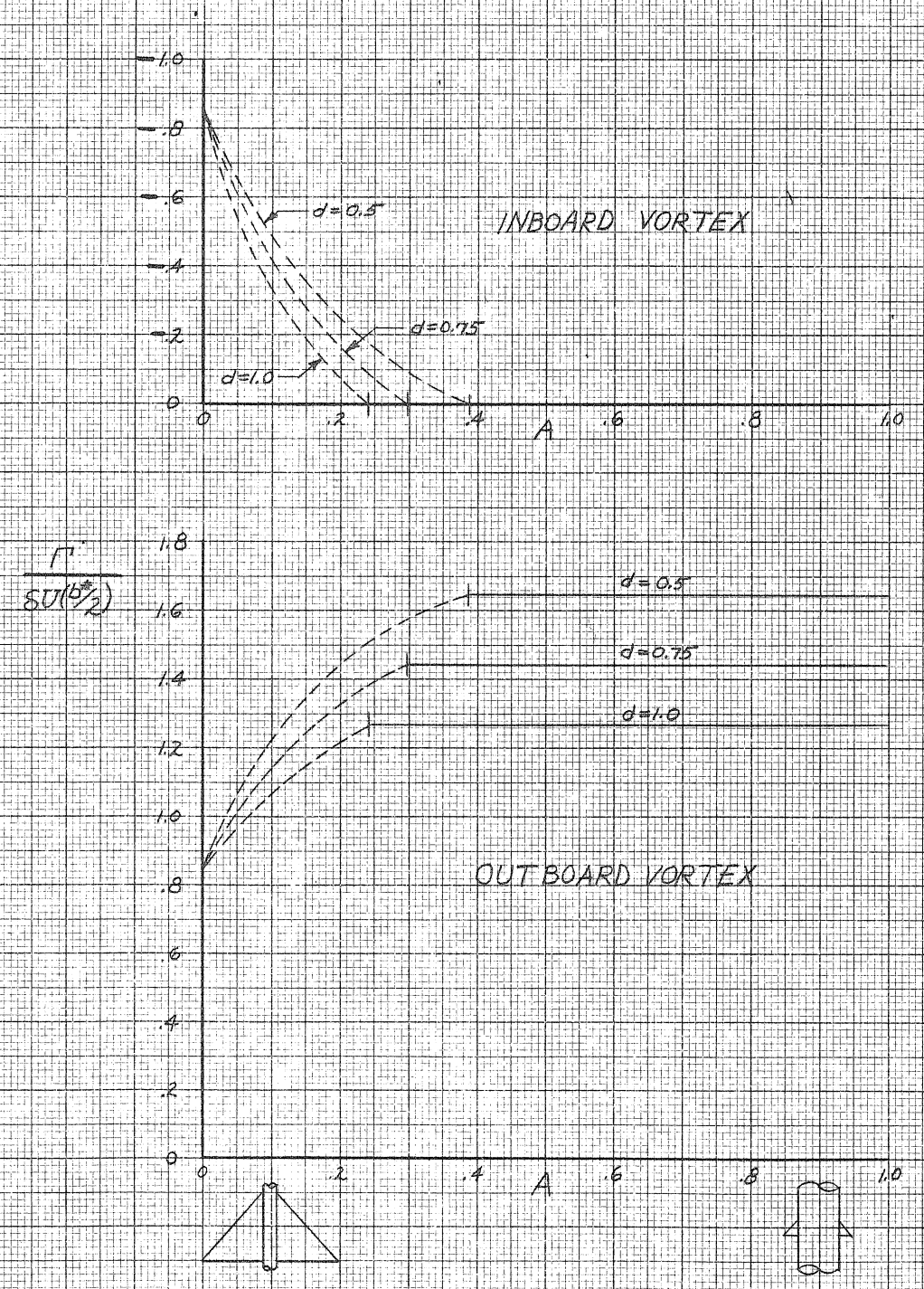

Fig. 61. Vortex Position Estimates for Plane Narrow-Delta Ailerons

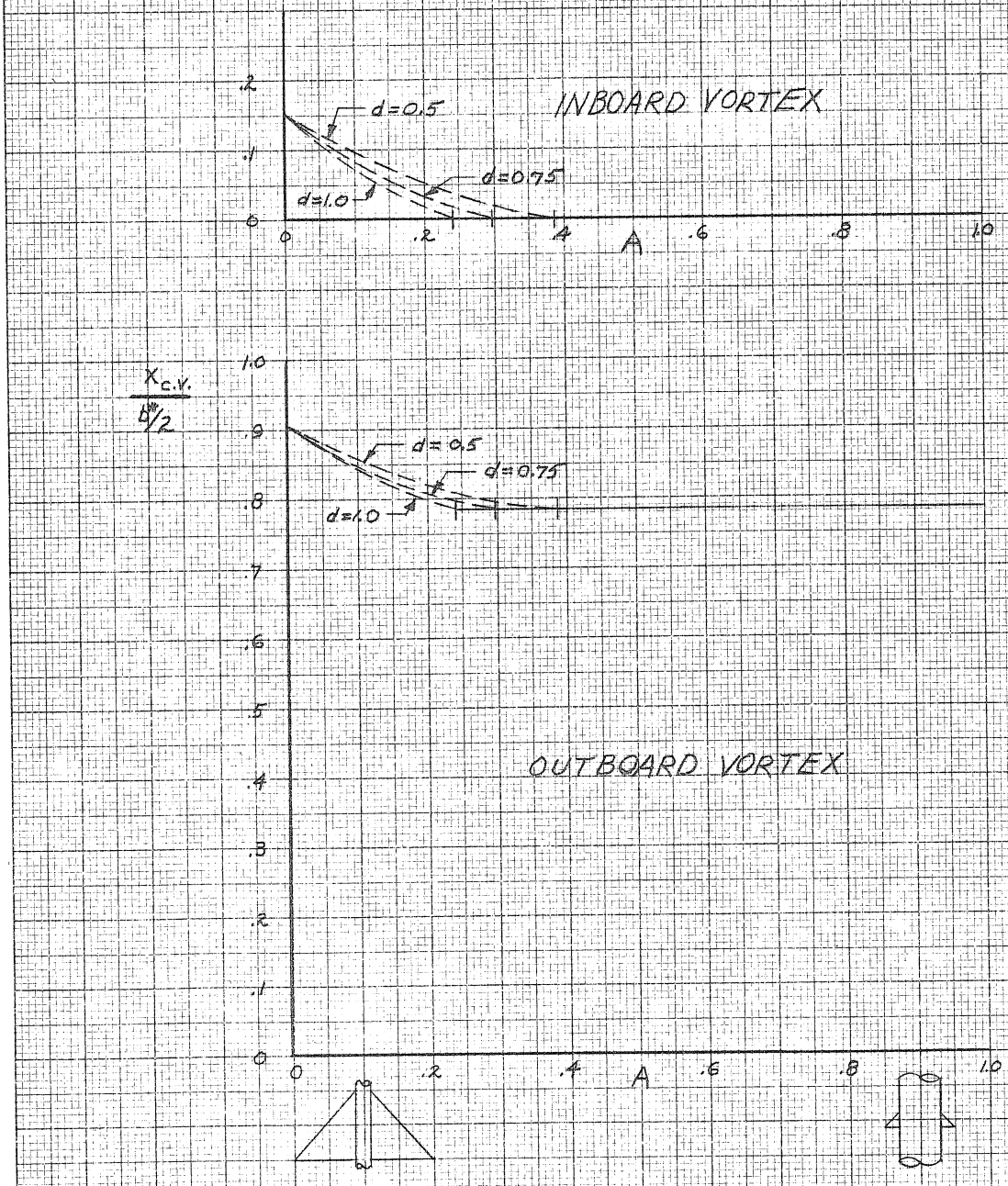

Fig. 62. Vorticity Distributions on Vertical Fins of Cruciform Wide-Delta Aileron (2 Fins Deflected)

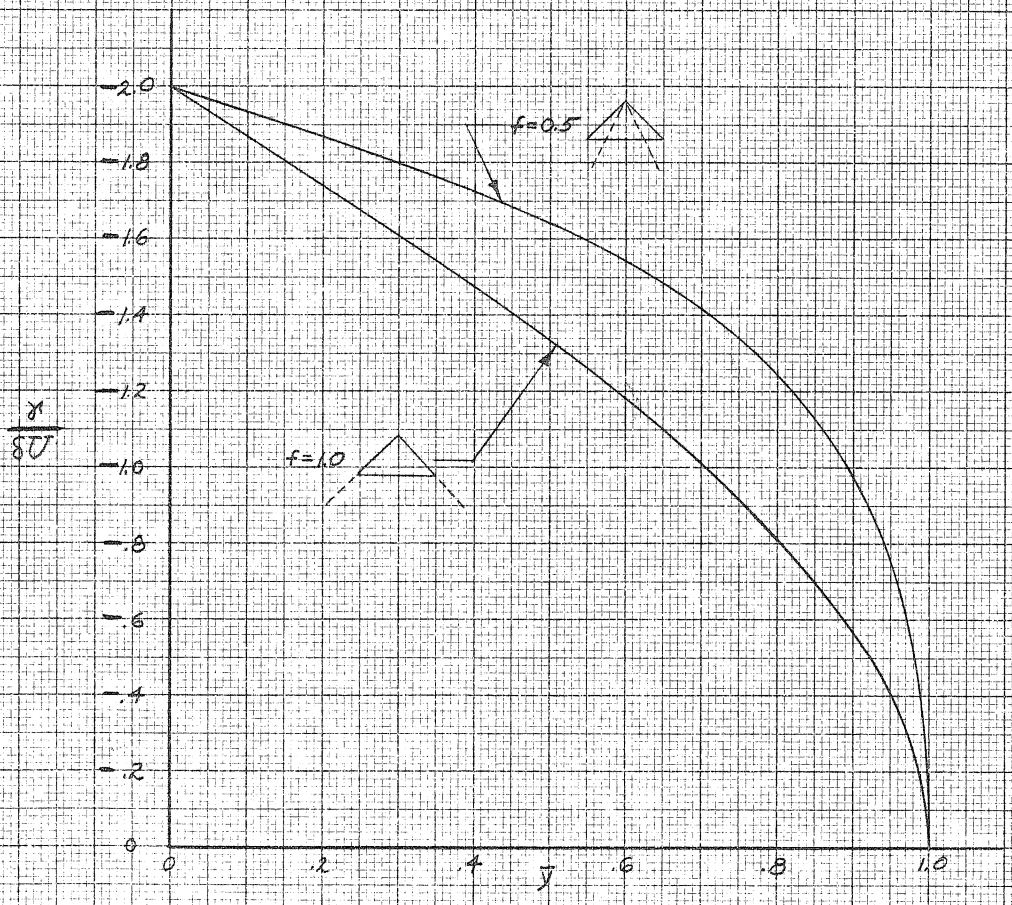

Fig. 63. Vorticity Distributions on Horizontal Fins of Cruciform Wide-Delta Ailerons (2 and 4 Fins Deflected)

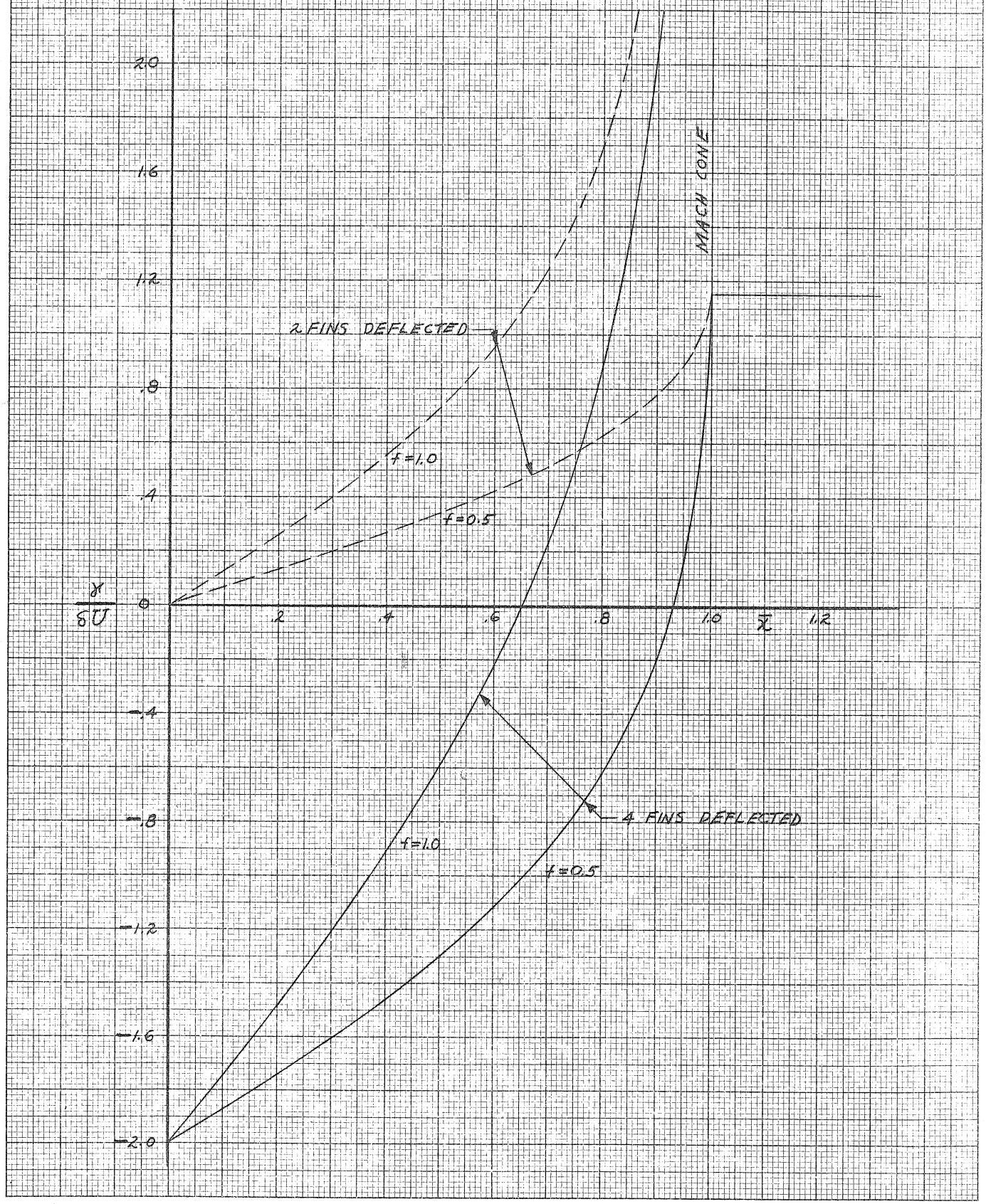

Fig. 64. Vorticity Distribution Overestimates for Damping in Roll for f = 1

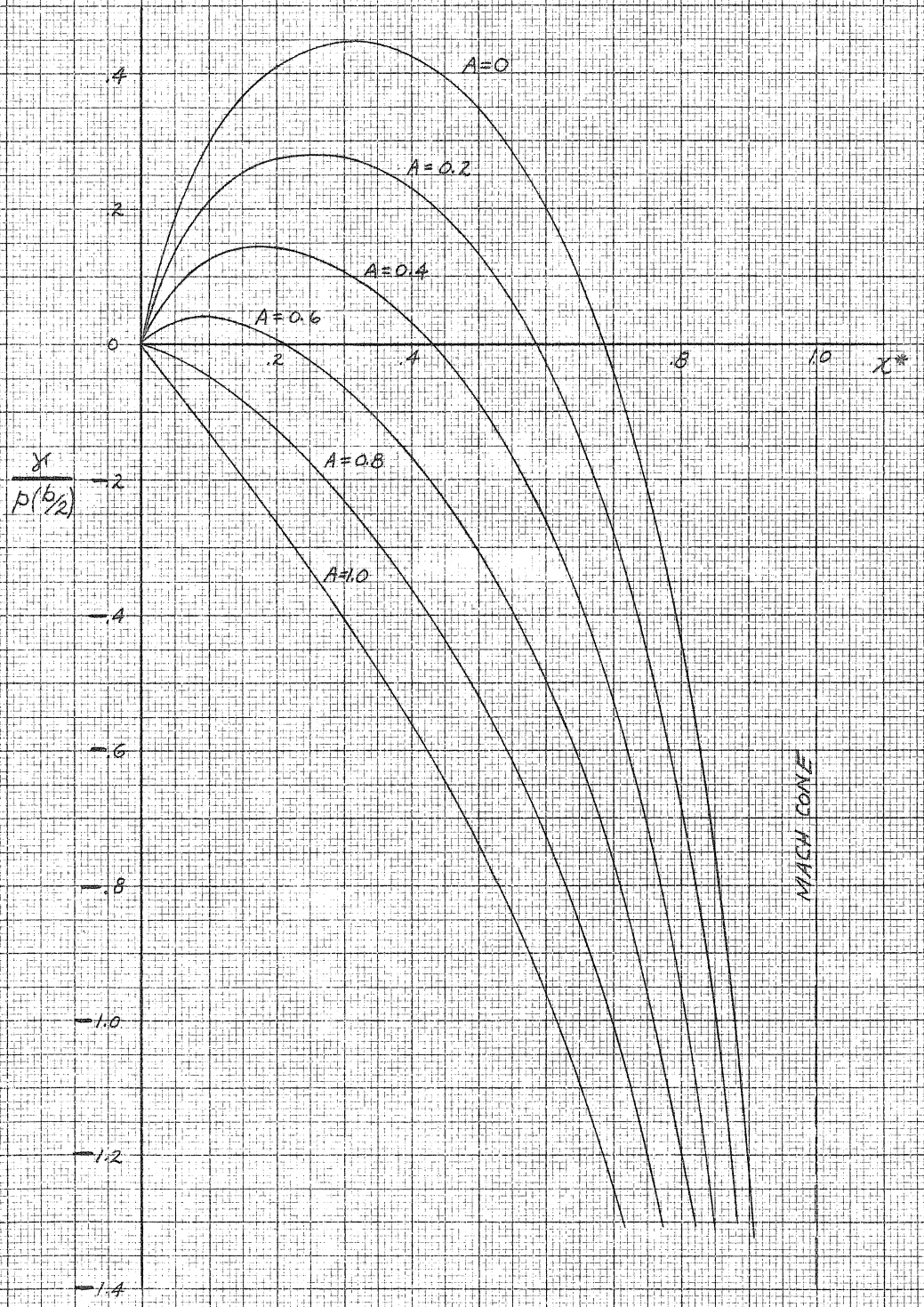

Fig. 65. Moments-of-Vorticity Distribution Overestimates for Damping in Roll for f = 1

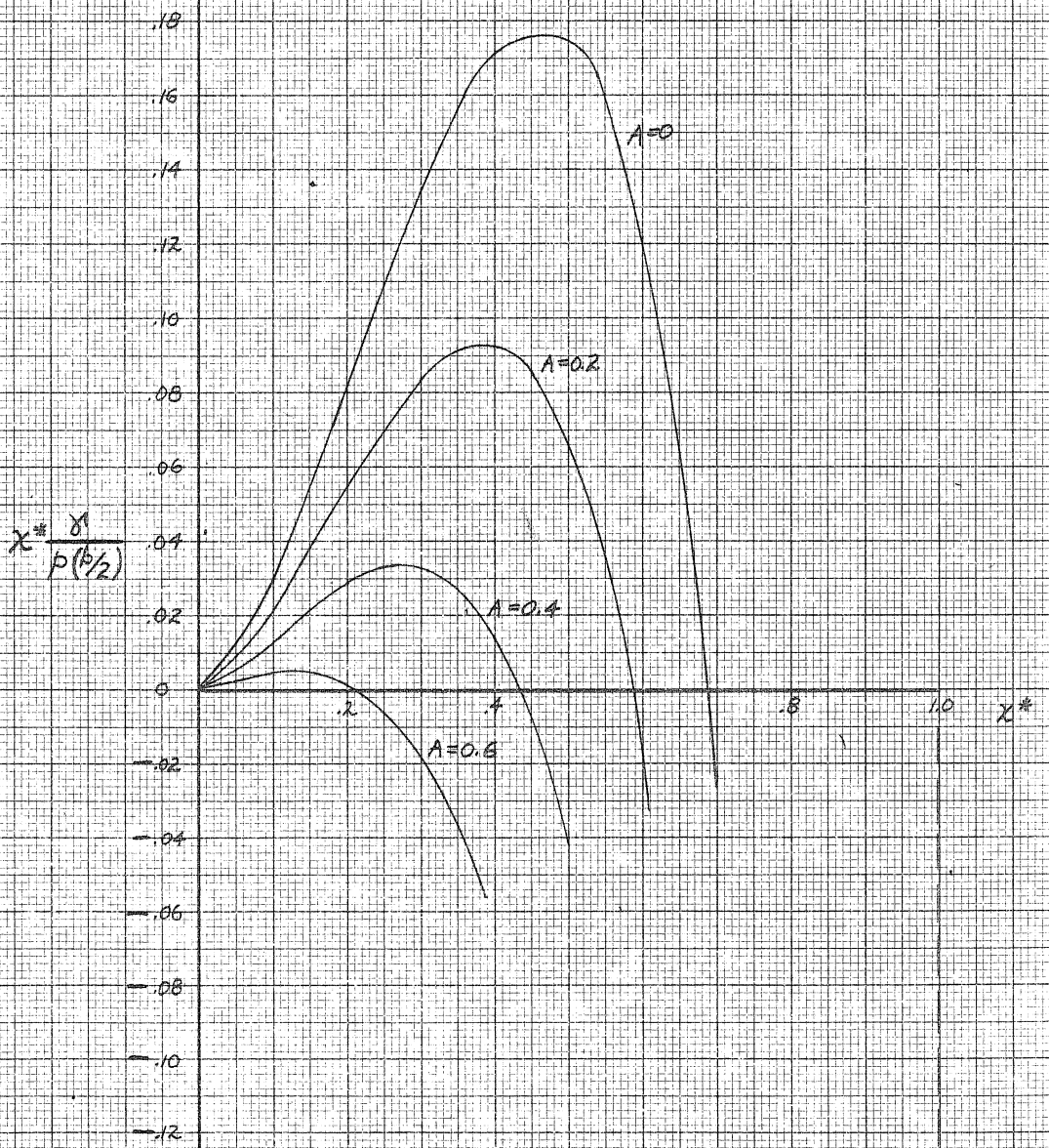

Fig. 66. Inboard Vortex Strength Estimates for Damping in Roll for Plane and Cruciform Wide-Delta Wings

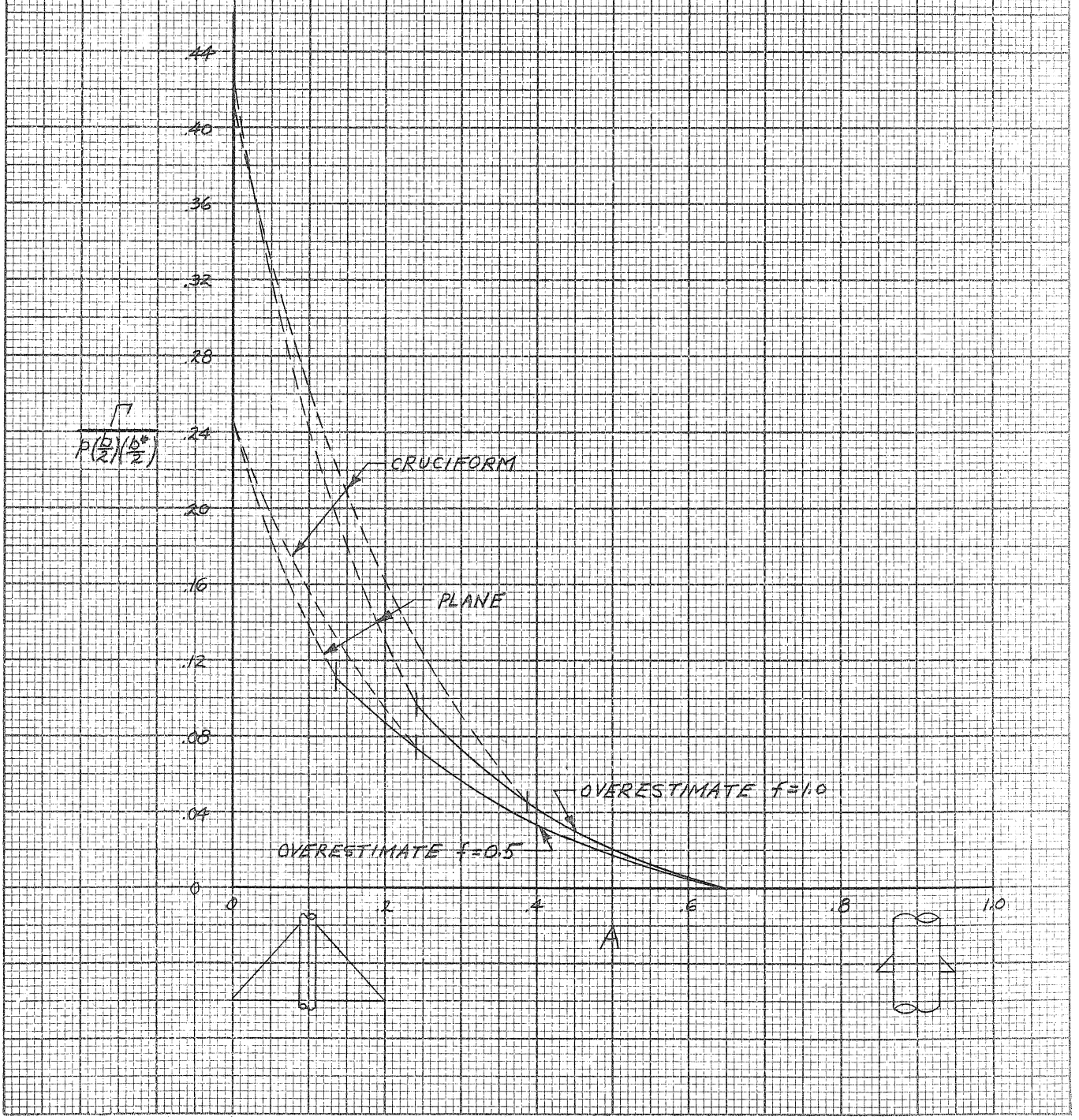

Fig. 67. Inboard Vortex Position Estimates for Damping in Roll for Plane and Cruciform Wide-Delta Wings

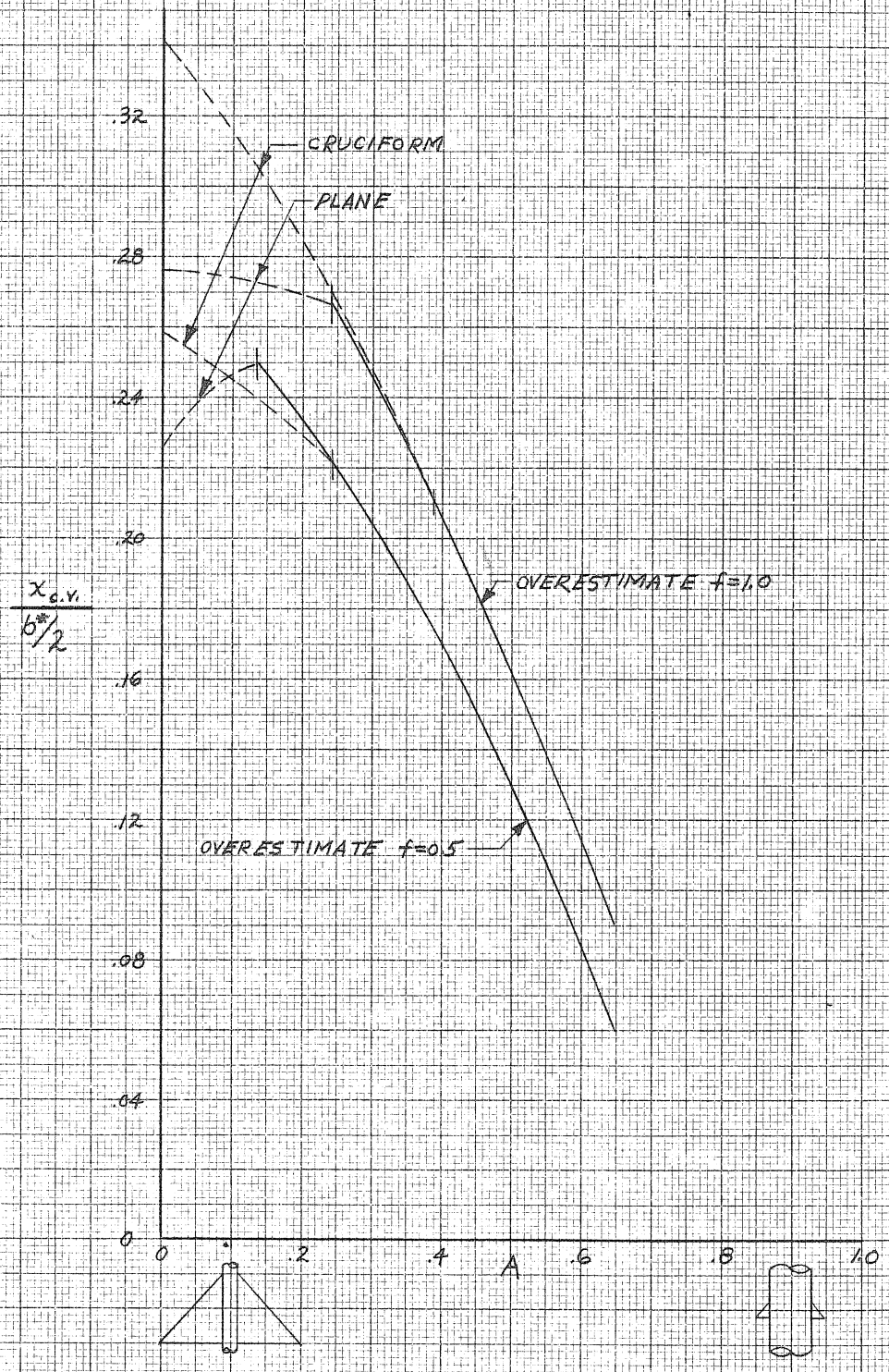

Fig. 68. Outboard Vortex Strength and Position Estimates for Damping in Roll for Plane and Cruciform Wide-Delta Wings

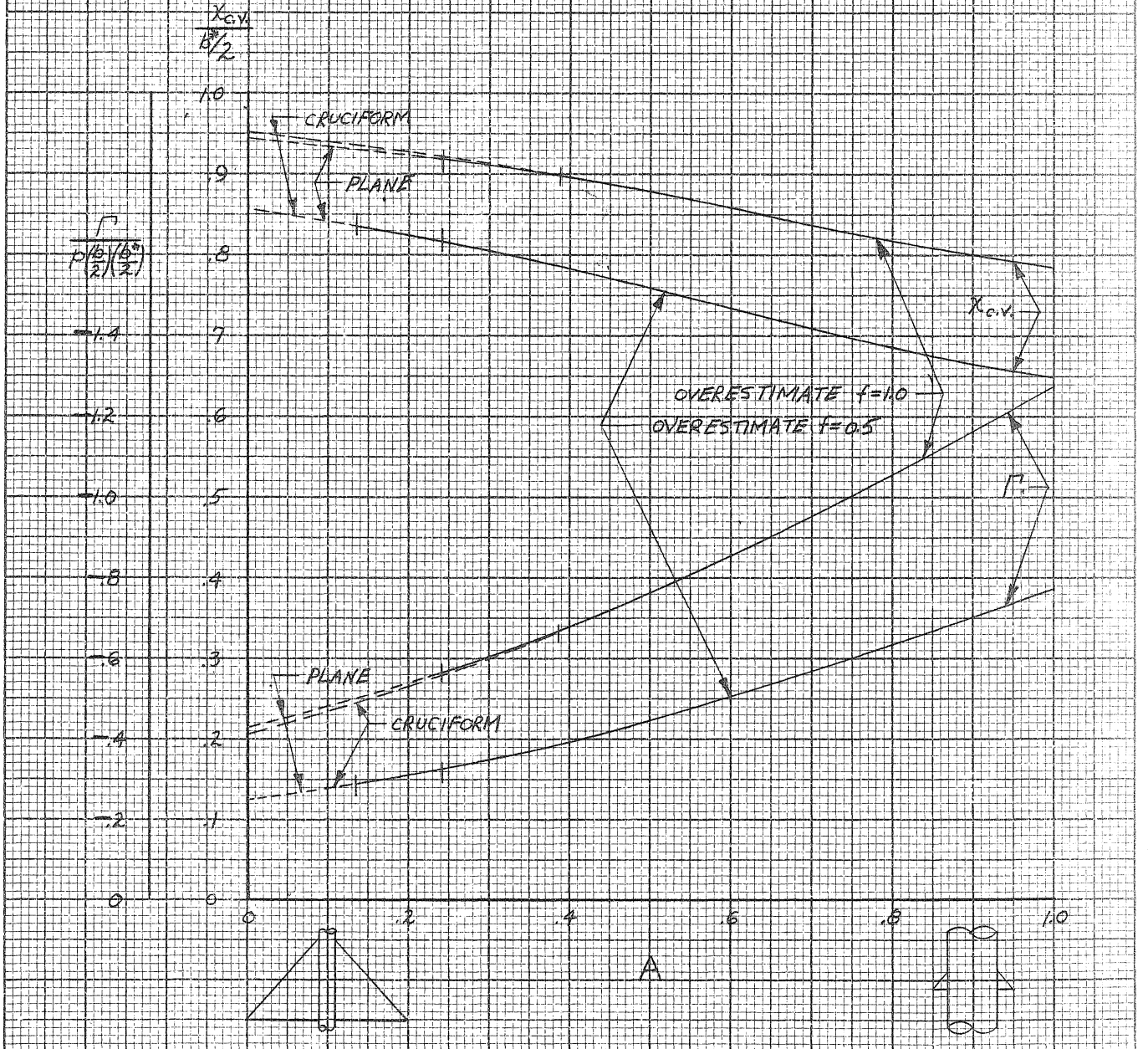

Fig. 69. Vorticity Distribution for Plane Wide-Delta Wing for Damping in Roll

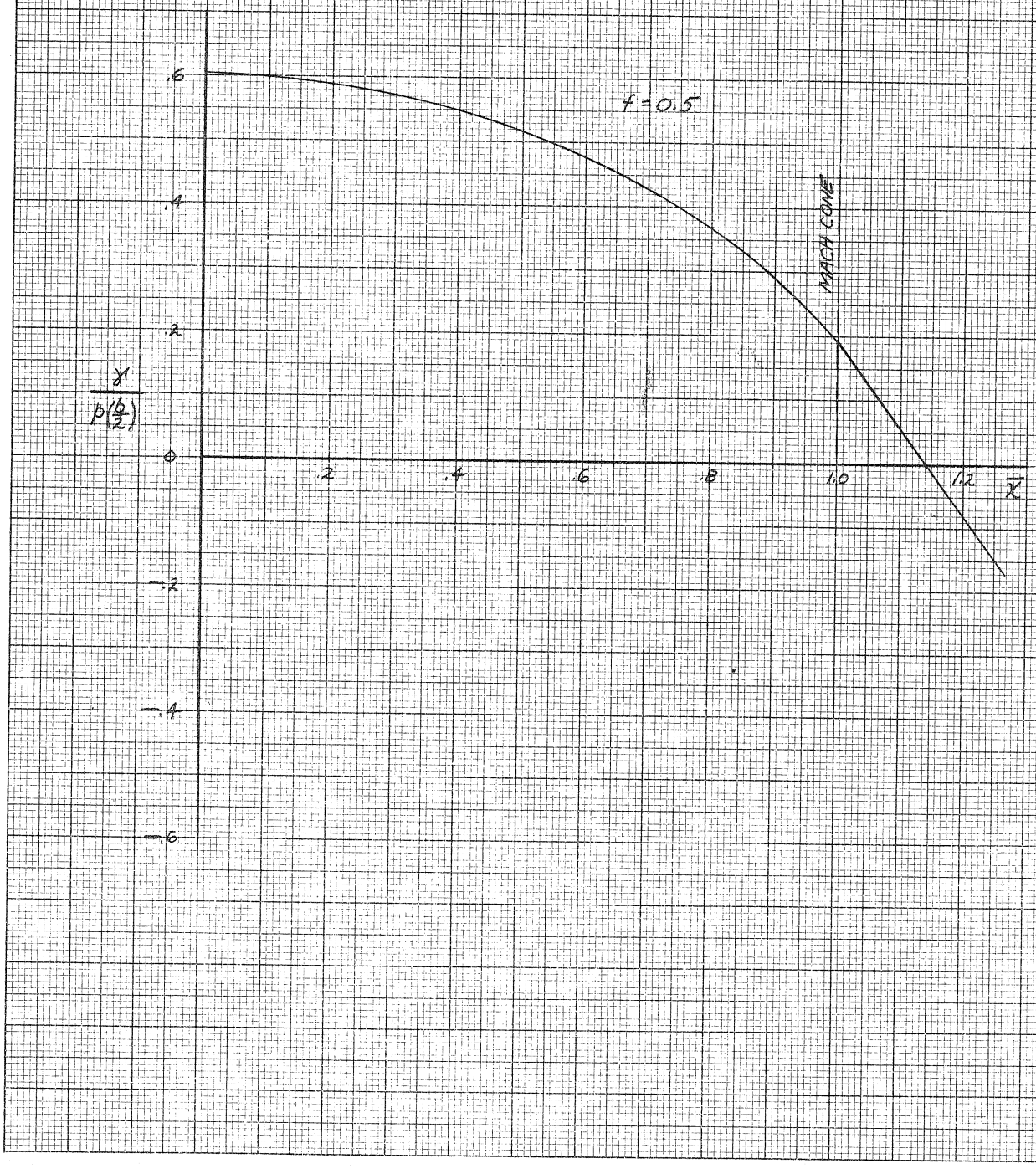

Fig. 70. Vorticity Distribution for Cruciform Wide-Delta Wing for Damping in Roll

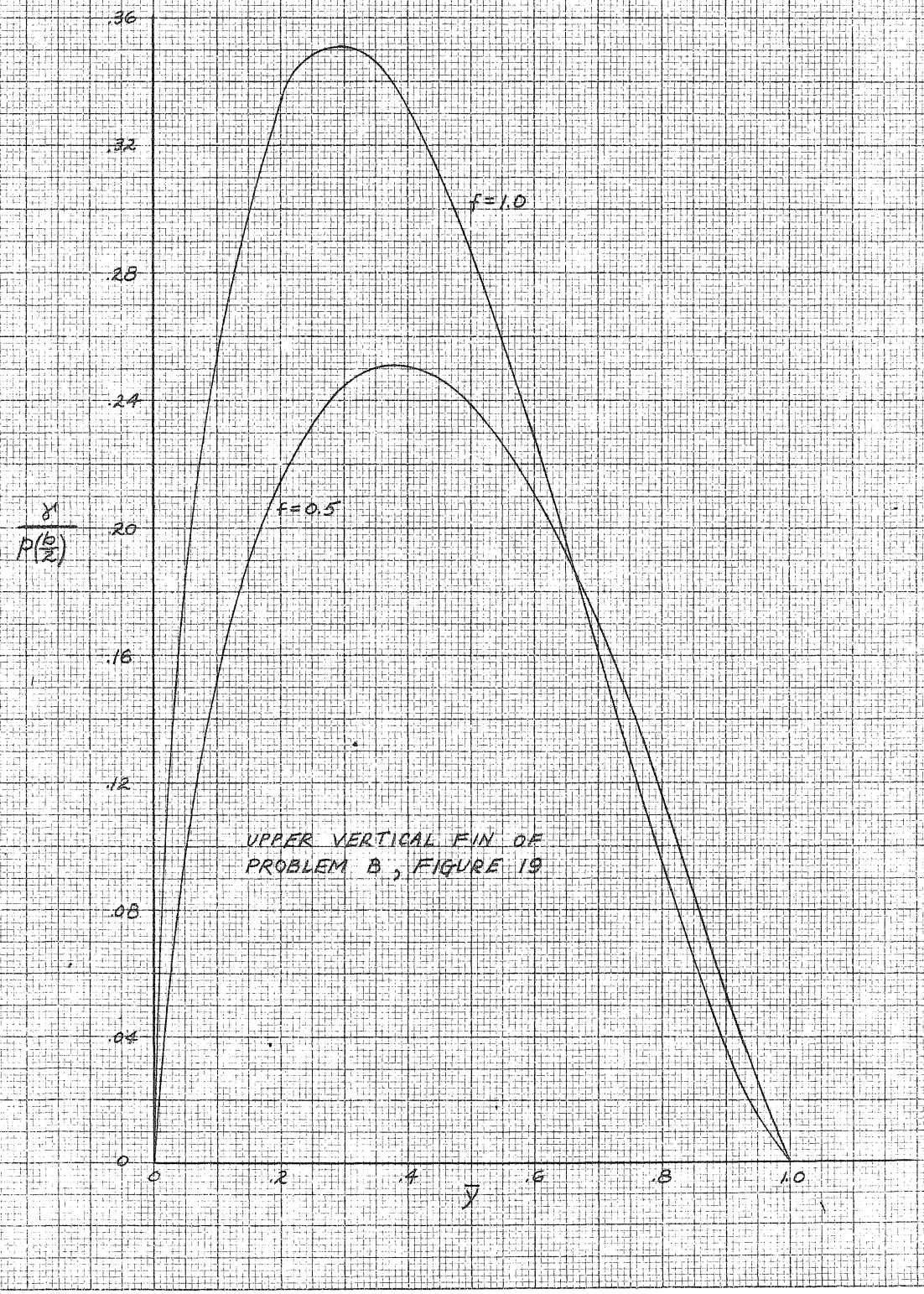

Fig. 71. Vorticity Distribution for Cruciform Wide-Delta Wing for Damping in Roll